AN ABSTRACT OF THE THESIS OF

Mark J. Redlinger for the degree of Master of Science in Civil Engineering and Forest Products presented on January 12, 1998. Title: Behavior of Metal-Plate-Connected Wood Truss Joints Under Wind and Impact Loads.

Abstract approved: Signature redacted for privacy. Thomas H. Miller Signature redacted for privacy. Rakesh Gupta

The objective of this research is to understand the behavior of metal-plate-connected (MPC) joints by examining actual MPC truss heel and tension splice joints subjected to hurricane wind load simulations and impact loads.

A hurricane wind load simulation was applied to MPC heel joints to determine if a large scale wind event would cause strength loss or change the joint stiffness. An "impact" load of one second duration (as defined by the American Forest and Paper Association (AFPA) (1991)) was also applied to MPC heel joints and tension splice joints. Two different impact loads were applied to MPC tension splice joints to determine if strength degradation or stiffness change occurs due to loads with short duration and high maximum load. Finally, MPC tension splice joints were subjected to a ramp load which linearly increased ten times faster than the control group ramp load to determine if shorter duration tests still produce "static" loading results. All observed

properties were compared to a control group which was subjected to a static ramp load.

Both MPC heel and tension splice joints exhibited non-linear behavior under static ramp loads and failed with little warning because the tests were load- controlled. Tooth withdrawal, wood shear failure, and plate failure modes were all seen for both types of MPC joints.

Heel joints tested with the top member in tension proved to have 17% higher average ultimate strength and 42% lower average ultimate deflection than heel joints tested with the top member in compression. The stiffness of heel joints increased by an average of 300% after the tension wind simulation. This stiffness increase is possibly due to wood densification near the metal teeth. The impact load, which increases from the dead load to double the design load caused a stiffness increase similar to the stiffness increase produced by the tension wind simulations. No significant strength degradation was caused by dynamic loadings on heel joints.

The accelerated ramp load produced the same results as the static ramp load in $1/10^{th}$ the time.

Joint stiffness decreased after the impact load for tension splice joints, but increased for heel joints. Impact loads caused no decrease in strength. Increasing the impact spike magnitude by 50% produced 360% more deflection during the spike.

Behavior of Metal-Plate-Connected Wood Truss Joints Under Wind and Impact Loads

by

Mark J. Redlinger

A THESIS

submitted to

Oregon State University

in partial fulfillment of
the requirements for the
degree of

Master of Science

Presented January 12, 1998
Commencement June 1998

Master of Science thesis of Mark J. Redlinger presented on January 12, 1998

APPROVED:

Signature redacted for privacy.

Co-Major Professor, representing Civil Engineering

Signature redacted for privacy.

Co-Major Professor, representing Forest Products

Signature redacted for privacy.

Head of Department of Civil, Construction, and Environmental Engineering

Signature redacted for privacy.

Head of Department of Forest Products

Signature redacted for privacy.

Dean of Graduate School

I understand that my thesis will become part of the permanent collection of Oregon State University libraries. My signature below authorizes release of my thesis to any reader upon request.

Signature redacted for privacy.

Mark J. Redlinger, Author

ACKNOWLEDGMENT

I wish to acknowledge the following for their contributions to this study:

- Alpine Engineered Products, Inc. for their donation of the metal plate connectors;
- Frank Lumber Company for their donation of lumber.

Table of Contents

Table of Contents (continued)

Table of Contents (continued)

List of Figures

List of Figures (continued)

List of Figures (continued)

Figure Page

List of Figures (continued)

List of Figures (continued)

List of Tables

List of Tables (continued)

Table Page

DEDICATION

I wish to dedicate this work to the loving memory of my father, Jacob Francis Redlinger, who was the most selfless person to ever grace my life and who redefined "success" for me as the presence of family and generosity. I also wish to thank my mother, who showed me how to be strong in times of adversity, my siblings, for being my truest friends, Leanne, who is the complementary yin to my yang, and my God, who supported me in ways I could never describe in words.

Behavior of Metal-Plate-Connected Wood Truss Joints Under Wind and Impact Loads

1. Introduction

1.1 Background

Using metal plates to connect wood truss members is the most frequently used method to produce roof systems for many types of structures including residences, apartments, and light commercial buildings. Metal-plate-connected (MPC) wood trusses are used so often because they are cost effective and allow for the construction of many different and sometimes complex joint configurations. Due to the relative ease of construction, using MPC trusses saves money in the form of labor. Also, because the trusses are manufactured in a factory instead of on site, they can be mass produced with great efficiency. This efficiency makes MPC trusses more cost and time efficient than many other construction methods. A typical metal-plate-connector is shown in Figure 1-1.

Although MPC trusses are considered to be an engineered product, the dynamic behavior of both the joints and the overall truss is largely unknown. This problem is important because MPC trusses are exposed to both dynamic wind loads and earthquake loads.

Currently, the American Forestry and Paper Association (AFPA) (1991) provides the guidelines used to determine the design strength from static

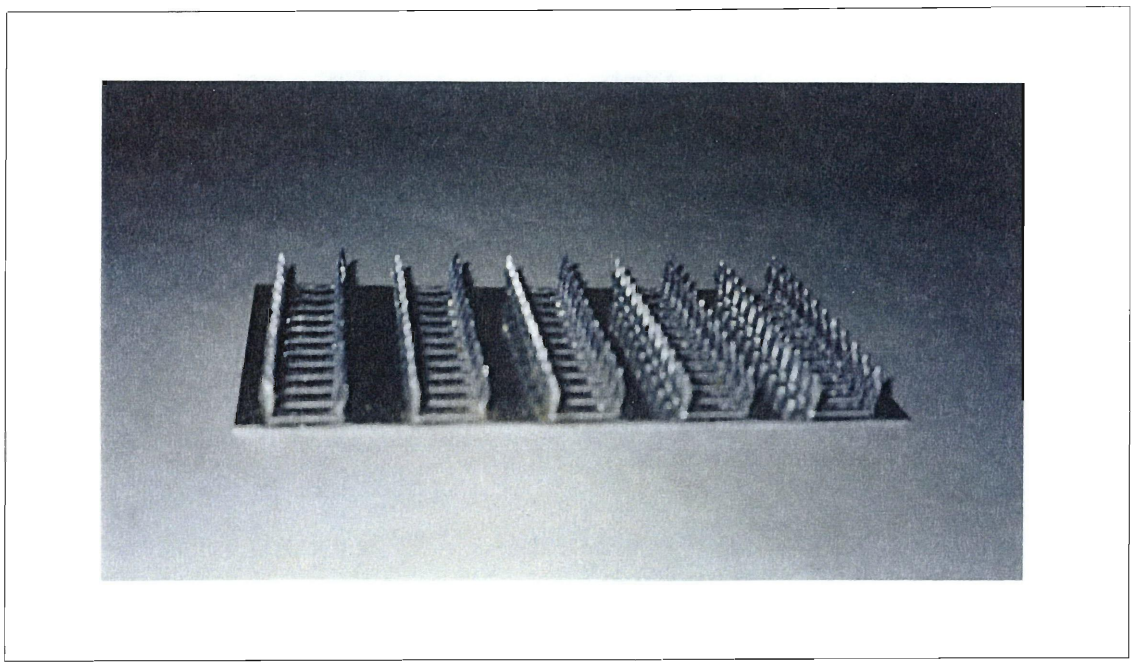

Figure 1-1: Typical metal-plate-connector

physical tests. The design strength, according to the AFPA (1991), is the lower of either the ultimate load divided by 3.0 or the load corresponding to 0.03 inches of deflection divided by 1.6. For the joints used in this study, one third of the ultimate load controls and is used as the design load.

Instead of performing tests on entire trusses, tests are usually performed on individual MPC joints. Tests are performed only on MPC joints because constructing and testing entire trusses would be costly and difficult. MPC joints are tested because understanding the behavior of MPC truss joints is required to accurately predict truss behavior. This project will analyze the behavior and failure modes of two different MPC wood truss joints when loaded with dynamic forces which simulate hurricane winds and impact loads on residential

structures. The impact loads used in this project is based on the AFPA (1991) definition of an impact load, which is a conservative version of an actual impact load. (Actual impact loads have very short durations, less than ¼ second, while the AFPA (1991) impact load has a one second duration.)

Most previous research has concentrated on the behavior of tension splice joints because they are easy to fabricate and test. The tension splice joint is often required to support large axial loads for many loading types, such as snow and dead loads, but high wind loads result in tension axial forces which are very small when compared to the tension splice joint ultimate strength as explained in Section 3.5.1.1.

However, heel joints receive high loads, in both tension and compression, due to winds. The forces produced in heel joints by hurricane winds are high enough, compared to the ultimate strength, to suggest that heel joint properties may be adversely affected. Therefore, wind load simulations are performed on heel joints in this project.

Impact load tests are performed on both MPC heel and tension splice joints to determine their response to short duration-high load conditions.

1.2 Objectives

The purpose of this study is to function as a preliminary investigation into the behavior of MPC heel and tension splice joints subjected to various dynamic loads. Dynamic loads used in this study include hurricane wind load simulations

and impact loads. The term "dynamic behavior" is used here to describe the time dependent behavior of joints subjected to time varying loads. This time dependent behavior is caused by the effect duration of load has on wood properties and is not concerned with the inertial effects. This study is not designed to determine the allowable dynamic load MPC joints can withstand before property degradation occurs.

Specifically, the objectives of this study are as follows:

1. Determine if hurricane wind load causes strength degradation or changes the stiffness of MPC heel and tension splice joints.
2. Determine if a single impact load causes strength degradation or changes the stiffness of MPC heel and tension splice joints.
3. Determine if a ramp load rate ten times higher than the static ramp load rate produces "static" results.

To achieve these objectives, the following tasks were performed:

1. Determine the properties of the control groups by subjecting the joints to a static ramp load. Three control groups are created for this study and are detailed in Section 4.4.1.1, Section 4.4.1.2, and Section 4.5.1 for heel joints in compression, heel joints in tension, and tension splice joints, respectively.

2. Evaluate the behavior of MPC heel joints subjected to hurricane wind loads in compression and tension. The hurricane wind load simulations are described in detail in Section 4.4.2.1 and Section 4.4.2.2 for compression and

tension, respectively. Strength, stiffness, dynamic deflection, and ultimate deflection will be examined to determine the hurricane simulation effects.

3. Investigate the effect of a single tension load spike from dead load to double the design load on MPC heel joints. This load condition is described in Section 4.4.3. This test will attempt to model an impact load as defined in the AFPA (1991). The AFPA (1991) defines an impact load as a load with a duration of approximately one second. (An actual impact load has a duration of less that ¼ second. This difference is acceptable because a longer duration will yield conservative results due to the time dependent strength of wood.) Determine if the double design impact load has the same effect as the hurricane simulation in tension. This is done to determine if dynamic loads applied over a 2 hour period with small magnitudes can be simulated by a short duration load with a high magnitude.

4. Determine if the testing time for the control group can be shortened by 90% for MPC tension splice joints by subjecting joints to an accelerated ramp load, described in Section 4.5.2, and comparing the results to the control group.

5. Investigate the effect, on MPC tension splice joints, of a single load spike with a maximum at double the design load and the effect of a single load spike with a maximum at the average ultimate load. These impact loads are described in Section 4.5.3 and Section 4.5.4 for the double design impact and ultimate impact, respectively.

6. Compare the results from the experimental groups to the corresponding control groups for MPC heel and tension splice joints.

2. Literature Review

The popularity growth of metal-plate-connected (MPC) truss joints over the last 40 years has created the need for information regarding their behavior and properties. Most research has focused on tension splice joints tested with static loads (Vatovec, et al. 1996, Gupta 1993, Gupta and Gebremedhin 1990, Suddarth, et al. 1979, Misra and Esmay 1966). Because understanding the behavior of all types of MPC joints is required to accurately predict truss behavior (Kirk, et al. 1989), research on other joint types is important. More recent studies have investigated the behavior and property changes which occur when MPC joints are subjected to dynamic loads (Dagher, et al. 1991, Emerson and Fridley 1996, Hayashi, et al. 1980). Information has also been gathered on MPC heel joints (Kent 1995, Kent, et al. 1995, Freilinger 1998) and MPC web joints (Gupta 1990).

2.1 Static Testing of MPC Wood Truss Joints

MPC truss joints have received substantial attention from previous researchers, much of which has focused on static properties of tension splice joints. Static tests, such as the ASTM D1761-88 (1994), have been the basis for design values and the stepping stone for dynamic tests.

Static tests have also resulted in many important conclusions about the basic nature of MPC joints. Gupta and Gebremedhin (1990) destructively tested tension splice, heel, and web at the bottom chord joints. These tests were used to determine ultimate strength, initial joint stiffness, and failure modes. Gupta and Gebremedhin (1990) concluded that the most common mode of failure was a combination of tooth withdrawal and wood failure. Failures were characterized for both the tension splice and web at the lower chord joints as non-ductile, but the heel joint failures were considered ductile. Average ultimate strength values were determined to be 6070 lb., 3750 lb., and 5100 lb. for the tension splice, web at the bottom chord, and heel joint, respectively. Lau (1987) also performed destructive tests on MPC joints, but only heel joints were included.

Gupta (1993) later performed destructive tests on MPC tension splice joints using a static axial ramp load as a control. The experimental groups used pure bending moment or one of four different levels of combined axial force and bending moment. The pure bending moment was applied using a two point loading system, while the combined axial load and bending moment was applied using axial loads with pre-defined eccentricities. Gupta (1993) determined three different stiffnesses: stiffness at design load, stiffness at critical slip, and stiffness from initial slope. The design load stiffness calculated by Gupta (1993) was based on the recommendations from the Truss Plate Institute (1985). Gupta (1993) concluded that the axial stiffness of the joint decreased as the moment, induced by the eccentricity, increased. Tooth withdrawal was the most common

form of failure for the combined loading tests, but failures in the steel plates were also seen. The results from the combined loading tests were used to create an interaction curve for MPC tension splice joints. Gupta (1993) concluded that the axial load capacity decreased 200 lb. for every additional 1000 lb.•in. of bending moment.

Vatovec, et al. (1996) evaluated the behavior of five different MPC joints from a scissors truss. Before testing began, a finite element model (FEM) was created to determine the relative magnitudes of the loads in the various members of the test joints. Static ramp loads were applied to heel joints, bottom chord splice joints at the web, crown joints, bottom chord ridge joints, and top chord splice joints at the web. For some members, the load was applied eccentrically to create a moment in the joint which was used to determine the rotational stiffness of the chords. Vatovec, et al. (1996) observed nonlinear load-deflection characteristics as did Gupta and Gebremedhin (1990) and Gupta (1993).

MPC tension splice joints were tested in compression to determine the effect of gap size on joint behavior by Kirk, et al. (1989). Tension splice joints were fabricated using 20-gauge and 16-gauge metal plates with 1/8 inch and 1/16 inch nominal gaps. Joints were loaded to the design level appropriate for the metal plate and held for five minutes. Creep deformation and permanent joint set were observed during and after the test, respectively. Joints which did not experience plate buckling were reloaded until plate buckling occurred. Kirk,

et al. (1989) found that both 20-gauge and 16-gauge plates buckled for 1/8 inch gaps, but 16-gauge plates did not buckle for 1/16 inch gaps. Closure of 1/16 inch gaps in the 16-gauge group occurred primarily due to slippage between the teeth and wood.

2.2 Numerical Models

Numerical models have been developed to analyze complex structural systems. If the results from a numerical model compare favorably to empirical results, it can often be concluded that the assumptions about the system and the system behavior are accurate.

Cramer, et al. (1990) created a finite element model which describes the nonlinear behavior of MPC tension splice joints in tension and bending. The model divided MPC tension splice joints into three components: the steel plate, tooth-wood springs, and the wood member. The metal plate was assumed to be a nonlinear, elastic, isotropic material, while the wood was treated as a linear, elastic, orthotropic material. The interaction between the metal teeth and the wood was modeled with nonlinear elastic spring elements with two degrees of freedom. These nonlinear spring elements were proposed by Foschi (1977) from load slip research on nailed wood connections. Deflections, internal stress conditions, and capacities of the MPC wood joints were calculated using a modified Newton-Raphson iteration algorithm. The model accurately (within 10%) predicted the ultimate bending moments of actual MPC tension splice

joints tested in bending. Cramer, et al. (1990) concluded that this model could be applied to more complex MPC joints, such as heel joints and joints with multiple members.

Gupta and Gebremedhin (1992) created a model to develop the resistance distribution of MPC Fink trusses. For the wood members, the model considered the modulus of elasticity (MOE), bending strength, and tensile strength. Wood member properties were simulated using a modified multivariate normal approach, developed by Taylor and Bender (1988). This property generation method preserved the natural correlation among the wood properties. The simulated properties were then randomly assigned to the members of a Fink truss. Three truss groups were created, each with a different assumption regarding the joint connectivity: pin connected joints, rigidly connected joints, and semi-rigidly connected joints. For the semi-rigid group, joint stiffnesses were generated based on joint tests and assigned randomly. After an initial load was applied, the combined stress interaction (CSI) index was calculated for each member. CSI index values greater than 1.0 indicated failure. The load on the truss was then increased until the highest CSI was 1.0, which indicated failure. The load on the truss at failure and the failure location were then recorded. Gupta and Gebremedhin (1992) found that the pin connected group had the lowest average load at failure, while the rigid and semi-rigid groups failed at approximately the same load.

Vatovec, et al. (1995) used the finite element analysis software ANSYS® to model the load-displacement behavior of MPC joints. The model used three spring elements to represent the stiffness of the wood-tooth interaction parallel to the slots, perpendicular to the slots, and perpendicular to the plane of the plate. The Vavotec, et al. (1995) model accounted for the different material properties, the orientations of the grain, teeth, and force, the wood to wood interaction, and gap between the joint members. The model produced load-deflection plots very similar to those produced from actual tests of MPC joints.

2.3 Wood Connections and Systems Under Various Loads

Much of the research performed with dynamic loads has concentrated on either nailed joints or component subsystems such as shear wall panels.

Polensek and Schimel (1991) investigated the damping ratio and dynamic stiffness of wood subsystems by applying static cyclic deflections on actual wall panels. Wall panels which were dynamically loaded perpendicular to the foundation were less stiff and had larger damping ratios than wall panels which were loaded parallel to the foundation.

Tests on nailed wood joints were performed by Girhammar and Andersson (1988) to determine the effect of deformation rate on the ultimate yield load. The thickness of the joint members, deformation rate, and angle between the load and the wood grain were all varied. Girhammar and

Andersson (1988) found that the increase in strength was linearly dependent on the logarithmic deformation rate for all groups.

Soltis and Mtenga (1985) examined nailed wood joints subjected to 1 Hz and 10 Hz deformation-controlled cyclic loadings, during which load was recorded every 10 cycles. They observed no change in stiffness for small cyclic amplitude and small number of cycles. However, at higher deformations and increased number of cycles, the stiffness of the cyclic loading groups decreases.

2.4 MPC Joint Behavior Under Dynamic Load

Testing has been performed on MPC joints with dynamic loads. Some researchers used cyclic loads to simulate actual dynamic loads because cyclic loads are easily generated by hydraulic testing machines. Cyclic loads have also been used to study the fatigue properties of MPC joints. Other research has attempted to recreate actual dynamic loading events for residential structures.

Tests on MPC joints by Emerson and Fridley (1996) used cyclic loads to emulate random dynamic loading. The cyclic tests consisted of three groups of 200 cycles, each with a different amplitude. The first, second, and third cyclic group had amplitudes of 20%, 40%, and 60% of the average maximum static load, respectively. After the cyclic load was finished, a linearly increasing static ramp load was applied until failure occurred. Tests were performed on six different joint configurations which varied the tooth-grain angle and the tooth-

force angle. Emerson and Fridley (1996) found three different failure modes: tooth withdrawal, shearing along a growth ring, and tension failure of the wood rings. The cyclic load produced a loss in initial stiffness, but no drop in strength was observed.

Fatigue testing on MPC tension splice joints was performed by Hayashi, et al. (1980) to determine the fatigue limit due to reversed and non-reversed cyclic loading. Two joint sizes were tested using cyclic loadings at 100 cycles per minute and 1000 cycles per minute. Hayashi, et al. (1980) found a linear relationship between the amplitude of the repeated load and the number of cycles before failure. The fatigue limit was determined to be approximately 20% to 25% of the static tensile strength for the non-reversed loading and 17% to 20% for the reversed loading. Hayashi, et al. (1980) also found a relationship between the failure mode and the repeated load levels. At high load level, tooth withdrawal occurred, while at low load levels, the teeth were sheared off the plate.

Kent (1995) tested MPC heel and tension splice joints with a variety of dynamic loads including a historical earthquake simulation, artificially generated earthquake simulation, sequential phased displacement (SPD) loading, and cyclic loads. The historical earthquake simulation forces were determined by performing a finite element analysis of a residential structure subjected to ground accelerations from the Northridge earthquake. The artificial earthquake simulation loads were generated using the computer program WES-RASCAL.

The SPD loading used by Kent (1995) was proposed by Dolan and McLain (1994) as a standard to determine the dynamic properties of wood connections. The cyclic loads were performed at various levels for 200 cycles. If a joint survived the dynamic loading, the load was increased statically until failure occurred. Kent (1995) found no strength degradation due to the earthquake simulations, but a slight difference was found in the heel joint axial stiffness. Kent (1995) concluded that the damage which accumulated in the connection during the SPD load was dependent on the level of displacement. Finally, large cyclic loads were found to cause significant strength loss in MPC joints.

Freilinger (1998) used cyclic loads to evaluate the duration of load factor from the AFPA (1991) for wind and earthquake loads on MPC heel and tension splice joints. Freilinger (1998) also found some stiffness degradation for both heel and tension splice joints due to dynamic load.

3. Determination of Heel and Tension Splice Joint Forces

Wind loads were calculated using the American Society of Civil Engineers Standard Minimum Design Loads for Buildings and Other Structures (ASCE 7-95) provisions. The truss examined throughout this study was a 30-ft spanFink truss. It was selected because it is similar to the trusses examined by Kent (1995) and Freilinger (1998) in earlier projects. Kent and Freilinger performed dynamic testing using historical earthquake loads, earthquake simulations, and other loadings such as the sequential phased displacement method proposed by Dolan and McLain (1994). The Fink truss was composed of nominal 2"x4" Douglas-fir members with a modulus of elasticity of 1,600,000 psi and a roof slope of 4/12.

3.1 Fink Truss Model

The wind loads, obtained from ASCE 7-95, were used with the linear finite element analysis computer program SAP90 (Computers and Structures, Inc., 1991) to determine the forces at the heel and tension splice joints. The joint connectivity and dimensions of the model used in SAP90 are shown in Figure 3-1.

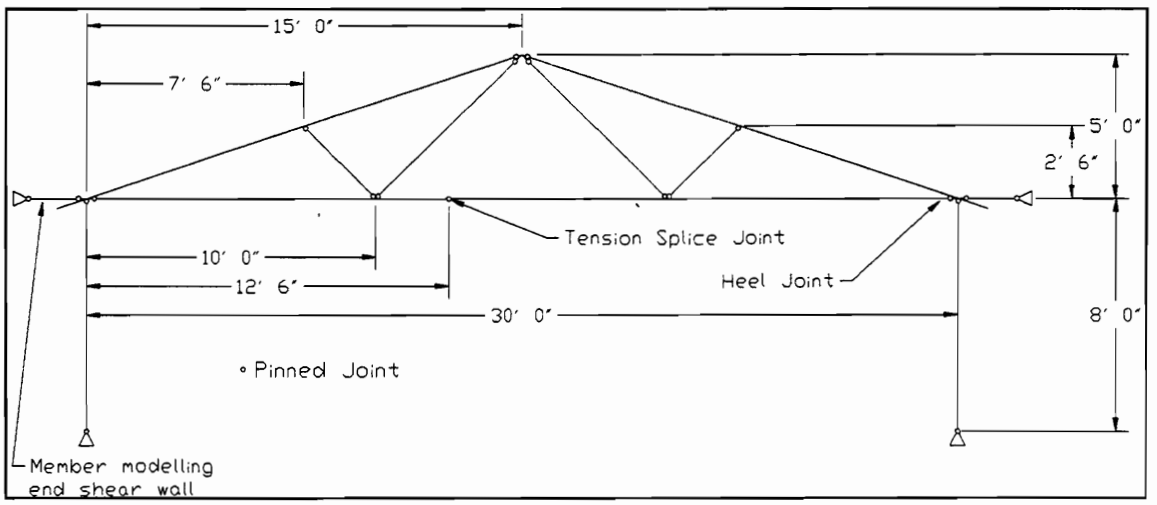

Figure 3-1: Dimensions and joint connectivity of the Fink truss modeled in SAP90 for this project

The truss bottom chord is 8 feet above the foundation and the trusses are spaced at 2 foot intervals. The importance of the truss base elevation is related to the wind analysis performed on this model. Table 6-3 in ASCE 7-95 shows that as the height increases, the wind pressure coefficient K_z also increases. This pressure coefficient is used in the calculation of the basic wind pressure. Therefore, as the height increases, so does the basic wind pressure. The spacing of the trusses affects the amount of tributary load the truss must carry. If the truss spacing is doubled, the load on the truss would also double. Other coefficients used in the ASCE 7-95 wind analysis, such as GC_p, are related to the effective tributary area as shown in Figure 6-5B of ASCE 7-95. (GC_p represents the gustiness of wind and the variability of actual wind pressure on a surface.)

A realistic simulation of joint connectivity is vital to obtaining accurate forces in the individual members once the roof loading is determined. Joints were assumed to be either pinned or continuous. Pinned joints cannot transfer moment, while continuous joints transfer moment. Members connected at the ends by metal plates were considered pinned. Continuous wood members were modeled as continuous.

For example, the top chord member in the Fink truss shown in Figure 3-1 is one continuous piece of lumber with several joints along it's length. The end of a web member connects to the middle of the top chord. This joint is modeled as continuous for the top chord member but pinned for the web member.

Therefore, the web member transfers no moment to the top chord member, but the top chord member can transfer moment across the joint. Another example of a pinned joint is the tension splice joint located on the bottom chord member. It consists of two members joined at the ends by a metal plate.

The assumptions regarding joint connectivity are not entirely accurate. In reality, joints connected with metal plates are able to transfer some moment to other members, and this will lead to some errors in the calculated member forces, particularly moments. Axial forces will generally be computed fairly accurately. The roof truss is assumed to be pin connected to the support walls at the ends of the bottom chord members. Figure 3-2 shows pre-manufactured truss connectors from Simpson (1997). Connectors such as these have little

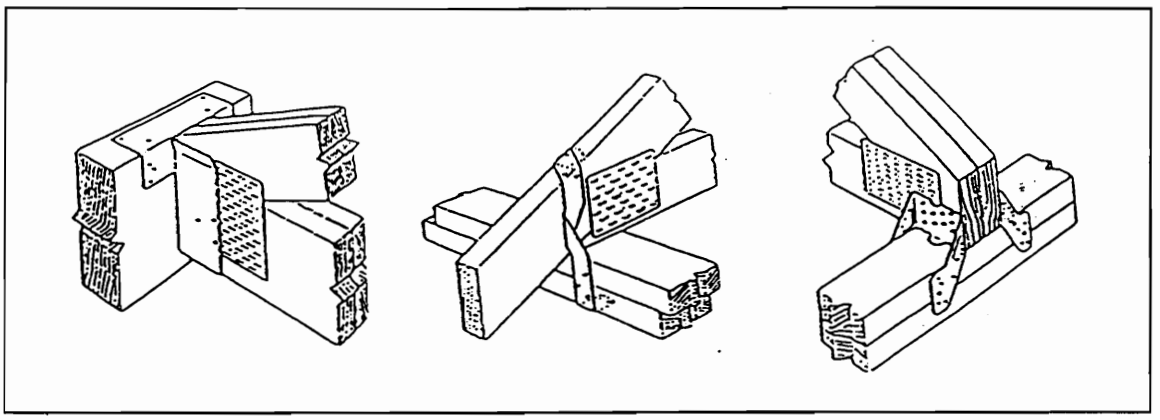

Figure 3-2: Pre-manufactured connectors which support trusses (Simpson 1997)

resistance to rotation and would be unable to transfer substantial moments from the truss to the supporting wall. Therefore, pinned end conditions will sufficiently represent the actual support case.

Most of the wind loadings applied to the truss, from ASCE 7-95, cause compression in the bottom chord. The compression forces, along with the dead load on the bottom chord, can cause lateral torsional or weak axis flexural buckling of the bottom chord member. SAP90, the structural analysis software used in this project, does not consider lateral torsional or weak axis flexural buckling of any members. (Lateral support is normally developed in the top chord by plywood sheathing which is securely nailed to the truss.)

3.2 Previous Finite Element Models of Metal-Plate-Connected Trusses

Previous research done by Kent (1995) examined a similar Fink truss, but the model was somewhat different. Kent's truss had the same basic geometry and joint connectivity, but had no need for the overhanging edges at the eaves because it was not used in a wind analysis. Kent's (1995) truss was supported vertically by stiff columns and horizontally by spring elements. These same truss support conditions were reproduced for this study with one small difference. Both models used a member which is very stiff in bending, but flexible axially, as a horizontal spring element. The horizontal spring element represents the stiffness of the end shear wall. The spring very stiff in bending so that all of the deformation of the spring is axial. This allows the stiffness to be controlled by adjusting the cross sectional area. Kent's (1995) model connected the spring member to a fixed support, while the model used here connects the spring member to a pin support. This difference is shown in Figure 3-3.

The spring element was modeled using a pin connection because of possible errors that could be attributed to fixing the spring support. A fixed support creates a cantilever beam effect in the spring. Since the spring is modeled as infinitely stiff in bending and fixed at one end, it becomes more stiff vertically than the support walls. This leads to the spring elements supporting more vertical load than the end walls.

Since Kent's (1995) model was used to analyze structural response to earthquake loading, mass properties were assigned to all members along with

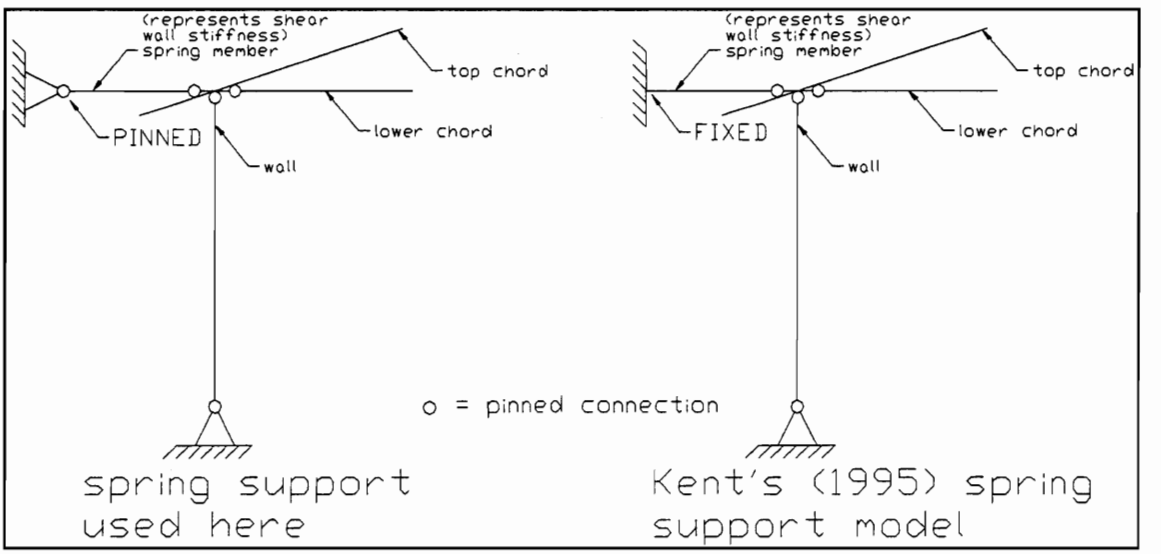

Figure 3-3: Comparing spring member support conditions between the model used here and Kent's (1995) model

dead loads on the top and bottom chords. The model used here has the same dead load and mass properties to ensure close agreement in dynamic analyses. Kent's (1995) model was not loaded using conventional span or point loads, instead, it was subjected to ground motion, while this model was loaded with distributed span loads.

Overall, Kent's (1995) model and the model used here are very similar and should give the same results given similar static loading conditions.

Vatovec, et al. (1996) created a model of a 40-ft span MPC scissors truss to determine the forces in the members before testing was started on five different MPC joints. While the Fink truss used in this project is geometrically different from a scissors truss, assumptions for the two models can be compared. Initially, Vatovec, et al. (1996) modeled all members as rigidly

connected at the joints to find the member forces. These member forces were used to load a variety of MPC joints. After the stiffnesses of the various joints were determined through actual testing, the model was re-examined with the test stiffnesses input for the corresponding model joints. Joints not tested were assumed continuous (rigid) through the chords, with web members pinned.

A pin connection was used in this project for all MPC joints. Continuous chord members which intersected at MPC joints were modeled as rigid. These joint assumptions were used because they result in a relatively simple model which reasonably predicts the axial forces in a truss.

3.3 ASCE 7-95 Wind Load Analysis

Computation of the wind loads was accomplished using ASCE 7-95.

An extreme wind speed is required if high forces are desired in the truss members. High forces are needed in the members because tests which do not sufficiently stress the joints will not reveal much about MPC dynamic load capacity. In other words, if the dynamic loads investigated in the testing are far below the ultimate strength of the joint, little or no change will be seen in the stiffness or ultimate strength. This would be due to a lack of damage accumulated during the dynamic loading portion of the test. Simulating a lower wind speed is less likely to produce damage during the dynamic loading and will reveal no new information about whether MPC joints are affected by high, yet realistic wind loads. Therefore, the structure was considered to be located in

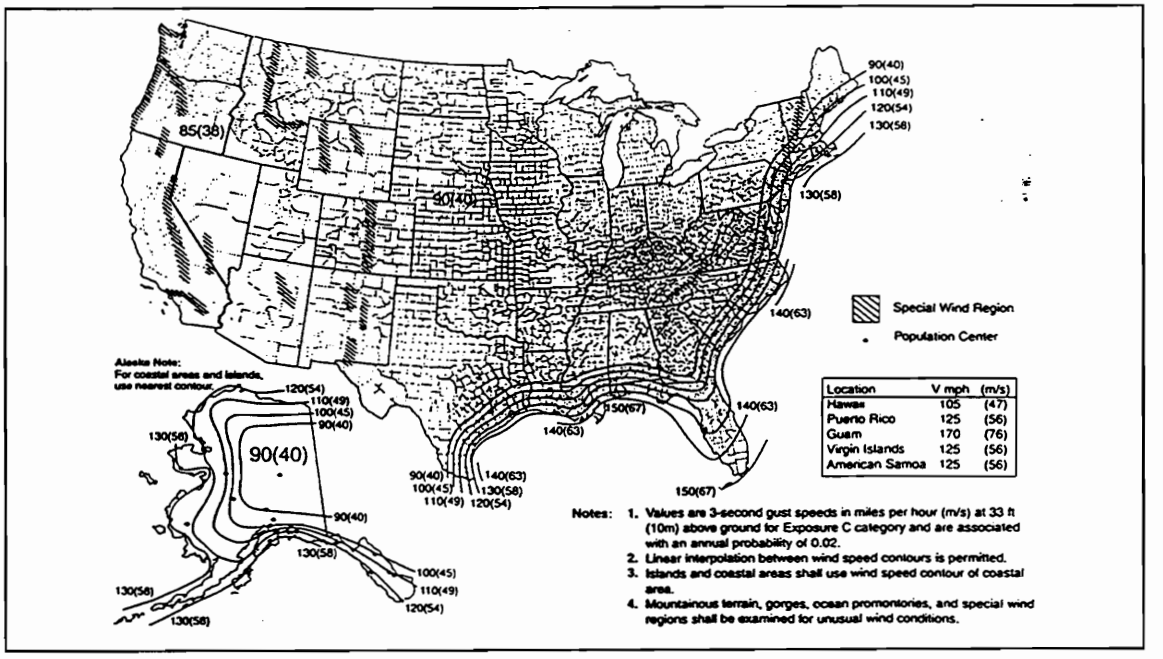

Figure 3-4: Basic wind speed map of the United States from ASCE 7-95

southern Florida, a 150 mph wind zone according to ASCE 7-95. The basic wind speed map from the ASCE 7-95 is shown in Figure 3-4.

The structure is considered rigid as described in Section 6.2 of ASCE 7-95. ASCE 7-95 states that a building is considered flexible if the height exceeds four times the least horizontal dimension. To be as similar to prior truss models as possible, the height of the bottom of the truss is 8 feet above the foundation to match Kent's (1995) model. Since the truss is 5 feet tall and rests 8 feet above the foundation, the average roof height for the residential structure is:

height = 8' + 5'/2 = 12.5'

The truss is 30 feet wide, so four times the width is much greater than the height, and the building is considered rigid instead of flexible.

ASCE 7-95 does not account for all wind phenomenon (across-wind loading, vortex shedding, galloping, flutter, channeling effects, and buffeting). It is assumed that open terrain with scattered obstructions surrounds the structure, so exposure C, as defined by ASCE 7-95, is used. It is further assumed that the structure is not located in or near any mountainous terrain, gorges, ocean promontories, or special wind regions as noted in Figure 6-1 of ASCE 7-95. Tornadoes were not considered in this analysis.

A simple residential structure such as this falls into Category II in ASCE 7-95. Category I represents structures which pose a low risk to human life if they failed, such as agricultural facilities, and minor storage facilities. Category III represents structures which are a substantial hazard to human life in the event of failure, such as gathering places, schools, jails, and general health care facilities. Category IV represents structures designated as essential, such as hospitals, police/fire stations, emergency shelters, and communication centers. Category II is described simply as all structures except those listed in Categories I, III, and IV.

The following set of calculations are used per ASCE 7-95 to translate various qualitative factors into a quantitative wind pressure. Global location, height above the ground, topography, and structure function are all included in this calculation.

The equation used to determine the basic wind pressure is:

$q_z = 0.00256 * K_z * K_{zt} * V^2 * I$ (ASCE 7-95 eqn 6-1)

where:

q_z = velocity pressure evaluated at height z above ground (psf)

q_h = velocity pressure evaluated at height z = h above ground (psf)

K_z = velocity pressure exposure coefficient evaluated at height z

K_{zt} = topographic factor

V = basic wind speed corresponding to a 3-second gust speed at 33 feet (mph)

I = importance factor

V = 150 mph Fig 6-1 (S. Florida)

Category II ASCE 7-95 Table 1-1

Any structure which falls into category II of ASCE 7-95 Table 1-1 is given an importance factor of:

I = 1.0 ASCE 7-95 Table 6-2

The velocity pressure exposure coefficient, otherwise known as K_z, represents two factors: the boundary-layer velocity profile and the exposure level. Simiu and Scanlan (1996) state that the shape of the boundary-layer velocity profile is due to the viscosity of the air. Experiments have shown that flowing air which comes in contact with a stationary surface adheres to it. The viscosity of the stationary air slows the air in the layer nearest to it. This layer is referred to as the boundary layer. As the distance from the stationary air

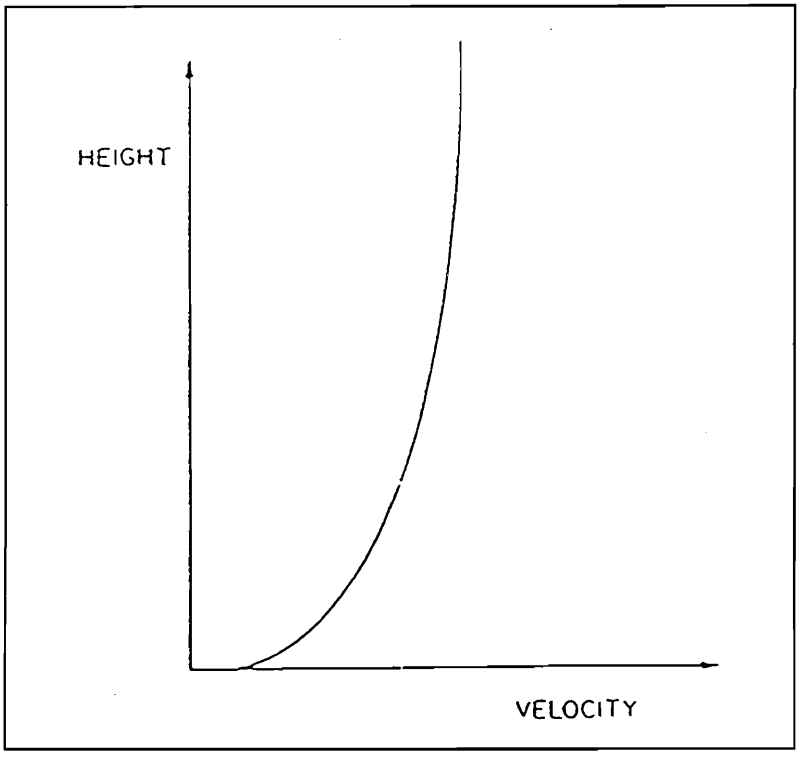

Figure 3-5: The boundary-layer wind velocity profile from Simiu and Scanlan (1996)

increases, its retarding effects decrease. The boundary-layer velocity profile is shown in Figure 3-5 as published by Simiu and Scanlan (1996).

Exposure level is a function of the wind cover around a building. For example, a small building located in a crowded urban setting is protected from the wind by the surrounding buildings, while the same building on the shore of a large lake has very little protection.

As stated previously K_z is a function of the wind velocity profile and the exposure level. Thus, K_z increases with building height and as wind protection decreases. The K_z coefficient for this case is found for exposure C at a height

less than 15 feet.

$K_z = 0.85$ ASCE 7-95 Table 6-3 (h <15', exposure C)

The topographic factor, otherwise known as K_{zt}, is a factor which represents the phenomenon of wind speeding up when going over hills and escarpments. ASCE 7-95 states, "The effect of wind speed up shall not be required to be considered when $H/L_h < 0.2$, or when $H < 15$ ft for exposure D, or < 30 ft for exposure C...", where H is the height of the hill or escarpment and L_h is the distance upwind of the crest of the hill or escarpment to where the difference in ground elevation is half the height of the hill or escarpment. Since this structure is only 13 feet tall and located in exposure C, K_{zt} can be considered to be 1.

$K_{zt} = 1.0$ ASCE 7-95 Section 6.5.5

Since the average roof height for the residential structure is 13', h = 13'. Therefore, the velocity pressure evaluated a height z = 13' above ground is:

$$q_{13'} = 0.00256 * K_z * K_{zt} * V^2 * I$$

Substituting for K_z, K_{zt}, V^2, and I gives:

$$q_{13'} = 0.00256 * 0.85 * 1.0 * 150^2 * 1.0$$

$$q_{13'} \approx 49 \text{ psf}$$

According to ASCE 7-95 (Section 6.2 of the commentary), components receive wind loads directly or from cladding, and transfer the load to the main wind force resisting system. Examples of components in ASCE 7-95 (Section 6.2 of the commentary under the definition of components and cladding) include

fasteners, purlins, girts, studs, roof decking, and roof trusses. While this might lead one to analyze roof trusses exclusively as a component, the code goes on to state (on the top of page 149 in the commentary), "trusses should be designed for loads associated with main wind-force resisting systems, and individual members of trusses should also be designed for component and cladding loads." The overall truss should be able to transfer wind loads prescribed for the main lateral force resisting system and the individual members should be designed to resist the forces prescribed for components and cladding. The roof truss was analyzed for both components and cladding and main wind force resisting system loads to conform to ASCE 7-95 recommendations.

3.3.1 Components and Cladding Analysis

Two types of wind pressures are accounted for by ASCE 7-95. They are external and internal wind pressures.

Actual wind pressure on a surface varies with position on that surface. This variability depends on proximity to edges, the ridge, overhangs, and other physical characteristics. This variability is accounted for in ASCE 7-95 (Figure 6-3) by the external pressure coefficient, C_p. C_p varies with location on the building walls and roof.

Since wind speed is variable, the actual pressure is factored upward because of gusting. Gusting accounts for the fact that wind speed is not constant, but changes rapidly and has the potential to markedly increase for

brief periods of time. Wind gusting is due to the fact that fluid flow can become turbulent when the velocity increases sufficiently according to Simui and Scanlan (1996). The gustiness of the wind is represented by G. C_p and G are found in ASCE 7-95 in Tables 6-5 through 6-7 already multiplied together.

Internal pressure and wind gustiness is accounted for in the GC_{pi} factor.

The equation used to convert the basic wind pressure to an actual wind pressure is:

$p = q_h * [(GC_p) - (GC_{pi})]$ Table 6-1 (Components & Cladding)

3.3.1.1 External Loading for Components and Cladding

The angle Θ ($\Theta = \tan^{-1}(5'/15') = 18.4°$) represents the slope of the roof and is used in determining GC_p. ASCE 7-95 provides different values of GC_p for different roof slopes. This is done because the magnitude of wind effects change as the roof slope changes.

The other factor which affects the GC_p coefficient is effective wind area. The effective wind area of any component or cladding is the tributary area it receives load from, adjusted for special cases. Special cases occur when the tributary length is much larger than the tributary width. ASCE 7-95 clearly states that roof trusses which are closely spaced should have adjusted effective wind areas. ASCE 7-95 commentary Section 6.2 states, "where components such as roofing panels, wall studs or roof trusses are spaced closely together; the area

served by the component may become long and narrow. To better approximate the actual load distribution in such cases, the width of the effective wind area used to evaluate GC_p need not be taken as less than one third the length of the area." This increase in effective wind area has the effect of reducing the average wind pressure acting on the component. (Note that the effective wind area is only used for the determination of the external pressure coefficients and is not used as the tributary area.)

As stated earlier, according to ASCE 7-95, trusses should be designed for main wind force resisting system loads, while individual members of trusses should be designed for components and cladding loads. Therefore, the components and cladding section of this analysis is concerned with individual members, not the entire truss. The commentary Section 6.2 of ASCE 7-95 defines cladding as members which receive wind loads directly, while components are defined as members which receive wind loads directly from cladding. For this analysis, the cladding would be plywood sheathing and components would include the top chord members of the truss.

In order to find the effective wind area for the top chord members modeled here, the adjusted tributary width was multiplied by the distance from the end of the overhang to the ridge. The length from the overhang to the ridge was determined using the Pythagorean theorem. The distance from the heel joint to the ridge is 15' horizontally and 5' vertically as shown in Figure 3-1. The overhang extends 1' horizontally and 4" vertically from the heel joint.

For components and cladding:

length = $[16^2 + 5.333^2]^{1/2}$ = 16.9'

$width_{actual}$ = 2'

$width_{min}$ = 1/3 length ≈ 5.6' ← controls Commentary 6.2

width = $width_{min}$ ≈ 5.6'

effective wind area = width * length

effective wind area = 5.6' * 16.9'

effective wind area = 94.8 sf ≈ 100 sf

The effective wind area is used in ASCE 7-95 Figure 6-5B to determine the various values of GC_p over the roof.

Some areas on the roof develop higher pressures than others. These higher pressure areas are located only on the leeward side for a simple gabled roof. Specifically, the areas near the ridge and the areas near the overhanging edge on the leeward side develop higher pressures due to non-direct wind pressure and other wind effects (ASCE 7-95 Figure 6-5B).

The width of the higher pressure coefficient zone is shown in Figure 3-8 as "a". This value is calculated in accordance with ASCE 7-95 Figure 6-5 note 11. The “a” value represents the distance from the ridge (or edge) on which the higher pressures.

According to ASCE 7-95, “a” is determined per several requirements. It is either 10% of the least horizontal dimension or 0.4 multiplied by the mean

height, whichever is smaller. The controlling value must be larger than either 4% of the least horizontal dimension or 3 feet.

a = 10% (30') = 3' ← controls

a = 0.4 (10.5') = 4.2 > 3'

4% (30') = 1.2' < 3' ok

3' ≤ 3' ok

a = 3'

Figure 3-6 shows the three different pressure zones for roofs with slopes ranging from 10° to 30° from Figure 6-5B in ASCE 7-95. It also shows where the distance "a" is applied. Figure 3-6 shows the edge of the overhang lining up well in both pictures, and the dashed line in the plan view coincidentally appears to line up with the wall in the profile view.

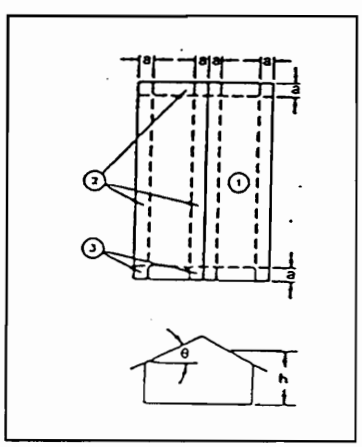

Figure 3-6: Pressure zones as shown in ASCE 7-95 in Figure 6-5B

This implies that the high pressure area starts at the edge of the overhang and extends inward a distance "a", and one might mistakenly think that it should not continue beyond the support wall. (In this case the support wall is located directly under the heel joint.) The distance "a" is defined in Figure 3-6 as the distance between the solid and dashed lines.

There is no interpretation of Figure 3-6 in ASCE 7-95 or in it's commentary, although other sources proved to be valuable. Mehta, et al. (1991) performed sample calculations of wind loading using ASCE 7-88. Figure 3-7 shows their interpretation of ASCE 7-88 Figure 6-5B for a warehouse with no roof overhang.

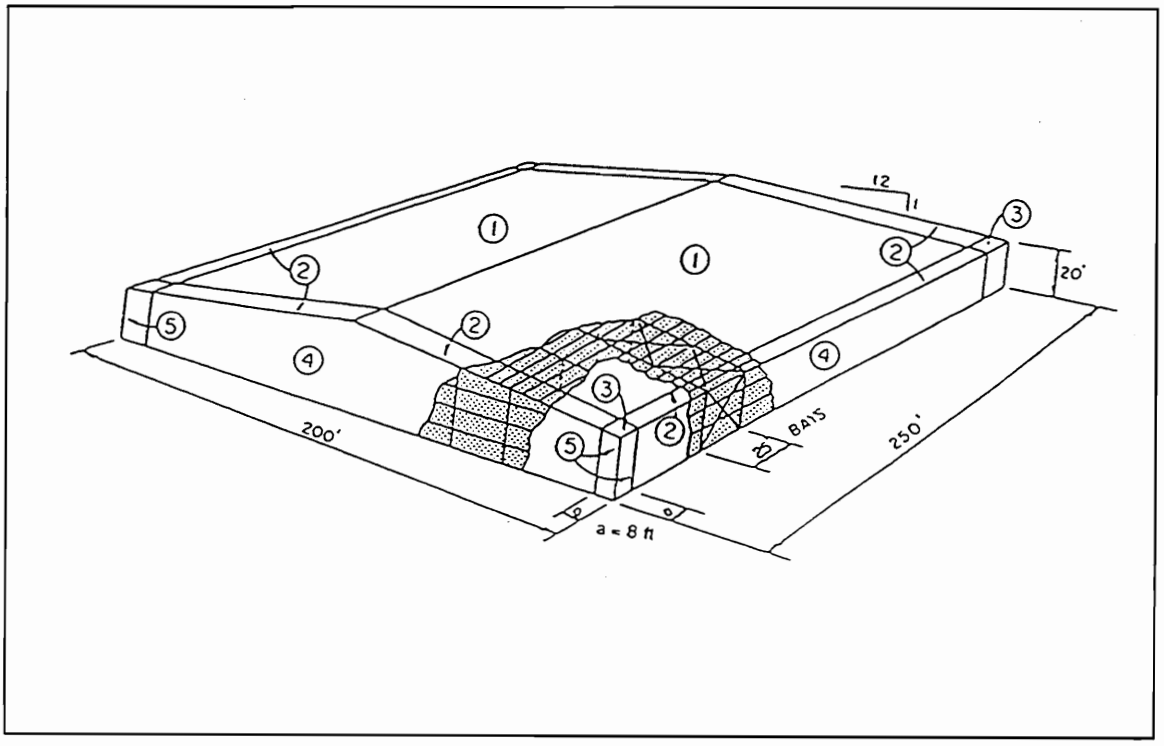

Figure 3-7: Wind pressure zones on a warehouse with no overhang

While ASCE 7-88 was used in the sample calculations, no change occurred in Figure 6-5B from ASCE 7-88 to ASCE 7-95. Therefore, Figure 3-7 is still applicable to ASCE 7-95.

Since the roof angle of the example by Metha, et al. (1991) is less than 10°, there is no high pressure region near the ridge, but notice that zone 2, in Figure 3-7, extends from the edge of the wall inward a distance "a". Therefore, it is concluded here that the high pressure area is not dependent on the length or presence of an overhang. For this analysis, "a" will be measured from the edge of the overhang to the full value of "a" regardless of the length of the overhang.

External pressure coefficients (C_p) along with gust coefficients (G) are found in Figure 6-5B of ASCE 7-95 combined into one variable (GC_p) for components and cladding. The subscript number after GC_p represents a section of the roof as shown in the plan view in Figure 3-8.

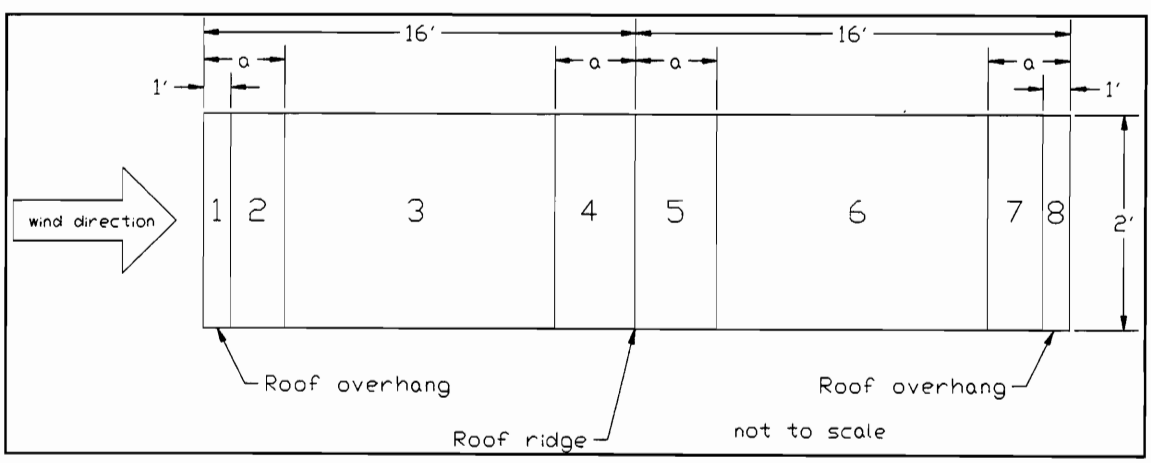

Figure 3-8: Plan view of a roof divided as in ASCE 7-95 in Fig. 6-5B (with roof overhang)

The GC_p values vary with the position and side of the roof to which they are applied. For example, the roof overhang on the windward side has a different GC_p value than the overhang on the leeward side. The GC_p values will be used to calculate external loads. Then these external loads will be used to examine various overall loading conditions when combined with internal loads.

The graph representing roof slopes from 10° to 30° in Figure 6-5B of ASCE 7-95 shows only one line representing the windward side. This results in a uniform external pressure distribution across the entire windward side regardless of location.

$GC_{p1} = GC_{p2} = GC_{p3} = GC_{p4} = +0.30$ ← windward side Fig 6-5B

For the area located within a distance "a" from the ridge of the roof the GC_p coefficient is higher than for the areas outside "a" as shown below.

$GC_{p5} = -1.4$ ← within distance "a" from ridge Fig 6-5B

$GC_{p6} = -0.8$ ← outside distance "a" from ridge Fig 6-5B

The leeward side of the roof within a distance "a", but not part of the overhang is a high wind pressure area.

$GC_{p7} = -1.4$ ← within distance "a" from edge of roof Fig 6-5B

The leeward side overhang is a special region like the area within "a" and thus has a higher GC_p coefficient.

$GC_{p8} = -2.2$ ← leeward side overhang Fig 6-5B

External pressures acting normal to the top chord are then calculated. This calculation combines the basic wind pressure, tributary width, gusting factor, and roof area coefficients together to obtain an effective wind load in pounds per linear foot which is defined here as "w".

For areas 1, 2, 3, and 4

$p = q * [(GC_p)] = 49 \text{ psf } (0.3) = 14.7 \text{ psf}$ > 10 psf ok

$w = p * (\text{trib. width}) = 14.7 \text{ psf} * (2 \text{ ft}) = 29.4 \text{ lb/ft}$

For area 5 and 7

$p = q * [(GC_p)] = 49 \text{ psf } (-1.4) = -68.5 \text{ psf}$ < -10 psf ok

$w = p * (\text{trib. width}) = -68.5 \text{ psf} * (2 \text{ ft}) = -137 \text{ lb/ft}$

For area 6

$p = q * [(GC_p)] = 49 \text{ psf } (-0.8) = -39.2 \text{ psf}$ < -10 psf ok

$w = p * (\text{trib. width}) = -39.2 \text{ psf} * (2 \text{ ft}) = -78.4 \text{ lb/ft}$

For area 8

$p = q * [(GC_p)] = 49 \text{ psf } (-2.2) = -107.7 \text{ psf}$ < -10 psf ok

$w = p * (\text{trib. width}) = -107.7 \text{ psf} * (2 \text{ ft}) = -216 \text{ lb/ft}$

3.3.1.2 Internal Pressures for Components and Cladding

Buildings are defined by ASCE 7-95 in Section 6.2 as either open, partially open, or enclosed. These cases are defined below.

Open buildings, or structures having all walls at least 80% open, do not develop internal pressures.

Partially enclosed buildings satisfy two conditions. First, the total area of openings in the windward wall must exceed the sum of the areas of openings in the rest of the building walls and roof by more than 10%. This means that one wall must have a majority of the openings. Second, the total area of openings in the windward wall must exceed 4 square feet or 1% of the area of that wall. This requirement ensures that openings are large enough to allow sufficient air flow into the building to create internal pressure.

Enclosed buildings are those that don't comply with the requirements for either open or partially enclosed buildings.

It must be decided which description best fits the building because ASCE 7-95 Table 6-4 lists internal pressure coefficients, GC_{pi}, (adjusted for gust effects) for each of these types. However, ASCE 7-95 states in Table 6-4 that buildings satisfying the following conditions use +0.80 and -0.30 as internal pressure coefficients: (1) buildings sited in hurricane-prone regions having a basic wind speed greater than or equal to 110 mph or located in Hawaii, and (2) buildings having glazed openings in the lower 60 feet which are not designed to resist wind-borne debris or are not specifically protected from wind-borne debris impact.

Since the structure in question is located in a hurricane prone region with a basic wind speed greater than 110 mph (southern Florida) it satisfies the first condition stated above. This analysis assumes that the glazed openings in the structure are ordinary glass windows which are considered glazed openings not

designed to resist wind-borne debris or protected from such. This assumption satisfies the second condition stated above. The reason the partially enclosed category is included in ASCE 7-95 is because structures with ordinary glass windows, which are caught in hurricanes, change from enclosed to partially enclosed when the windows are destroyed by flying debris. Note that the internal pressure coefficients are the same in hurricane-prone regions for buildings with ordinary windows as the coefficients for partially enclosed buildings.

The internal pressure is applied to the underside of the top chord member. The equation which combines internal and external pressures in ASCE 7-95 Table 6-1 is:

$p = q_h * [(GC_p) - (GC_{pi})]$ ← for components and cladding

This equation implies that the internal and external pressures act on the same member.

Positive internal pressures act toward surfaces and negative internal pressures act away from surfaces. These internal pressures will be combined with external pressures to account for all possible loading combinations. ASCE 7-95 states in Table 6-4 note 3 that, "Two cases shall be considered to determine the critical load requirements for the appropriate condition: a positive value of GC_{pi} applied to all internal surfaces, and a negative value of GC_{pi} applied to all internal surfaces." The positive and negative GC_{pi} values from

ASCE 7-95 Table 6-4 are listed below. Combinations of external and internal loads are analyzed to find the most extreme loading condition in Section 3.4.

GC_{pi} = 0.80, -0.30 Table 6-4

$p_{internal} = q * [(GC_{pi})]$ = 49 psf * (0.8,-0.3) = 39.2 psf, -14.7 psf

w = p * (trib. width) = 39.2 psf * (2 ft) = 78.4 lb/ft

w = p * (trib. width) = -14.7 psf * (2 ft) = -29.4 lb/ft

3.3.2 Main Wind Force Resisting System Analysis

The following equation is used for main wind force resisting systems (MWFRS) to calculate design pressures, given basic wind pressures, for low-rise buildings.

$p = q_h * [(GC_{pf}) - (GC_{pi})]$ (ASCE 7-95 Table 6-1 (MWFRS))

This equation is similar to the one used for the components and cladding analysis. It accounts for both internal and external wind pressures on the structure. GC_{pf} represents the external pressure coefficient multiplied by the gusting factor and is found in Figure 6-4 of ASCE 7-95 and is shown in Figure 3-9.

3.3.2.1 External Loading for Main Wind Force Resisting Systems

Figure 3-9 presents two different possibilities. The first option is if the wind flow is normal to the roof ridge, referred to as case A. Note that a range of

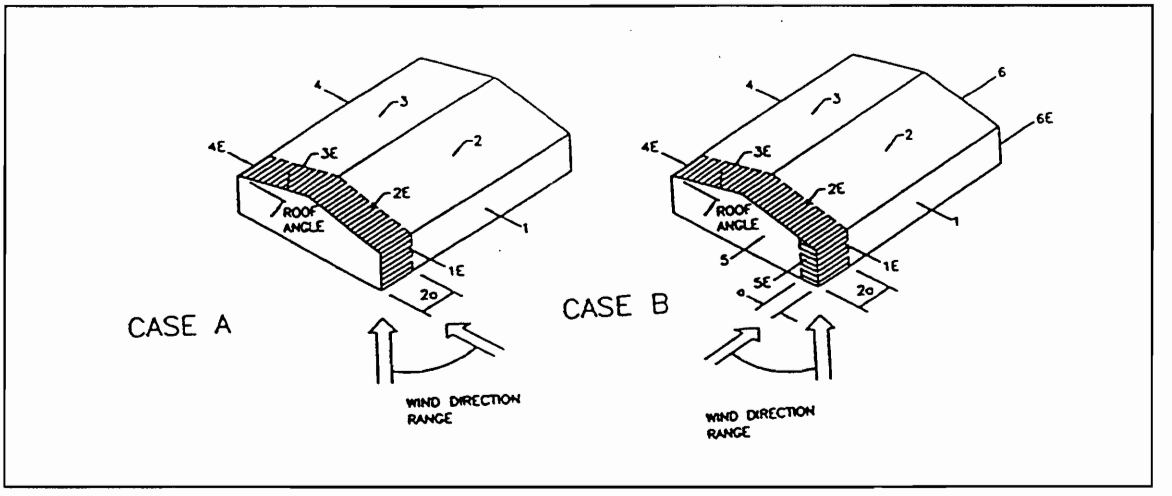

Figure 3-9: M.W.F.R.S illustration of case A and case B from ASCE 7-95 Figure 6-4

wind directions is given and thus the wind direction does not have to be exactly normal to the ridge. The second option is if the wind flow is parallel to the roof ridge, referred to as case B. Case B also allows the wind direction to deviate from perfectly parallel to the ridge.

External pressure coefficients are listed for different roof locations, different walls, and (for case A) different roof angles. While the roof is not divided into several sections for each side, it is divided at the ridge to account for the leeward and windward sides.

A special region on the roof and walls is designated as a shaded area in Figure 3-9. The area within a distance of 2*a (for this case a = 3 feet) from the windward wall has higher external pressure coefficients. (The value of "a" was previously calculated in Section 3.3.1.) The external wind loading is 44% to

55% higher in the shaded portion of Figure 3-9, which leads to the issue of the location of the truss being analyzed.

The Structural Engineers Association of Washington (SEAW) (1995) discuss this higher wind load area as addressed by the Uniform Building Code (UBC). (Both the UBC and ASCE 7-95 account for increased pressures on the area near the windward side of a structure by increasing the design wind load.) The SEAW (1995) states, "trusses parallel to the ends of the building located within 5 feet of the edge will be governed by Case 2 loading. Since only two trusses at each end are within the zone of discontinuity, it would be rather uneconomical to design a different truss type for these few trusses. A better approach would be to provide double trusses combined with effective bridging along the trusses that could distribute the uplift forces to the end wall and to several other interior trusses located outside the zone of discontinuity."

The truss being modeled here is assumed to be outside of the special region near the windward wall for two reasons. First, the statement made by the SEAW (1995) above implies that individual trusses are generally not designed to resist forces in the discontinuous region. Secondly, the vast majority of the trusses in this structure will be outside of this region.

Θ is defined as the angle defining the slope of the truss top chord member. It is found from Figure 3-1:

$$\Theta = \tan^{-1}(5'/15') = 18.4^\circ \cong 20^\circ$$

Θ is approximated by 20° to eliminate the need for linear interpolation of the coefficients from the values given in Figure 6-4 of ASCE 7-95. The external pressure coefficients for the various sides of the roof and different cases are listed below.

Wind Normal to Roof Ridge Case A

Windward Side Roof

GC_{pf} = -0.69 (ASCE 7-95 Fig 6-4 case A)

Windward Wall

GC_{pf} = +0.53 (ASCE 7-95 Fig 6-4 case A)

Leeward Side Roof

GC_{pf} = -0.48 (ASCE 7-95 Fig 6-4 case A)

Leeward Wall

GC_{pf} = -0.43 (ASCE 7-95 Fig 6-4 case A)

Wind Parallel to Roof Ridge Case B

Windward Side Roof

GC_{pf} = -0.69 (ASCE 7-95 Fig 6-4 case B)

Windward Wall

GC_{pf} = -0.45 (ASCE 7-95 Fig 6-4 case B)

Leeward Side Roof

GC_{pf} = -0.37 (ASCE 7-95 Fig 6-4 case B)

Windward Wall

GC_{pf} = -0.45 (ASCE 7-95 Fig 6-4 case B)

Even though the wind is flowing parallel to the roof ridge for case B, there is still a leeward and windward side. This is because ASCE 7-95 assumes that the wind does not flow perfectly parallel to the roof ridge, but rather the wind direction is considered within a range. The angle between the wind flow and the roof ridge results in different pressures on the two sides of the roof.

Here the external roof loads are calculated by combining the basic wind pressure, gust factor, external pressure coefficients, and tributary width.

Wind Normal to Roof Ridge

Leeward Side Roof

$p = q * [(GC_{pf})] = 49 \text{ psf } (-0.48) = -23.5 \text{ psf}$ < -10 psf ok

$w = p * (\text{trib. width}) = -23.5 \text{ psf} * (2 \text{ ft}) = -47.0 \text{ lb/ft}$

Windward Side Roof

$p = q * [(GC_{pf})] = 49 \text{ psf } (-0.69) = -33.8 \text{ psf}$ < -10 psf ok

$w = p * (\text{trib. width}) = -33.8 \text{ psf} * (2 \text{ ft}) = -67.6 \text{ lb/ft}$

Windward Wall

$p = q * [(GC_{pf})] = 49 \text{ psf } (+0.53) = +26.0 \text{ psf}$ $> +10$ psf ok

$w = p * (\text{trib. width}) = +26.0 \text{ psf} * (2 \text{ ft}) = +51.9 \text{ lb/ft}$

Leeward Wall

$p = q * [(GC_{pf})] = 49 \text{ psf } (-0.43) = -21.1 \text{ psf}$ < -10 psf ok

$w = p * (\text{trib. width}) = -21.1 \text{ psf} * (2 \text{ ft}) = -42.1 \text{ lb/ft}$

Wind Parallel to Roof Ridge

Leeward Side

$p = q * [(GC_{pf})] = 49 \text{ psf } (-0.37) = -18.1 \text{ psf} \quad < -10 \text{ psf} \quad \text{ok}$

$w = p * (\text{trib. width}) = -18.1 \text{ psf} * (2 \text{ ft}) = -36.3 \text{ lb/ft}$

Windward Side

$p = q * [(GC_{pf})] = 49 \text{ psf } (-0.69) = -33.8 \text{ psf} \quad < -10 \text{ psf} \quad \text{ok}$

$w = p * (\text{trib. width}) = -33.8 \text{ psf} * (2 \text{ ft}) = -67.6 \text{ lb/ft}$

Windward and Leeward Wall

$p = q * [(GC_{pf})] = 49 \text{ psf } (-0.45) = -22.1 \text{ psf} \quad < -10 \text{ psf} \quad \text{ok}$

$w = p * (\text{trib. width}) = -22.1 \text{ psf} * (2 \text{ ft}) = -44.1 \text{ lb/ft}$

According to Section 6.7.2.1 of ASCE 7-95, for main wind force resisting systems, a positive pressure on the bottom surface of windward roof overhangs must be considered. C_p, listed as 0.8, must be combined with a gust factor G and the upward pressure combined with the usual windward load. The gust factor used is found in Section 6.6.1, where it is listed as 0.85 for exposures C and D. The resultant loading is then used in combination with the pressure developed in prior sections.

Overhang on Windward Side

$C_p = 0.8$ 6.7.2.1

$G = 0.85$ 6.6.1

$p_{special} = q *[(GC_p)] = 49 \text{ psf} * (0.8) * (0.85) = 33.3 \text{ psf}$

$w_{special} = p_{special} * (\text{trib. width}) = 33.3 \text{ psf} * (2 \text{ ft}) = 66.7 \text{ lb/ft}$

Since this special overhang pressure (calculated above) acts upwards on the bottom side of the overhang and the windward pressure acts negatively on the top of the overhang, the resulting forces add together.

$w_{overhang} = w + w_{special}$ ← for the overhang

Wind Normal to Roof Ridge

Windward Overhang

$w_{overhang}$ = -67.6 lb/ft - 66.7 lb/ft = -134 lb/ft (upwards)

Wind Parallel to Roof Ridge

Windward Overhang

$w_{overhang}$ = -67.6 lb/ft - 66.7 lb/ft = -134 lb/ft (upwards)

3.3.2.2 Internal Loading for Main Wind Force Resisting Systems

Internal pressure coefficients are found in the same way for the main wind force resisting system as for components and cladding. They are shown below.

GC_{pi} = 0.80 and -0.30 (ASCE 7-95 Table 6-4)

$p = q * [(GC_{pi})]$ = 49 psf * (0.8 and -0.3) = 39.2 psf and -14.7 psf

w = p * (trib. width) = 39.2 psf * (2 ft) = 78.4 lb/ft

w = p * (trib. width) = -14.7 psf * (2 ft) = -29.4 lb/ft

Internal, external, and special region uniform loads are combined in Section 3.4.

3.4 Load Combinations

Combinations of the uniform loads previously calculated in Section 3.3 are described in this section. These load combinations will be analyzed using SAP90 to determine the member and reaction forces.

The two methods described by ASCE 7-95 to calculate the load on a roof system are the "components and cladding" method and the "main wind force resisting system" method. Loads from both methods were calculated previously. This section combines the external, internal, and special loads.

Internal pressure may be developed by external wind and must be considered when combining loads to determine the most critical combination of internal and external load. Positive pressure is developed if the building has openings on the windward side. Negative pressure is developed if the building has openings on the leeward side. The relationship between opening side and the sign of internal pressure is shown in Figure 3-10 from Cook (1990).

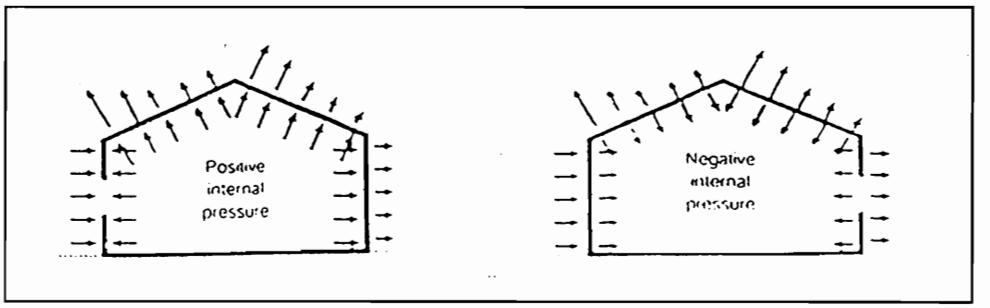

Figure 3-10: Internal pressure developed by openings in a building wall

Because positive or negative internal pressure can be developed in any structure due to openings and different wind directions, both types of internal pressure must be considered when forming load combinations.

Note that these loading combinations consider wind loads only. When the analysis was actually done, a 20 lb/ft dead load was added to the top and bottom chord members to account for the weight of plywood, gypsum, shingles, self weight of members, etc. Figures relating to the wind loads do not show the dead load to keep them as simple as possible.

The following are descriptions of the wind load cases illustrated in the corresponding figures. For each figure, uniform loads are calculated for the different areas of the roof.

3.4.1 Load Case 1

From the components and cladding analysis, positive (windward) and negative (leeward) forces on top chord members of the truss are combined while exposing the underside of the top chord members and support walls to positive internal pressure. The tension splice joint is located on the windward side of the truss. This case is shown in Figure 3-11.

For area 1

Since the roof overhang is not subjected to internal pressure variations, the external pressure is also the total pressure.

p_{tot} = 29.4 lb/ft

For areas 2, 3, and 4

$p_{tot} = p_{external} + p_{internal}$

p_{tot} = 29.4 lb/ft - 78.4 lb/ft = -49.0 lb/ft

For areas 5 and 7

p_{tot} = -137 lb/ft - 78.4 lb/ft = -215 lb/ft

For area 6

p_{tot} = -78.4 lb/ft - 78.4 lb/ft = -157 lb/ft

For area 8

Since area 6 is the overhang of the roof, there is no internal pressure acting on the inside of the top chord member.

p_{tot} = -216 lb/ft

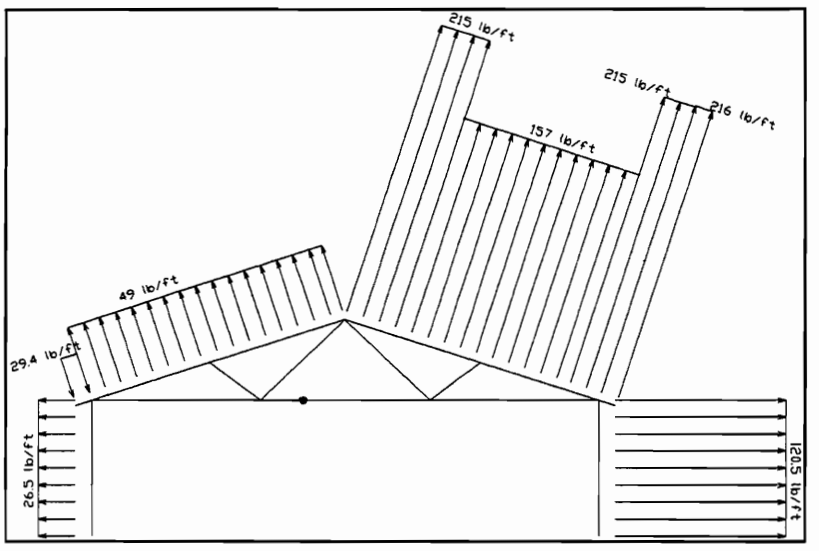

Figure 3-11: Components and cladding roof analysis with positive internal pressure and windward tension splice joint

For windward wall

$$p_{tot} = p_{external} + p_{internal}$$

$$p_{tot} = 51.9 \text{ lb/ft} - 78.4 \text{ lb/ft} = -26.5 \text{ lb/ft}$$

For leeward wall

$$p_{tot} = -42.1 \text{ lb/ft} - 78.4 \text{ lb/ft} = -120.5 \text{ lb/ft}$$

3.4.2 Load Case 2

As shown in Figure 3-12, load case 2 is the same as load case 1, but the tension splice joint is located on the leeward side.

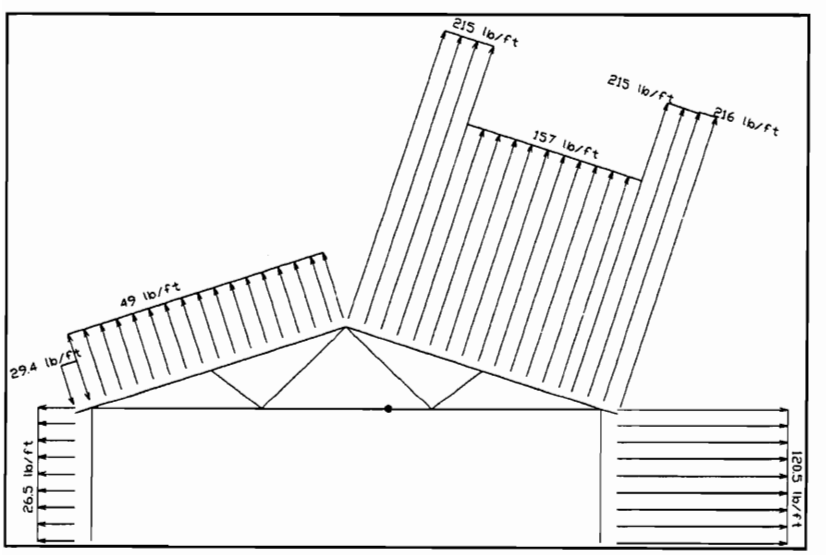

Figure 3-12: Components and cladding roof analysis with positive internal pressure and leeward tension splice joint

3.4.3 Load Case 3

From the components and cladding analysis, positive (windward) and negative (leeward) forces on top chord members of the truss are combined while exposing the underside of the top chord members and support walls to negative internal pressure. The tension splice joint is located on the windward side of the truss. This case is shown in Figure 3-13.

For area 1

The overhang is not subjected to internal pressure.

p_{tot} = 29.4 lb/ft

For areas 2, 3, and 4

p_{tot} = 29.4 lb/ft + 29.4 lb/ft = 58.8 lb/ft

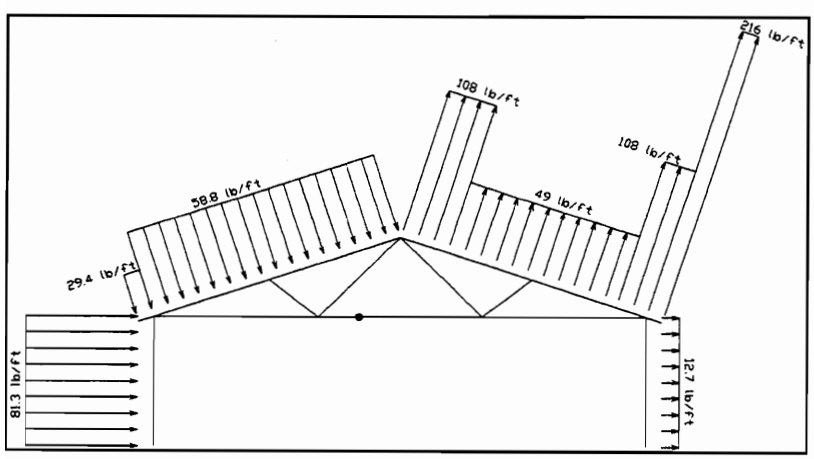

Figure 3-13: Components and cladding roof analysis with negative internal pressure and windward tension splice joint

For area 5 and 7

$$p_{tot} = -137 \text{ lb/ft} + 29.4 \text{ lb/ft} = -108 \text{ lb/ft}$$

For area 6

$$p_{tot} = -78.4 \text{ lb/ft} + 29.4 \text{ lb/ft} = -49.0 \text{ lb/ft}$$

For area 8

Again, since area 8 is the overhang of the roof, there is no internal pressure acting on the inside of the top chord member.

$$p_{tot} = -216 \text{ lb/ft}$$

For windward wall

$$p_{tot} = p_{external} + p_{internal}$$

$$p_{tot} = 51.9 \text{ lb/ft} + 29.4 \text{ lb/ft} = 81.3 \text{ lb/ft}$$

For leeward wall

$$p_{tot} = -42.1 \text{ lb/ft} + 29.4 \text{ lb/ft} = -12.7 \text{ lb/ft}$$

3.4.4 Load Case 4

As shown in Figure 3-14, load case 4 is the same as load case 3, but the tension splice joint is located on the leeward side.

3.4.5 Load Case 5

This case considers the main wind force resisting system analysis, using the forces calculated for wind approaching the structure normal to the ridge. An

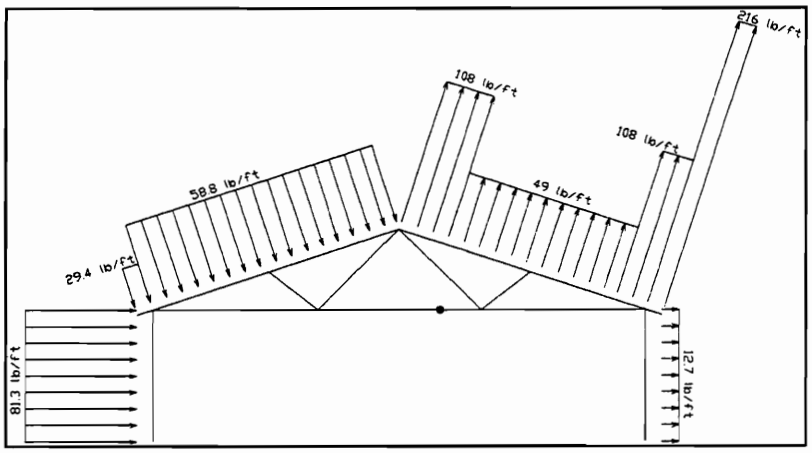

Figure 3-14: Components and cladding roof analysis with negative internal pressure and leeward tension splice joint

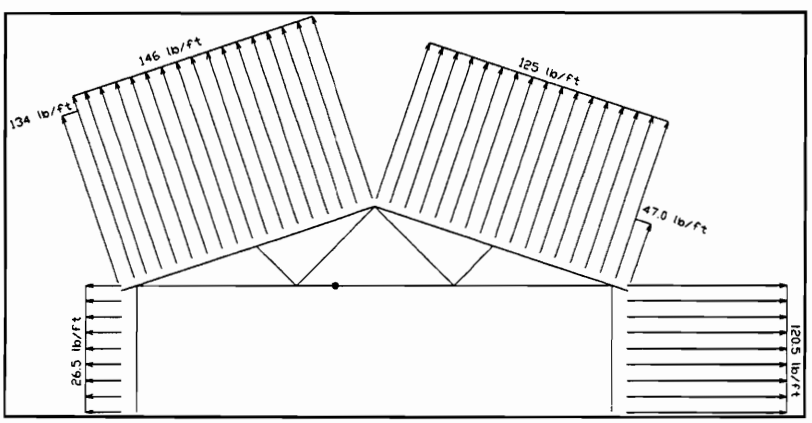

Figure 3-15: MWFRS with wind normal to the ridge with positive internal pressure and windward tension splice joint

additional load is applied on the underside of the windward overhang as required by ASCE 7-95 Section 6.7.2.1. Finally, the underside of the top chord members of the truss and the support walls are exposed to a positive internal

pressure. The tension splice joint is located on the windward side. This load case is shown in Figure 3-15.

Windward side

overhang

Since the overhang on both sides has no internal pressure affecting it, there is no $p_{internal}$, but there is an adjustment for the windward overhang.

$p_{tot} = p_{external} + p_{special}$

p_{tot} = -67.6 lb/ft - 66.7 lb/ft = -134 lb/ft

roof section

$p_{tot} = p_{external} + p_{internal}$

p_{tot} = -67.6 lb/ft - 78.4 lb/ft = -146 lb/ft

Leeward side

overhang

Since the overhang has no internal pressure acting on it, there is no adjustment required.

p_{tot} = -47.0 lb/ft

roof section

p_{tot} = -47.0 lb/ft - 78.4 lb/ft = -125 lb/ft

For windward wall

$p_{tot} = p_{external} + p_{internal}$

p_{tot} = 51.9 lb/ft - 78.4 lb/ft = -26.5 lb/ft

For leeward wall

p_{tot} = -42.1 lb/ft - 78.4 lb/ft = -120.5 lb/ft

3.4.6 Load Case 6

As shown in Figure 3-16, load case 6 is the same as load case 5, but the tension splice joint is located on the leeward side.

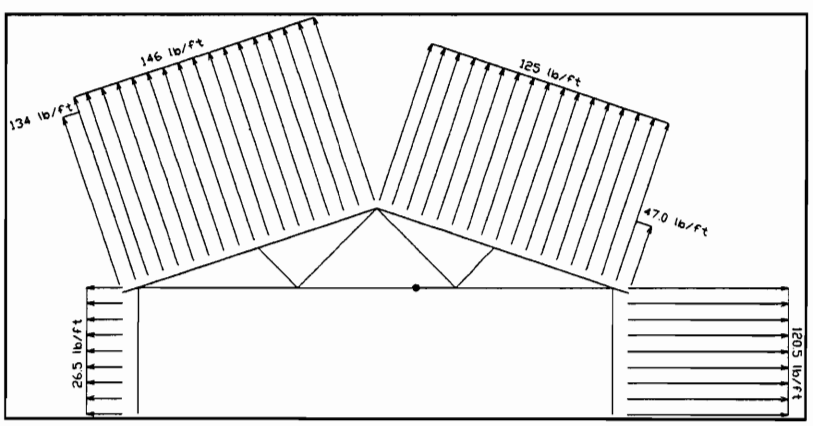

Figure 3-16: MWFRS with wind normal to the ridge with positive internal pressure and leeward tension splice joint

3.4.7 Load Case 7

This case considers the main wind force resisting system analysis, using the forces calculated for wind approaching the structure normal to the ridge. An additional load is applied on the underside of the windward overhang as

required by ASCE 7-95 Section 6.7.2.1. Finally, the underside of the top chord members of the truss and the support walls are exposed to a negative internal pressure. The tension splice joint is located on the windward side. This load case is shown in Figure 3-17.

Windward side

overhang

Since the overhang on both sides has no internal pressure affecting it, there is no $p_{internal}$, but there is an adjustment for the windward overhang.

$p_{tot} = p_{external} + p_{special}$

p_{tot} = -67.6 lb/ft - 66.7 lb/ft = -134 lb/ft

roof section

$p_{tot} = p_{external} + p_{internal}$

p_{tot} = -67.6 lb/ft + 29.4 lb/ft = -38.2 lb/ft

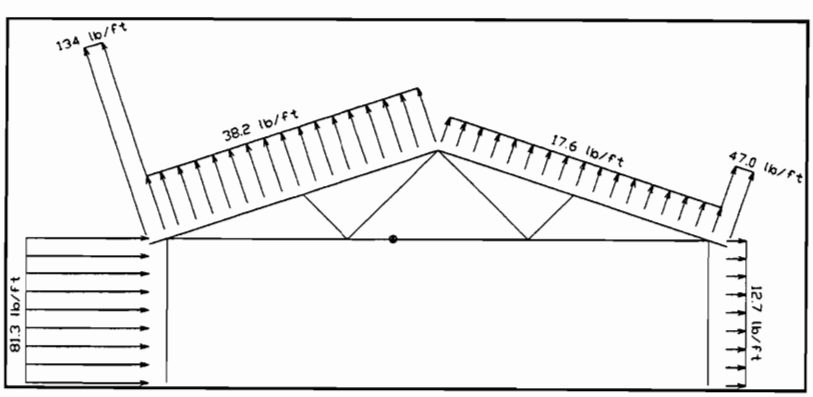

Figure 3-17: MWFRS with wind normal to the ridge with negative internal pressure and windward tension splice joint

Leeward Side

overhang

Since the overhang has no internal pressure acting on it, there is no adjustment required.

p_{tot} = -47.0 lb/ft

roof section

p_{tot} = -47.0 lb/ft + 29.4 lb/ft = -17.6 lb/ft

For windward wall

$p_{tot} = p_{external} + p_{internal}$

p_{tot} = 51.9 lb/ft + 29.4 lb/ft = 81F.3 lb/ft

For leeward wall

p_{tot} = -42.1 lb/ft + 29.4 lb/ft = -12.7 lb/ft

3.4.8 Load Case 8

As shown in Figure 3-18, load case 8 is the same as load case 7, but the tension splice joint is located on the leeward side.

3.4.9 Load Case 9

This case considers the main wind force resisting system analysis, using the forces calculated when the wind approximately approaches parallel to the ridge of the building. (ASCE 7-95 assumes that the wind approaches the

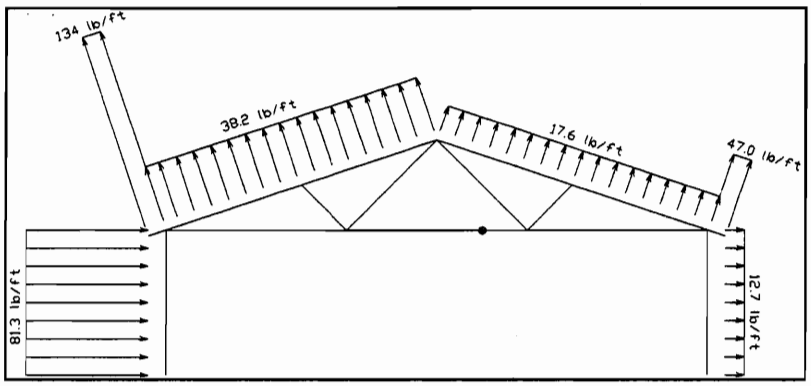

Figure 3-18: MWFRS with wind normal to the ridge with negative internal pressure and leeward tension splice joint

building at some angle, ranging from 0° to 45°, from parallel from the ridge. This angle causes a difference in loading between the two sides of the roof ridge. The side of the roof ridge with the higher wind load is considered the windward side.) An additional load is applied on the underside of the windward overhang as required by ASCE 7-95 Section 6.7.2.1. Finally, the underside of the top chord members of the truss and the support walls are exposed to a positive internal pressure. The tension splice joint is located on the windward side. This load case is shown in Figure 3-19.

Windward side

overhang

$$p_{tot} = p_{external} + p_{special}$$

$$p_{tot} = -67.6 \text{ lb/ft} - 66.7 \text{ lb/ft} = -134 \text{ lb/ft}$$

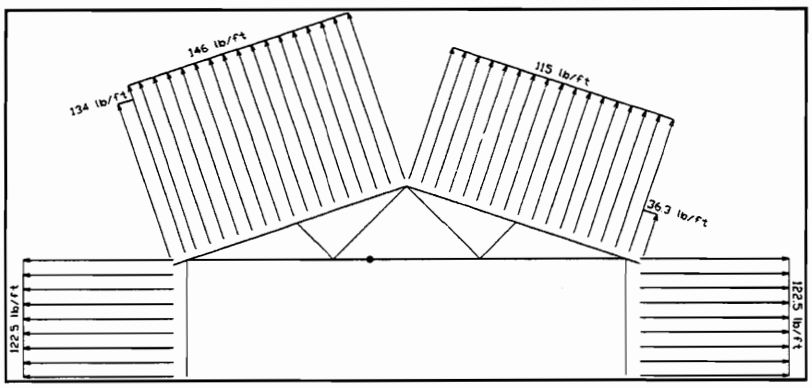

Figure 3-19: MWFRS with wind parallel to the ridge with positive internal pressure and windward tension splice joint

roof section

$p_{tot} = p_{external} + p_{internal}$

p_{tot} = -67.6 lb/ft - 78.4 lb/ft = -146 lb/ft

Leeward side

overhang

Since the overhang has no internal pressure acting on it,

there is no adjustment required.

p_{tot} = -36.3 lb/ft

roof section

p_{tot} = -36.3 lb/ft - 78.4 lb/ft = -115 lb/ft

For windward wall

$p_{tot} = p_{external} + p_{internal}$

p_{tot} = -44.1 lb/ft - 78.4 lb/ft = -122.5 lb/ft

For leeward wall

$$p_{tot} = -42.1 \text{ lb/ft} - 78.4 \text{ lb/ft} = -122.5 \text{ lb/ft}$$

3.4.10 Load Case 10

As shown in Figure 3-20, load case 10 is the same as load case 9, but the tension splice joint is located on the leeward side.

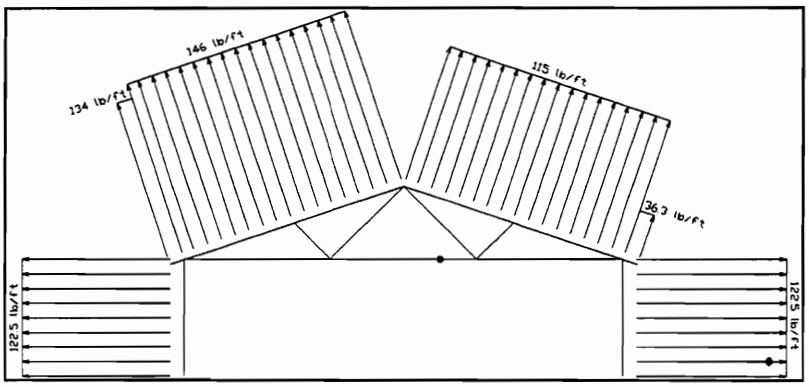

Figure 3-20: MWFRS with wind parallel to the ridge with positive internal pressure and leeward tension splice joint

3.4.11 Load Case 11

This case considers the main wind force resisting system analysis, using the forces calculated for wind approaching the structure parallel to the ridge. An additional load is applied on the underside of the windward overhang as required by ASCE 7-95 Section 6.7.2.1. Finally, the underside of the top chord members of the truss and the support walls are exposed to a negative internal

pressure. The tension splice joint is located on the windward side. This load case is shown in Figure 3-21.

Windward side

overhang

$p_{tot} = p_{external} + p_{special}$

p_{tot} = -67.6 lb/ft - 66.7 lb/ft = -134 lb/ft

roof section

$p_{tot} = p_{external} + p_{internal}$

p_{tot} = -67.6 lb/ft + 29.4 lb/ft = -38.2 lb/ft

Leeward side

overhang

Since the overhang has no internal pressure acting on it, there is no adjustment required.

p_{tot} = -36.3 lb/ft

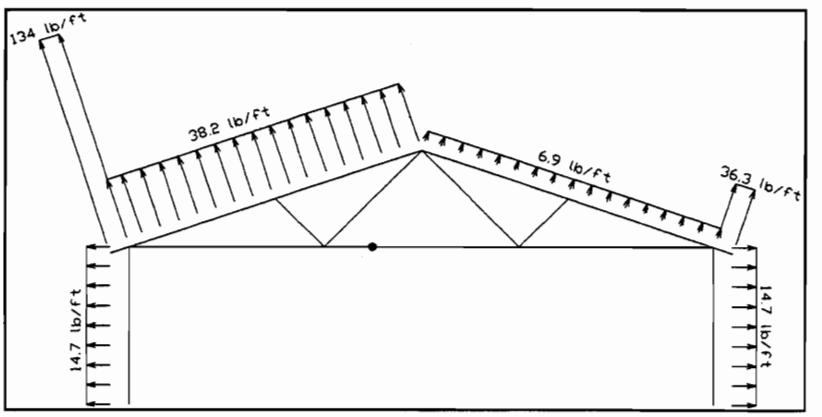

Figure 3-21: MWFRS with wind parallel to the ridge with negative internal pressure and windward tension splice joint

roof section

$$p_{tot} = -36.3 \text{ lb/ft} + 29.4 \text{ lb/ft} = -6.9 \text{ lb/ft}$$

For windward wall

$$p_{tot} = p_{external} + p_{internal}$$

$$p_{tot} = -44.1 \text{ lb/ft} + 29.4 \text{ lb/ft} = -14.7 \text{ lb/ft}$$

For leeward wall

$$p_{tot} = -44.1 \text{ lb/ft} + 29.4 \text{ lb/ft} = -14.7 \text{ lb/ft}$$

3.4.12 Load Case 12

As shown in Figure 3-22 , load case 12 is the same as load case 10, but the tension splice joint is located on the leeward side.

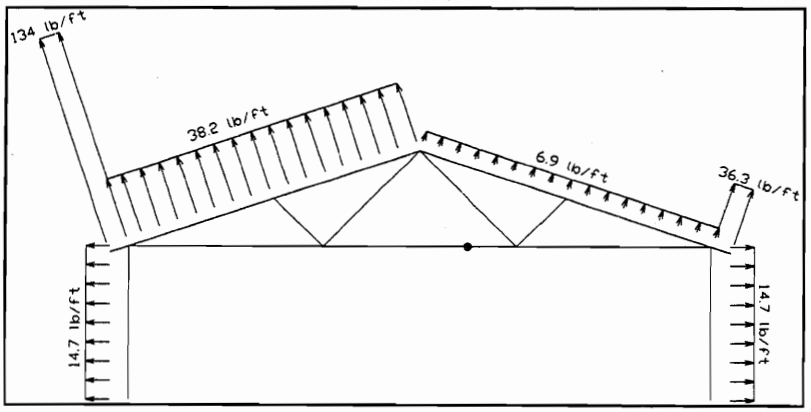

Figure 3-22: MWFRS with wind parallel to the ridge and negative internal pressure and leeward tension splice joint

3.5 SAP90 Finite Element Analysis

The Fink truss discussed in Section 3.1 was modeled using linear elastic beam elements. Both top chord members are continuous from the overhang to the ridge. The bottom chord member is continuous except at the tension splice joint, where it is modeled as a pin connection. All of the web members are pinned at both ends. The joint connectivity is shown in Figure 3-1, along with the dimensions.

A dynamic analysis was performed on the structure using the wind loads to excite the system, but little dynamic effect was seen. Therefore, the member forces were determined using the static loads calculated using the ASCE 7-95.

The truss is supported by end walls vertically and springs horizontally. The horizontal springs model the support provided by the end shear wall.

The load combinations shown in Figure 3-11 through Figure 3-22 were analyzed in SAP90 to determine the maximum forces on the heel and tension splice joints. SAP90 requires that span loads be defined with reference to the global axes, not the local axes. The local axes are defined with respect to an individual member, while the global axes are the same throughout the system. Therefore, the wind loads must first be transformed into global axes system. After member forces were determined for the wind loads, the member forces produced by the dead load were added to obtain the total member force. The analysis was accomplished in two steps so that the wind loads could be scaled to various wind speeds, while not affecting the dead load forces.

Since there are two heel joints in the model, both must be checked. Since physical testing will be performed by applying the load through the top chord member of each heel joint, only the forces in members 13 and 6, from Figure 3-23, are examined for the heel joints. The force in member 16 is also examined because it corresponds to the force exerted on the tension splice joint. (The force in member 17 is checked to ensure it has the same magnitude and sign, but it is not recorded.)

Members were defined in SAP90 such that the forces at the j end of member 13, the j end of member 16, and the i end of member 6 describe the desired forces. Tension is listed as positive and compression is listed as negative. The forces in pounds are listed in Table 3-1 for each joint and loading case.

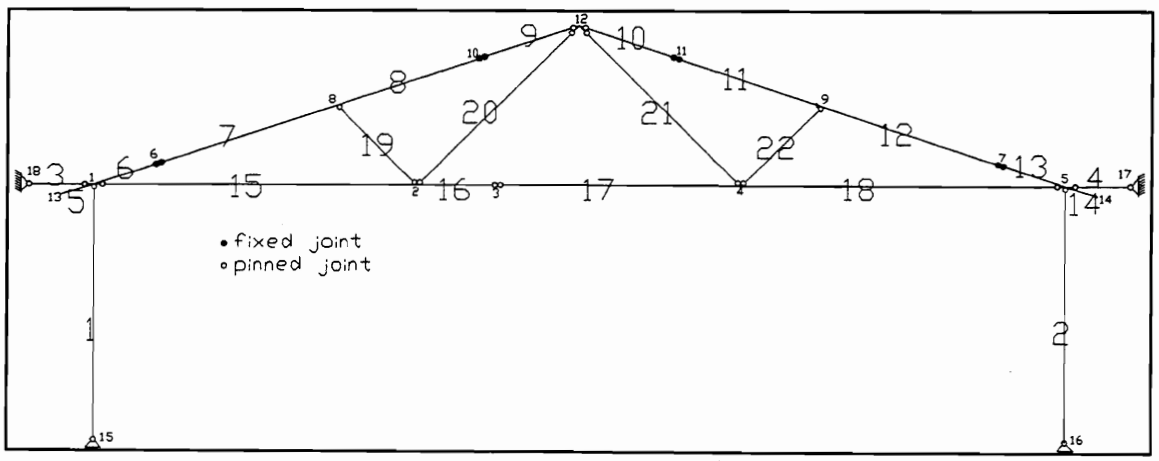

Figure 3-23: Member and joint numbers used in SAP90 analysis

Joints 6, 10, 11, and 7 in Figure 3-23 were defined because the uniform wind load across the top chord changes at the location of the joints. (The joints are located 3 ft from the edge or the eaves. 3 ft corresponds to the distance "a" as defined by ASCE 7-95 and described in Section 3.3.)

Table 3-1: Joint force and description versus load case

Load Case	Description Analysis Type	Tension Splice Joint Side	Joint Windward Heel (lb.)	Leeward Heel (lb.)	Tension Splice (lb.)
1	C&C with positive internal pressure	Windward	1910	3337	-1147.4
2		Leeward	1902	3349	-1148.4
3	C & C with negative internal pressure	Windward	-2128	-580	619.6
4		Leeward	-2126	-577	617.6
5	M.W.F.R.S with positive internal	Windward	3662	3369	-1546.4
6	pressure and wind normal to ridge	Leeward	3649	3381	-1546.4
7	M.W.F.R.S with negative internal	Windward	-323	-596	188.6
8	pressure and wind normal to ridge	Leeward	-326	-594	189.6
9	M.W.F.R.S with positive internal	Windward	3540	3107	-1249.4
10	pressure and wind parallel to ridge	Leeward	3528	3118	-1249.4
11	M.W.F.R.S with negative internal	Windward	-447	-864	487.6
12	pressure and wind parallel to ridge	Leeward	-449	-862	488.6

Some of the load cases listed in Table 3-1 are very similar. The difference between load case 1 and load case 2 is only in the placement of the tension splice joint. Load case 2 has the tension splice joint located on the leeward side, while load case 1 has it on the windward side. (The change in tension splice joint side represents the wind approaching from the opposite direction.) Note that this similarity repeats throughout Table 3-1. Case 3 is similar to case 4, case 5 is similar to case 6, and so on.

Comparing the forces of the similar load cases shows that changing the side the wind approaches from has little effect on the member forces. Therefore, half of the load cases are disregarded because they are already represented. The reduced load cases are shown in Table 3-2, with values for the tension splice joint on the windward side shown.

The data in Table 3-2 is shown graphically in Figure 3-24. Note that negative forces are in compression while positive forces are in tension. (Description C&C in Table 3-2 stands for components and cladding while M. W. F. R. S. stands for main wind force resisting system.)

Table 3-2: Joint force vs. load condition table

Load Case	Description Analysis Type	Joint		
		Windward Heel (lb.)	Leeward Heel (lb.)	Tension Splice (lb.)
1	C&C with positive internal pressure	1910	3337	-1147.4
3	C & C with negative internal pressure	-2128	-580	619.6
5	M.W.F.R.S with positive internal pressure and wind normal to ridge	3662	3369	-1546.4
7	M.W.F.R.S with negative internal pressure and wind normal to ridge	-323	-596	188.6
9	M.W.F.R.S with positive internal pressure and wind parallel to ridge	3540	3107	-1249.4
11	M.W.F.R.S with negative internal pressure and wind parallel to ridge	-447	-864	487.6

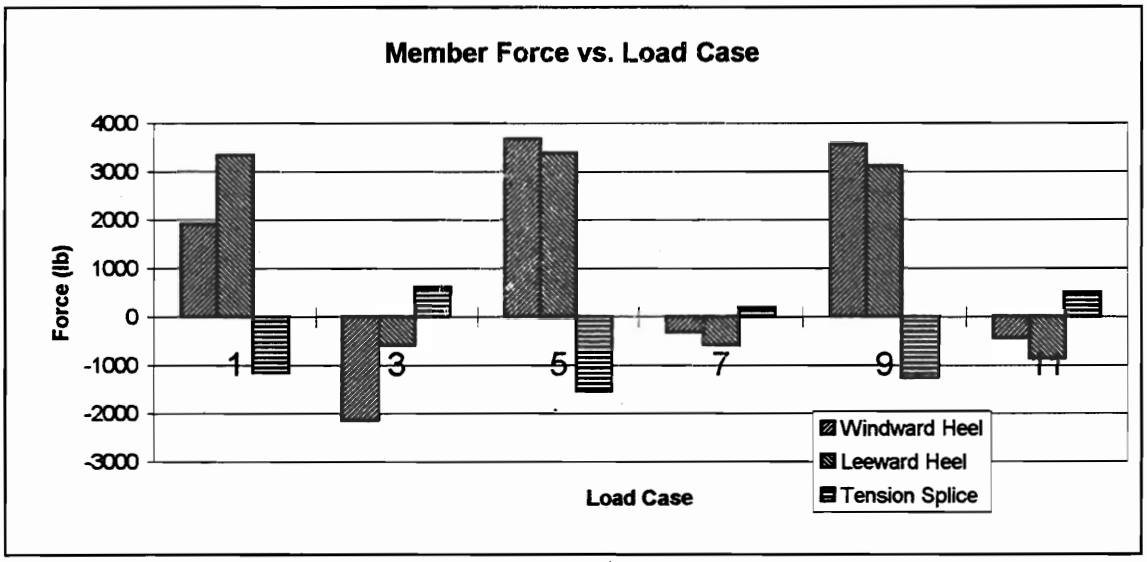

Figure 3-24: Member forces plotted versus load case

3.5.1.1 Wind Force Discussion for Tension Splice Joints

For tension splice joints, the largest force magnitude is 1546 lb. in compression, found in load case 5. Unfortunately, loading tension splice joints to failure in compression would be difficult and the results would yield little or no information concerning tension splice joint behavior. This is due to the unpredictable nature of tension splice joint behavior when loaded in compression.

If the tension splice joint was laterally unsupported, then the joint would likely fail in a buckling mode. Data from this type of failure would not be comparable to control group data. (For this project, control members are loaded in tension at a constant load rate until failure occurs.)

If the tension splice joints were completely supported in the lateral direction, the characteristics of the tension splice joint would only be observable when the joint deflection is small. The gap between the two members in a tension splice joint would close under high load and the two members would be in direct contact. After contact occurs, the behavior of the two members would be seen, not the behavior of the tension splice joint. (Also, the lateral support condition a tension splice joint in a structure can vary. Sturdy blocking with a gypsum board ceiling results in good lateral support, while some garages have no blocking or gypsum board on the ceiling.) Because of the incomparable nature of tension tests and compression tests, the compression values for the tension splice joints were disregarded.

Therefore, only the tension wind load forces are considered for the tension splice joint. The maximum tension force in the tension splice joint is 619 lb., which is found in load case 3. The 619 lb. represents the dead load force added to the wind load force. The member force due to the wind is 244 lb. in compression, while the member force due to the dead loading is 864 lb. in tension. (Adding these two member forces together gives approximately 619 lb.)

For this project, the dead load forces are constant and the wind load forces contain the dynamic part of the overall loading. Since the wind force is small, the corresponding wind load simulation would have little load variation. According to Freilinger (1998) the ultimate strength of a tension splice joint tested in tension is approximately 5760 lb. The proposed test force of 619 lb. is

nine times smaller than the ultimate strength of the joint. The proposed tension splice joint test is neither significantly dynamic nor large enough in magnitude when compared to the ultimate strength of the joint to be interesting. Therefore, a tension wind load force test using tension splice joints was not performed for this project.

3.5.1.2 Wind Force Discussion for Heel Joints

The largest heel joint force is 3662 lb. in tension, which is found on the windward side of load case 5. It is possible to load a heel joint in tension as accomplished by Kent (1995) and Freilinger (1998), but the maximum load, for a heel joint, is generally dependent on how securely the roof trusses are connected to the walls in actual construction. (A heel joint tested in tension is defined here as a heel joint with the top chord in tension. Conversely, compression load heel joint tests have compression forces in the top chord of the heel joint.) If the mechanical connections which tie the truss to the wall are not strong enough to resist the reaction forces, then the members will never experience the loads calculated. If the reaction force is larger than the strength of the truss tie downs, then testing the heel joint would be pointless because the corresponding force level could never be developed in a realistic situation.

The similarities between load cases result in very similar reaction forces. Because reaction force values are so close between similar load cases, there is

no need to consider the duplicate reaction forces. The non-duplicate vertical reaction forces are listed in Table 3-3.

Table 3-3: Vertical reaction forces for representative load cases

Load Case	Description	Reaction Forces	
		Vertical Force on Windward Wall (lb.)	Vertical Force on Leeward Wall (lb.)
1	C&C with positive internal pressure	-542.4	-1631.2
3	C & C with negative internal pressure	1020.6	-87.2
5	M.W.F.R.S with positive internal pressure and wind normal to ridge	-1532.4	-1306.2
7	M.W.F.R.S with negative internal pressure and wind normal to ridge	24.6	251.8
9	M.W.F.R.S with positive internal pressure and wind parallel to ridge	-1493.4	-1183.2
11	M.W.F.R.S with negative internal pressure and wind parallel to ridge	63.6	377.8

For the vertical reactions, negative forces act downward and require truss tie downs, while positive forces act upward and only require a bearing support. The reaction forces listed in Table 3-3 are also shown graphically in Figure 3-25.

To determine if the roof will be lifted off the support before the maximum member force is reached, the uplift force associated with the maximum member force must be compared to the strength of the truss connector. As stated before, the largest heel joint force is 3662 lb. in tension, which is found on the windward side of load case 5. The windward reaction force for load case 5 is 1532 lb. in the downward direction.

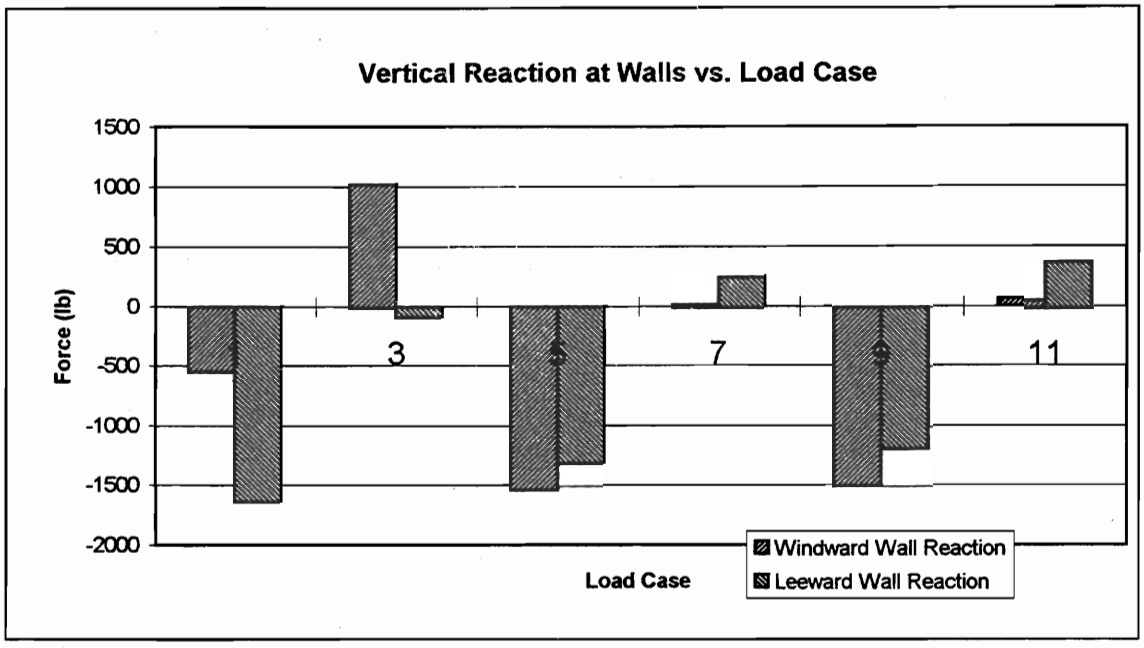

Figure 3-25: Reaction force versus load case

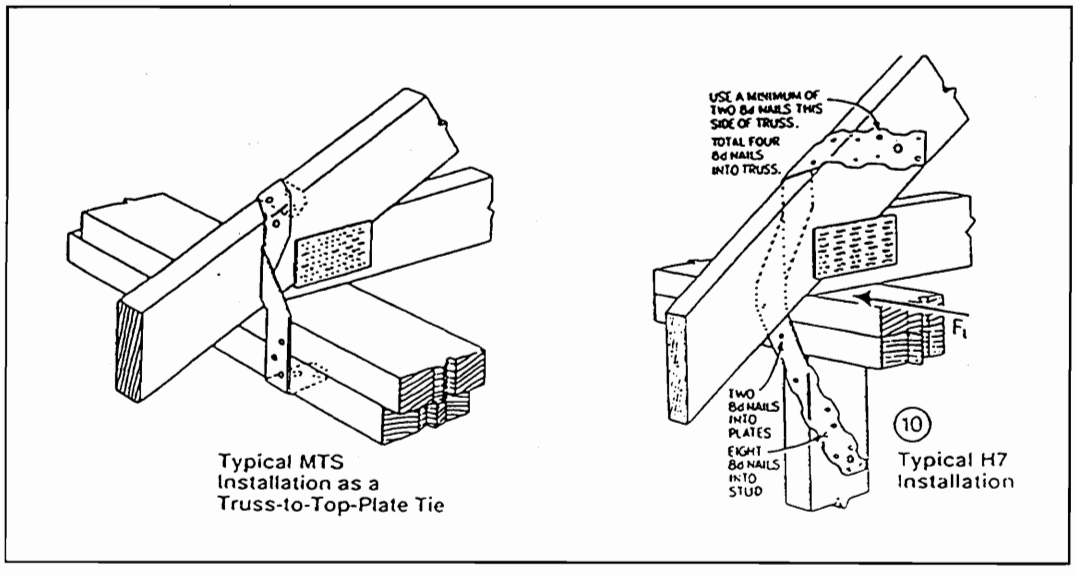

Figure 3-26: Simpson (1997) seismic and hurricane wood truss tie-down connectors

Many different truss tie down support possibilities exist. In Figure 3-26, several seismic and hurricane ties are shown from Simpson (1997).

It assumed here that Simpson H15 truss ties were used to secure the Fink truss to the supports. H15 tie-downs were used in this project because they are the strongest connectors available from Simpson (1997). If a weaker tie-down connector was used, the controlling wind load from Section 3.3 may not be reached before failure occurs in the tie-down. Design values for Simpson H15 truss ties are 1300 lb. in uplift and 480 lb. in lateral load. The average ultimate uplift load is 6070 lb. according to Simpson (1997).

While the design uplift load of the Simpson H15 is exceeded by 232 lb. for load case 5, the average ultimate uplift force is 4538 lb. higher than the actual uplift force. The maximum reaction force for all load cases is 1631 lb., as found in the leeward reaction of load case 1. This reaction force is also considerably lower than the ultimate uplift force.

Although the reaction uplift forces exceed the design capacity of the truss ties used, the ultimate capacity is significantly higher than the uplift forces developed by any of the load cases. Therefore, it is reasonable to assume that heel joints loaded to 3662 lb. (as developed in load case 5) would not be pulled off of the reaction points if tied down with a Simpson H15 truss tie. Consequently, testing heel joints in tension is an acceptable method.

The largest compressive force in the heel joints, as seen in Table 3-2, is found in the windward heel joint of load case 3, which is 2128 lb. While this

compressive force is considerably less than the maximum tensile force, it is still significantly large and should be addressed. Properties of MPC heel joints could be significantly different in tension than in compression. This lower compressive force could potentially cause more damage to the heel joints than the larger tensile force. Therefore, it is necessary to perform heel joint tests in both tension and compression.

Tests will be performed to determine the effects of wind loading on heel joints in both tension and compression, but no wind simulation tests will be done on tension splice joints as explained previously in Section 3.5.1.1. The controlling member forces are listed in Table 3-4.

Table 3-4: Controlling member forces

Joint	Load Case	Joint Side	Force (lb.)	Force Type
Heel	5	windward	3662	tension
Heel	3	windward	2128	compression

Since this project is concerned with the dynamic properties of MPC joints, the static forces listed in Table 3-1 must be transformed into a dynamic time history which can be used during testing. This is accomplished using real time wind speed data from a hurricane, provided by the U.S. Army Corps of Engineers (1991). Data from hurricane Bob, which passed through southern

Florida and Louisiana in September of 1991, was available and is used in this project.

First the data from hurricane Bob must be adjusted to match the wind speeds indicated on the Basic Wind Speed map in Figure 6-1 of ASCE 7-95. The wind speed values in ASCE 7-95 are 3-second gust speeds in miles per hour at 33 ft above the ground for Exposure C and are associated with an annual probability of 0.02. The data from hurricane Bob is not averaged, but it was recorded at a height of 33 feet. Therefore, the wind speed data must be altered so the 3 second average is equal to the design speed. For this project the design speed is 150 mph as stated in Section 3.3. The original wind speed data is shown in Figure 3-27. Only a small amount of the hurricane data is shown in this figure for clarity, but the entire data set for the hurricane is shown in Figure 3-28. Note the data has been averaged from approximately 64,000 points to approximately 250 points so the entire 2 ¼ hours of data could all fit on one plot. Averaging the data caused the points to move towards the average, therefore the actual maximums and minimums are not shown. The purpose of displaying is to Figure 3-28 show the general trend of the average wind speed during the test.

First, the hurricane Bob data was subjected to a running 3 second average which is shown in Figure 3-29. Again, only a small amount of the hurricane data is shown here for clarity.

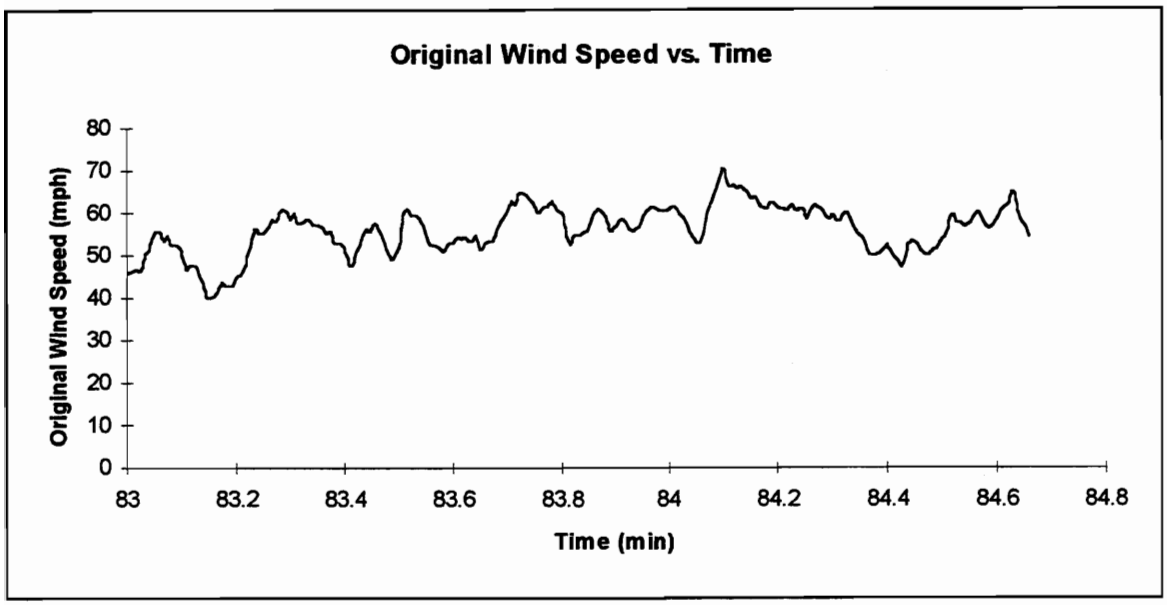

Figure 3-27: Original wind speed data

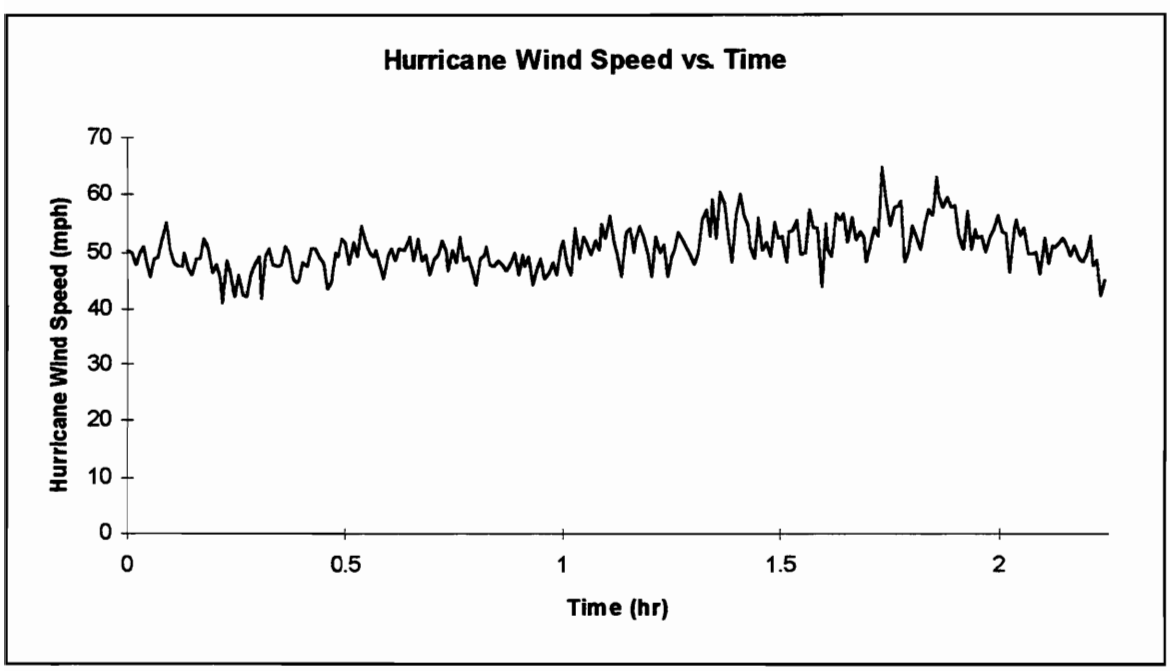

Figure 3-28: General trend of the average wind speed during test

The ratio between the design speed, 150 mph, and the maximum value of the 3 second average was determined. The original hurricane Bob wind data was then multiplied by this ratio. The result is a set of data, whose maximum 3 second average value is 150 mph as shown in Figure 3-30. The modified hurricane Bob wind speed data combined with the controlling member forces to create a force time history which was used to test heel joints.

The formula used to combine the variables is:

$$TestForce(t) = \frac{velocity(t)^2}{150mph^2} * MemberForce_{WIND} + MemberForce_{DEADLOAD}$$

TestForce(t) = force exerted by the modified hurricane Bob wind loading on the top chord of a heel joint at and time t (lb)

velocity(t) = speed of the modified hurricane Bob wind at any time t (mph)

$MemberForce_{WIND}$ = controlling force (from Table 3-4) exerted on the top chord of a heel joint according to the ASCE 7-95 due to a 150 mph wind (lb)

$MemberForce_{DEADLOAD}$ = force exerted on the top chord of a heel joint due to the structure dead load (lb)

The TestForce(t) is the force used during the hurricane wind load tests on heel joints. The velocity(t) is a set of modified wind speed values from hurricane Bob. The wind speed data used for velocity(t) has been modified such that the maximum of the 3-second average is 150 mph. This modification is done so the wind data matches the ASCE 7-95 design wind speed requirements. The

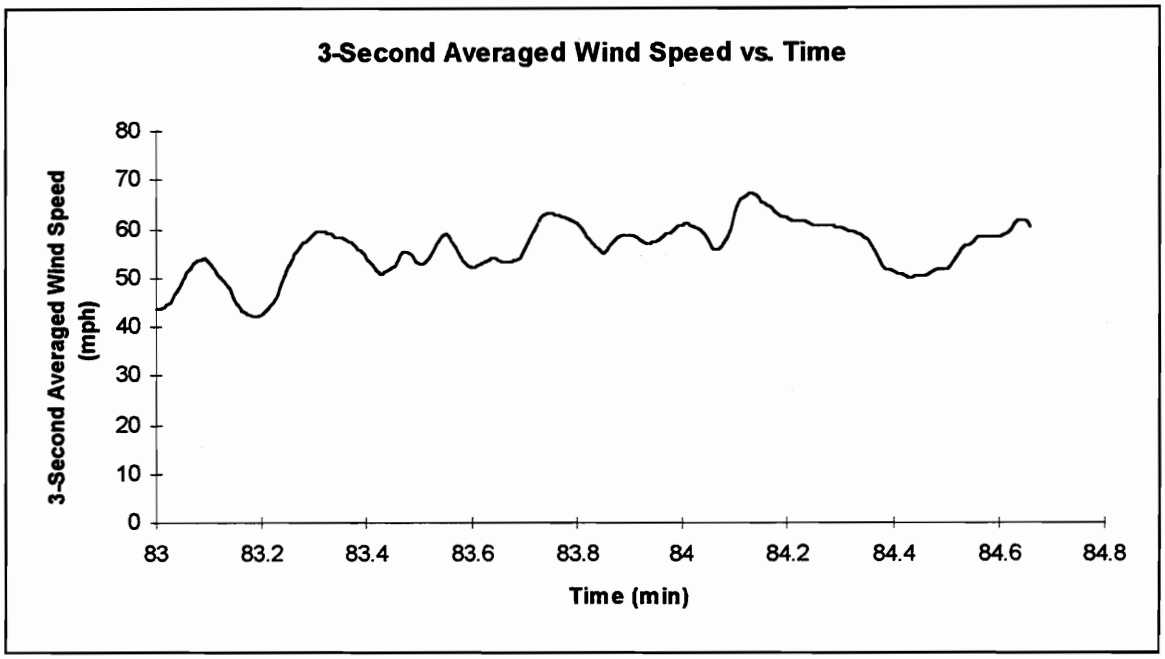

Figure 3-29: Original wind speed data subjected to a running three second average

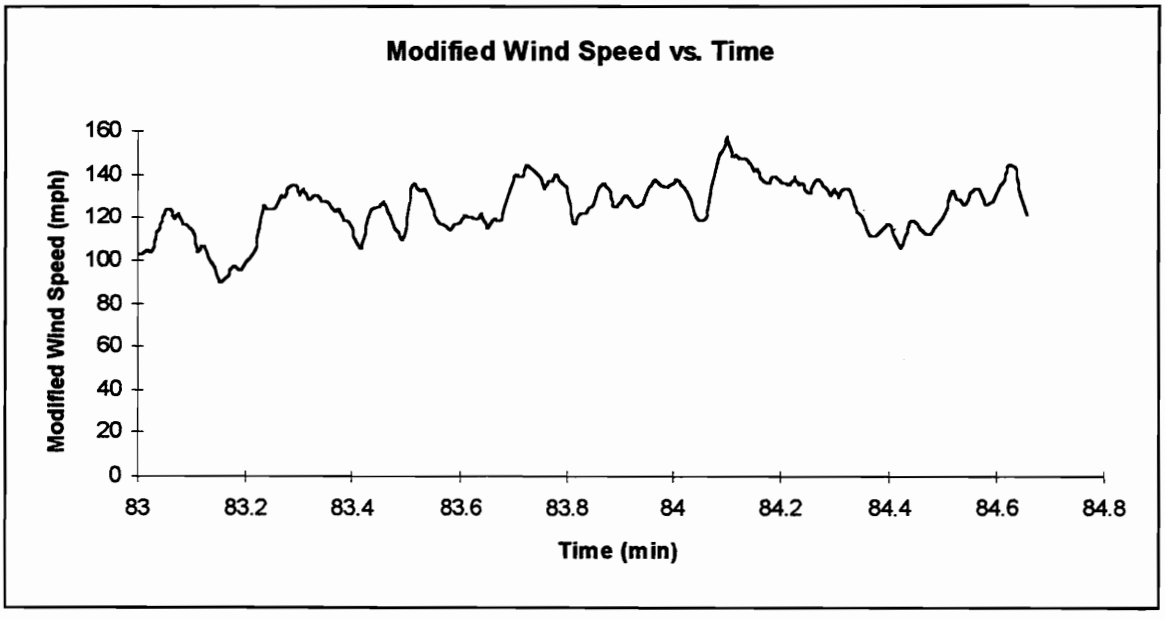

Figure 3-30: Hurricane wind speed data modified to make the maximum of the running 3-second average 150 mph

$MemberForce_{WIND}$ is the controlling force in the top chord of the heel joints based on the ASCE 7-95 analysis detailed in Section 3.3. This force is either in tension or compression depending on which test is being performed. For the hurricane wind load simulation tests on heel joints with the top member in compression, the controlling force (found in Table 3-4) in compression is used as the $MemberForce_{WIND}$. The controlling tension force is used for the hurricane wind load simulation tests in tension. The $MemberForce_{DEADLOAD}$ is the force in the top chord of a heel joint due to the dead weight of the structure. The $MemberForce_{DEADLOAD}$ is 1465 lb in compression on the top chord of the heel joint. For the hurricane wind simulation in tension, the $MemberForce_{WIND}$ and $MemberForce_{DEADLOAD}$ subtract from each other, while the opposite is true for the hurricane wind simulation in compression.

4. Experimental Design and Methods

4.1 Materials

MPC heel joints were constructed from lumber and metal plates supplied by Frank Lumber Company (Mill City, Oregon) and Alpine Engineered Products, Inc. (Pompano Beach, Florida), respectively. The 2"x4" (nominal) machine stress rated (MSR) Douglas-fir (1800f-1.6E) lumber was conditioned in a 70°F and 65% relative humidity standard room to an approximate equilibrium moisture content of 12%. 3"x4" and 3"x5" metal plates were used to construct the tension splice and heel joints, respectively.

Kent (1996) concluded that using metal plates from different batches can result in different results. To avoid this confounding variable, all metal plates tested were from the same batch. All metal plates were made from 20 gauge sheet metal and had ¼" by 0.12 inch teeth. The metal plates were pressed using a 450 ton Cliffton hydraulic press. To prevent over pressing or under pressing of the metal plates, only one metal plate was pressed at a time and each joint was carefully observed during the operation. Specifically, each plate was pressed until the teeth embedded enough that the plate touched the wood and made a slight indentation. The operator attempted to keep the indentation in the wood less than one-half the thickness of the plate. Over pressing, indenting the plate into the wood more than one-half the thickness, was avoided

by increasing the press deflection slowly. Under pressing, leaving a gap between the plate and the wood, was avoided by watching each pressing operation for such a gap.

Arbek (1979) concluded that the strength of MPC joints changes as the wood fibers relax for approximately one week after they are fabricated. All joints were allowed to relax in the standard room for a minimum of one week to ensure joint age was not a significant factor in strength measurement.

Both the top and bottom chords of the heel joints were constructed from 20 inch long sections of 2"x4" (nominal) lumber. Also, both sides of the tension splice joints were constructed from two 20 inch long sections of 2"x4" (nominal) lumber. The dimensions of both heel and tension splice joints are shown in Figure 4-1.

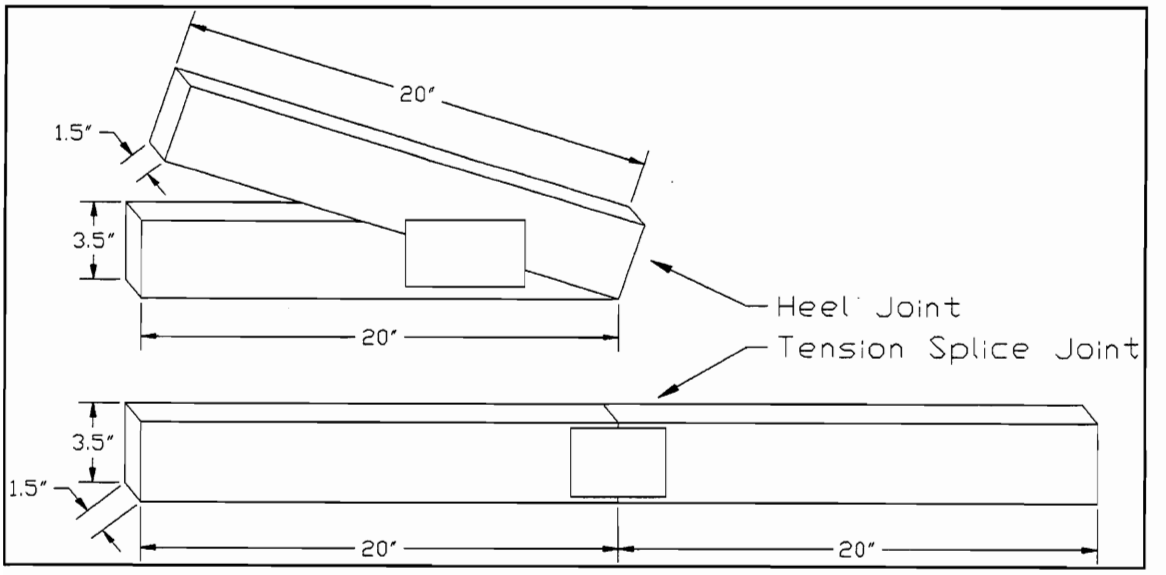

Figure 4-1: Dimensions of test heel and tension splice joints

4.2 Experimental Design

This project was designed to add to the knowledge base pertaining to the dynamic behavior of MPC joints. Specifically, this project addresses the issue of wind and impact loading on heel and tension splice joints of MPC trusses from residential structures. The hypothesis being tested is that wind and impact loads decrease the strength and change the stiffness of MPC joints. The different load scenarios for heel and tension splice joints are described in detail in Section 4.4 and 4.5, respectively.

The ultimate strength, ultimate deflection (defined as the deflection at the ultimate load), and stiffness values from the experimental groups are compared to the corresponding property values in the control group. The control group varies for different experimental groups.

For heel joints, experimental groups subjected to dynamic compressive loads are compared to the group subjected to a compressive static ramp load. Conversely, experimental groups subjected to dynamic tension loads are compared to the group which experienced a tension static ramp load.

Since all tension splice joints were tested in tension, only one control group exists. All tension splice joint experimental groups were compared to the tension static ramp load group.

A t-test procedure is used to comparing group values. For the statistical analysis, it is assumed that the variances for the two groups are not equal and a

95% confidence interval is used. Interpretation of p-values is described in Section 4.6.

The coefficient of variation (COV), defined as the standard deviation divided by the group average, is listed along with the corresponding property for each test. The COV is presented to indicate the amount of spread in a data set. Low COV values, less than 5%, indicate that the data does not vary significantly from the average, while high COV values, greater than 40%, indicate that the data has considerable variability.

Table 4-1 and Table 4-2 list the tests examined in this study with the sample size for heel joints and tension splice joints, respectively.

Table 4-1: Heel joint tests

Heel Joint Test	Sample Size
Control Group (Compression Static Ramp Load)	10
Control Group (Tension Static Ramp Load)	10
Hurricane Wind Load Simulation in Compression	10
Hurricane Wind Load Simulation in Tension	10
Double Design Impact Load in Tension	10

Table 4-2: Tension splice joint tests

Tension Splice Joint Test	Sample Size
Control Group (Tension Static Ramp Load)	9
Accelerated Ramp Load	10
Double Design Impact Load	10
Ultimate Impact Load	10

The sample size listed in these tables indicates how many joints were subjected to the corresponding test, but does not indicate how many property values were collected. The sample size was not always the number of property values collected because, for some joints, problems with the data collection equipment made calculation of some properties impossible. Some joints failed in the middle of the test which also decreased the number of property values available.

For the tension splice joint control group, one joint was inadvertently destroyed before the test could begin, causing only 9 samples to be available for comparison.

Specific gravity and moisture content were measured according to ASTM D2395-93 (Method A, Volume by Measurement) and ASTM D4442-92 (Method A, Oven Drying Primary), respectively. The MOE was measured before the lumber was cut into smaller pieces using an E-computer system (Metriguard, Model 390). The E-computer can determine the MOE of a member if given the length and cross section dimensions by measuring the natural frequency and mass of the member.

4.3 Apparatus

All joints were tested using a horizontal trapezoid shaped testing frame developed by Gupta and Gebremedhin (1990). This frame was used because its shape allows many different joint configurations to be tested. The forces were

applied to the joints using a Materials Testing System (MTS) hydraulic actuator which had an 11 kip capacity. Figure 4-2 shows the horizontal testing frame, MTS hydraulic actuator, and support device for a heel joint test.

The set-up used to test tension splice joints is simpler because no complex support conditions were modeled. Figure 4-3 shows the testing frame set up to test a tension splice joint.

Applied force and joint deflection was measured and recorded. The force applied to the joint was measured by 20 kip capacity Sensotec load cells. For the heel joints, a load cell was placed between the MTS hydraulic actuator and the top chord member of the joint. Another load cell was placed on the bottom chord member of the heel joint. The load cell on the bottom chord was used to compare and check the readings from the top load cell. For tension splice joints, only one load cell was used, placed between the MTS hydraulic actuator and the end of the tension splice joint.

For this project, heel joint tests are described by the type of force exerted on the top chord of the heel joint. The top chord is identified in Figure 4-4 and Figure 4-5 for a compression test and a tension test, respectively.

Joints which are tested with compression forces on the top chord member and tension forces on the bottom chord are referred to as compression tests. The setup for a compression test on a heel joint is shown in Figure 4-4.

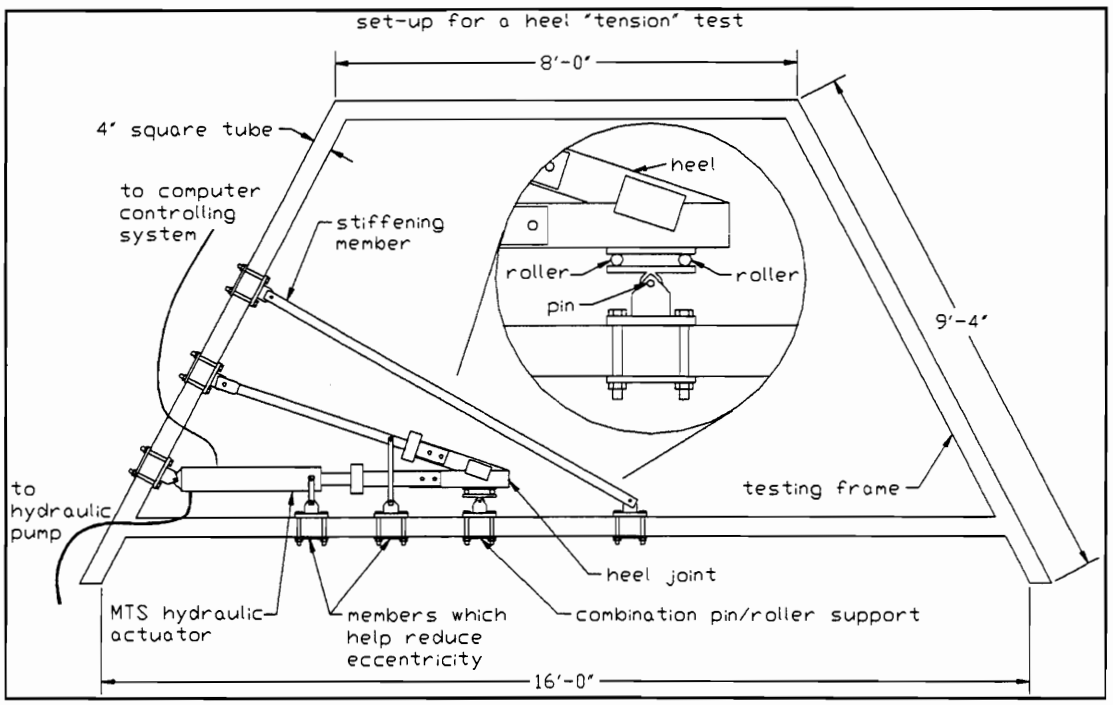

Figure 4-2: Trapezoid testing frame with heel joint and support

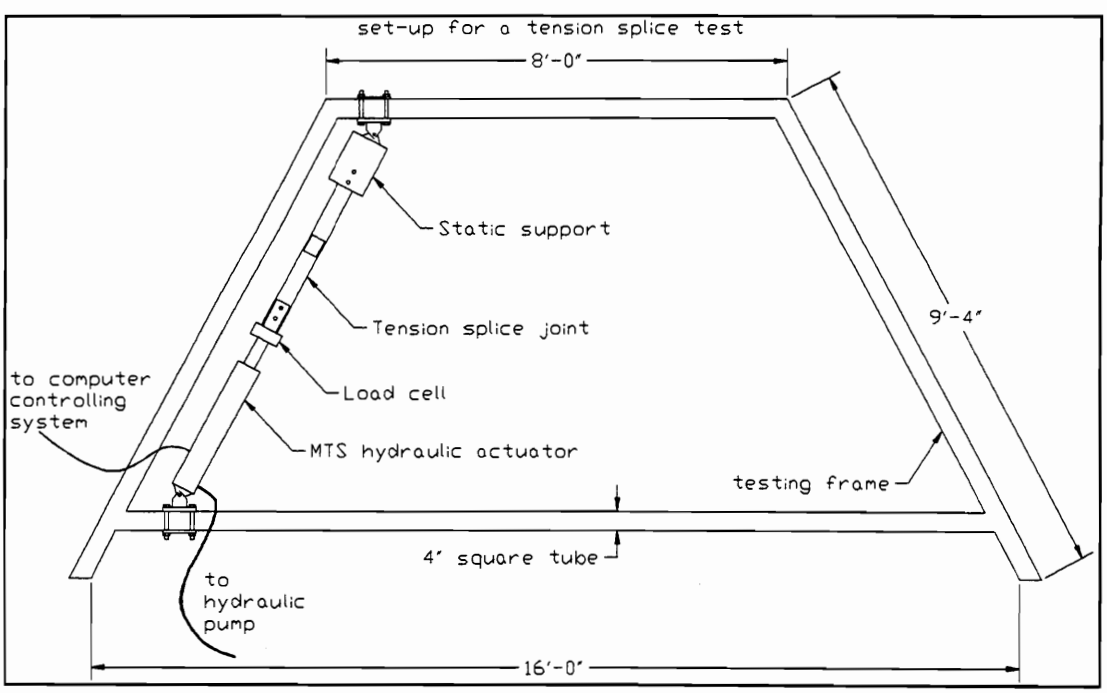

Figure 4-3: Trapezoid testing frame with tension splice joint setup

Joints which are tested with tension on the top chord and compression forces on the bottom chord member are referred to as tension tests. The setup for a tension test on a heel joint is shown in Figure 4-5.

Displacement was measured using direct current linearly variable differential transducers (LVDT). For the heel joint tests, one LVDT measured the slip deflection between the two members while another LVDT measured the opening deflection of the joint. The LVDT configuration for a heel joint test is shown in Figure 4-4 and Figure 4-5 for a compression test and tension test,

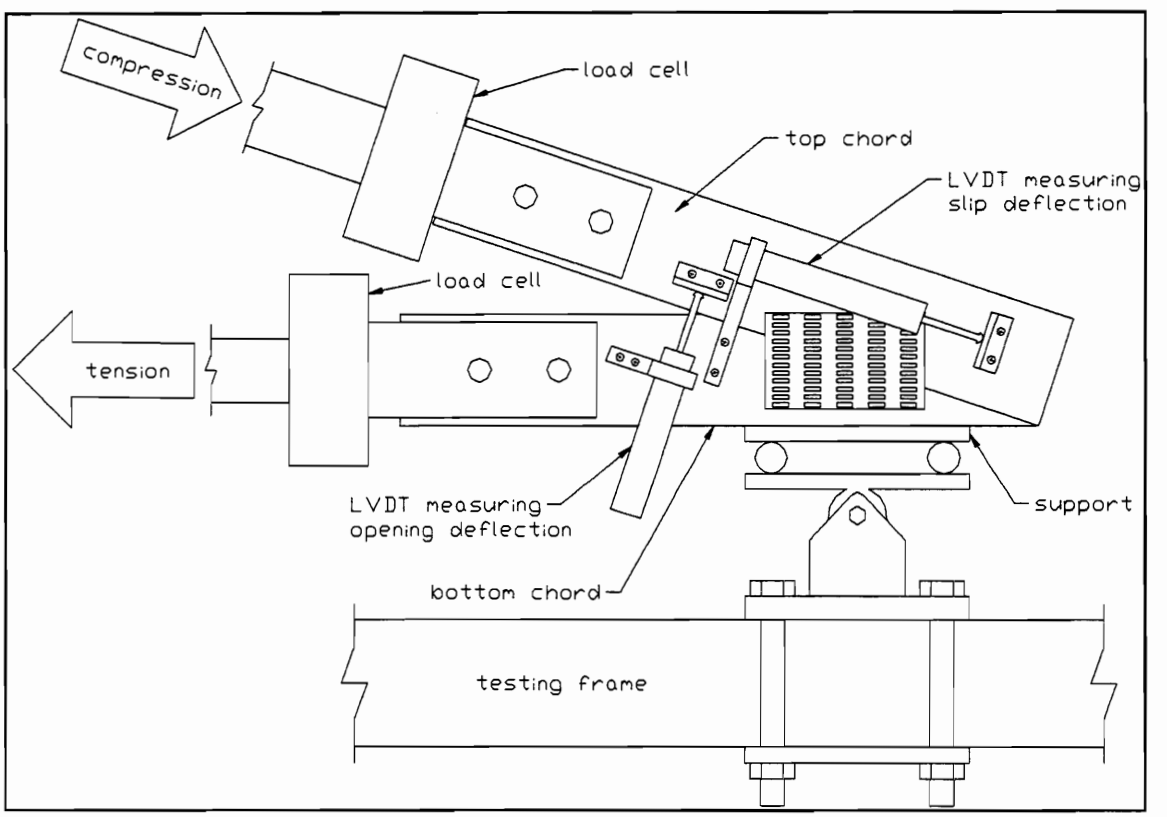

Figure 4-4: LVDT configuration for a heel joint test in compression

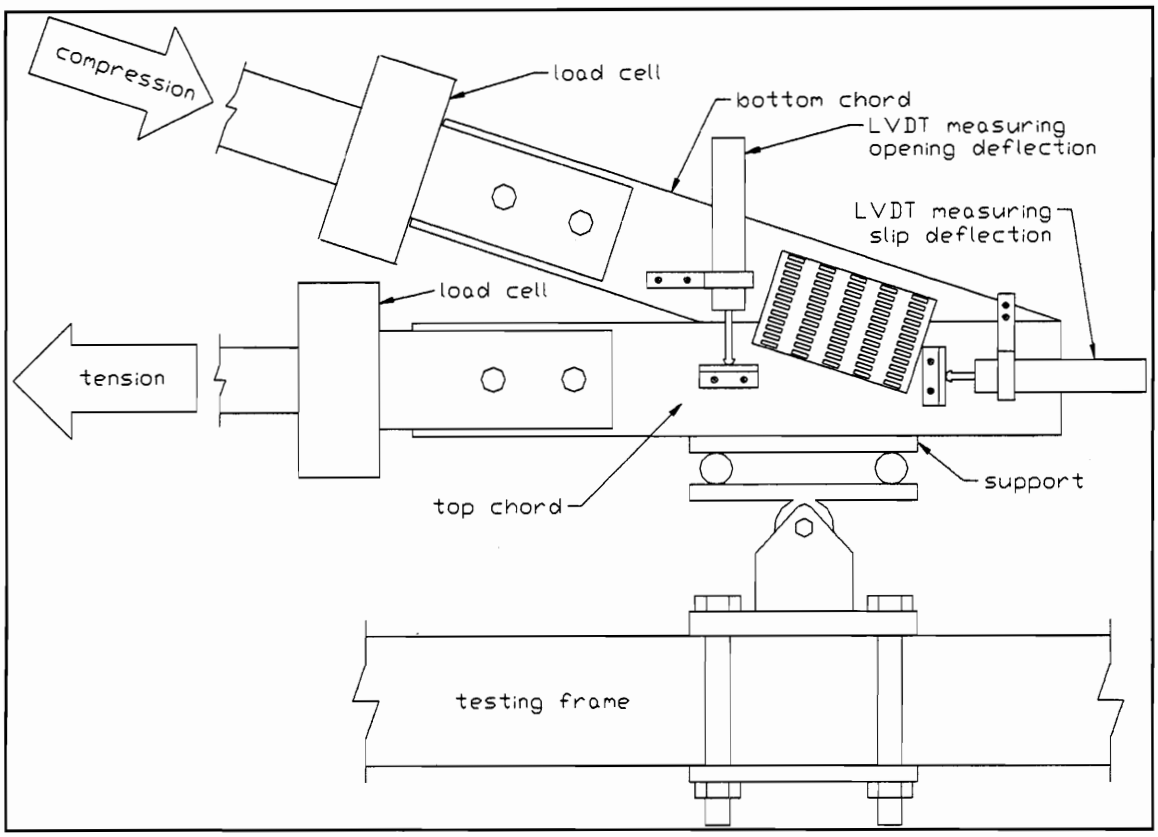

Figure 4-5: LVDT configuration for a heel joint test in tension

respectively. For this project, slip deflection is defined as the distance the top chord moves with respect to the bottom chord measured in the direction of the top member. The opening deflection measures how much the joint members rotate towards or away from each other.

For the tension splice joint tests, one LVDT was placed on either side of the metal plate to measure deflection between the two members of the joint as shown in Figure 4-6.

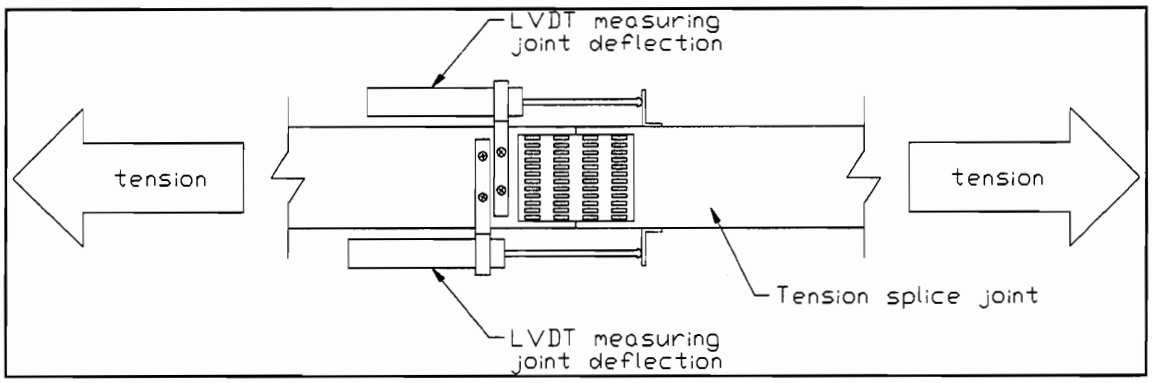

Figure 4-6: LVDT configuration for a tension splice joint test.

The load cells and LVDTs were connected to an analog to digital card, which was in turn connected to a personal computer with a 80486 processor. The load cell which was placed between the joint and the MTS hydraulic actuator was connected to an MTS 403.11 controlling unit. The controlling unit was then connected to the analog to digital card. The function of the MTS 403.11 controller was to ensure that the proper force was being applied to the joint. The MTS controller receives two input voltages. One voltage comes from the load cell, which indicates the actual force in the joint, and the second voltage comes from the computer, which indicates the desired force in the joint. The computer calculates the difference between the two voltages and sends an adjusted voltage to the MTS hydraulic actuator. The adjusted voltage causes the actual force in the joint to change to the desired force ordered by the computer. Then the MTS controller passes the voltage from the top load cell to the computer to be recorded. These connections are shown in Figure 4-7.

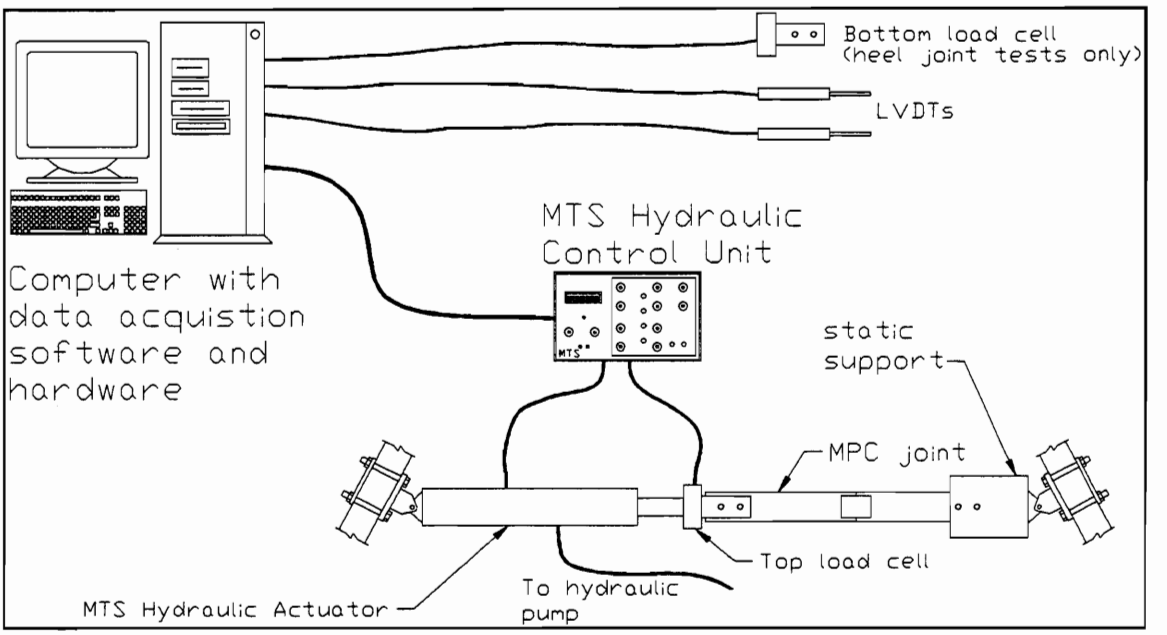

Figure 4-7: Schematic of the testing set up

Workbench software from Strawberry Tree Incorporated (1995) was used to record data and create output voltages for the MTS controller. The output voltages were determined in two ways. For most cases, a voltage is written as a function of time. For example, a ramp load was calculated by multiplying the time by a constant slope. Some tests required a different load generating procedure. In tests with complex dynamic loads, load values were predetermined and saved in an ASCII text file. These values were read by the software and output to the MTS controller. Output voltages from the LVDTs and load cells were displayed along with the corresponding deflection and load values during the test. The deflections and load values were recorded as an ASCII text file.

4.4 Heel Joint Load Scenarios

Heel joints were tested using five different loading conditions: 1) a static compression ramp load which serves as the control group for dynamic tests in compression, 2) a static tension ramp load which serves as the control group for dynamic tests in tension, 3) a hurricane wind compression load simulation 4) a hurricane wind tension load simulation, and 5) a double design impact load in tension. The test set-ups for all heel joints are shown in Figure 4-4 and Figure 4-5.

4.4.1 Static Ramp Load

For this project, heel joints tested with static ramp loads are used as the control group. Results from the static ramp load groups are compared to the results from the experimental groups.

4.4.1.1 Compression Static Ramp Load

A group of ten heel joints was subjected to a compression static ramp load to establish a control group as shown in Figure 4-4. The end wall support is modeled as a simple roller support as shown in Figure 4-8.

A compressive static ramp load of 900 lb/min was applied to ten heel joints until failure occurred. This ramp load rate was chosen to cause failure in 5

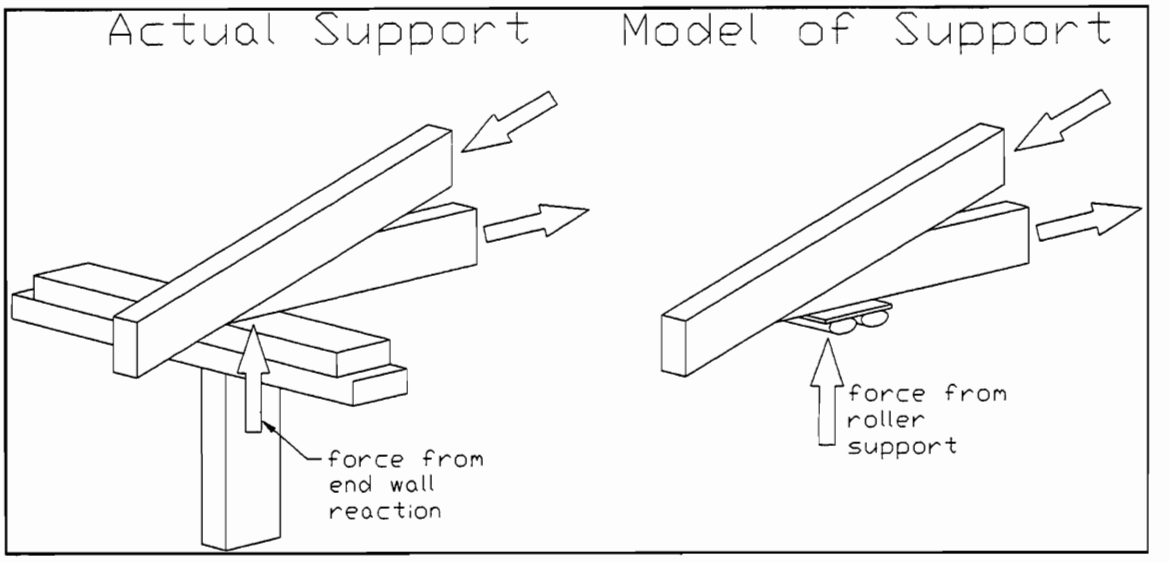

Figure 4-8: Heel joint support by end wall and the model used here for compression tests

to 10 minutes. This time to failure is used to approximate the time to failure used by Kent (1995) and Freilinger (1998). This project assumes that a joint which fails in 5 to 10 minutes produces static results. Data from LVDTs and load cells were collected and recorded twice every second.

4.4.1.2 Tension Static Ramp Load

A group of ten heel joints was subjected to a tension static ramp load to establish a control group as shown in Figure 4-5. The tie down support is modeled as a simple roller support as shown in Figure 4-9.

A truss system, loaded by high winds, relies on truss tie down connectors to prevent the roof from being lifted off the support walls. For this project, a Simpson Strong-Tie connector is modeled as shown in Figure 4-9.

The roller support used in the actual tests is placed in the approximate position the Strong-Tie connector would contact the top of the heel joint. It is possible that a heel joint supported with a Simpson Strong-Tie connector would not behave precisely as the model used here.

Differences include support stiffness, deflection constraint, and support friction. The roller support used in the model is very stiff in the direction of the force, but the connector is only made of light gauge metal, which makes it less stiff.

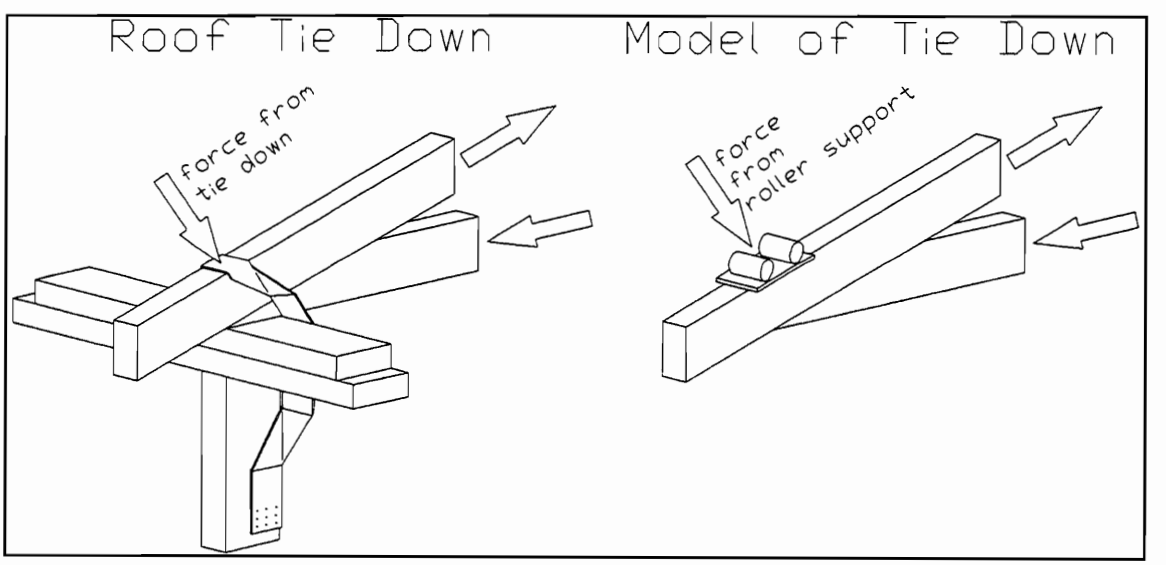

Figure 4-9: Heel joint Simpson Strong-Tie connector and the model used here for tension tests

The actual heel joint support condition may also restrain the movement of the joint differently because of the presence of the end wall. Finally, the roller support device has very little friction, while the Strong-Tie connector has some stiffness in the direction perpendicular to the reaction force.

While these differences may affect the behavior of the joint, actual Simpson Strong-Tie connectors were not used because this project is focused on the behavior of the joint, not the behavior of heel-connector systems.

A static tensile ramp load of 900 lb/min was applied to ten heel joints until failure occurred. This ramp load rate was chosen to cause failure in 5 to 10 minutes. Data from LVDTs and load cells were collected and recorded twice every second.

4.4.2 Hurricane Wind Load Simulation

Hurricane wind load simulation tests were performed in three different stages: the beginning stage, the wind stage, and the ending stage. During each stage, values from the LVDTs and load cells were recorded. The dead load stiffness and the design load stiffness is measured during the beginning ramp load and during the ending ramp load. The dynamic deflection is measured during the wind load. These properties are shown in Figure 4-10.

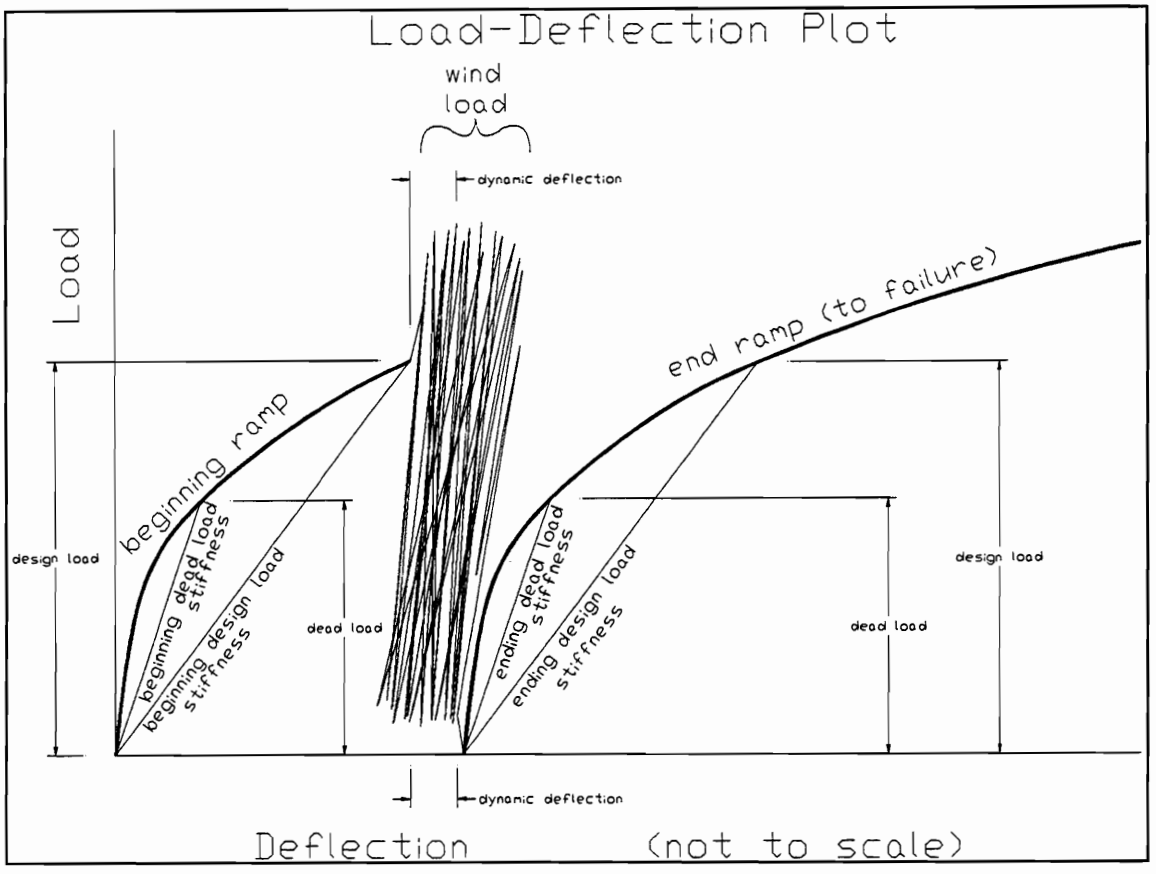

Figure 4-10: Graphic representation of the calculated stiffnesses and the dynamic deflection for wind simulation tests

During the beginning stage, a ramp load was applied to the heel joint at a rate of 900 lb/min. When the load in the joint was equal to the design load (1/3 of the average ultimate load from the static tests), the ramp was stopped. This stage was used to determine the beginning design load and beginning dead load stiffnesses. (The beginning design load stiffness is the stiffness of the joint before the wind load simulation is applied measured at the design load of the individual joint. The beginning dead load stiffness is the stiffness of the joint

before the wind load simulation is applied measured at the dead load. For heel joints, the dead load is approximately 1465 lb.)

During the wind stage, the hurricane wind load simulation was sent from the computer memory to the MTS controlling system. The wind stage was the dynamic portion of the loading and lasted for approximately 2 hours 15 minutes for each joint. The purpose of this stage was to apply the hurricane loading and measure the amount of dynamic deflection.

The difference between the deflection before and after the wind load is called the dynamic deflection here. The before deflection reading is taken immediately before the dynamic load is applied, while the after deflection reading is taken immediately after the dynamic load ends. Both of these deflection readings are taken at the design load, which is the beginning and ending load of the wind load simulation. (The before and after deflection readings taken for the impact tests are also taken immediately before and after the dynamic load, but the impact tests start and end at the dead load. Therefore, the deflection readings are taken at the dead load for the impact tests.)

A dynamic deflection of zero means that the deflection caused by the dynamic load is completely recovered after the dynamic load is removed. Therefore, the joint behaved elastically. A dynamic deflection greater than zero means that not all the deflection caused by the dynamic load was recovered

after the load was removed, which means the joint behaved inelastically. Large dynamic deflections indicate the wind load had a perceptible effect on the joint.

The ending stage begins after the wind load simulation finishes. After the load returns to zero, the ramp load algorithm is restarted at a rate of 900 lb/min and continued until failure occurs. The purpose of this stage is to determine the ultimate load, ultimate deflection, ending design load stiffness, and ending dead load stiffness. (The ending design load stiffness and ending dead load stiffness are both measured after the dynamic load is removed. The ending design load stiffness is measured at the joints design load, while the dead load stiffness is measured at the dead load (approximately 1465 lb).

4.4.2.1 Hurricane Wind Compression Load Simulation

For the hurricane wind simulation tests in compression, a compression ramp load is used during both the beginning and ending stages. The compressive wind load simulation values ranged from approximately 1600 lb. to 2150 lb. Figure 4-11 is a graphical representation of the three loading stages. Only a small part of the hurricane loading function is included here because of the extremely large size of the full plot.

Figure 4-12 shows the range and distribution of the wind simulation compressive load in the form of a histogram.

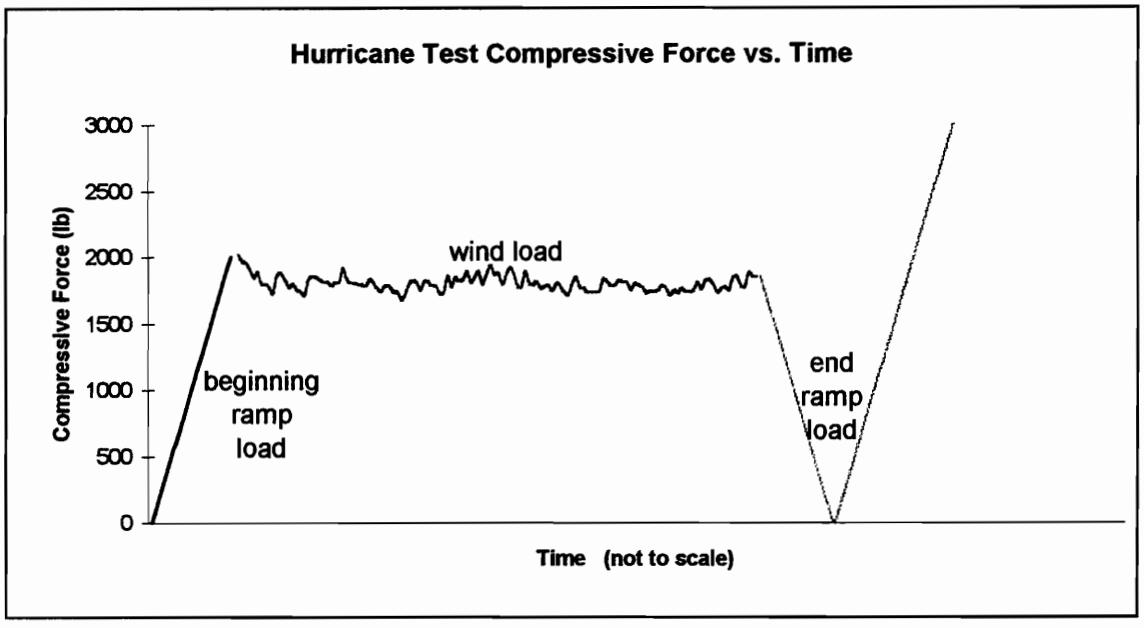

Figure 4-11: Hurricane compressive load function

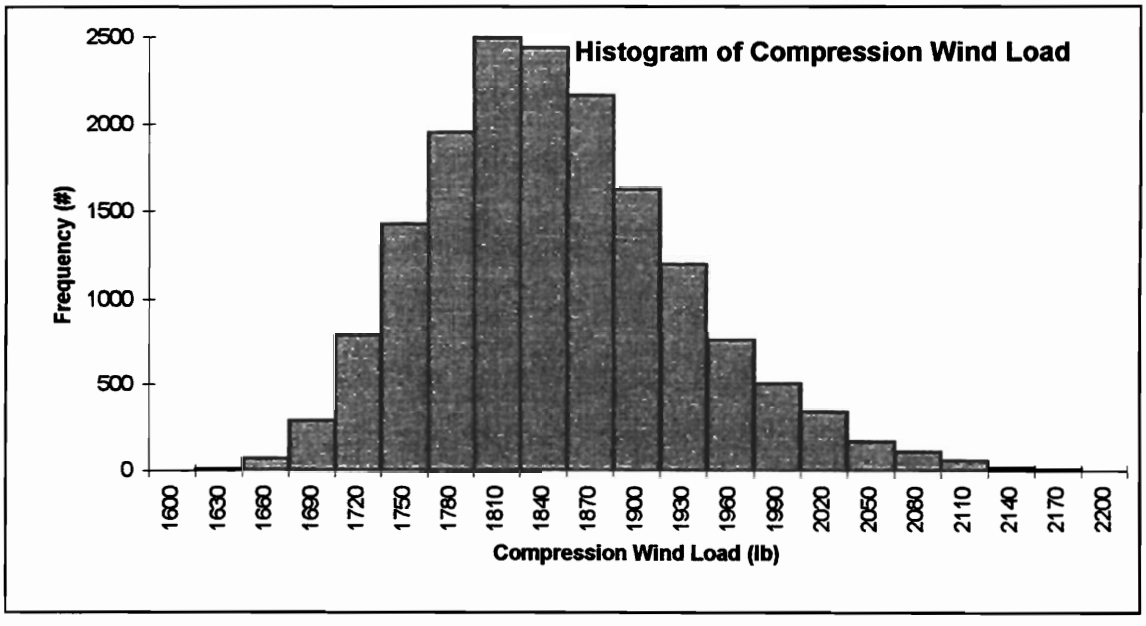

Figure 4-12: Histogram of the compressive wind load simulation

4.4.2.2 Hurricane Tension Load Simulation

For the hurricane wind simulation tension tests, a tension ramp load is used during both the beginning and ending stages. The tension wind load simulation values ranged from approximately 50 lb. to 3900 lb. Figure 4-13 is a graphical representation of the three loading stages. Again, only a small part of the hurricane loading function is included in the plot.

Figure 4-14 shows the range and distribution for the tension wind simulation load in the form of a histogram. Comparing the histograms for the tension and compression wind load simulation tests in Figure 4-12 and Figure 4-14, respectively, it can be seen that the tension test has a higher maximum load and a lower minimum load. The average force for the tension load wind

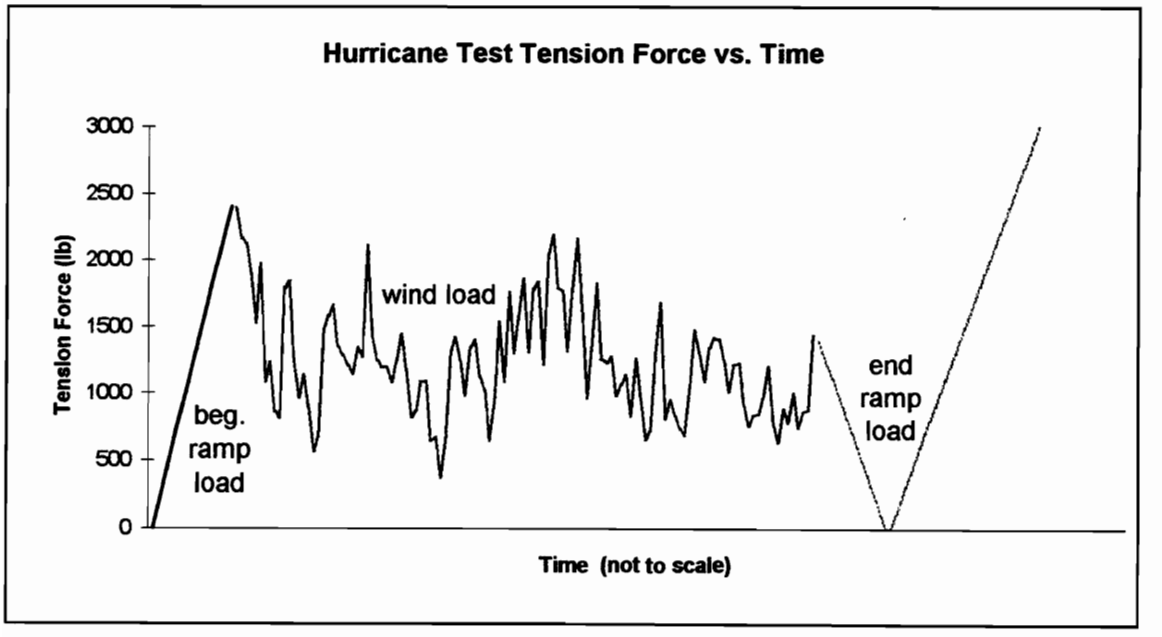

Figure 4-13: Tension hurricane load function

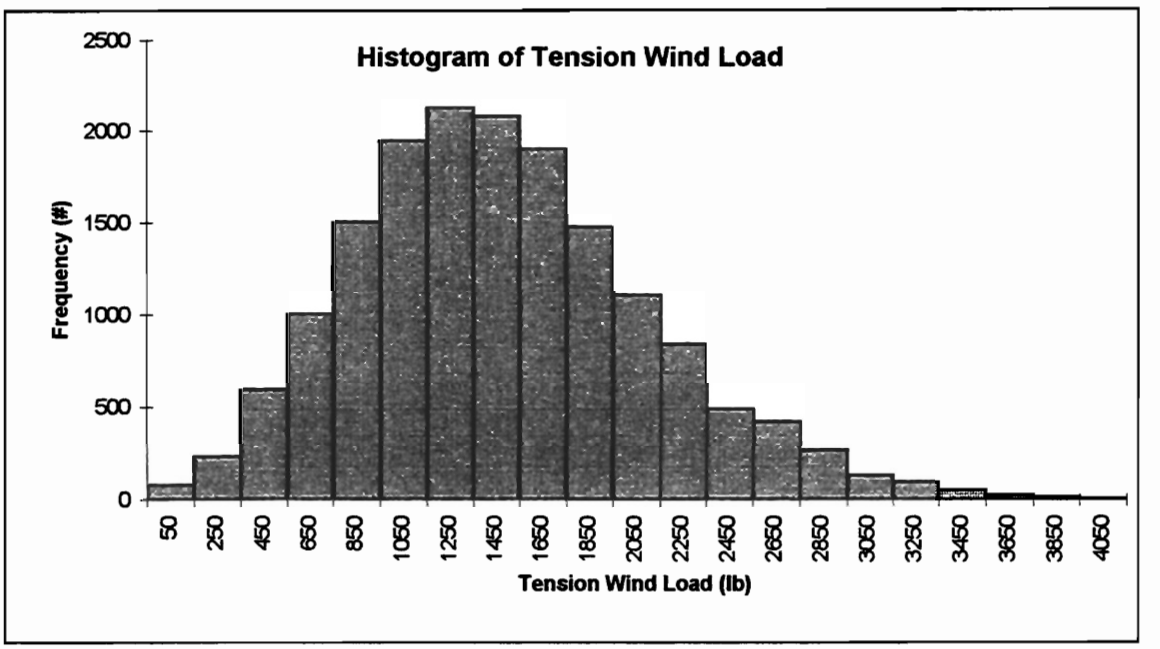

Figure 4-14: Histogram of the tension wind load simulation

simulation is slightly lower than the average load for the compression load wind simulation, but overall, the tension load simulation is probably a more extreme test because of the large load range. This load range makes the tension test more dynamic and potentially more damaging to the heel joint.

4.4.3 Double Design Impact Load

The properties measured during the double design impact load tests on heel joints are shown graphically in Figure 4-17. The impact load is applied only in tension for heel joints because insufficient heel joints existed from the same batch to perform the test in both tension and compression. The impact tests

were performed in tension because the results from the compression load wind simulations showed little difference when compared to the static group results. It was believed that the tension load wind simulation results would be more comparable to impact load results.

The dynamic load used for this test is based on design factors found in the AFPA (1991). The AFPA defines an impact load as a loading with a duration of one second or less. It allows design values to be multiplied by 2.0 for impact loads. The AFPA (1991) states, "The impact load duration factor shall not apply to connection design values." Other duration factors apply to wood connections as seen in Table 7.3.1 of the AFPA (1991) which includes C_D in the calculation of design values and footnote 1 of that same table, which states, "the load duration factor, C_D, shall not exceed 1.6 for connections." The AFPA (1991) specification also states, "Load duration factors, $C_D \leq 1.6$, apply to design values for connections, except when connection capacity is based on design of metal parts" and "When the capacity of a connection is controlled by metal strength, rather than wood strength, allowable metal strength shall not be multiplied by the adjustment factors in this Specification."

Previous researchers, such as Vatovec, et al. (1996) and Hayashi et al. (1980), observed failures in the metal plates of some MPC joints, while different joints failed in other modes, such as tooth withdrawal. According to the AFPA (1991), joints which failed in the metal plate are given a C_D value of 1.0, while

joints which failed in the wood are given C_D values according to the type of load. (Load types with a longer duration of maximum load receive lower C_D values.)

Although the AFPA (1991) guidelines, described above, are not applicable the joints being tested, the AFPA (1991) is still used to define "impact" for tests on MPC joints. This is done because the purpose of this project is not to determine if the C_D factor used on MPC connections by the AFPA is suitable. The AFPA (1991) is used only as a guide to determine duration and magnitude of the "impact" tests performed for this project.

The maximum value of the spike is set at double the design value. The design value is found by dividing the average ultimate strength from the static test heel joint group by 3.0. For heel joint double design impact load tests, the peak load is 4793 lb. The peak load is double the design value. (The design value is the average ultimate strength from the static heel joint group divide by 3.0.) Figure 4-15 shows the load versus time plot for the double design impact test.

The AFPA (1991) defines an impact load with a duration of 1 second (or less), but does not give details on how long the load takes to go from the minimum to the maximum value. This time is referred to as the change time in this project. Selecting an appropriate change time is important because it can potentially alter the effects of the impact load. If the change time is very long, the spike becomes a static ramp load instead of a dynamic load. If the change time is very short, the joint could be affected more by the rapid change than by

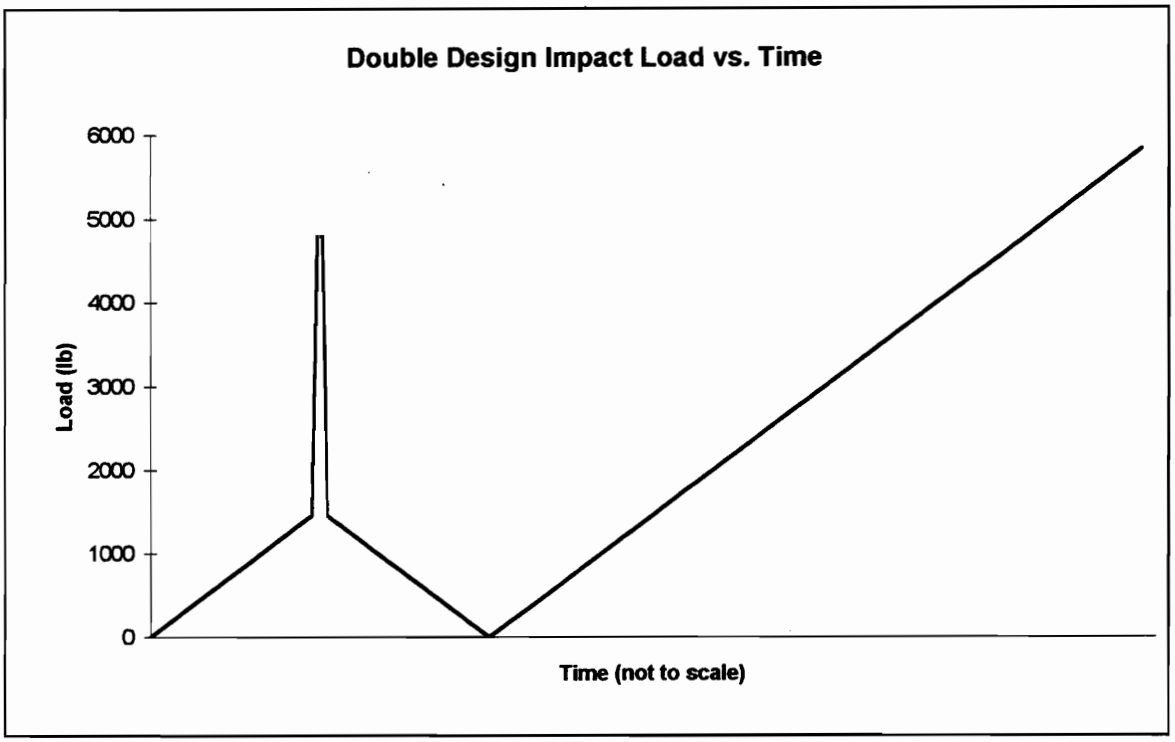

Figure 4-15: Load versus time plot for double design impact load test on heel joints

the maximum value of the load spike. It was hypothesized that a one second change time is short enough to keep the load from acting static, but not so short that it dominates the behavior of the joint.

During the initial stage of the test, the joint is loaded to 1465 lb., which simulates the dead load, at a rate of 900 lb/min. This portion of the test is used to determine the beginning dead load stiffness.

The load is then spiked from dead load to double the design value, or 4793 lb. This takes one second. The load is held at double the design load for one second, then it returns to the dead load in one second. Although the entire

load spike takes three seconds, the maximum value of the spike is held only for one second. The deflection readings taken immediately before the impact load is applied and immediately after the impact load is finished are used to determine the dynamic deflection. The dynamic deflection is the deflection reading immediately after the impact load is finished minus the deflection reading immediately before the impact load is applied.

When the impact load is finished, the joint is unloaded and a static ramp load (900 lb/min) is applied until failure occurs. The ending stage of the impact test is used to determine the ultimate load, ultimate deflection, ending design load stiffness, and ending dead load stiffness. A magnified view of the spike portion of the impact load is shown in Figure 4-16.

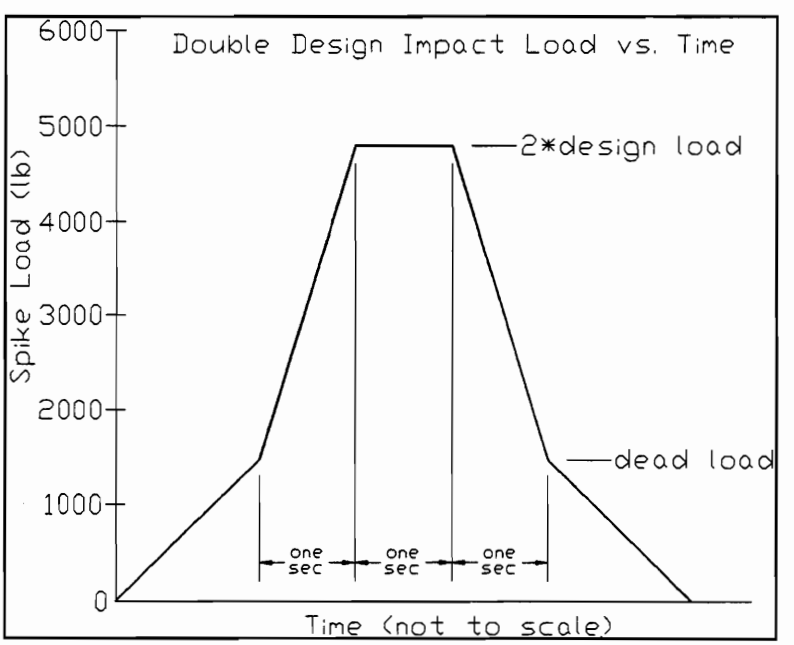

Figure 4-16: Magnified view of spike portion of double design impact load for heel joints

4.5 Tension Splice Joint Load Scenarios

Tension splice joints were tested using four different loading conditions: 1) a static ramp load in tension which serves as the control group, 2) an accelerated ramp load in tension, 3) a tension impact to double the design value, and 4) a tension impact to the ultimate strength. The test set-up for all tension splice joints is shown in Figure 4-3.

4.5.1 Static Ramp Load

A tension static ramp load of 900 lb/min was applied to nine tension splice joints until failure occurred. Ten joints were assigned to this group, but one was inadvertently destroyed before the test was started. The static ramp load group is used as the control group, to which all other tension splice joint groups are compared.

The ramp load rate was chose to cause failure in 5 to 10 minutes. Data from LVDTs and the load cell were collected and recorded twice every second.

4.5.2 Accelerated Ramp Load

In the accelerated ramp load tests, a tensile ramp load which linearly increases at a rate of 9000 lb/min was applied to ten tension splice joints until failure occurred. The ramp load rate was selected to cause failure in

approximately 30 to 60 seconds. The accelerated ramp load was performed to determine if "static" results could be attained in a shorter period of time. Data from LVDTs and the load cell were collected and recorded four times every second. A higher data recording rate is used for the accelerated ramp load tests to ensure that enough data points were recorded to accurately describe the load-deflection behavior of the joints. (A faster rate was not used because the computer recording device was recording data points as fast as possible without the risk losing data.) If the standard recording rate of two points per second was used for the accelerated tests, it is possible that not enough points would be recorded to accurately plot the load-deflection relationship.

4.5.3 Double Design Impact Load

The double design impact load for tension splice joints is based on design factors in the AFPA (1991). As described in Section 4.4.3, the double design impact load is double the design load. (The design load is 1/3 of the average ultimate strength from the static ramp load tests.) For tension splice joint the design load is approximately 2275 lb, which makes the double design impact load 4549 lb.

The dead load stiffness is measured before and after the impact load is applied, but the design load stiffness is only measured after the impact load. The beginning design load stiffness can not be measured because the beginning ramp load stops at the dead load. A graphical presentation of the beginning

dead load stiffness, ending dead load stiffness, ending design load stiffness, and the dynamic deflection is shown in Figure 4-17.

The impact loading is three seconds long to match the duration of the impact load used for the heel joint spike load test described in Section 4.4.3. The loading function is shown in Figure 4-18.

During the initial stage of the test, the joint is loaded to the dead load, 865 lb, at a load rate of 900 lb/min. (The dead load is determined by loading the

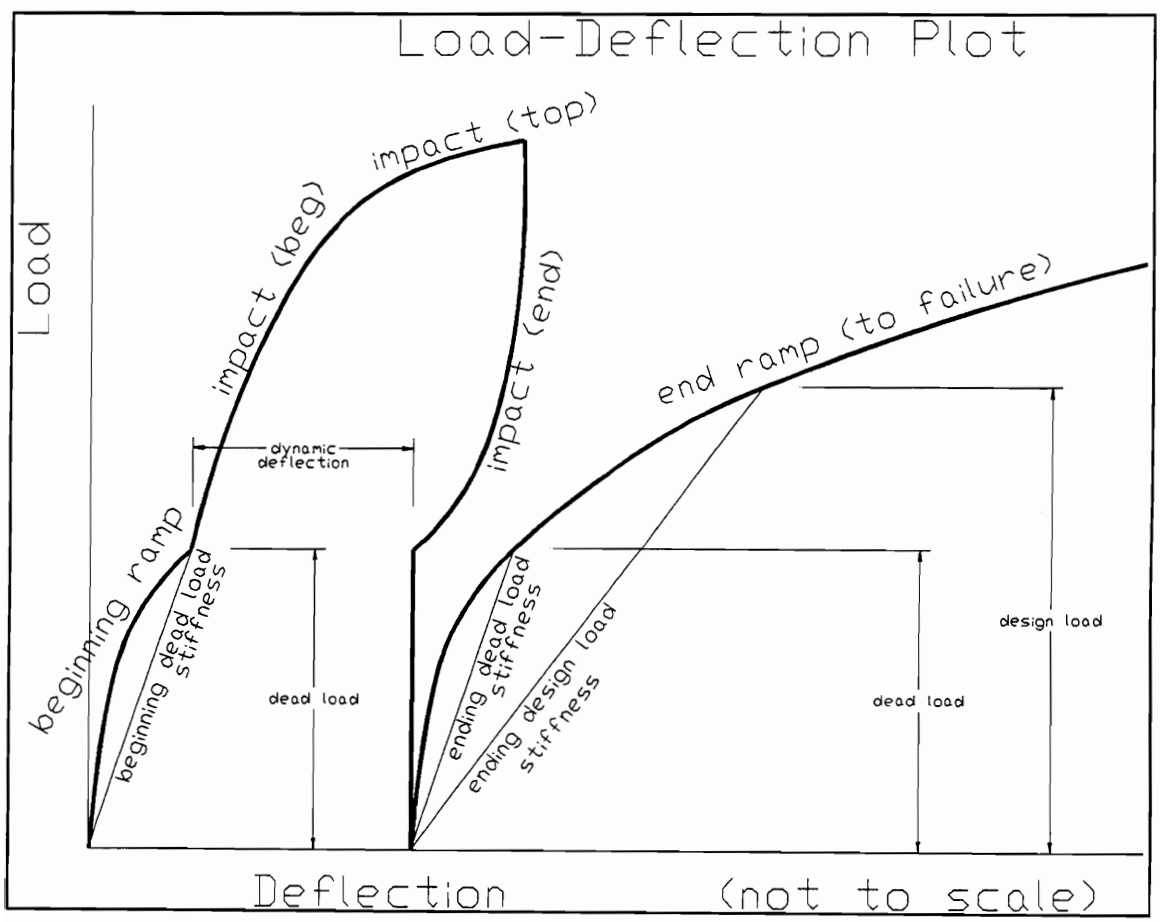

Figure 4-17: Graphic representation of the calculated stiffnesses and the dynamic deflection for impact load tests

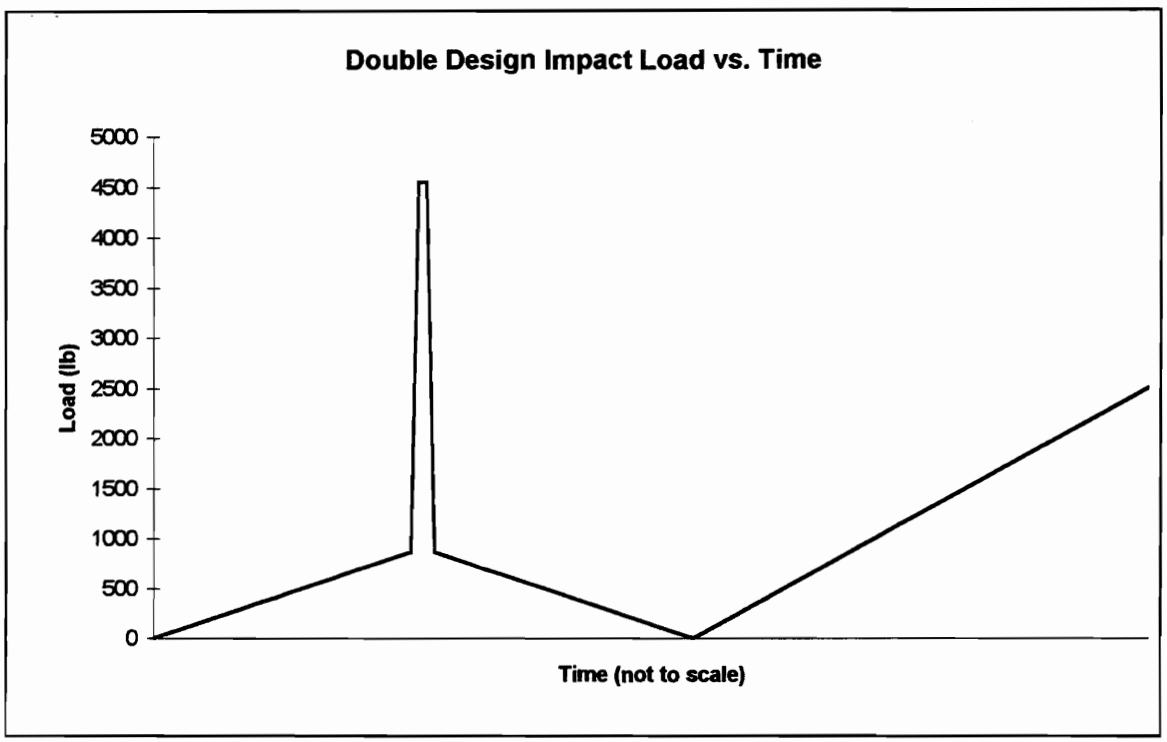

Figure 4-18: Load vs. time for double design impact load test on tension splice joints

upper chord of the Fink truss model with the dead load (20 lb/ft) in the SAP90 model and checking the force in the tension splice joint.) This portion of the test is used to determine the beginning dead load stiffness.

Then the load is spiked from dead load to double the design value. This takes one second. The load is held at double the design load for one second, then it returns to the dead load in one second. The deflection readings taken during the spike load are used to determine the dynamic deflection. The dynamic deflection was calculated by subtracting the deflection reading taken

immediately before the impact load was applied from the deflection reading taken immediately after the impact load finished.

When the impact load is finished, the joint is unloaded and a static ramp load (900 lb/min) is applied until failure occurs. The ramp load is continued until failure occurs. The ending ramp load section is used to determine the ultimate load, ultimate deflection, ending design load stiffness, and ending dead load stiffness.

A magnified view of the spike portion of the impact load is shown in Figure 4-19.

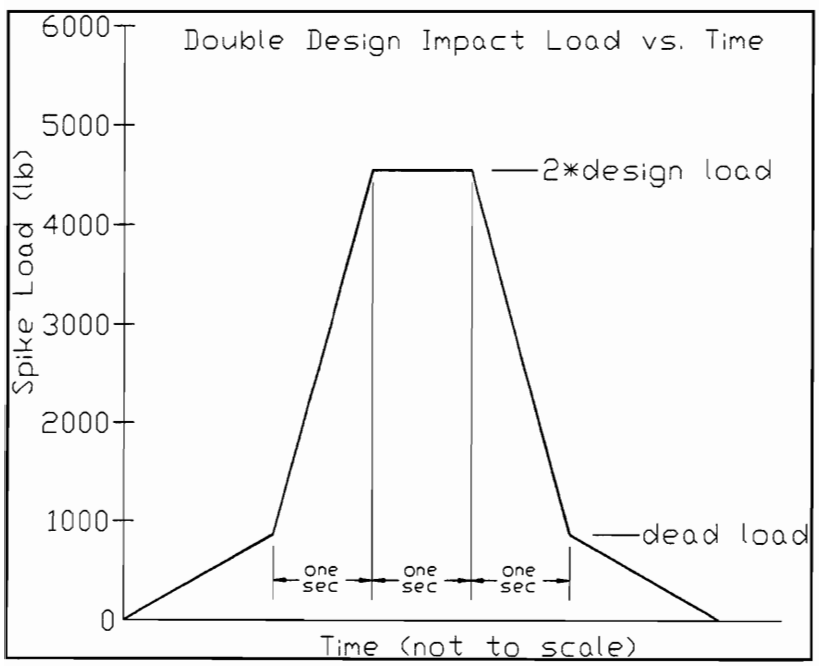

Figure 4-19: Magnified view of spike portion of double design impact load for tension splice joints

4.5.4 Ultimate Impact Load

The ultimate impact load is shown in Figure 4-20. The ultimate impact load test for tension splice joints is identical to the double design impact load test with two exceptions. First, the maximum load in the spike is 50% higher for the ultimate impact tests. Second, the load rate for the ultimate impact tests is also higher than the load rate for the double design impact tests (on tension splice joints). The load rate is higher in the ultimate impact tests because the load increases more in the same amount of time.

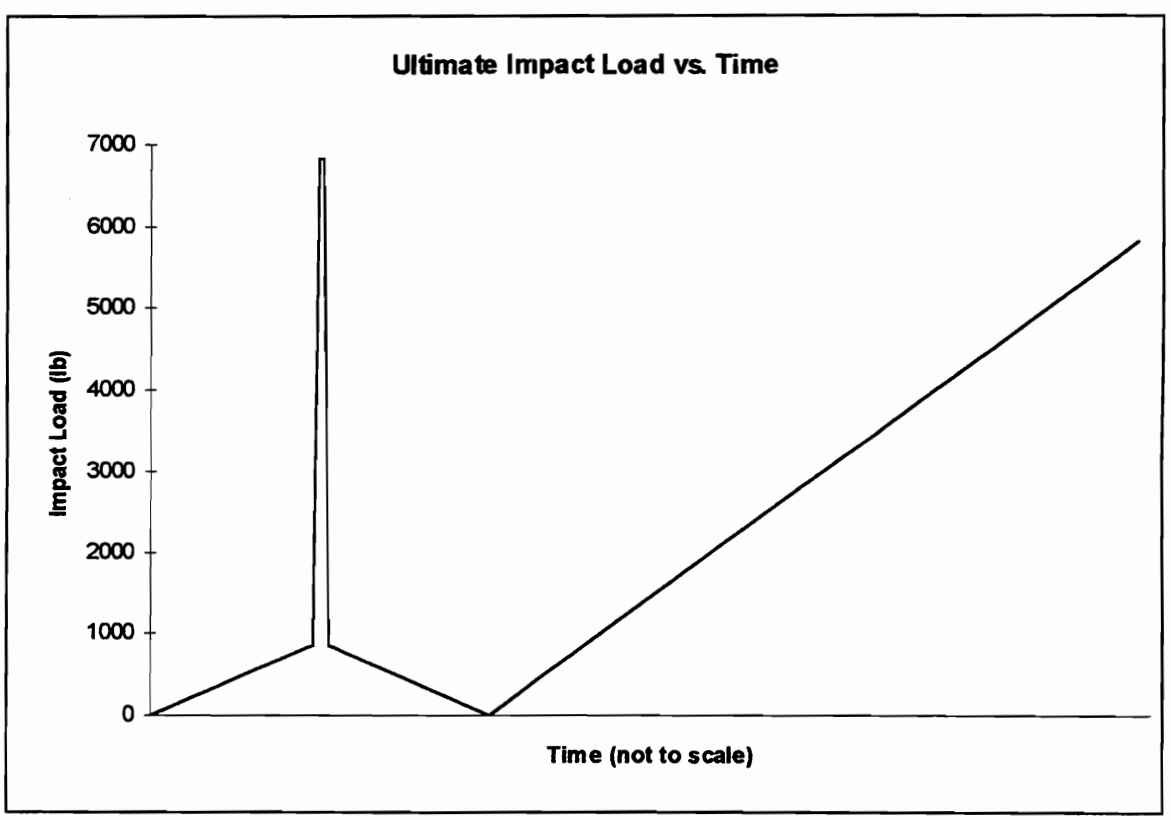

Figure 4-20: Load versus time for ultimate load spike test on tension splice joints

The ultimate load, 6824 lb., is the average ultimate strength found from the static ramp load tests on tension splice joints.

First, the joint is statically loaded up to the dead load value of 865 lb. at 900 lb/min, then the load is spiked to 6824 lb in one second, held there for one second, and then returned to the dead load in one second. (The dead load is determined by loading the upper chord of the Fink truss model in SAP90 with the dead load (20 lb/ft) and checking the force in the tension splice joint. The

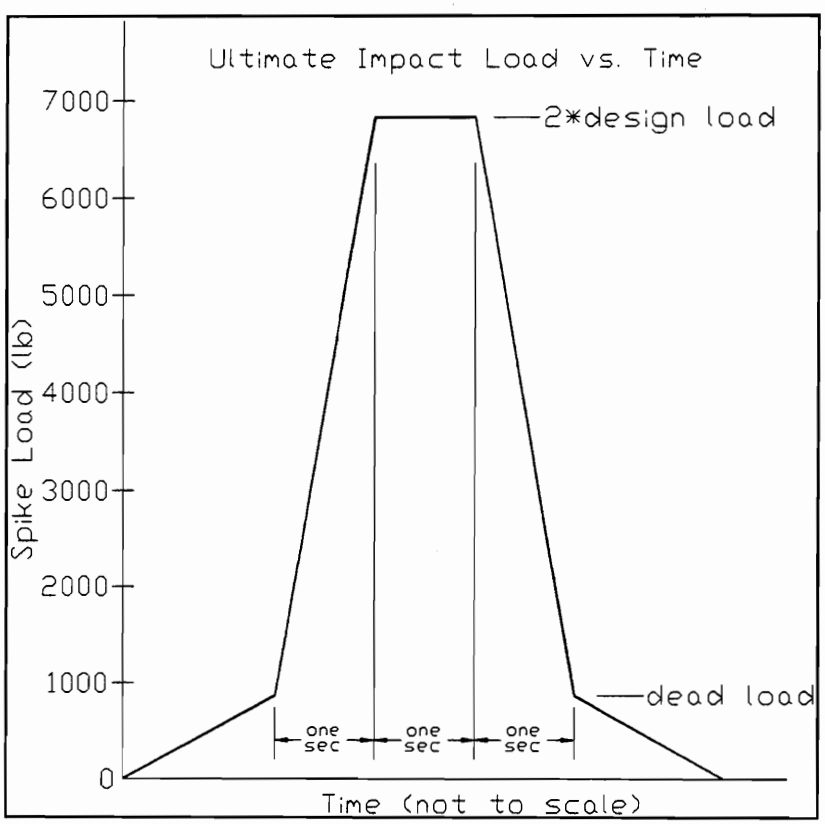

Figure 4-21: Magnified view of spike portion of ultimate impact load for tension splice joints

maximum value of the ultimate impact load was determined by averaging the ultimate strength values from the static ramp load tests on tension splice joints.) Then the joint is unloaded and a static ramp load (900 lb/min) is applied until failure occurs. A magnified view of the spike portion of the impact load is shown in Figure 4-21.

4.6 Statistical Analysis

A student's t-test procedure is used when comparing two groups. For the statistical analysis, it is assumed that the variances for the two groups are not equal and a 95% confidence interval is used.

The choice between using a one sided or a two sided p-value depends on the hypothesis set forward. When the goal is to determine if a difference between the experimental group and control group exists, a two-sided p-value is used. When the goal is to determine if the control group has either a higher or lower value than the experimental group, a one sided p-value is used. For ultimate strength and ultimate deflection, a one sided p-value is used because the goal of the comparison is to determine if the experimental strength and deflection values are decreased by the dynamic loading. For stiffness comparisons, a two sided p-value is used because the goal is to determine if the experimental group is different from the control group. This hypothesis was selected because the effect of dynamic loading on stiffnesses was unknown before the tests were performed.

A method to determine the number of samples required, given the approximate coefficient of variation, is described by ASTM D2915-94. Using an approximate coefficient of variation of 10%, from Gupta and Gebremedhin (1990), 18 samples are required to determine the lower 5% exclusion limit for a 95% confidence interval. Only 10 joints were used for each test here, so the lower 5% exclusion limit cannot be determined. This is acceptable because the purpose of this research is to determine the effects of wind and impact loading on metal-plate-connected joints, not to set statistical exclusion limits.

P-values from a t-test can be interpreted in two ways. The first method is to set a cut-off value and accept the hypothesis if the p-value is lower than the cut-off and reject it if the p-value if it is higher than the cut-off value. There are two problems with this approach which are described by Ramsey and Schafer (1997).

The first problem can be illustrated in the following example. Two p-values from two different tests are very close together, but the cut off falls between them. One hypothesis is rejected and the other is accepted even though they both have approximately the same evidence of a difference. In this way, using the cut-off method can lead to different conclusions based on very similar evidence.

The second problem can be seen if p-values from two different tests are both below the cut off, but one is much lower than the other. A p-value of 0.000001 is strong evidence of a difference, while 0.049 shows less evidence of

a difference. Both p-values could fall below a cut off of 0.05 and be "accepted" even though they provide very different amounts of evidence of a difference. In this way, using the cut-off method can lead to the same conclusion based on very different evidence.

The second way to interpret a p-value is by assigning a range of adjectives to p-values as shown in Figure 4-22 from Ramsey and Schafer (1997).

Care must be taken when using Figure 4-22 to describe p-values. The description must be presented with the magnitude of the p-value. This is important because stating that a p-value is "convincing" can be dangerous if the author's and reader's definitions of "convincing" are different. Presenting a combination of adjectives and p-values, the author is able to interpret the

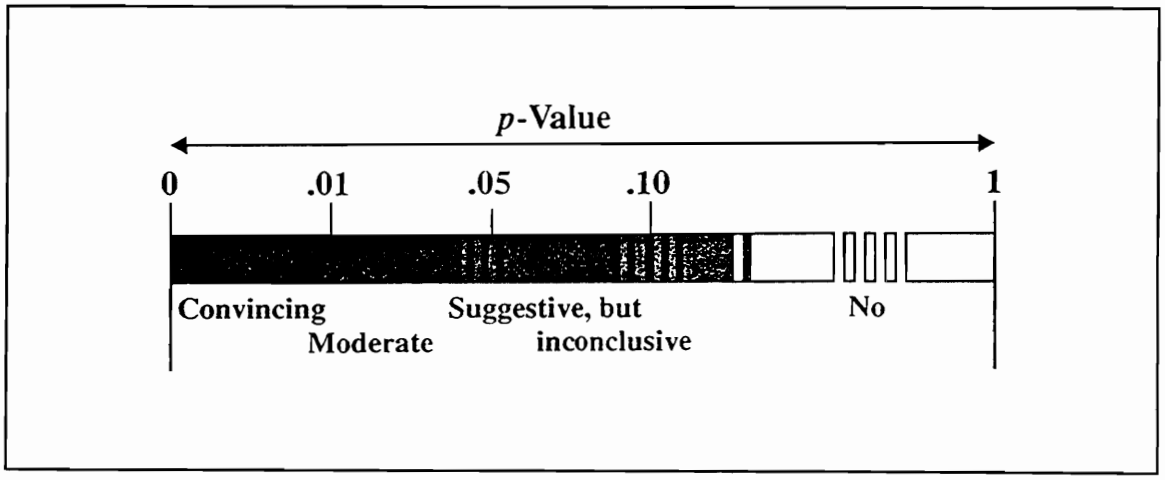

Figure 4-22: Adjectives which describe p-value magnitude

data, while giving the reader enough information to form a separate opinion about the magnitude of evidence.

For this project, Figure 4-22 is used to describe p-values instead of using the cut off method.

5. Results

5.1 General Heel Joint Results

All the properties of heel joints which were calculated or measured for this study are shown in Appendix B. Properties include ultimate strength, dead load stiffness, design load stiffness, ultimate deflection, specific gravity, modulus of elasticity (MOE), moisture content, growth rings per inch, grain orientation, late wood content, and failure mode. Along with the property, the respective coefficient of variation (COV) is listed. A brief summary of the heel joint test results is shown in Table 5-1.

Due to LVDT problems, some properties were deemed unusable, therefore the sample size can vary within a test group. For example, one of the samples in the compression static ramp load group resulted in useless deflection data, but the load data was not affected. This caused there to be one more

Table 5-1: Summary of heel joint results

Test Description	Sample Size	Average Strength (lb)	Average Specific Gravity	Average M. C. (%)	Average Wood MOE (x10^6 psi)
Tension Static Ramp Load	10	7,189	0.51	12.1	1.78
Compression Static Ramp Load	10	5,959	0.52	11.9	1.89
Hurricane Tension Simulation	10	7,807	0.52	12.1	1.81
Hurricane Compression Simulation	10	6,437	0.48	11.6	1.89
Double Design Impact Load	10	7,021	0.52	11.7	1.76

sample point for strength than for deflection or stiffness. For Table 5-1, the sample size is considered the number of ultimate strength values.

No dominant failure mode was identified for heel joints. Wood shear failure was seen 11 times, tooth withdrawal 15 times, and a combination of tooth withdrawal and wood shear 19 times. For one sample, both metal plates were sheared into two pieces along the interface between the two chords. Combinations involving plate failure occurred four times.

Wood shear failure occurs when the shear strength of the wood is lower than the applied shear stress. Wood shear failures usually occurred along the connection between the late and early wood.

Tooth withdrawal failures are caused by crushing of the wood in contact with the plate teeth and slight bending of the plate and the plate teeth. As the joint approaches failure, the wood in contact with the metal teeth deforms plastically due to large stress concentrations. As the hole the teeth sit in increases in size, the force holding the teeth in the wood decreases. Bending moment is induced in the plate because of eccentric loading between the tooth force and the plate force. The eccentricity is shown in Figure 5-1 as "d".

The bending moment in the plate causes it to bend slightly upward, partially withdrawing the outside teeth. The remaining teeth are required to resist even higher loads, which encourages tooth withdrawal to continue until failure occurs.

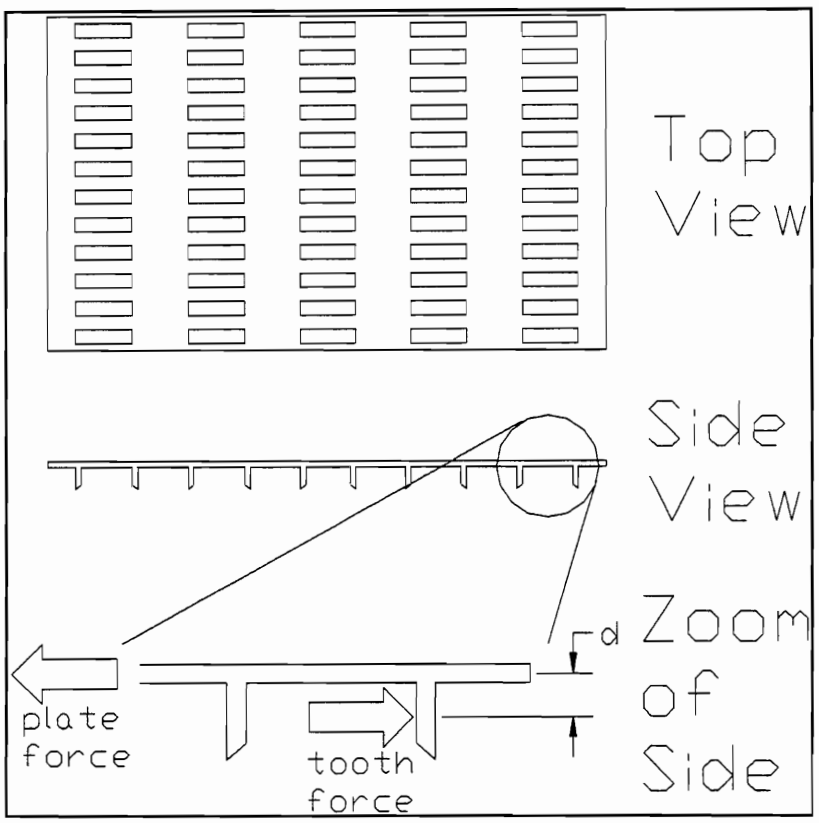

Figure 5-1: The distance "d" between the force in the plate and the force exerted on the teeth

Figure 5-2 and Figure 5-3 show examples of wood failure mode and tooth withdrawal failure mode, respectively, for heel joints. Gupta and Gebremedhin (1990) observed similar failure modes.

The load-deflection plots for heel joints exhibit non-linear behavior, as shown in Figure 5-4, which is typical of wood members and wood joints. In heel joints, the shape of the load-deflection plot is affected by the behavior of both the metal plate and the wood fibers. All heel joint load-deflection curves show the same general non-linear shape and are included in Appendix C.

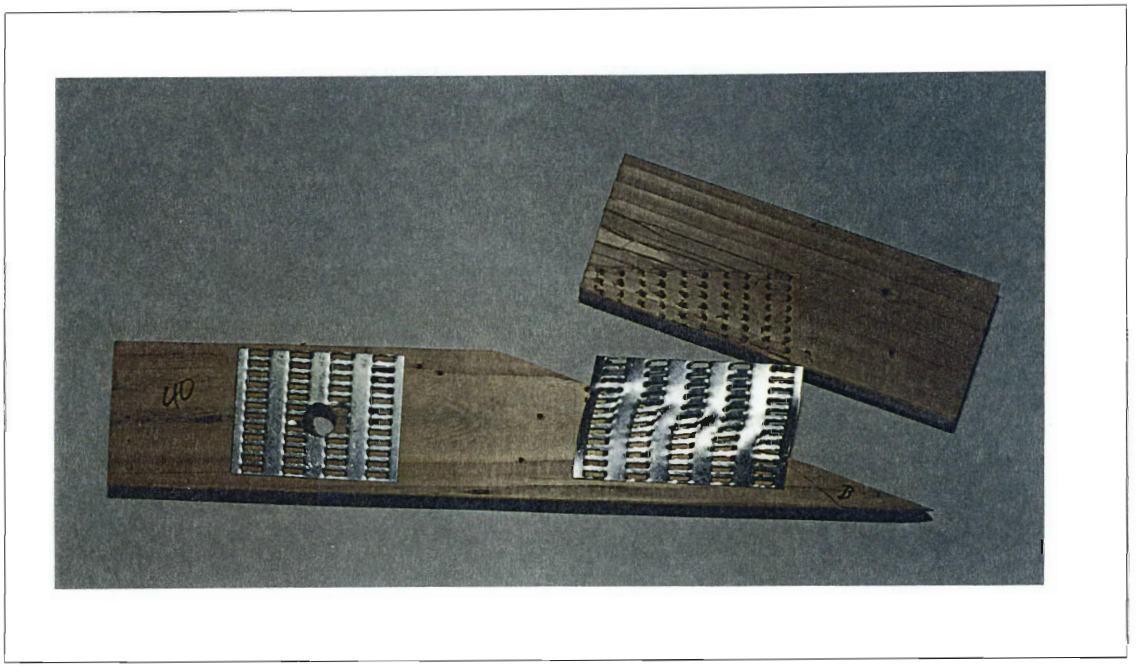

Figure 5-2: Wood shear failure mode for a heel joint

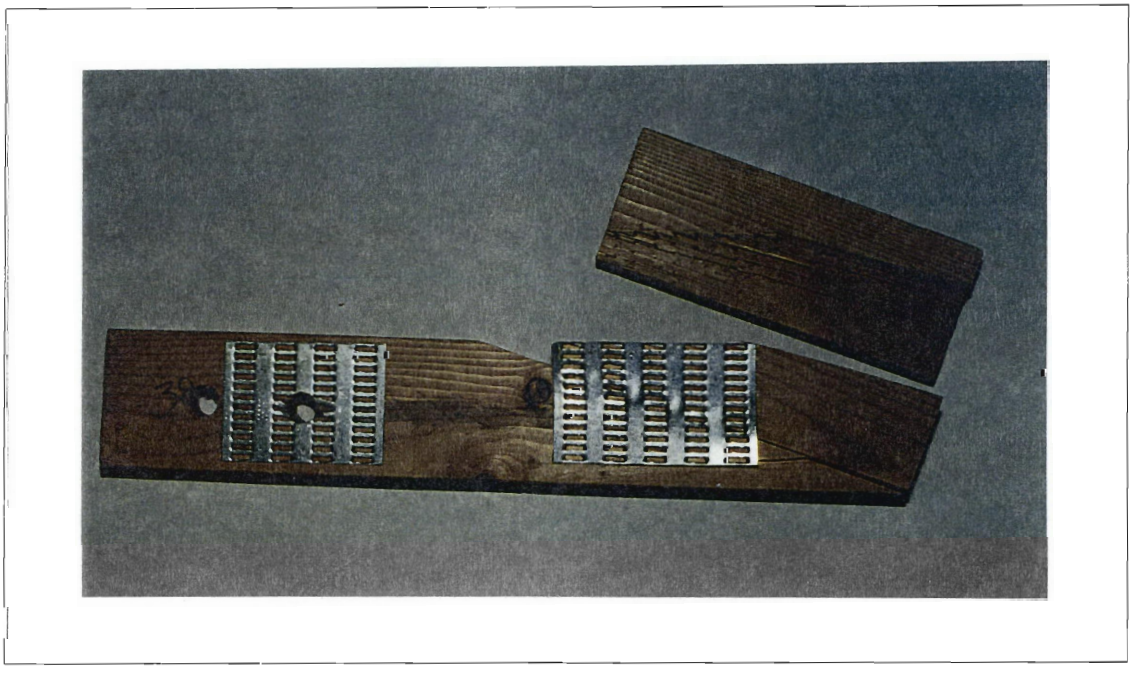

Figure 5-3: Tooth withdrawal failure for a heel joint

When the load is low, wood fibers closest to the metal teeth deform elastically. As the load increases, the wood nearest to the metal teeth crushes, the corner teeth begin to bend and withdraw. Failure of the joint is preceded by deformation of the metal plate along the gap line due to the shear forces in the joint, partial tooth withdrawal of the outside teeth, and crushing of the wood near the teeth.

Heel joint stiffness was measured using a secant stiffness approach which calculated the ratio of the load in the upper chord to the corresponding slip deflection. Because the load-deflection plot is non-linear, the stiffness was measured at two different loads. First, the stiffness was measured at the dead load level which was found by analyzing a Fink truss loaded with 20 lb/ft on the

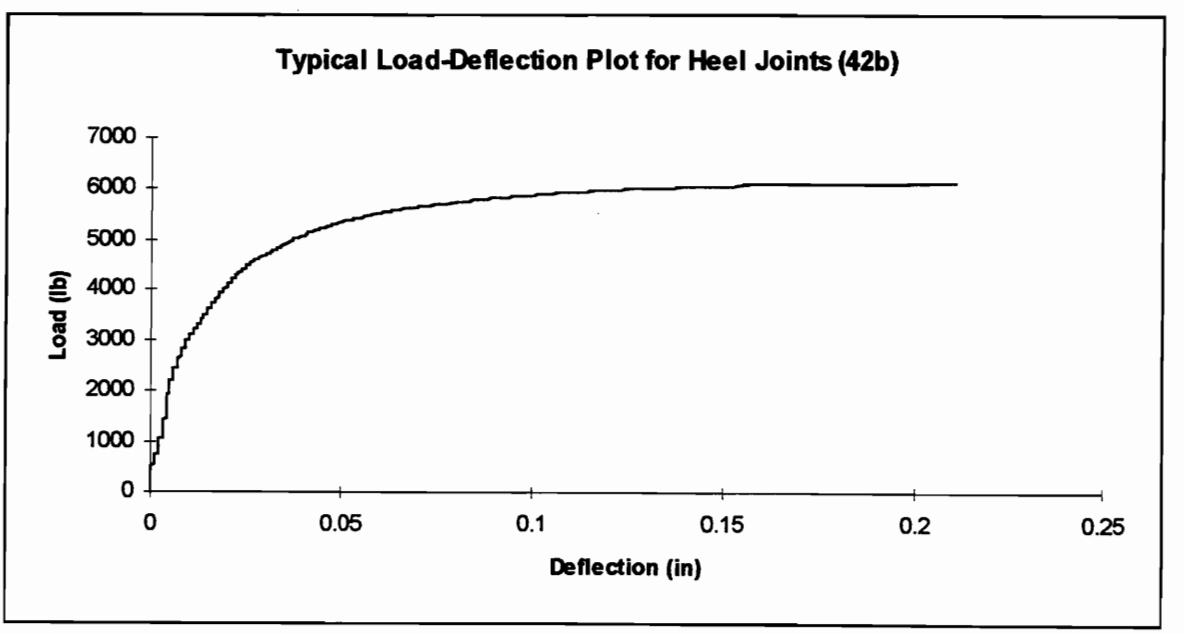

Figure 5-4: Typical load-deflection curve for a heel joint

top and bottom chords (plus member self weight) using a finite element modeling (FEM) program, SAP90, as described in Section 3.5. The stiffness was also measured at the design load.

The four different stiffnesses measured for the experimental groups, described in Sections 4.4.2.1 and 4.4.2.2, are: beginning dead load stiffness, beginning design load stiffness, ending dead load stiffness, and ending design load stiffness. For the double design impact load test, described in Section 4.4.3, the beginning design load stiffness was not measured because the initial ramp load was stopped before the design load was reached.

Comparing the beginning stiffnesses from the static group to the beginning stiffnesses from the experimental group can help determine if a difference exists between the two groups before the dynamic load is applied. If no difference is seen before the impact load, comparisons of static and experimental ending stiffnesses can determine if the dynamic load has affected the joint stiffness.

5.1.1 Static Ramp Load Results

5.1.1.1 Tension Static Ramp Load Results

The average properties, COV values, and sample size for heel joints tested in tension with the static ramp load are shown in Table 5-2. Property values for all heel joint samples are given in Appendix B.

Table 5-2: Tension static ramp load heel joint property values, COV, and sample size

Property Description	Average Value	C. O. V.	Sample Size
Dead Load Stiffness (lb/in)	333,000	63.2%	8
Design Load Stiffness (lb/in)	223,000	28.4%	8
Ultimate strength (lb)	7,189	12.0%	10
Time to Failure (s)	8.0	12.0%	10
Ultimate deflection (in)	0.167	28.3%	10

All heel joint load-deflection curves are included in Appendix C. While the general shapes of the load-deflection plots were consistent, there was variation among the curves. For some joints, the slip deflection was immediately measurable, while other joints showed no deflection until the load exceeded 1500 lb. This initial lack of deflection could be caused by opening or closing of the joint. The energy which would normally be stored in slip deflection is stored in rotational deflection. Rotation of the joint is encouraged by slight loading eccentricities induced by human error. The COV for stiffness is high partially because the amount of eccentricity varies from joint to joint. Vatovec, et al.(1996) also found a higher coefficient of variation for stiffness than for ultimate strength. The COV for dead load stiffness is much higher than the COV for design load stiffness because the initial lack of deflection, mentioned earlier, has a greater effect on the dead load stiffness because it is measured at a lower load, and thus at lower deflection readings. The lower deflection readings are affected more by LVDT noise, which increases the COV.

5.1.1.2 Compression Static Ramp Load Results

The average properties, COV values, and sample size for heel joints tested in compression with the static ramp load are shown in Table 5-3. Property values for all heel joint samples are given in Appendix B.

Table 5-3: Compression static ramp load heel joint property values, COV, and sample size

Property Description	Average Value	C. O. V.	Sample Size
Dead Load Stiffness (lb/in)	338,000	50.9%	9
Design Load Stiffness (lb/in)	325,000	39.8%	9
Ultimate strength (lb)	5,959	8.9%	10
Time to Failure (min)	6.6	8.9%	10
Ultimate deflection (in)	0.237	19.0%	9

All heel joint load-deflection curves show the same general non-linear shape and are included in Appendix C. The static average ultimate strength found here, 5959 lb. (COV = 8.9%), is comparable to the results found by other researchers. Freilinger (1998), Kent (1995), and Gupta and Gebremedhin (1990) tested very similar heel joints with compression static ramp loads and found the average ultimate strength to be 5763 lb. (COV = 6%), 6211 lb. (COV = 6.9%), and 5100 lb. (COV = 6.7%), respectively.

Because of LVDT problems, no reliable deflection readings were collected for one of the ten samples. High COV values for stiffness can likely be

attributed to the same source of variation in compression as described for tension in Section 5.1.1.1.

5.1.1.3 Static Ramp Load Results Comparison

Table 5-4 shows the average property values for both tension and compression static ramp tests along with the p-values from a statistical t-test comparing the two groups. Two sided t-tests were used because the proposed hypothesis is concerned with whether a difference exists between the two groups, not whether one group has a higher mean than the other. Property values for all heel joint samples are given in Appendix B.

There is insufficient evidence to conclude that there is a difference between tension stiffnesses and compression stiffnesses (two sided p-values of 0.93 and 0.88 for dead load stiffness and design load stiffness, respectively). It is possible that a difference exists between the stiffnesses, but because of the high COV, no difference can be determined. There is convincing evidence that

Table 5-4: Comparison of compression and tension static ramp load heel joint property values

Property Description	p-Value (two-sided)	Average Value		C.O.V. and {Sample Size}	
		Tension	Compression	Tension	Compression
Dead Load Stiffness (lb/in)	0.93	333,000	338,000	63% {8}	51% {9}
Design Load Stiffness (lb/in)	0.88	223,000	325,000	28% {8}	40% {9}
Ultimate strength (lb)	0.002	7,189	5,959	12% {10}	9% {10}
Ultimate deflection (in)	0.004	0.167	0.237	28% {10}	19% {9}

a difference exists between the tension and compression ultimate strength and ultimate deflection values (two sided p-values of 0.002 and 0.004 for ultimate strength and ultimate deflection, respectively). Heel joints tested in tension have a 17% higher average ultimate strength and a 42% lower average ultimate deflection than heel joints tested in compression.

Differences between tension properties and compression properties may be understood by comparing the deflected shapes of loaded heel joints. If a heel joint opens, then the angle between the two chords increases. Conversely, a heel joint which closes has a decreasing angle between the two chords.

Table 5-4 shows convincing evidence (two sided p-value of 0.004) of a difference between the compression ultimate deflection and the tension ultimate deflection. Figure 5-5 shows how heel joints tested in compression opened as the load increased. As the joint opens, the loading forces become more eccentric and the joint opens more. Because there is more force opening the joint, less force is causing the chords to slip with respect to one another. Because the angle changes very little, the axial force would not be reduced enough to cause a significant change in the ultimate strength.

Figure 5-5 and Figure 5-6 show heel joints subjected to a low load, then a high load in compression and in tension, respectively, on the top chord. The deflected shape of the loaded heel joint is purposely exaggerated to emphasize the differences between compression and tension deflections. Compression loads tended to open the joint, while tension loads closed the joint.

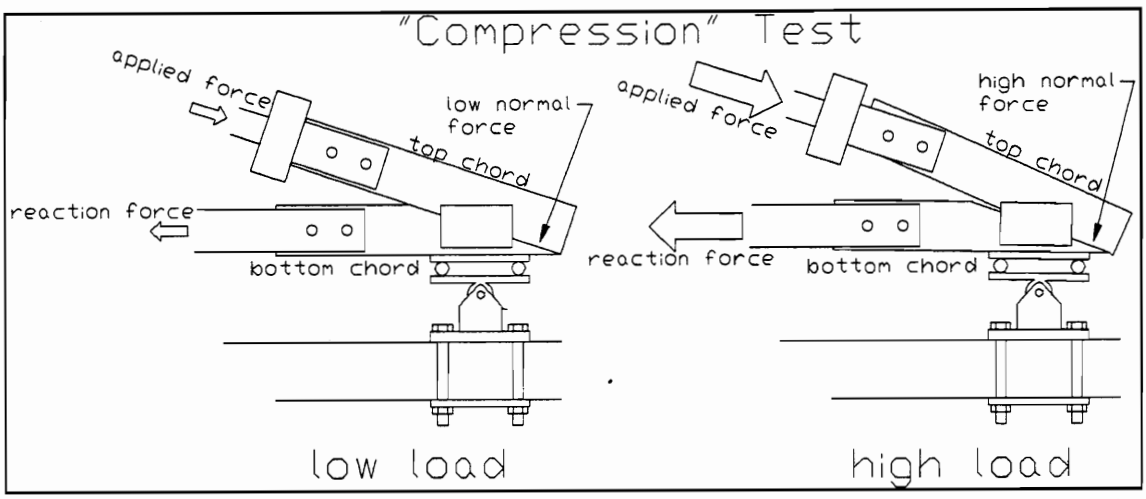

Figure 5-5: Heel joint subjected to both low and high compression loads

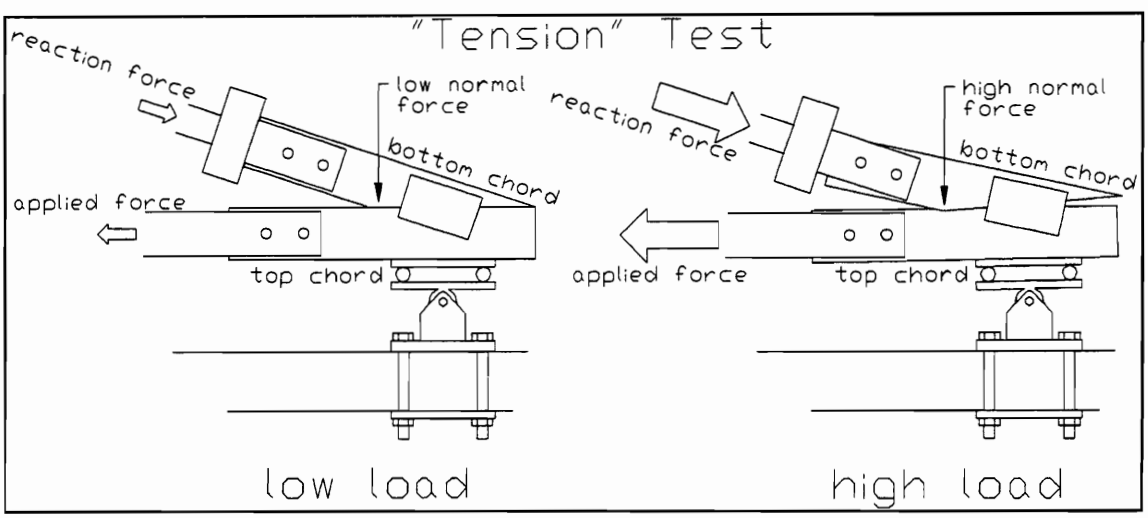

Figure 5-6: Heel joint subjected to both low and high tension loads

Table 5-4 also shows convincing evidence (two sided p-value of 0.002) of a difference between the compression ultimate strength and tension ultimate strength. This difference could be attributed to the higher amount of friction between the chords in the tension case. When the force increases in the

compression case, the heel joint opens. As it opens, the normal force between the chord members increases near the outside of the joint as shown in Near the outside of the heel joint, the bottom chord is thin and flexible, which means it deflects more easily against the force applied by the top chord. This leads to less normal force and thus a lower frictional force.

The opposite is true for the tension case, which is shown in Figure 5-6. As load increases, the joint closes and the normal force between the chord members increases near the inside of the heel joint. Near the inside of the heel joint, the bottom chord is thick, which means it does not deflect as easily against. Since the deflection is lower, the normal force between the chords is higher, thus, the frictional force between the two chord is relatively high compared to the compression case. Also, as the heel joint closes, the bottom chord begins to crush the wood fibers on the contact surface of the top chord. As failure nears, the bottom chord must crush the wood fibers at the contact point before deflecting more.

The higher friction forces and wood crushing which occurs in the tension tests result in higher ultimate strength. Lower ultimate deflection values for tension tests could also be attributed to the high friction forces. The friction forces resist the movement of the chords with respect to each other which reduces the ultimate deflection.

5.1.2 Wind Simulation Results

5.1.2.1 Hurricane Wind Tension Load Simulation Results

The average properties, COV values, and sample size for heel joints tested in tension with the hurricane simulation load are shown in Table 5-5. Property values for all heel joint samples are given in Appendix B.

All load-deflection curves show the same general non-linear shape and are included in Appendix C. For one sample, LVDT problems occurred just as the joint was approaching failure, therefore, only 9 ultimate deflection values were collected. A typical wind simulation tension load-deflection plot is shown in Figure 5-7. High stiffness COV values are attributed to the same source of variation in the tension wind simulation as in the tension static ramp load, explained in Section 5.1.1.1.

Table 5-5: Hurricane wind tension load simulation heel joint property values, COV, and sample size

Property Description		Average Value	C. O. V.	Sample Size
Dead Load Stiffness (lb/in)	begin	334,000	35.1%	10
	end	1,290,000	28.2%	10
Design Load Stiffness (lb/in)	begin	318,000	43.8%	10
	end	952,000	34.1%	10
Ultimate Strength (lb)		7,807	10.8%	10
Ultimate Deflection (in)		0.158	20.2%	9
Dynamic Deflection (in)		0.006	38.6%	10

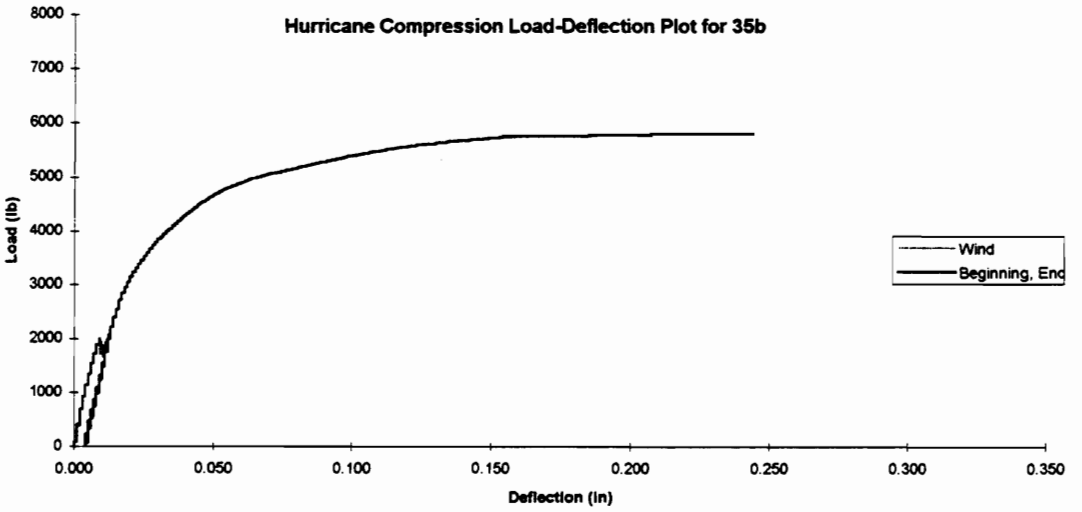

Figure 5-7: Typical wind simulation tension load-deflection plot

The difference between the deflection before and after the wind load is called the dynamic deflection here. The before deflection reading is taken immediately before the dynamic load is applied, while the after deflection reading is taken immediately after the dynamic load ends. Both of these deflection readings are taken at the design load, which is the beginning and ending load of the wind load simulation. For the tension load wind simulations, an average of 0.006 inches of dynamic deflection occurs during the wind load simulation. This deflection is the distance the two chords move with respect to one another, measured along the contact surface between the chords.

Table 5-6 shows the average property values for both static ramp load and wind simulation in tension along with p-values from a statistical t-test comparing the two groups. Both one-sided and two-sided t-tests were used. Because the effect of dynamic load on stiffness was unknown, a two-sided t-test was used to test the hypothesis that there is no difference between the two

Table 5-6: Comparison of wind simulation and static ramp heel joint property values in tension

Property Description		p-Value (two-sided)	Average Value Wind	Average Value Static	C.O.V. and {Sample Size} Wind	C.O.V. and {Sample Size} Static
Dead Load	begin	0.99	334,000	333,000	35% {10}	63% {8}
Stiffness (lb/in)	end	4.E-06	1,290,000	333,000	28% {10}	63% {8}
Design Load	begin	0.08	318,000	223,000	44% {10}	28% {8}
Stiffness (lb/in)	end	4.E-05	952,000	223,000	34% {10}	28% {8}
Ultimate strength (lb)		0.06 *	7,807	7,189	11% {10}	12% {10}
Ultimate deflection (in)		0.32 *	0.158	0.167	20% {9}	28% {10}

* one-sided test used

groups. However, another goal of the tests was to determine if dynamic loads reduce the strength or ultimate deflection of MPC joints. This leads to the hypothesis that the mean static value is higher than the mean wind simulation value for strength and ultimate deflection. Because the hypothesis is concerned with whether one group has higher values than another, a one-sided p-value is used.

Insufficient evidence exists to conclude that the dynamic load caused a decrease in the ultimate deflection (one-sided p-value of 0.32). However, suggestive, but inconclusive evidence exists of a difference between the control and experimental ultimate strengths (one-sided p-value of 0.06). Because the static strength is lower than the strength from the wind simulation and some evidence of a difference exists, the conclusion could be made that dynamic wind loading increases the strength of MPC heel joints. Because only suggestive evidence of a difference exists and the apparent difference is rather small (~ 8%), chance is assumed to cause the difference between the two groups.

Comparing the control group stiffness to the experimental group stiffnesses gives two-sided p-values of 0.99 and 0.08 for dead load stiffness and design load stiffness, respectively. A p-value of 0.99 shows no evidence of a difference while a p-value of 0.08 shows slight evidence of a difference. For this project, insufficient evidence was revealed by the t-test to conclude the groups were different before the dynamic load was applied. Therefore, it is assumed that the joints in the two groups came from the same population.

After the dynamic load was applied to the experimental group, a definite difference between the stiffnesses of the two groups is seen (two-sided p-values of 4.E-6 and 4.E-5 for dead load stiffness and design load stiffness, respectively). Before the dynamic load, the stiffness of the experimental groups was approximately the same as the control group. Not only is the evidence of a difference overwhelming, the difference between the two groups is very large. The dead load stiffness increased by approximately 290%, while the design load stiffness increased by approximately 325%.

The increase in stiffness after the dynamic load can be explained if the deflection of the joint is closely examined. The slip deflection of the joint has three different causes. First, the metal plate, connecting the two chords, deflects in shear. Shear deflection of the metal plate is shown in Figure 5-8.

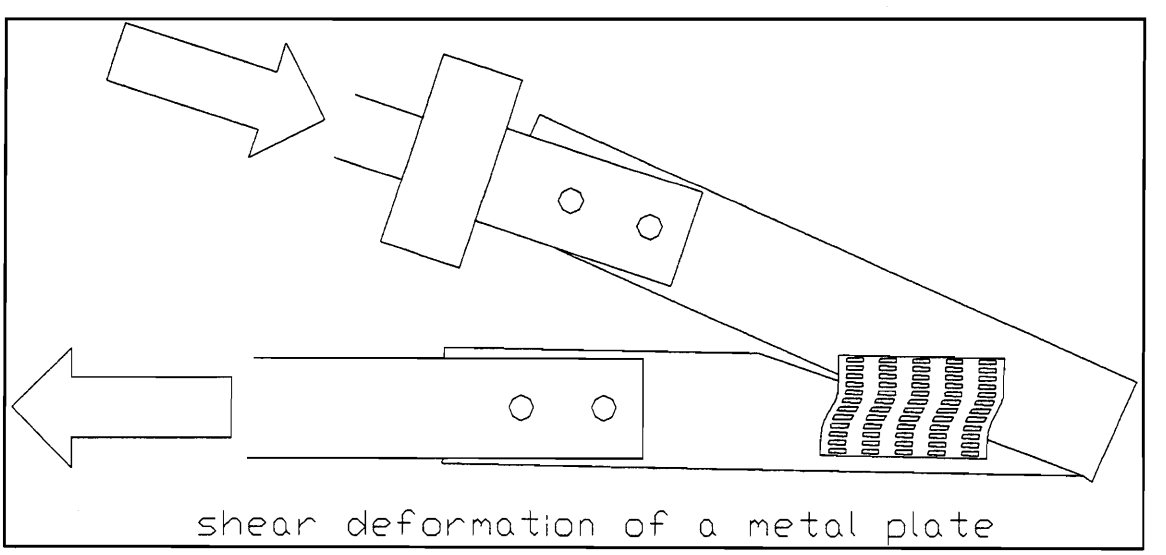

Figure 5-8: Shear deformation of a metal plate under high loads

Second, the teeth of the metal plate bend and withdraw just prior to failure. Third, wood fibers in direct contact with the teeth crush.

The third source of deflection may explain the increase in stiffness after the dynamic load. As the dynamic load progresses, the wood fibers close to the teeth are plastically crushed and densified. After the dynamic load ends and the load is removed, the wood fibers only slightly rebound. As the joint is reloaded, the densified wood fibers do not deflect as much as they did initially. After the ramp load exceeds the maximum dynamic load, the stiffness changes to approximate the stiffness of the control group joint at that load. The load-deflection graph, shown in Figure 5-7, shows the change in stiffness as a change in the slope of the plot.

This change in stiffness could be useful. If an estimate of the maximum previous dynamic load on a truss is needed, it could be determined by cutting a heel joint out of an existing truss and testing it. The maximum previous load would be at the point where the stiffness changes. Since many factors can affect the stiffness of a heel joint, more specific testing would be required before this theory could be confirmed.

5.1.2.2 Hurricane Wind Compression Load Simulation Results

The average properties, COV values, and sample size for heel joints tested in compression with the hurricane simulation are shown in Table 5-7. Property values for all heel joint samples are given in Appendix B.

Table 5-7: Hurricane wind compression load simulation heel joint property values, COV, and sample size

Property Description		Average Value	C. O. V.	Sample Size
Dead Load Stiffness (lb/in)	begin	280,000	19.9%	10
	end	258,000	18.1%	10
Design Load Stiffness (lb/in)	begin	267,000	24.8%	10
	end	256,000	16.2%	10
Ultimate strength (lb)		6,437	5.3%	10
Ultimate deflection (in)		0.276	16.1%	10
Dynamic Deflection (in)		0.002	48.4%	10

All heel joint load-deflection curves show the same general non-linear shape and are included in Appendix C. High stiffness COV values are attributed to the same source of variation in wind compression load simulation as in the tension static ramp load, explained in Section 5.1.1.1. A typical hurricane simulation compression load-deflection plot is shown in Figure 5-9.

Table 5-8 shows the average property values for both static ramp load and wind simulation in compression along with the p-values from a statistical t-test comparing the two groups. Both one-sided and two-sided t-tests were used for reasons explained in Section 5.1.2.1.

Comparing initial stiffnesses from the wind simulation group to the control group shows no evidence of a difference (two-sided p-values of 0.34 and 0.25 for dead load stiffness and design load stiffness, respectively). This is also the case for the ending stiffnesses (two-sided p-values of 0.20 and 0.16 for dead load stiffness and design load stiffness, respectively). The lack of a difference

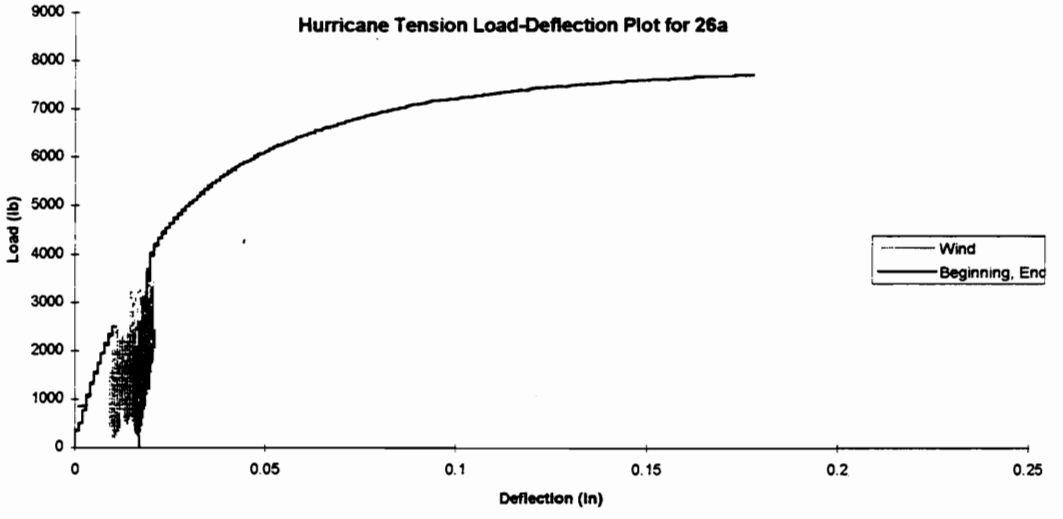

Figure 5-9: Typical hurricane simulation compression load-deflection plot

Table 5-8: Comparison of wind simulation and static ramp heel joint property values in compression

Property Description		p-Value (two-sided)	Average Value Wind	Average Value Static	C.O.V. and {Sample Size} Wind	C.O.V. and {Sample Size} Static
Dead Load	begin	0.34	280,000	338,000	20% {10}	51% {9}
Stiffness (lb/in)	end	0.2	258,000	338,000	18% {10}	51% {9}
Design Load	begin	0.25	267,000	325,000	25% {10}	40% {9}
Stiffness (lb/in)	end	0.16	256,000	325,000	16% {10}	40% {9}
Ultimate strength (lb)		0.01 *	6,437	5,959	5% {10}	9% {10}
Ultimate deflection (in)		0.04 *	0.276	0.237	16% {10}	19% {9}

* one-sided test used

between the ending stiffness and the control group stiffness is probably due to the relatively low dynamic load used in the compression tests. The compression test average load was approximately 1830 lb. and varied by only about 550 lb. More specifically, the joints didn't become stiffer after the wind simulation because the wood fibers closest to the metal teeth were not plastically crushed and densified enough to cause a stiffening effect. If the wind simulation load had a higher average load and amplitude, the joints may have been stiffer after the dynamic load.

Even though no stiffness increase occurred after the dynamic load, the theory, detailed in Section 5.1.2.1, that wood fiber densification is generally responsible for a stiffness increase is still proposed. Comparing the dynamic deflection for wind simulation groups in tension and compression shows that there is approximately three times more dynamic deflection in the tension group than in the compression group. (Dynamic deflection values for tension and

compression are 0.006 inches and 0.002 inches, as taken from Table 5-5 and Table 5-7, respectively. Dynamic deflection is the permanent deflection which occurs between the beginning and ending of the dynamic load.) The higher dynamic deflection in the tension case caused enough wood fiber densification near the teeth to increase the stiffness. In the compression case, the dynamic deflection is too small to create enough wood fiber densification to increase the stiffness.

Moderate to suggestive evidence exists which shows a difference between the wind simulation compression load group and the compression static load group for strength and ultimate deflection (one-sided p-values of 0.01 and 0.04, respectively). While moderate evidence of a difference between the wind simulation load group and the control group exists for strength, the static group is only approximately 7% lower than the experimental group. The cause of this apparent increase in strength is not completely clear. Several possibilities exist.

Only moderate evidence exists of a difference between the two groups. It is possible, however unlikely, that the difference is solely attributed to a chance grouping of stronger joints into the experimental group and weaker joints into the control group.

Also, the apparent difference between the two groups could be caused by low COV values, 5.3% and 8.9% for the compression load wind group and the compression static load group, respectively. The low COV values could have been caused by a chance grouping of joints which were very similar in strength

and ductility. (Lower COV values make the difference between the two groups appear to be more significant.)

Finally, it is possible, however unlikely, that the wind simulation load caused an increase in joint strength.

5.1.3 Double Design Impact Load Results

The average properties, COV values, and sample size for heel joints tested in tension with the double design impact load are shown in Table 5-9. Property values for all heel joint samples are given in Appendix B.

All heel joint load-deflection curves show the same general non-linear shape and are included in Appendix C. High stiffness COV values are attributed to the same source of variation in the double design impact load tests as for the tension static ramp load, explained in Section 5.1.1.1. A typical load-deflection

Table 5-9: Double design impact load heel joint property values, COV, and sample size

Property Description	Average Value	C. O. V.	Sample Size
Dead Load Stiffness (lb/in) begin	294,000	56.3%	10
end	830,000	55.4%	10
Design Load Stiffness (lb/in)	565,000	41.6%	10
Ultimate strength (lb)	7,021	9.8%	10
Ultimate deflection (in)	0.155	18.0%	9
Dynamic Deflection (in)	0.025	24.3%	10

plot for a heel joint subjected to the double design impact load is shown in Figure 5-10.

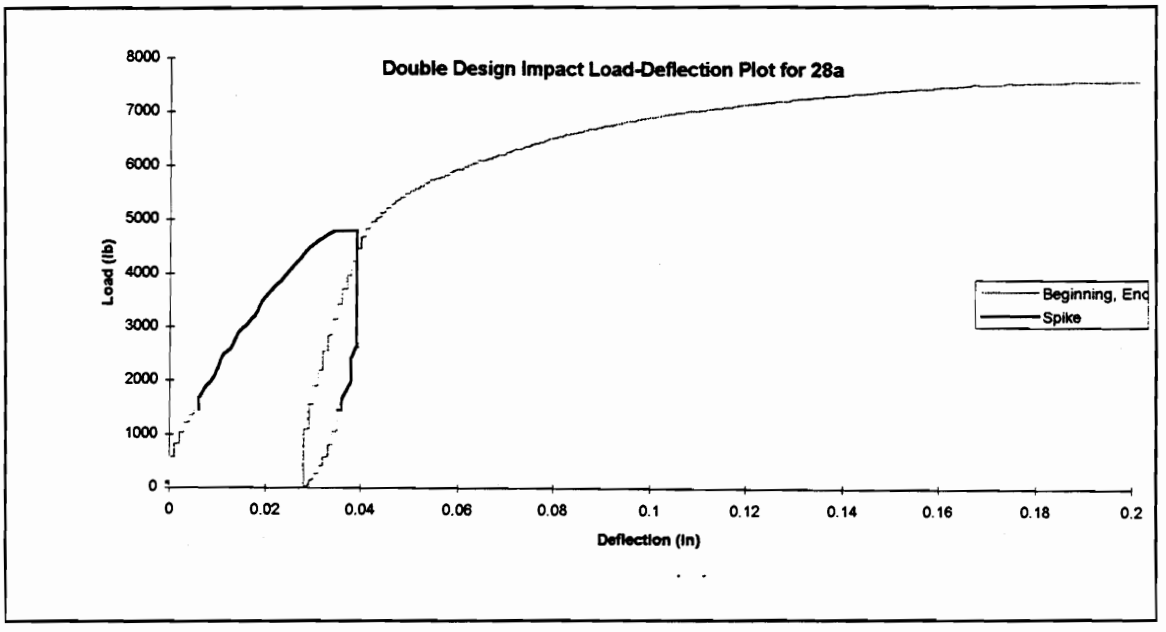

Figure 5-10: Typical load-deflection plot for a heel joint subjected to the double design impact load

Table 5-10: Comparison of double design impact and static ramp heel joint property values in tension

Property Description		p-Value (two-sided)	Average Value Impact	Average Value Static	C.O.V. and {Sample Size} Impact	C.O.V. and {Sample Size} Static
Dead Load	begin	0.67	294,000	333,000	56% {10}	63% {8}
Stiffness (lb/in)	end	0.01	830,000	333,000	55% {10}	63% {8}
Design Load Stiffness (lb/in)		0.001	565,000	223,000	42% {10}	28% {8}
Ultimate strength (lb)		0.32 *	7,021	7,189	10% {10}	12% {10}
Ultimate deflection (in)		0.27 *	0.155	0.167	18% {9}	28% {10}

* one-sided test used

Table 5-10 shows the average property values for both static ramp load in tension and double design impact load in tension along with the p-values from a statistical t-test comparing the two groups. Both one-sided and two-sided t-tests were used for reasons explained in Section 5.1.2.1.

In the beginning phase, the load was only increased to the dead load, therefore the beginning design load stiffness was not available. Comparing the beginning dead load stiffness to the control group shows no evidence of a difference (two-sided p-value of 0.67), but after the spike was applied, the impact group stiffnesses increased dramatically compared to those of the control group (two-sided p-values of 0.01 and 0.001 for dead load stiffness and design load stiffness, respectively). The dead load stiffness p-value of 0.01 shows only moderate evidence of a difference, but the design load stiffness p-value of 0.001 shows convincing evidence of a difference. Not only is the evidence compelling, but the difference between the group averages is very significant. Both the dead load stiffness and the design load stiffness increased by approximately 150%.

This stiffness change is similar to the stiffness increase caused by the hurricane simulation tension load (where the stiffnesses increased an average of 308%). If the spike load was increased to the ultimate load, the stiffness change would likely become even closer to the stiffness change seen in the tension wind simulation. Therefore, it is possible that a long duration dynamic load can be simulated using a single dynamic event, but the magnitude of the force in the short duration dynamic load must be much greater than the magnitude of the

force in the long duration dynamic load. The maximum force in the tension load wind load simulation is only 3954 lb. while the double design impact load maximum force is 4815 lb.

No differences between the control group and impact load group were observed for strength or for ultimate deflection (one-sided p-values of 0.32 and 0.27). No differences between the control group and the tension load wind simulation group were seen for strength or for ultimate deflection either.

5.2 General Tension Splice Joint Results

All the properties of tension splice joints which were calculated or measured for this study are shown in Appendix D. Properties include ultimate strength, dead load stiffness, design load stiffness, ultimate deflection, specific gravity, modulus of elasticity (MOE), moisture content, growth rings per inch, grain orientation, late wood content, and failure mode. Along with the property, the respective coefficient of variation (COV) is also listed.

A brief summary of the tension splice joint tests done for this study is shown in Table 5-11. Due to LVDT problems and premature failure, some properties were not recorded or deemed unusable, therefore the sample size can vary within a test. For example, only 7 of 10 samples subjected to the ultimate impact load survived the spike portion of the test. Therefore, only 7 strength values were measured for that test. In Table 5-11, the sample size

Table 5-11: Summary of tension splice joint results

Test Description	Sample Size	Average Strength (lb)	Average Specific Gravity	Average Moisture Content (%)	Average Wood MOE (x10^6 psi)
Tension Static Ramp Load	9	6,824	0.52	11.9	1.79
Accelerated Ramp Load	10	7,185	0.52	12.1	1.85
Double Design Impact Load	10	7,235	0.52	9.8 *	1.81
Ultimate Impact Load	7	7,520	0.52	10.1*	1.81

* Unreliable Moisture Content - samples were left out of standard room

listed is the number of ultimate strength values. The sample size for all other properties in Table 5-11 is ten.

Specific gravity and moisture content were measured according to ASTM D2395-93 (Method A, Volume by Measurement) and ASTM D4442-92 (Method A, Oven Drying Primary), respectively. Failed joints from the two impact load groups were accidentally removed from the standard room for the approximate one week period before moisture content samples could be taken. Since the COV for all reliable moisture content readings is low, 4.7%, it was assumed that all moisture content readings are the same. Even if the moisture content averages, shown in Table 5-11, are correct, the 2% difference between the impact groups and the other groups is not enough to cause a significant change in properties.

MOE was determined with an E-computer (Metriguard, Model 390) given the length and cross sectional measurements by measuring the natural frequency and mass of the member.

Load-deflection curves were analyzed to determine the stiffnesses. Load was measured as the axial force in the tension splice joint, while the deflection was measured at the spice joint over the length of the metal plate as shown in Figure 4-6.

No dominant failure mode was identified for tension splice joints. Failure modes were distributed quite equally among wood shear, tooth withdrawal, and plate failure. Failure completely due to wood shear occurred 11 times, tooth withdrawal 7 times, and plate failure 2 times. Twenty joints experienced a combination of these failure modes. The failure modes seen for tension splice joints are described in Section 5.1. Figure 5-11, Figure 5-12, and Figure 5-13 show the wood shear, tooth withdrawal, and plate failure modes of tension splice joints tested for this project.

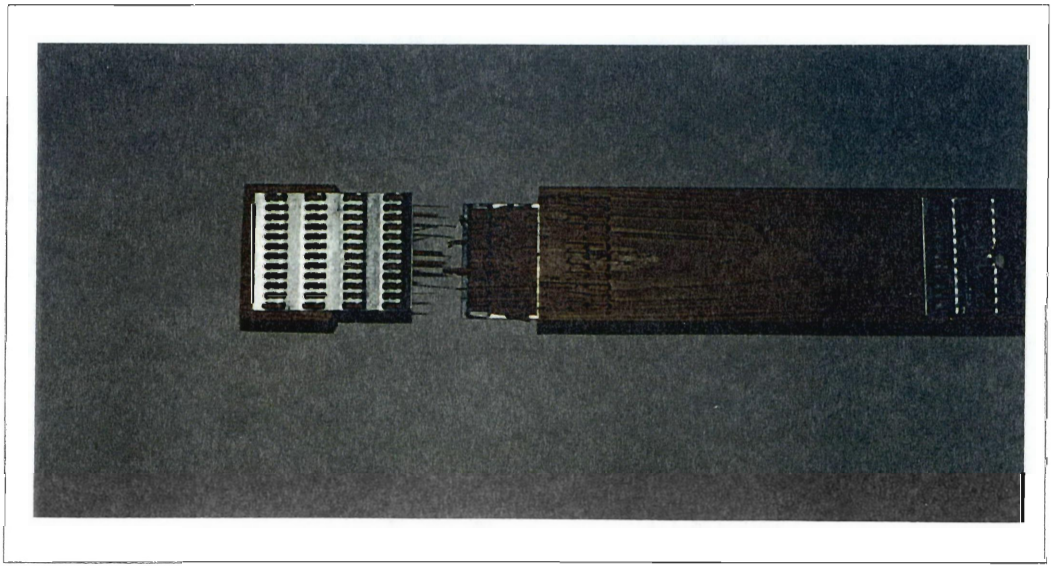

Figure 5-11: Wood shear failure of a tension splice joint

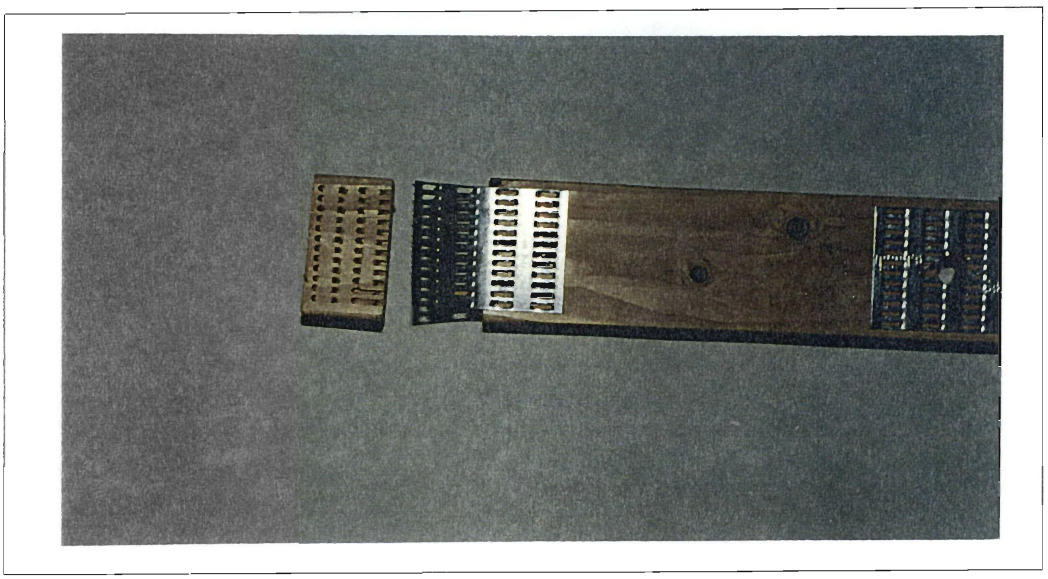

Figure 5-12: Tooth withdrawal failure of a tension splice joint

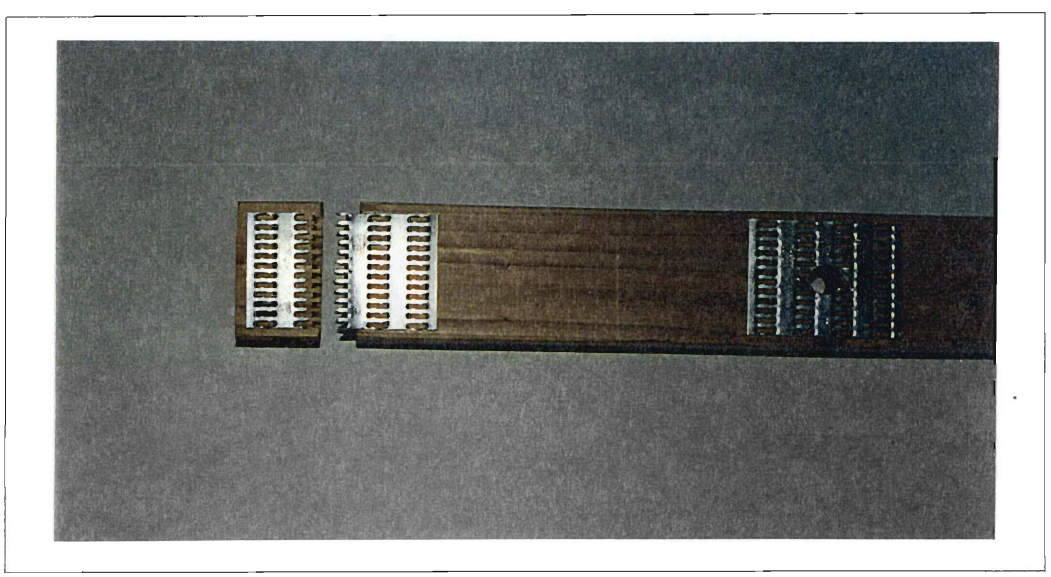

Figure 5-13: Plate failure of a tension splice joint

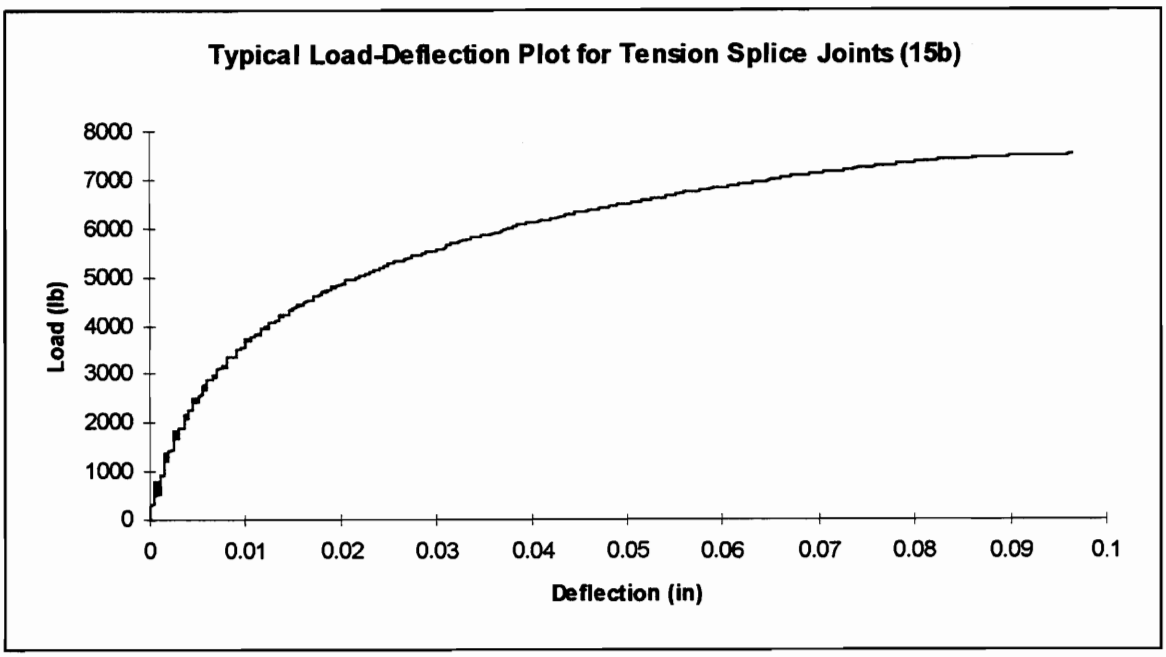

Figure 5-14: Typical load-deflection curve for a tension splice joint

The load-deflection plots show that tension splice joints behave in a non-linear fashion as shown in Figure 5-14. The non-linear behavior of tension splice joints is typical of wood members and wood joints. In tension splice joints, the shape of the load-deflection plot is affected by both the metal plate and the wood fibers. When the load is low, the wood fibers in contact with the metal teeth deform elastically and the plate elastically deflects in tension. Increased load causes the wood nearest to the metal teeth to crush and deform. If the yield strength of the metal plate is exceeded, a plate failure mode generally follows plastic deformation of the plate. If a weak shear plane in the wood exists near the connection, a wood shear failure generally occurs. Tooth withdrawal failures is likely caused by crushing of the wood fibers in contact with the metal

teeth and bending of the metal teeth. Tension splice joint stiffness was measured for each joint using a secant stiffness approach, which is defined as the axial load divided by the corresponding axial deflection. Because the load-deflection plot is non-linear, the stiffness was measured at two different load levels. First, the stiffness was measured at the dead load level which was found by analyzing a Fink truss loaded with 20 lb/ft on the top and bottom chords (plus member self weight) using the FEM program SAP90, as described in Section 3.5. The stiffness was also measured at the design load.

Three different stiffnesses were calculated for the impact tests, described in Sections 4.5.3 and 4.5.4, because there are two sections of loading which use a static ramp load. Before the impact load is applied, the tension splice joint is subjected to a ramp load which stops at the dead load value of 865 lb. After the impact load is applied, the load is removed and the ramp load is applied again. Therefore, both the dead load stiffness and the design load stiffness is calculated both before and after the spike load. The three different stiffnesses are referred to as: beginning dead load stiffness, ending dead load stiffness, and ending design load stiffness. The beginning dead load stiffness is defined as the dead load divided by the deflection caused by the dead load measured before the dynamic load is applied. The ending dead load stiffness is the same as the beginning dead load stiffness, except it is measured after the dynamic load is applied and all load is removed from the joint. Ending design load stiffness is the design load divided by the deflection caused by applying the

design load. The ending design load stiffness is also measured after the dynamic load is applied. The design load level used to determine the design load stiffness is the average ultimate load from the static load group divided by 3.0. Multiple stiffness measurements are used in comparisons to determine if a difference exists between the static load group and the impact load group before and after the dynamic load. If no difference is seen before the dynamic load, comparisons of static load and impact load ending stiffnesses can help determine if the dynamic load affected the joint stiffness.

5.2.1 Static Ramp Load Results

The average properties, COV values, and sample size for tension splice joints tested in tension with the static ramp load are shown in Table 5-12. Property values for all tension splice joint results are given in Appendix D.

Table 5-12: Static ramp load tension splice joint property values, COV, and sample size

Property Description	Average Value	C. O. V.	Sample Size
Dead Load Stiffness (lb/in)	650,000	27.1%	9
Design Load Stiffness (lb/in)	437,000	22.0%	9
Ultimate Strength (lb)	6,824	15.2%	9
Time to Failure (min)	7.6	15.2%	9
Ultimate Deflection (in)	0.081	30.3%	9

Load-deflection curves for all tension splice joints show the same general non-linear shape and are included in Appendix E. Variation among static stiffnesses is much lower for tension splice joint tests than for heel joints tested in either tension or compression. This difference in variability is seen in Table 5-13 and Table 5-14 as higher COV values for heel joints and lower COV values for tension splice joints.

The average ultimate strength of tension splice joints found here, 6824 lb. (COV = 15.2%), is fairly comparable to results from previous researchers. Kent (1995) did similar tests on tension splice joints, but determined two different ultimate strength values depending on which plate batch was used. Kent's (1995) two different ultimate strength averages for tension splice joints are 7284 lb. (COV = 6%) and 6712 lb. (COV = 8.1%). Freilinger (1998) and Gupta and Gebremedhin (1990) also tested similar tension splice joints with static ramp loads and determined the average ultimate strength to be 5760 lb. (COV = 12%) and 6070 lb. (COV = 17.6%), respectively.

Table 5-13: Comparison of tension splice joint results to heel joint results tested in tension

Property Description	p-Value (two-sided)	Average Value		C.O.V. and {Sample Size}	
		TSJ	Heel Joint	TSJ	Heel Joint
Dead Load Stiffness (lb/in)	0.59	650,000	554,000	27% {9}	91% {10}
Design Load Stiffness (lb/in)	0.10	437,000	313,000	22% {9}	63% {10}
Ultimate strength (lb)	0.42	6,824	7,189	15% {9}	12% {10}
Ultimate deflection (in)	0.00017	0.081	0.167	30% {9}	28% {10}

Table 5-14: Comparison of tension splice joint results to heel joint results tested in compression

Property Description	p-Value (two-sided)	Average Value		C.O.V. and {Sample Size}	
		TSJ	Heel Joint	TSJ	Heel Joint
Dead Load Stiffness (lb/in)	0.0005	650,000	325,000	27% {9}	40% {9}
Design Load Stiffness (lb/in)	0.16	437,000	338,000	22% {9}	51% {9}
Ultimate strength (lb)	0.04	6,824	5,959	15% {9}	9% {10}
Ultimate deflection (in)	9.E-07	0.081	0.237	30% {9}	19% {9}

Some heel joints did not show any deflection at low loads (under 1500 lb.), but almost all tension splice joints deflected immediately after load was applied. The lack of initial deflection of some of the heel joints caused the COV for heel joint stiffness to be high. This difference in initial behavior could be caused by the frictional force between the members of an MPC joint, which affects heel joints, but not tension splice joints. Static friction exists between the chords of MPC joints because the two members are in direct contact with one another. Since heel joint tests all involve forcing the two chords together, this friction must be overcome before the joint will deflect. (While some tension splice joints have internal static friction (produced during joint construction), behavior of the joint would not be affected because the force applied to the joint is orthogonal to the plane along which the friction forces act. The friction forces in heel joints do affect the behavior of the joint because it acts in the direction of the applied force. This is shown in Figure 5-15.)

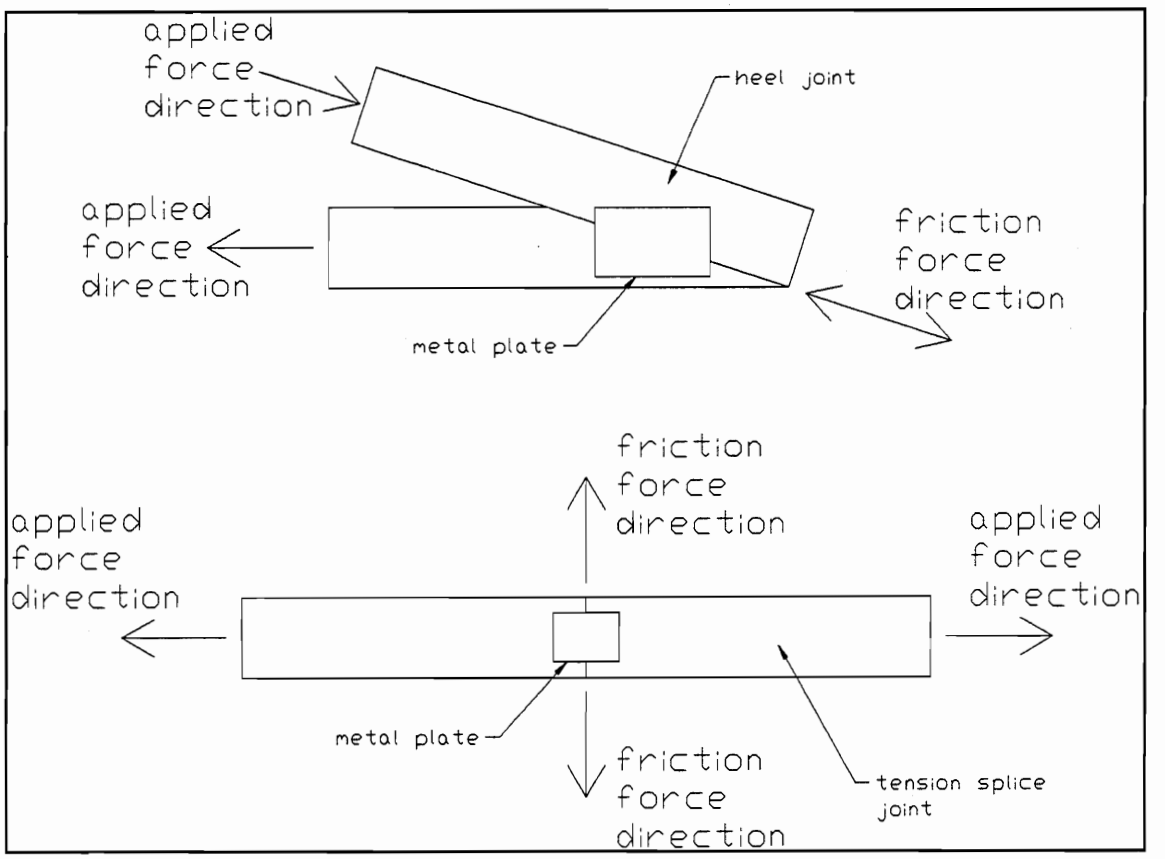

Figure 5-15: Direction of friction and applied forces for heel and tension splice joints

The effect of static friction would vary among heel joints, thus causing higher COV values, while static friction does not affect tension splice joint behavior.

Also, both LVDTs are aligned with the axis of the joint for a tension splice joint, while for heel joint tests the LVDTs are aligned at angles to one or both of the chords. Because of the simple way the tension splice joints deflect (compared to heel joints) there is less chance of getting inaccurate deflection readings due to accidental LVDT rotation or joint rotation.

The COV for ultimate strength and ultimate deflection values is approximately the same for both tension splice joints and heel joints (tested in either tension or compression) as shown in Table 5-14 and Table 5-15.

Overwhelming evidence exists of a difference in ultimate deflection between tension splice joints and heel joints tested in both tension and compression (two-sided p-value of 0.00017 and 9E-7, respectively). This difference is not surprising because heel joints and tension splice joints deform differently. Tension splice joint ultimate deflection values are approximately 52% smaller and 66% smaller than heel joint ultimate deflection values from tension and compression tests, respectively. The difference between heel joint and tension splice joint ultimate deflection can be seen graphically in the load-deflection plots included in Appendix C and Appendix E, respectively. Prior to failure, heel joints show very large deformations for small increases in load. For tension splice joints near failure, the amount of deflection for a small increase in load is not nearly as high. This difference in behavior is shown in the load-deflection plots as a long flat inelastic region before failure for heel joints and a much less defined inelastic region for tension splice joints.

Suggestive evidence exists for a difference between tension splice joint strength and heel joint strength when tested in compression (two-sided p-value of 0.04). The averages imply that tension splice joints are about 1000 lb. stronger than heel joints tested in compression.

There is inadequate evidence to conclude that a difference exists between tension splice joint strength and heel joint strength when tested in tension (two-sided p-value of 0.42).

Convincing evidence exists for a difference between tension splice joint dead load stiffness and heel joint (tested in compression) dead load stiffness (two-sided p-value of 0.0005). Other comparisons show insufficient evidence to conclude that a difference exists between heel joint and tension splice joint stiffnesses (two-sided p-values of 0.59 and 0.10 for dead load stiffness and design load stiffness comparing tension splice joints and heel joints tested in tension and 0.16 for dead load stiffness comparing tension splice joints and heel joints tested in compression) for various comparisons of stiffnesses detailed in Table 5-13 and Table 5-14). Because three of the four stiffness comparisons between heel joints and tension splice joints show little evidence of a difference, it may be concluded that tension splice joint stiffness is approximately the same as heel joint stiffness.

5.2.2 Accelerated Ramp Load Results

The average properties, COV values, and sample size for tension splice joints tested in tension with the accelerated ramp load are shown in Table 5-15.

Table 5-15: Accelerated ramp load tension splice joint property values, COV, and sample size

Property Description	Average Value	C. O. V.	Sample Size
Dead Load Stiffness (lb/in)	750,000	19.9%	10
Design Load Stiffness (lb/in)	492,000	17.0%	10
Ultimate strength (lb)	7,185	17.9%	10
Time to Failure (s)	47.9	17.9%	10
Ultimate deflection (in)	0.084	31.8%	10

Property values for all tension splice joint results are given in Appendix D. Table 5-16 shows the comparison of the static ramp load results to the accelerated ramp load results. COV values are approximately the same for static and accelerated properties.

Table 5-16: Comparison of accelerated ramp and static ramp tension splice joint property values

Property Description	p-Value (two-sided)	Average Value		C.O.V. and {Sample Size}			
		Static	Accelerated	Static		Accelerated	
Dead Load Stiffness (lb/in)	0.20	650,000	750,000	27%	{9}	20%	{10}
Design load stiffness (lb/in)	0.20	437,000	492,000	22%	{9}	17%	{10}
Ultimate strength (lb)	0.51	6,824	7,185	15%	{9}	18%	{10}
Ultimate deflection (in)	0.80	0.081	0.084	30%	{9}	32%	{10}

P-values produced from comparisons of static ramp load and accelerated ramp load groups show no evidence of a difference for any properties (two-sided p-values of 0.20, 0.20, 0.51, and 0.80 for dead load stiffness, design load stiffness, ultimate strength, and ultimate deflection, respectively).

It is not surprising that no difference is seen between the two groups. While the accelerated ramp load rate is approximately ten times higher than the static ramp load rate, the accelerated rate still takes approximately 45 seconds to fail a joint. The accelerated load rate used in this test produced "static" results, but it is still possible that even higher load rates would produce results which significantly differ from the "static" group. 5.2.4 briefly discusses the effects of very high load rates on tension splice joint properties.

5.2.3 Double Design Impact Load Results

The average properties, COV values, and sample size for tension splice joints tested in tension with the double design impact load are shown in Table 5-17. Property values for all tension splice joint results are given in Appendix D.

Table 5-17: Double design impact load tension splice joint property values, COV, and sample size

Property Description	Average Value	C. O. V.	Sample Size
Dead Load Stiffness (lb/in) begin	721,000	21.1%	10
end	435,000	19.4%	10
Design load stiffness (lb/in)	389,000	19.0%	10
Ultimate strength (lb)	7,235	8.3%	10
Ultimate deflection (in)	0.081	20.6%	10
Dynamic Deflection (in)	0.007	35.3%	10

Table 5-18 shows the comparison of the static ramp load results to the double design impact load results. COV values are approximately the same for static and double design properties.

Table 5-18: Comparison of double design impact and static ramp tension splice joint property values

Property Description		p-Value (two-sided)	Average Value Static	Average Value Impact	C.O.V. and {Sample Size} Static	C.O.V. and {Sample Size} Impact
Dead Load	begin	0.36	650,000	721,000	27% {9}	21% {10}
Stiffness (lb/in)	end	0.007	650,000	435,000	27% {9}	19% {10}
Design Load Stiffness (lb/in)		0.25	437,000	389,000	22% {9}	19% {10}
Ultimate strength (lb)		0.16 *	6,824	7,235	15% {9}	8% {10}
Ultimate deflection (in)		0.47 *	0.081	0.081	30% {9}	21% {10}

* one-sided test used

Before the spike load, the dead load stiffness was the same for the double design impact group and the static group (two-sided p-value of 0.36). The data collected after the load spike shows convincing evidence of a difference between the dead load stiffness for the spike group and the static group (two-sided p-value of 0.007). The dead load stiffness drops by approximately 40% after the double design impact. This decrease in dead load stiffness is suspicious because the design load stiffness does not experience a similar decrease.

Because of the low dead load stiffness p-value (two-sided p-value of 0.007), it is unlikely that the stiffness decrease is completely due to chance. It is equally unlikely that a difference exists between the impact and static design

load stiffness, but is not revealed by the statistical t-test because of the high resulting p-value (two-sided p-value of 0.36). Therefore, the double design impact must be affecting the dead load stiffness, but not the design load stiffness.

The only explanation for this joint behavior is that the design load stiffness was not affected by the spike because of the relative magnitudes of the spike and the design load. For the double design impact group, the maximum load during the spike is approximately 4550 lb. Comparing the impact magnitude to the design load where the stiffness is measured shows the spike load is only 90% larger for design load stiffness, but 425% larger for dead load stiffness. A larger spike magnitude would likely cause a similar decrease in design load stiffness.

The double design impact load had little effect on the design load stiffness, ultimate strength, and ultimate deflection property values (two-sided p-value of 0.25 for design load stiffness and one-sided p-values of 0.16 and 0.47 for ultimate strength and ultimate deflection, respectively).

Tension splice joints loaded with the double design impact load displayed interesting behavior which is not quantified in the property table. Figure 5-16 and Figure 5-17 show the load-deflection plots from a typical tension splice joint tested with the static ramp load and the double design impact load, respectively. (Load-deflection plots were included for all tension splice joints in Appendix E.)

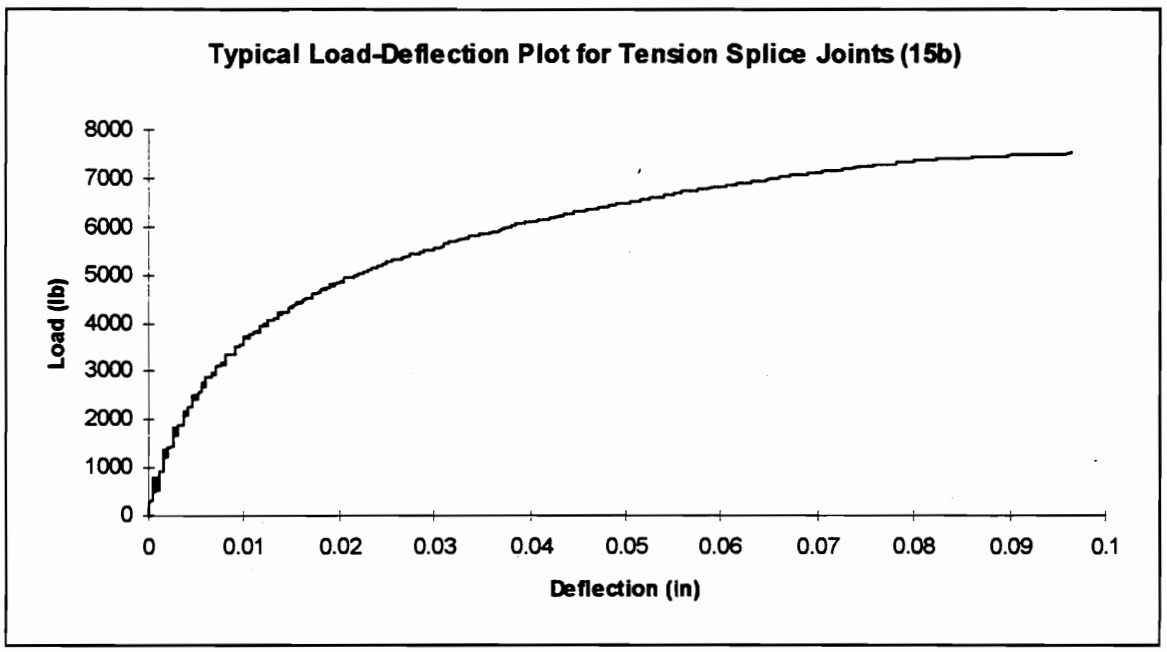

Figure 5-16: Load-deflection plot for a typical tension splice joint tested with the static ramp load

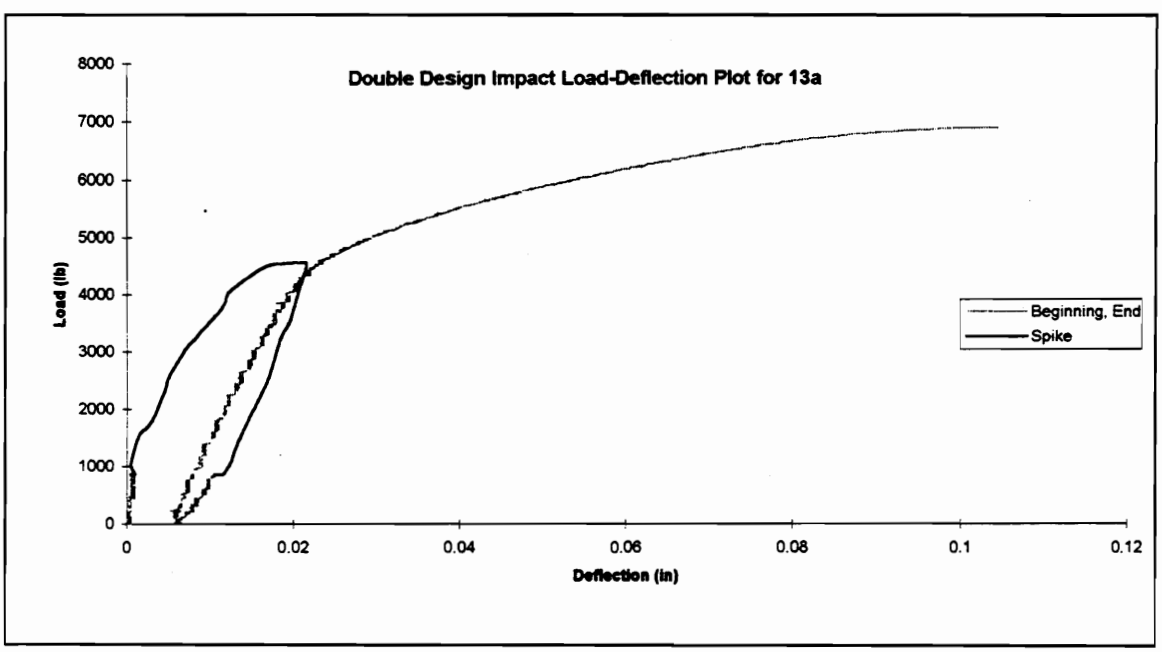

Figure 5-17: Load-deflection plot for a typical tension splice joint tested with the double design impact load

The load-deflection curve in Figure 5-17 is divided into the beginning, spike, and ending stages. During the beginning stage, the load slowly increases from 0 lb. to the dead load. The spike stage shows the load-deflection relationship as the load quickly increases from the dead load to the top of the spike, through the load plateau, and back down to the dead load. During the ending stage, the load is slowly decreased to 0 lb. and then slowly increased until failure occurs.

When comparing Figure 5-16 and Figure 5-17, a major difference is seen between the static plot and the ending stage of the double design impact plot. The slope of the static load-deflection curve changes from the beginning to the end of the load, but the slope of the spike load-deflection curve is very constant until the load reaches the spike maximum, at approximately 4800 lb. After the maximum spike load is reached, the slope of the load-deflection curve decreases dramatically.

Figure 5-18 shows the typical load-deflection plot for the static group and for the double design impact group when the load is above the maximum spike load. The general shapes of both curves are approximately the same.

Therefore, the load-deflection curve of a tension splice joint subjected to the double design impact load is linear until the maximum spike load is exceeded. After the maximum spike load, the joint behaves approximately like a joint tested only with a ramp load.

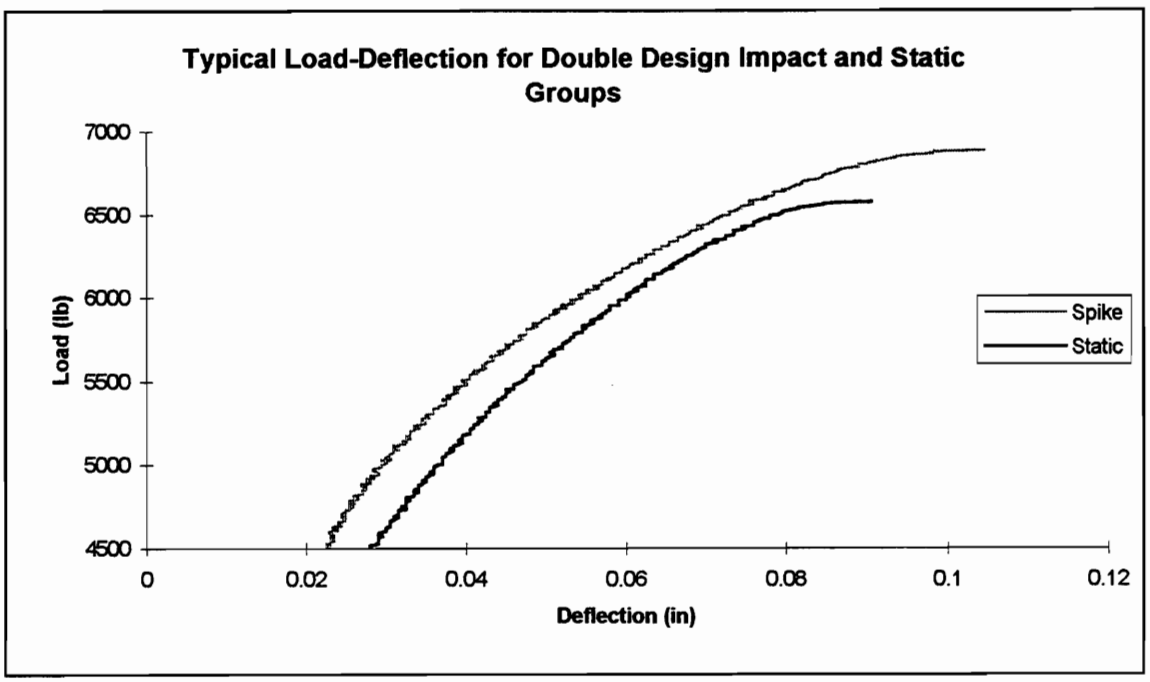

Figure 5-18: Load-deflection plot for static ramp load and the ending stage for the double design impact load cases above the maximum spike load

5.2.4 Ultimate Impact Load Results

The average properties, COV values, and sample size for tension splice joints tested in tension with the ultimate impact load are shown in Table 5-19. Property values for all tension splice joint results are given in Appendix D.

The COV value is particularly small for the ultimate strength. This low COV is likely caused by the exclusion of the three joints which failed during the ultimate impact load from the COV calculations. For this group, the spike load is filtering out the weaker joints by failing them. These excluded joints would otherwise be outliers which would increase the variation and thus the COV.

Table 5-19: Ultimate impact load tension splice joint property values, COV, and sample size

Property Description	Average Value	C. O. V.	Sample Size
Dead Load Stiffness (lb/in) begin	865,000	47.1%	7
end	441,000	15.4%	7
Design Load Stiffness (lb/in)	341,000	5.0%	7
Ultimate strength (lb)	7,520	5.6%	7
Ultimate deflection (in)	0.069	31.2%	7
Dynamic Deflection (in)	0.032	20.3%	7

The ratio of joints which failed during the spike load to joints which survived the spike load is interesting because it infers that tension splice joints are stronger when loaded very quickly. This The spike load used for this test changes from dead load, 865 lb, to the average of the static ultimate strength values, 6824 lb, in one second. If the maximum value of the impact load is equal to the average strength of the joints being tested, 50% of the joints would be weaker than the average and 50% would be stronger. Therefore, 50% of the joints subjected to the ultimate impact load should fail before the spike maximum is reached. The 30% failure ratio seen in this test implies that loading tension splice joints very quickly increases the ultimate strength. This observation supports the well established relationship between duration of load and strength of wood.

Table 5-20 shows the comparison of the static ramp load results to the ultimate impact load results.

Table 5-20: Comparison of ultimate impact and static ramp tension splice joint property values

Property Description		p-Value (two-sided)	Average Value Static	Average Value Impact	C.O.V. and {Sample Size} Static	C.O.V. and {Sample Size} Impact
Dead Load	begin	0.11	650,000	865,000	27% {9}	47% {7}
Stiffness (lb/in)	end	0.004	650,000	441,000	27% {9}	15% {7}
Design Load Stiffness (lb/in)		0.009	437,000	341,000	22% {9}	5% {7}
Ultimate strength (lb)		0.05 *	6,824	7,520	15% {9}	6% {7}
Ultimate deflection (in)		0.17 *	0.081	0.069	30% {9}	31% {7}

* one-sided test used

The data presented insufficient evidence to conclude that a difference exists between the ultimate impact loading and the static loading ultimate deflection and beginning dead load stiffness (one-sided p-value of 0.17 and two-sided p-value of 0.11, respectively).

After the ultimate impact load, convincing evidence of a difference between the ultimate impact loading and static loading dead load stiffnesses is seen (two-sided p-value of 0.004). The dead load stiffness for the ultimate impact group drops by approximately 49% because of the ultimate impact. The data also shows convincing to moderate evidence for a difference between the ultimate impact loading and static loading ending design load stiffnesses (two-sided p-value of 0.009). The ultimate impact loading design load stiffness is only about 22% lower than the static loading design load stiffness.

Stiffness increased for heel joints subjected to the double design impact load, but decreased for tension splice joints subjected to the same load. The difference in stiffness change is partially due to the different amounts of dynamic

deflection which occurred during the impact loads. Heel and tension splice joint dynamic deflection averages are compared in Table 5-21.

Table 5-21: Comparison of double design impact load dynamic deflection averages for heel and tension splice joints

Property Description	p-Value (two-sided)	Average Value		C.O.V.	
		Heel	Tension Splice	Heel	Tension Splice
Dynamic Deflection (in)	2.E-06	0.025	0.007	24%	35%

Overwhelming evidence exists of a difference between the dynamic deflections of heel and tension splice joints (two-side p-value of 2.E-06). In heel joints, the large amount of dynamic deflection likely caused wood fiber densification near the metal teeth, but for tension splice joints, the dynamic deflection was only enough to slightly enlarge the holes in which the teeth sit. For heel joints, the densified wood fibers caused increased stiffness, but for tension splice joints, the enlarged holes caused a decrease in stiffness. After the dynamic load was applied in heel joint tests, small gaps were seen between the metal teeth and the wood. Based on this simple observation, it was assumed that wood densification was occurring on the opposite side of the teeth.

Moreover, the different stiffness change in heel joints compared to tension splice joints, subjected to the same dynamic load, is likely caused by the fundamental differences in joint geometry and loading.

When a tension splice joint is loaded, bending moment is induced about the weakest axis in the metal teeth because the force direction and the flat side of the teeth are aligned. Therefore, the teeth bend considerably.

When a heel joint is loaded the metal teeth are less inclined to bend because the force and the flat side of the teeth are not aligned, they are more secure in the wood holes because the plate teeth must withdraw further for a given deflection. Also, the angle between the heel joint teeth and the applied force results in the applied force being distributed on a smaller area. The resultant higher stress on the wood fibers causes more wood densification. The combination of wood densification and higher plate tooth security makes the joint stiffer after the dynamic load is applied.

For tension splice joints, the teeth are more flexible, and thus they are less likely to cause wood densification. More flexible teeth bend if the metal plate is pushed through the wood while stiff teeth crush the wood fibers as shown in Figure 5-19.

The greater tooth bending in tension splice joints results in teeth which are less secure in the wood because they are not required to withdraw as much for a given deflection. The combination of low wood densification and low plate tooth security makes the joint less stiff after dynamic load is applied.

Suggestive evidence exists for a difference between the static loading and ultimate impact loads (one-sided p-value of 0.05). The data suggests that the ultimate load for the ultimate impact group is approximately 10% higher than

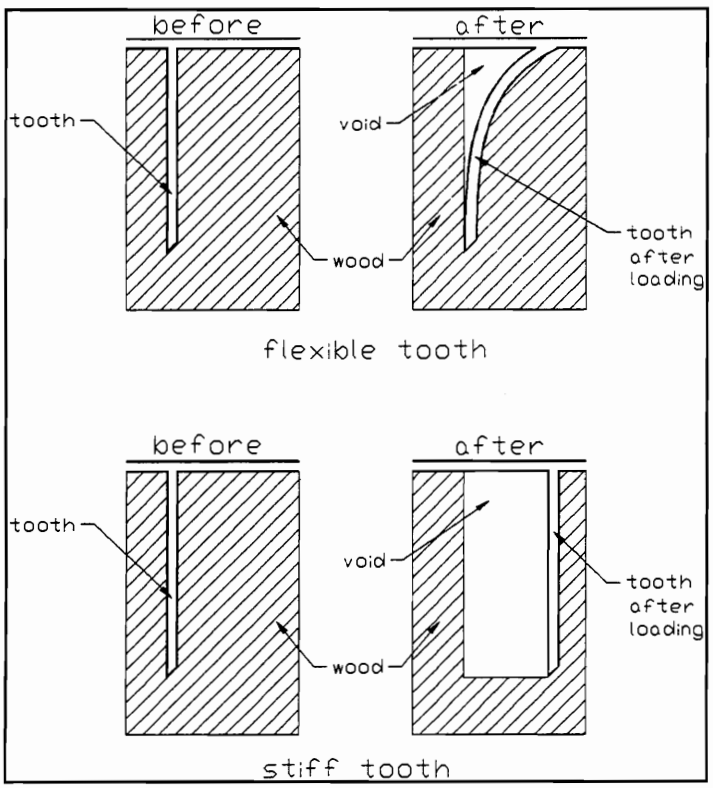

Figure 5-19: Flexible and stiff metal teeth before and after being pushed into wood fibers

the static loading group. This difference could be attributed to the filtering of weaker joints by the load spike. Weaker joints are more likely to fail during the spike, and thus less likely to be included in the group average, which increases the average ultimate strength.

Table 5-22 shows the comparison of selected properties from the double design impact group and the ultimate impact group.

Table 5-22: Comparison of double design impact group and ultimate impact group properties

Property Description	p-Value (two-sided)	Average Value 2*Design	Average Value Ultimate	C.O.V. {Sample Size} 2*Design	C.O.V. {Sample Size} Ultimate
Beginning Dead Load Stiffness (lb/in)	0.40	721,000	865,000	21% {10}	47% {7}
Ultimate Strength (lb)	0.27	7,235	7,520	8% {10}	6% {7}
Dynamic Deflection (in)	3.E-05	0.007	0.032	35% {10}	20% {7}

Comparing the beginning dead load stiffness reveals insufficient evidence to conclude that a difference exists between the two groups (two-sided p-value of 0.40). Although only one pre-spike property can be compared to the static group, it is assumed that the double design impact and ultimate impact groups are approximately the same before the spike load.

The dynamic deflection is a measure of the permanent deflection caused by the spike load. Large dynamic deflections would suggest that the spike load had a large effect on the joint, while the absence of dynamic deflection would imply that the spike load had little or no effect. Convincing evidence exists for a difference between the dynamic deflection values of the double design impact group and the ultimate impact group (two-sided p-value of 3.E-5).

Larger dynamic deflection is expected for the ultimate impact group than for the double design impact group because the ultimate impact magnitude is much larger. The spike maximum for the ultimate impact test is 50% larger than the spike maximum for the double design impact, but the dynamic deflection for the ultimate impact group is approximately 360% larger than the dynamic

deflection for the double design impact group. In short, a 50% increase in load produced 360% increase in permanent deflection.

The 50% load increase did not create a 50% deflection increase because joints subjected to the ultimate impact experienced large inelastic deformations while the load was at the spike maximum. At the double design impact maximum, some joints had very small inelastic deformations, while others did not yield at all. A comparison of typical double design impact and ultimate impact load-deflection plots is shown in Figure 5-20. Only the spike portion of the load-deflection plot is shown for simplicity.

Both curves start at the same point and follow the same approximate path until the load increases over the double design value. The deflection from the

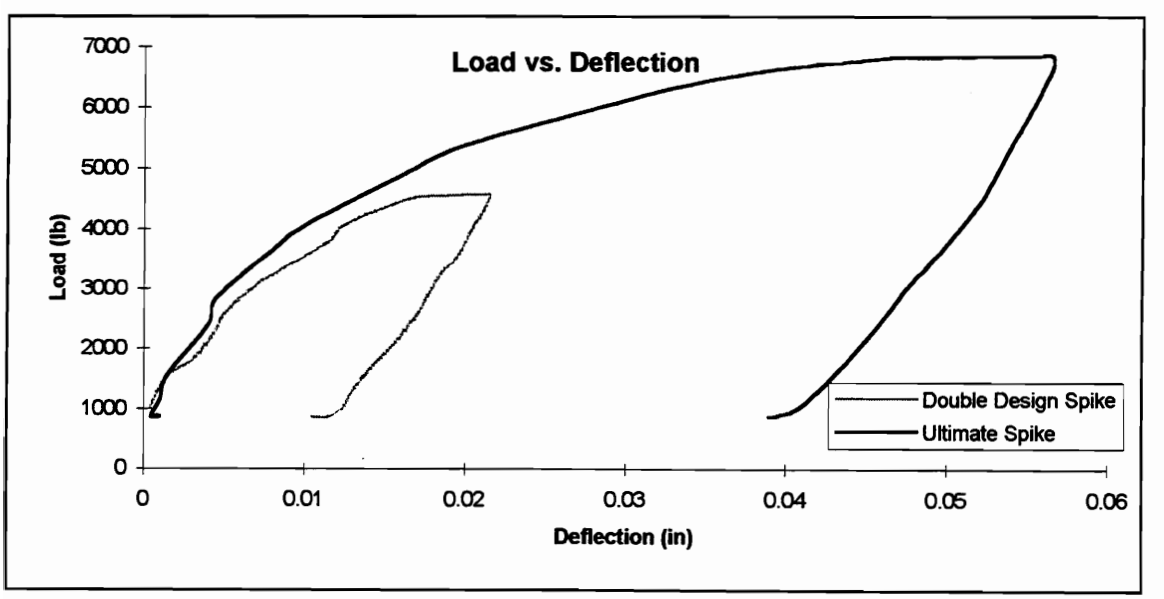

Figure 5-20: Typical load-deflection plots for double design impact and ultimate impact groups

ultimate impact test becomes much larger than the deflection for the double design impact test. The ultimate impact curve has an extensive inelastic deformation region, but the corresponding area for the double design impact is quite small. These curves are part of the hysteresis curve for MPC tension splice joints. If the complete hysteresis curve was available, the energy dissipation would be the area which it encloses. Because the area under the load-deflection plot for the ultimate impact group is larger than the area under the load-deflection plot for the double design impact group, joints from the ultimate impact group dissipated more energy than those from the double design impact group. This is expected because the energy input into the joint is also higher in the ultimate impact group. The input energy is related to the maximum load and deflection (during the hysteresis curve). Over half of the dynamic deflection for the ultimate impact curve occurs when the load is greater than 4500 lb.

Figure 5-21 shows a typical load-deflection plot from the ultimate impact group.

Several similarities exist between the load-deflection plots of tension splice joints from the double design impact group and the ultimate impact group. The beginning portion of each plot is almost identical. Figure 5-20 shows that the general shape of the load-deflection plot is the same for the double design impact group and the ultimate impact group during the load spike. For both groups, the spike caused a non-linear positive curve during the increasing

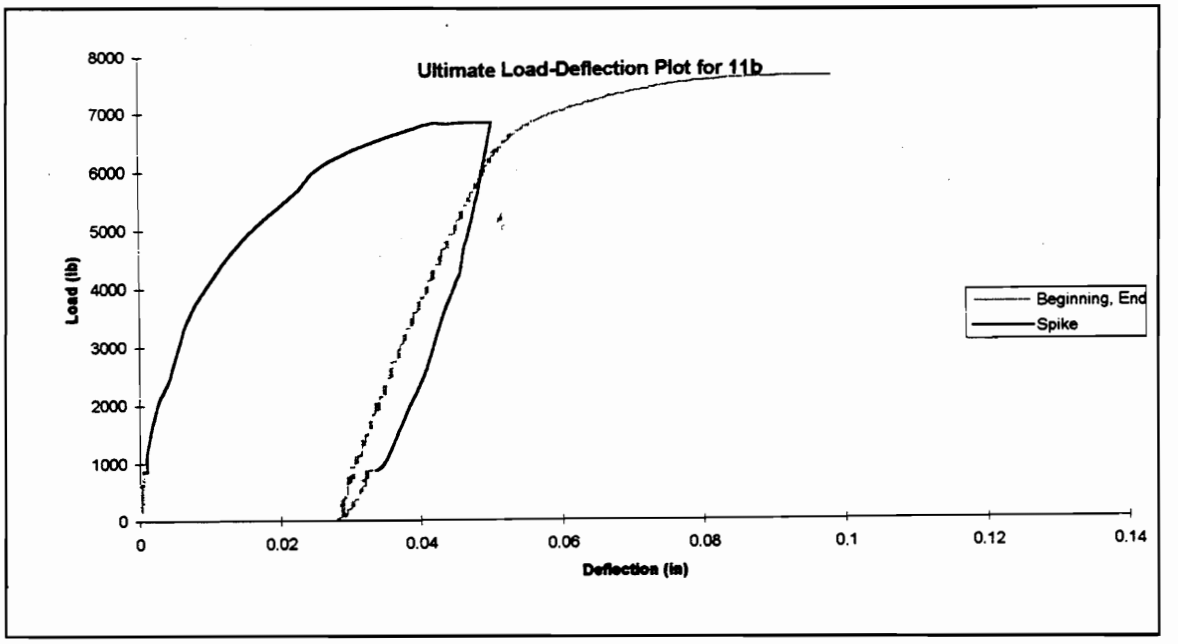

Figure 5-21: Typical load-deflection plot of a tension splice joint from the ultimate impact group

portion of the spike, inelastic deformation when the spike was at the maximum, and a non-linear negative curve during the decreasing portion of the spike. (A positive curve has a positive change in slope and curves like this symbol ∪. A negative curve has a negative change in slope and curves like this symbol ∩).

Both groups showed that after the spike load was applied, the joint behaved in a much more linear fashion. Both Figure 5-17 and Figure 5-21 show that the ending portion of the load-deflection curve is very straight and does not change slope appreciably until the load exceeds the spike maximum. After the spike maximum is reached, both groups show a large decrease in stiffness.

6. Conclusions

The load-deflection plots for metal-plate-connected (MPC) heel and tension splice joints show non-linear behavior under static ramp loads. Heel and tension splice joints subjected to load controlled static ramp loads (900 lb/min) fail with little warning. Failure is generally preceded by partial withdrawal of the outside teeth, tooth hole elongation, and plate shear deformation (for heel joints only). These failure warnings are only visible if close attention is paid to the joint as load is increased.

No distinct failure mode was seen for either heel or tension splice joints. Heel joints failed in either wood shear, tooth withdrawal, or a combination of the two. Tension splice joints failed in three different modes: wood shear, tooth withdrawal, and tension plate failure. Combinations of two of these three modes were common.

The effect of multiple dynamic loads on MPC joints is currently unknown. In this study, MPC joints in the experimental groups were subjected to either one wind load simulation or one impact load, after which, the joints were failed using a static ramp load. Strength, stiffness, and deflection properties were compared to properties of joints subjected only to the static ramp load. It is possible that using one dynamic load would have little or no effect on a joint while several iterations of the same dynamic load would have a more profound effect.

For most groups, the COV for the stiffness properties was higher than the COV for the other properties. It is possible that stiffness has a higher variation because of the larger number of variables which contribute to the stiffness. Measured stiffness is likely affected by LVDT noise, metal teeth stiffness, wood-to-plate interaction, and friction between members, while the ultimate strength is affected by only one or a combination of two variables. These variables include steel strength, wood shear strength, and wood-to-plate interaction, which predict plate failure, wood shear failure, and tooth withdrawal, respectively.

6.1 Metal-Plate-Connected Heel Joint Conclusions

Static ramp load tests revealed that heel joints tested with the top member in tension had 17% higher average ultimate strength and 42% lower average ultimate deflection than heel joints made of similar material tested with the top member in compression. No significant difference exists between stiffnesses of heel joints tested in compression and heel joints tested in tension.

Heel joints subjected to the wind simulation tension load initially had the same stiffness as the static load control group, but after the wind simulation, the joints became much stiffer. The dead load stiffness and design load stiffness increased by 290% and 325%, respectively. The stiffness increase is caused by densification of the wood closest to the metal teeth. The wind simulation tension load caused no significant change in heel joint ultimate strength or ultimate deflection.

Heel joints subjected to the wind simulation compression load have the same initial and ending stiffnesses. No change is seen because the wind simulation compression loads are neither very large nor do they significantly range (compared to the average ultimate joint strength). Moderate evidence was found for a difference between the static load control group and the wind simulation compression load group for ultimate strength and ultimate deflection. This difference is believed to be caused by a chance grouping of stronger, more ductile joints into one group.

Heel joints subjected to the double design impact load condition behaved similar to joints subjected to the wind simulation tension load. Before the spike, the dead load stiffness was the same for the control and impact groups, but after, the stiffness dramatically increased. Again, this increase in stiffness is attributed to wood densification near the metal teeth caused by prior loading. No difference was found between the static load control and impact load groups ultimate strengths or ultimate deflections.

Similarities exist between the properties from the double design impact load group and the hurricane wind simulation tension load group. For both groups, the dynamic loading had little to no effect on either ultimate deflection or ultimate strength. Also, for both groups, the dynamic load caused a significant increase in stiffness. The stiffness increase was more dramatic for the wind simulation tension load group than for the double design impact group. An

impact load to the average ultimate strength would probably produce stiffness changes closer to those seen in the wind simulation tension load group.

Because all the dynamic loads, used in all the experimental groups, were only applied once, the effect of multiple dynamic loads on the strength, stiffness, and ductility is unknown.

6.2 Metal-Plate-Connected Tension Splice Joint Conclusions

Tension splice joints and heel joints tested in tension have similar dead load stiffness, design load stiffness, and ultimate strength values when tested with a static ramp load. The major difference for the two groups is that heel joints loaded in tension deflect over twice as much before failure as tension splice joints. Although similarities exist between tension splice joints and heel joints tested in tension, these similarities must be coincidental because of the major differences between the geometry and plate size of the two joint types.

Tension splice joint properties are much less similar to the properties of heel joints tested in compression. Heel joints tested in compression are less stiff, have lower strength, and deflect more before failure than tension splice joints.

Joints subjected to the accelerated ramp load produced the same results as the joints subjected to the static ramp load. Using the accelerated ramp load as a control group for MPC tension splice joints would produce "static" results in $1/10^{th}$ the time.

The effect of the double design impact load on tension splice joint stiffnesses was opposite to the effect on heel joint stiffnesses. The double design impact load caused heel joint stiffness to increase and tension splice joint stiffness to decrease. The different changes are attributed to the amount of dynamic deflection the impact load caused. Stiffness decreased in tension splice joints because of partial tooth withdrawal, while stiffness increased in heel joints because of wood fiber densification.

Joints in the double design impact group behaved in a very similar to manner those in the ultimate impact group. Neither the double design impact load or ultimate impact load caused strength or ultimate deflection changes. The shapes of the load-deflection curves for both impact groups were very similar, while the magnitudes of the loads and deflections were quite different. The ultimate impact was only 50% larger than the double design impact, but joints in the ultimate group deflected 360% more during the spike compared to the joints in the double design group.

6.3 Recommendations for Further Study

- Examine the effect of multiple wind simulations on the strength, stiffness, and ductility of MPC joints. Buildings in hurricane prone areas are expected to survive several wind events. Subject joints to multiple wind load simulations.

Then, attempt to reproduce the results from the multiple wind simulation tests, but this time using multiple spike loads.

- Construct tension splice joints with the metal plates at varying angles to the axis of the joint. The control would consist of a group of tension splice joints which are properly constructed (no angle between the axis of the tension splice joint and the metal plate). Expose both control and experimental groups to the same dynamic load. Examine changes in the stiffness to determine if higher angles between the metal teeth and the applied force cause a stiffening effect as hypothesized in this thesis.
- Construct a testing apparatus which uses timber end walls and Simpson Strong-Tie connectors as support conditions for heel joints.
- Develop a testing system able to apply both compression and tension forces to heel joints in the same test. Using this system, apply the hurricane wind tension load simulation used in this project. After the wind simulation is finished, apply a compression static ramp load to the joint until failure. This would model a truss which was subjected to a hurricane and then a large gravity load (such as construction or snow loads). Any decrease in stiffness during the gravity load could be explained by the presence of voids between the wood fibers and the metal teeth.
- Develop a testing apparatus which is able to apply both axial forces and moments to the heel joints. Axial forces and moments should be applied to model a truss loaded with the actual static and dynamic loads.

- Investigate how the alignment of the metal plates affects the behavior of MPC joints. Metal plates should be positioned correctly for the static load control group, while the experimental groups would consist of joints with metal plates in the correct position, but rotated at various angles.
- Determine the effects of water saturation on a joint which was constructed at a normal moisture content. This project would model a joint which was properly constructed, but saturated with water by a leak in the roof.
- Determine the effect of encased knots on the behavior of MPC joints. The metal plate would be placed directly over the encased knot. The varying grain direction and specific gravity of the knot could potentially affect the failure mode and ultimate strength of the joint. (Shear wood failure modes would not be expected because of the varying grain pattern in the knot.)
- Determine the effect of storing or shipping a truss bundle on the flat side by performing tests on actual trusses. After a set amount of time passes, remove the joints and fail them using a ramp load and compare to a static load control group.
- Construct MPC joints at 14% moisture content, but perform static ramp load tests after the joints have equilibrated to 20% moisture content. This would simulate joints which were properly built, but which experience a hot humid environment, such as an attic during the summer.
- Construct MPC joints at 25% moisture content, but perform a static ramp load test after joints have equilibrated to 14% moisture content. These tests

would help determine the effect of shrinkage and drying stresses on MPC joints.

- Test the densification theory proposed in this thesis. This could be done by performing the dynamic tests as described previously, but not testing the joints to failure. After the dynamic load is finished, the density of the wood in contact with the metal teeth would be compared to the density of the wood which was not in contact with the metal teeth. The density of the wood should be determined using methods which do not unnecessarily stress the wood fibers. This could potentially be done using x-ray density meters or similar technology.

Bibliography

American Society for Testing and Materials. 1994. ASTM D1761-88: Standard Methods of Testing Mechanical Fasteners in Wood., D2395-93: Standard Test Methods for Specific Gravity of Wood and Wood-Base Materials., ASTM D2915-94: Standard Practice for Evaluating Allowable Properties for Grades of Structural Lumber., ASTM D4442-92: Standard Test Methods for Direct Moisture Content Measurement of Wood and Wood-Base Materials. Vol. 04.10. Philadelphia, PA.

American Society of Civil Engineers. 1995. Minimum Design Loads for Buildings and Other Structures. American Society of Civil Engineers. New York, NY.

Arbek, T. 1979. The Effect of Time on the Strength of Truss Plate Joints. Unpublished report submitted to the Department of Civil Engineering, Carleton University. Ottawa, Canada.

AFPA. 1991. ANSI/NFPA NDS-1991 National Design Specification for Wood Construction. American Forest and Paper Association, Washinton DC.

Callahan, E.E. 1993. Metal-Plate-Connected Wood Truss Handbook. Wood Truss Council of America. Madison, WI.

Computers & Structures, Inc. 1991. SAP90 - A Series of Computer Programs for the Finite Element Analysis of Structures - Structural Analysis User's Manual. Version 5.31. Berkeley, CA.

Cook, N.J. 1990. The Designer's Guide to Wind Loading of Building Structures: Part 2 Static Structures. Butterworths. London.

Cramer, S.M., D. Shrestha, and W.B. Fohrell. 1990. Theoretical Consideration of Metal-Plate-Connected Wood-Splice Joints. Journal of Structural Engineering. 116(12):3458-3473.

Dagher, H.J., V. Cacese, Y. Hsu. 1991. Feasibility of Metal Connector Plates in Timber Bridges: Fatigue Study. Technical Report. Department of Civil Engineering. University of Maine. Orono, MA.

Dolan, J.D. and T.E. McLain. 1994. Proposed Test Method For Dynamic Properties of Connections Assembled With Mechanical Fasteners. Journal of Testing and Evaluation, 22(6):542-547.

Emerson, R. and Fridley, K.J. 1996. Resistance of Metal-Plate-Connected Truss Joints to Dynamic Loading. Forest Products Journal. 46(5):83-90.

Freilinger, S. 1998. Characteristics and Duration of Load Performance of Metal Plate-Connected Truss Joints. draft MS Thesis. Oregon State University. Corvallis, OR.

Foschi, R.O. 1974. Load-Slip Characteristics of Nails. Wood Science. 7(1):69-76.

Foschi, R.O. 1977. Load-Slip Characteristics for Connections with Common Nails. Wood Science. 9(3):118-123.

Girhammar, U.A. and H. Andersson. 1988. Effect of Loading Rate on Nailed Timber Joint Capacity. Journal of Structural Engineering. 114(11):2439-2456.

Gupta, R. 1993. Metal-Plate Connected Tension Joints Under Different Loading Conditions. Wood and Fiber Science. 26(2):212-222.

Gupta, R. 1990. Reliability Analysis of Semirigidly Connected Metal Plate Residential Wood Trusses. Ph.D. thesis. Cornell University. Ithaca, N.Y.

Gupta, R. and K.G. Gebremedhin. 1990. Destructive Testing of Metal Plate Connected Wood Truss Joints. Journal of Structural Engineering. 116(7):1971-1982.

Gupta, R. and K.G. Gebremedhin. 1992. Resistance Distributions of a Metal-Plate-Connected Wood Truss. Forest Products Journal. 42(7/8):11-16.

Hayashi, T., H. Sasaki, and M. Masuda. 1980. Fatigue Properties of Wood Butt Joints with Metal Plate Connectors. Forest Products Journal. 30(2):49-54.

Hoover, C.C. 1993. Lessons of Hurricane Andrew. Good Connections. Alpine Engineering Products, Inc. Pompano Beach, FL.

Kent, S. 1995. Dynamic Behavior of Metal-Plate-Connected Wood Truss Joints. MS Thesis. Oregon State University. Corvallis, OR.

Kirk, L.S., T.E. McLain, and F.E. Woeste. 1989. Effect of Gap Size on Performance of Metal-Plated Joints in Compression. Wood Fiber Science. 21(3):274-288.

Lau, P.W. 1987. Factors Affecting the Behavior and Modeling of Toothed Metal-Plate Joints. Canadian Journal of Civil Engineering. 14(2). 183-195

Link, C.L., C.C. Gerhards, and J.F. Murphy. 1988. Estimation and Confidence Intervals for Parameters of a Cumulative Damage Model. United States Department of Agriculture. FRL-RP-484. Madison, WI.

Mehta, K.C., R.D. Marshall, and D.C. Perry. 1991. Guide to the Use of the Wind Load Provisions. American Society of Civil Engineers. New York, NY.

Misra, R.D. and M.L. Esmay. 1966. Stress Distributions in the Punched Metal Plate of a Timber Joint. Transcript. American Society of Agricultural Engineers. 9(6). 839-845.

Polensek, A. and B.D. Schimel, 1991. Dynamic Properties of Light-Frame Wood Subsystems. Journal of Structural Engineering. 117(4):1079-1095.

Ramsey, F.L. and D.W. Schafer. 1997. The Statistical Sleuth: A Course in Methods of Data Analysis. Duxbury Press. Belmont CA.

Simiu, E. and R. Scanlan. 1996. Wind Effects on Structures: Fundamentals and Applications to Design. John Wiley & Sons, Inc. New York, NY.

Simpson. 1997. Connectors for Wood Construction Product & Instruction Manual. Simpson Strong-Tie Company, Inc., Pleasanton. CA.

Soltis, L.A. and P. Mtenga. 1985. Strength of Nailed Wood Joints Subjected to Dynamic Load. Forest Products Journal. 35(11/12):14-18.

Suddarth, S.K., D.H. Percival, and Q.B. Comus. 1979. Variability in Tension Performace of Metal Plate Connections. Procedure of the Metal Plate Wood Conference. Forest Products Research Society. 98-104.

Structural Engineers Association of Washington. 1995. Wind Commentary to the Uniform Building Code. Structural Engineers Association of Washington. Seattle, WA.

Taylor, S.E. and D.A. Bender. 1988. Simulating Correlated Lumber Properties Using a Modified Multivariate Normal Approach. Transactions of the American Society of Agricultural Engineers. 31(3):182-186.

Truss Plate Institute. 1985. Design Specifications for Metal-Plate-Connected Wood Trusses: TPI-85. Madison, WI.

United States Army Corps of Engineers Field Research Facility. 1991. Hurricane Bob Wind Data. unpublished data. Kitty Hawk, NC.

Vatovec, M., T.H. Miller, and R. Gupta. 1995. Modeling of Metal-Plate-Connected Wood Truss Joints. Transactions of the ASAE. 39(3):1101-1111.

Vatovec, M., R. Gupta, and T. Miller. 1996. Testing and Evaluation of Metal-Plate-Connected Wood Truss Joints. Journal of Testing and Evaluation. March. 24(2):63-72.

Appendices

Appendix A
Finite Element Model (SAP90) Input File for Fink Truss

SAP90 input file used to analyze Fink truss member forces.

```
C SAP90 Input File
C Fink Truss, 4/12 pitch, 30 foot span
C 20 lb/ft dead load on top and bottom chords
C includes dead weight of web members.
C Using 2x4 truss members
C E = 1.6E6 psi
C Units are POUND INCHES
SYSTEM
 R=0  L=1  C=0  V=20  T=0.0001  P=0  W=0  Z=0
GRID
 XN=1    YN=1    ZN=1    OG=0
 0
 0
 0

C Defines the location of all joints
JOINTS
 1    X=0 Y=0 Z=0
 2    X=120 Y=0 Z=0
 3    X=150 Y=0 Z=0
 4    X=240 Y=0 Z=0
 5    X=360 Y=0 Z=0
 6    X=24 Y=0 Z=8
 7    X=336 Y=0 Z=8
 8    X=90 Y=0 Z=30
 9    X=270 Y=0 Z=30
 10   X=144 Y=0 Z=48
 11   X=216 Y=0 Z=48
 12   X=180 Y=0 Z=60
 13   X=-12 Y=0 Z=-4
 14   X=372 Y=0 Z=-4
 15   X=0 Y=0 Z=-96
 16   X=360 Y=0 Z=-96
 17   X=384 Y=0 Z=0
 18   X=-24 Y=0 Z=0

Defines properties of the materials for the different members
FRAME
 NM=4 NL=26 NSEC=0
 1   A=0.012 J=0 I=0,999999 AS=0,0 E=1.6E+006 G=0 W=0 M=0 TC=0
 2   A=8.25 J=0 I=20700,20700 AS=0,0 E=1.6E+006 G=0 W=0.65 M=0.0016927 TC=0
 3   A=5.25 J=0 I=0,5.35 AS=0,0 E=1.6E+006 G=0 W=0.09479 M=0.0002468 TC=0
 4   A=5.25 J=0 I=0,5.35 AS=0,0 E=1.6E+006 G=0 W=1.6667 M=0.0043403 TC=0

C Defines uniform loads
 1   WL=0,0,0 WG=0.183333,0,0.541667 T=0,0,0
 2   WL=0,0,0 WG=-1.00833,0,3.01667 T=0,0,0
 3   WL=0,0,0 WG=0.958333,0,2.86667 T=0,0,0
 4   WL=0,0,0 WG=3.025,0,9.08333 T=0,0,0
 5   WL=0,0,0 WG=0.466667,0,1.39167 T=0,0,0
 6   WL=0,0,0 WG=-1,0,3.01667 T=0,0,0
 7   WL=0,0,0 WG=1.23333,0,3.71667 T=0,0,0
 8   WL=0,0,0 WG=3.29167,0,9.91667 T=0,0,0
 9   WL=0,0,0 WG=-3.84167,0,11.5833 T=0,0,0
```

```
10  WL=0,0,0 WG=-3.525,0,10.5833 T=0,0,0
11  WL=0,0,0 WG=4.13333,0,12.4167 T=0,0,0
12  WL=0,0,0 WG=5.65833,0,17 T=0,0,0
13  WL=0,0,0 WG=-1.29167,0,3.875 T=0,0,0
14  WL=0,0,0 WG=1.225,0,0 T=0,0,0
15  WL=0,0,0 WG=-1.225,0,0 T=0,0,0
16  WL=0,0,0 WG=10.2083,0,0 T=0,0,0
17  WL=0,0,0 WG=-10.2083,0,0 T=0,0,0
18  WL=0,0,0 WG=10.0417,0,0 T=0,0,0
19  WL=0,0,0 WG=-2.20833,0,0 T=0,0,0
20  WL=0,0,0 WG=1.05833,0,0 T=0,0,0
21  WL=0,0,0 WG=6.775,0,0 T=0,0,0
22  WL=0,0,0 WG=5.68333,0,17.0833 T=0,0,0
23  WL=0,0,0 WG=1.29167,0,3.875 T=0,0,0
24  WL=0,0,0 WG=2.84167,0,8.54167 T=0,0,0
25  WL=0,0,0 WG=1.55,0,-4.65 T=0,0,0
26  WL=0,0,0 WG=0.775,0,-2.325 T=0,0,0

C Places members between the joints and assigns connectivity to ends
1   15  1   M=2,2,1 LP=3,0 LR=1,1,0,1,1,1  \
            NSL=21
2   16  5   M=2,2,1 LP=3,0 LR=1,1,0,1,1,1  \
            NSL=20
3   18  1   M=1,1,1 LP=0,0 LR=1,1,0,1,1,1
4   5   17  M=1,1,1 LP=0,0 LR=1,1,0,1,1,1
5   13  1   M=4,4,1 LP=0,0 LR=1,0,0,1,0,1  \
            NSL=26
6   1   6   M=4,4,1 LP=0,0 LR=0,0,0,0,0,1  \
            NSL=25
7   6   8   M=4,4,1 LP=0,0 LR=0,0,0,0,0,1  \
            NSL=25
8   8   10  M=4,4,1 LP=0,0 LR=0,0,0,0,0,1  \
            NSL=25
9   10  12  M=4,4,1 LP=0,0 LR=0,1,0,0,1,1  \
            NSL=25
10  12  11  M=4,4,1 LP=0,0 LR=1,0,0,1,0,1  \
            NSL=24
11  11  9   M=4,4,1 LP=0,0 LR=0,0,0,0,0,1  \
            NSL=23
12  9   7   M=4,4,1 LP=0,0 LR=0,0,0,0,0,1  \
            NSL=23
13  7   5   M=4,4,1 LP=0,0 LR=0,0,0,0,0,1  \
            NSL=24
14  5   14  M=4,4,1 LP=0,0 LR=0,1,0,0,1,1  \
            NSL=12
15  1   2   M=4,4,1 LP=0,0 LR=1,0,0,1,0,1
16  2   3   M=4,4,1 LP=0,0 LR=0,1,0,0,1,1
17  3   4   M=4,4,1 LP=0,0 LR=1,0,0,1,0,1
18  4   5   M=4,4,1 LP=0,0 LR=0,1,0,0,1,1
19  8   2   M=3,3,1 LP=0,0 LR=1,1,0,1,1,1
20  2   12  M=3,3,1 LP=0,0 LR=1,1,0,1,1,1
21  12  4   M=3,3,1 LP=0,0 LR=1,1,0,1,1,1
22  4   9   M=3,3,1 LP=0,0 LR=1,1,0,1,1,1
```

```
C Defines the restraint (support) of the joints
RESTRAINTS
 15   15   1    R=1,1,1,1,0,1
 16   16   1    R=1,1,1,1,0,1
 13   13   1    R=0,1,0,1,0,1
 1    1    1    R=0,1,0,1,0,1
 6    6    1    R=0,1,0,1,0,1
 8    8    1    R=0,1,0,1,0,1
 2    2    1    R=0,1,0,1,0,1
 10   10   1    R=0,1,0,1,0,1
 3    3    1    R=0,1,0,1,0,1
 12   12   1    R=0,1,0,1,0,1
 11   11   1    R=0,1,0,1,0,1
 4    4    1    R=0,1,0,1,0,1
 9    9    1    R=0,1,0,1,0,1
 7    7    1    R=0,1,0,1,0,1
 5    5    1    R=0,1,0,1,0,1
 14   14   1    R=0,1,0,1,0,1
 18   18   1    R=1,1,1,1,0,1
 17   17   1    R=1,1,1,1,0,1


TIMEH
 ATYPE=0 NSTEP=1000 DT=0.5 NF=1 NV=20 D=0.1
 NF=1 PRIN=0 DT=0.5 NPL=1 NAM=SAPWIND2.TXT
 LC=1 NF=1 S=1 AT=0 ANGLE=0
```

Appendix B
Heel joint test results

Static Compression Ramp	Ultimate Strength (lb)	Design Load Stiffness (lb/in)	Dead Load Stiffness (lb/in)	Ultimate Deflection (in)	Moisture Content (%)	Time to Failure (min)
53a	5,768	274,660	241,667	0.168	11.5	6.4
48b	7,119	593,285	725,000	0.262	12.8	7.9
46a	5,719	272,344	290,000	0.248	12.5	6.4
45a	5,398	299,862	290,000	0.176	11.6	6.0
42a	6,311	350,594	290,000	0.223	11.8	7.0
42b	6,136	409,038	362,500	0.211	11.8	6.8
40b	5,300	176,668	181,250	0.281	12.6	5.9
38a	5,608	373,881	483,333	0.275	11.7	6.2
37b	6,173	171,480	181,250	0.290	11.7	6.9
32a	6,061	NA	NA	NA	10.8	6.7
Average	5,959	325,000	338,000	0.237	11.9	6.6
COV	8.9%	39.8%	50.9%	19.0%	5.0%	8.9%
# of samples	10	9	9	9	10	10

Static Compression Ramp	Rings per inch	% Late Wood	Specific Gravity	Modulus of Elasticity (10^6 psi)	Failure Mode	Grain Orientation
53a	16	15	0.48	1.95	WS	Both
48b	17	30	0.43	1.88	PF	Flat
46a	7	30	0.56	1.81	WS	Quarter
45a	5	25	0.53	1.92	WS and TW	Both
42a	4	25	0.51	1.96	WS	Both
42b	4	15	0.52	1.96	WS and TW	Both
40b	5	35	0.55	1.88	TW	Flat
38a	8	20	0.54	1.73	WS and TW	Flat
37b	10	30	0.57	1.92	TW	Quarter
32a	12	25	0.56	1.90	WS and TW	Flat
Average	9	25	0.52	1.89		
COV	54.8%	26.7%	7.9%	3.8%		
# of samples	10	10	10	10		

NA: Not Available
Flat: Flat-Sawn Lumber (Growth Rings Parallel to Wide Face of Lumber)
Quarter: Quarter-Sawn Lumber (Growth Rings Perpendicular to Wide Face of Lumber)
Both: Combination of Flat and Quarter-Sawn Lumber
TW: Tooth Withdrawal Failure
WS: Wood Shear Failure
PF: Metal Plate Failure

Static Tension Ramp	Ultimate Strength (lb)	Design Load Stiffness (lb/in)	Dead Load Stiffness (lb/in)	Ultimate Deflection (in)	Moisture Content (%)	Time to Failure (min)
45B	6,406	142,354	162,222	0.126	11.6	7.1
44A	8,634	261,650	243,333	0.205	12.2	9.6
40A	7,796	324,835	730,000	0.200	12.6	8.7
39B	7,292	220,959	486,667	0.105	12.1	8.1
38B	8,164	NA	NA	0.125	11.7	9.1
36A	6,962	290,100	486,667	0.195	11.7	7.7
33B	7,627	181,597	182,500	0.214	13.1	8.5
31A	6,692	171,602	162,222	0.233	13.6	7.4
30B	6,382	193,387	208,571	0.146	11.1	7.1
30A	5,933	NA	NA	0.118	11.2	6.6
Average	7,189	223,000	333,000	0.167	12.1	8.0
COV	12.0%	28.4%	63.1%	28.3%	6.7%	12.0%
# of samples	10	8	8	10	10	10

Static Tension Ramp	Rings per inch	% Late Wood	Specific Gravity	Modulus of Elasticity (10^6 psi)	Failure Mode	Grain Orientation
45B	5	35	0.50	1.92	TW	Quarter
44A	9	25	0.46	1.88	TW and PF	Quarter
40A	5	35	0.53	1.88	WS and PF	Flat
39B	9	25	0.52	1.78	WS	Quarter
38B	8	20	0.55	1.73	WS	Flat
36A	3	20	0.54	1.74	TW	Flat
33B	19	40	0.49	1.74	TW	Flat
31A	3	20	0.55	1.67	TW	Flat
30B	7	25	0.51	1.74	WS	Flat
30A	7	25	0.50	1.74	WS and TW	Flat
Average	8	27	0.51	1.78		
COV	61.3%	26.5%	5.6%	4.6%		
# of samples	10	10	10	10		

NA: Not Available
Flat: Flat-Sawn Lumber (Growth Rings Parallel to Wide Face of Lumber)
Quarter: Quarter-Sawn Lumber (Growth Rings Perpendicular to Wide Face of Lumber)
Both: Combination of Flat and Quarter-Sawn Lumber
TW: Tooth Withdrawal Failure
WS: Wood Shear Failure
PF: Metal Plate Failure

Wind Simulation (compression)	Ultimate Strength (lb)	Design Load Stiffness (lb/in)		Dead Load Stiffness (lb/in)		Ultimate Deflection (in)	Dynamic Deflection (in)	Moisture Content (%)
		beginning	ending	beginning	ending			
51a	6,918	384,342	329,436	365,000	365,000	0.266	0.001	11.8
48a	6,633	368,525	315,879	365,000	292,000	0.286	0.002	12.7
35b	5,799	214,785	241,634	243,333	243,333	0.24	0.002	11.4
27b	6,433	268,054	268,054	292,000	292,000	0.17	0.001	11.1
25c	5,958	180,534	198,587	208,571	208,571	0.304	0.003	11.7
25b	6,480	196,378	240,017	208,571	243,333	0.331	0.002	11.8
23c	6,549	272,895	242,574	292,000	243,333	0.301	0.001	11.1
23a	6,339	264,115	234,769	292,000	208,571	0.282	0.001	11.8
21c	6,767	250,617	214,815	243,333	243,333	0.298	0.003	11.2
21b	6,494	270,569	270,569	292,000	243,333	0.277	0.001	11.6
Average	6,437	267,000	256,000	280,000	258,000	0.276	0.002	11.6
COV	5.30%	24.83%	16.19%	19.88%	18.12%	16.09%	48.43%	4.1%
# of samples	10	10	10	10	10	10	10	10

Wind Simulation (compression)	Time to Failure (min)	Rings per inch	% Late Wood	Specific Gravity	Modulus of Elasticity (10^6 psi)	Failure Mode	Grain Orientation
51a	7.7	6	35	0.40	1.99	WS and PF	Flat
48a	7.4	17	45	0.37	1.88	TW and PF	Flat
35b	6.4	22	35	0.51	1.97	WS	Quarter
27b	7.1	14	30	0.41	2.00	WS and TW	Both
25c	6.6	6	25	0.52	2.07	TW	Flat
25b	7.2	8	20	0.53	2.07	TW	Flat
23c	7.3	4	20	0.52	1.76	TW	Both
23a	7.0	5	20	0.53	1.76	WS and TW	Flat
21c	7.5	4	20	0.48	1.68	TW	Flat
21b	7.2	4	20	0.49	1.68	WS and TW	Flat
Average	7.2	9	27	0.48	1.89		
COV	5.29%	71.0%	32.9%	12.3%	8.2%		
# of samples	10	10	10	10	10		

NA: Not Available
Flat: Flat-Sawn Lumber (Growth Rings Parallel to Wide Face of Lumber)
Quarter: Quarter-Sawn Lumber (Growth Rings Perpendicular to Wide Face of Lumber)
Both: Combination of Flat and Quarter-Sawn Lumber
TW: Tooth Withdrawal Failure
WS: Wood Shear Failure
PF: Metal Plate Failure

Wind Simulation (tension)	Ultimate Strength (lb)	Design Load Stiffness (lb/in)		Dead Load Stiffness (lb/in)		Ultimate Deflection (in)	Dynamic Deflection (in)	Moisture Content (%)
		beginning	ending	beginning	ending			
52b	7,803	325,125	1,300,433	292,000	1,460,000	0.142	0.005	12.5
44b	7,739	234,515	644,958	292,000	486,667	0.165	0.005	12.2
34b	7,185	342,143	798,339	486,667	1,460,000	0.105	0.006	11.9
31b	6,787	174,026	452,490	208,571	730,000	0.15	0.004	13.5
28c	7,730	429,444	858,936	486,667	1,460,000	0.147	0.007	12.2
27c	9,426	628,400	1,047,310	486,667	1,460,000	0.222	0.002	11.5
27a	8,929	372,042	1,488,205	365,000	1,460,000	0.183	0.005	11.5
26b	6,769	150,422	752,078	182,500	1,460,000	0.148	0.009	11.5
26a	7,717	257,233	1,286,198	292,000	1,460,000	0.162	0.006	12.1
24b	7,981	266,033	886,781	243,333	1,460,000	NA	0.009	11.6
Average	7,807	318,000	952,000	334,000	1,290,000	0.158	0.006	12.1
COV	10.83%	43.80%	34.14%	35.06%	28.20%	20.15%	38.56%	5.1%
# of samples	10	10	10	10	10	9	10	10

Wind Simulation (tension)	Time to Failure (min)	Rings per inch	% Late Wood	Specific Gravity	Modulus of Elasticity (10^6 psi)	Failure Mode	Grain Orientation
52b	8.7	5	30	0.51	1.70	TW	Flat
44b	8.6	7	25	0.43	1.88	TW	Both
34b	8.0	4	15	0.46	1.81	WS	Both
31b	7.5	4	25	0.55	1.67	WS and TW	Flat
28c	8.6	15	25	0.52	1.66	WS and TW	Flat
27c	10.5	8	20	0.53	2.00	WS and TW	Both
27a	9.9	10	30	0.51	2.00	WS and TW	Quarter
26b	7.5	6	20	0.56	1.76	WS	Quarter
26a	8.6	6	20	0.56	1.76	WS and TW	Quarter
24b	8.9	4	20	0.52	1.86	TW	Both
Average	8.7	7	23	0.52	1.81		
COV	10.83%	49.9%	21.0%	8.3%	6.9%		
# of samples	10	10	10	10	10		

NA: Not Available
Flat: Flat-Sawn Lumber (Growth Rings Parallel to Wide Face of Lumber)
Quarter: Quarter-Sawn Lumber (Growth Rings Perpendicular to Wide Face of Lumber)
Both: Combination of Flat and Quarter-Sawn Lumber
TW: Tooth Withdrawal Failure
WS: Wood Shear Failure
PF: Metal Plate Failure

Double Design Impact	Ultimate Strength (lb)	Design Load Stiffness (lb/in) ending	Dead Load Stiffness (lb/in) beginning	Dead Load Stiffness (lb/in) ending	Ultimate Deflection (in)	Dynamic Deflection (in)	Moisture Content (%)
21a	7,479	623,234	293,000	732,500	0.115	0.017	11.5
23b	6,677	445,156	183,125	488,333	0.177	0.025	11.4
24c	7,659	364,701	244,167	366,250	0.177	0.026	11.4
25a	6,327	527,236	209,286	732,500	0.16	0.023	11.4
26c	6,246	416,404	209,286	732,500	NA	0.037	11.7
28a	7,616	634,635	293,000	1,465,000	0.175	0.029	12.0
28b	7,524	836,055	366,250	1,465,000	0.144	0.023	11.7
43a	6,261	347,856	162,778	366,250	0.105	0.028	12.0
46b	6,430	1,071,626	732,500	1,465,000	0.172	0.021	11.4
52a	7,988	380,363	244,167	488,333	0.174	0.017	12.0
Average	7,021	565,000	294,000	830,000	0.155	0.025	11.7
COV	9.83%	41.64%	56.32%	55.37%	18.00%	24.25%	2.3%
# of samples	10	10	10	10	9	10	10

Double Design Impact	Time to Failure (min)	Rings per inch	% Late Wood	Specific Gravity	Modulus of Elasticity (10^6 psi)	Failure Mode	Grain Orientation
21a	8.3	4	20	0.51	1.68	WS	Both
23b	7.4	5	25	0.52	1.76	WS and TW	Flat
24c	8.5	5	20	0.54	1.86	WS	Both
25a	7.0	7	25	0.52	2.07	WS and TW	Flat
26c	6.9	7	25	0.57	1.76	TW	Quarter
28a	8.5	13	35	0.48	1.66	TW	Flat
28b	8.4	12	25	0.47	1.66	WS and TW	Flat
43a	7.0	5	25	0.53	1.62	WS and TW	Flat
46b	7.1	6	30	0.56	1.81	WS and TW	Quarter
52a	8.9	5	25	0.51	1.70	WS and TW	Flat
Average	7.8	7	26	0.52	1.76		
COV	9.83%	45.0%	17.2%	5.7%	7.5%		
# of samples	10	10	10	10	10		

NA: Not Available
Flat: Flat-Sawn Lumber (Growth Rings Parallel to Wide Face of Lumber)
Quarter: Quarter-Sawn Lumber (Growth Rings Perpendicular to Wide Face of Lumber)
Both: Combination of Flat and Quarter-Sawn Lumber
TW: Tooth Withdrawal Failure
WS: Wood Shear Failure
PF: Metal Plate Failure

Appendix C
Load-deflection plots for heel joint

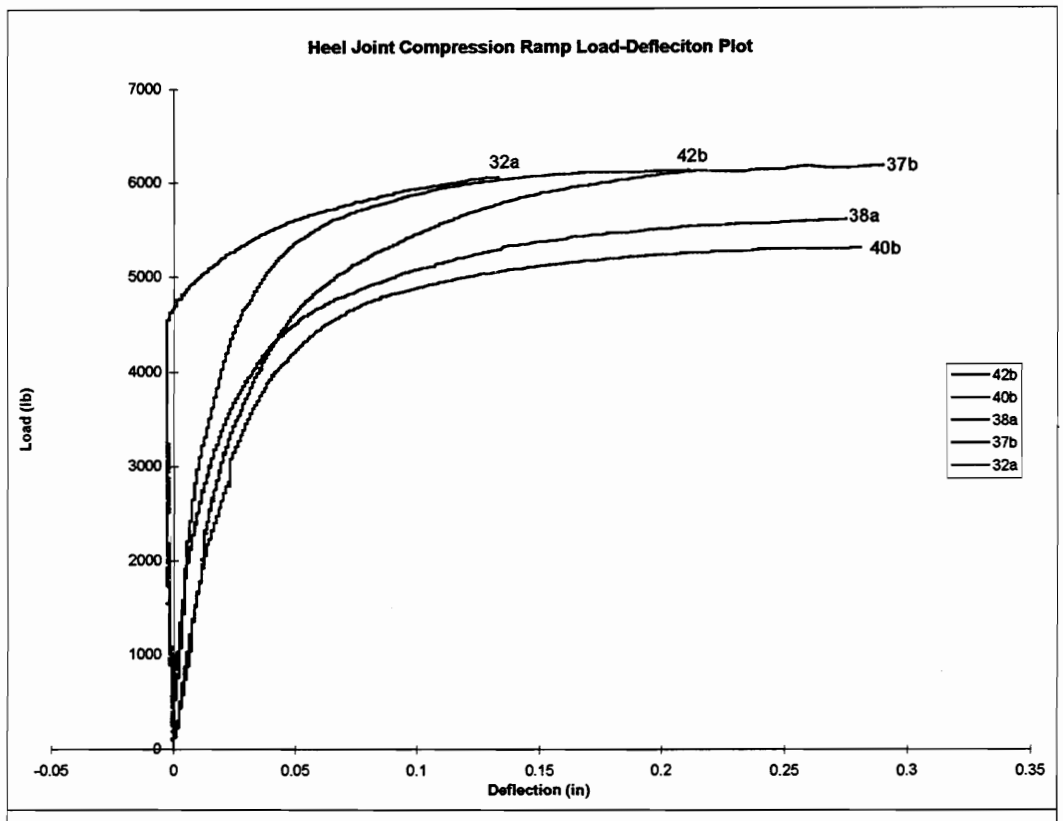
Heel Joint Compression Ramp Load-Defleciton Plot
Load (lb)
Deflection (in)
32a
42b
37b
38a
40b
42b
40b
38a
37b
32a

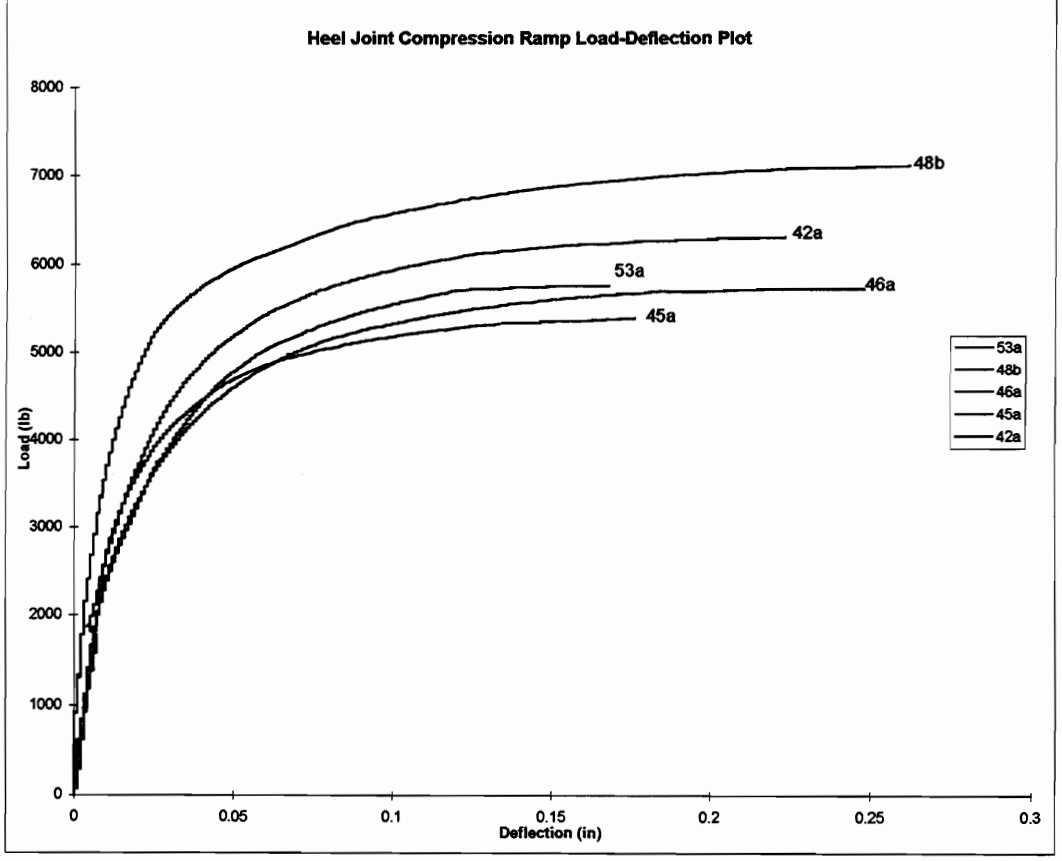
Heel Joint Compression Ramp Load-Deflection Plot
Load (lb)
Deflection (in)
48b
42a
53a
46a
45a
53a
48b
46a
45a
42a

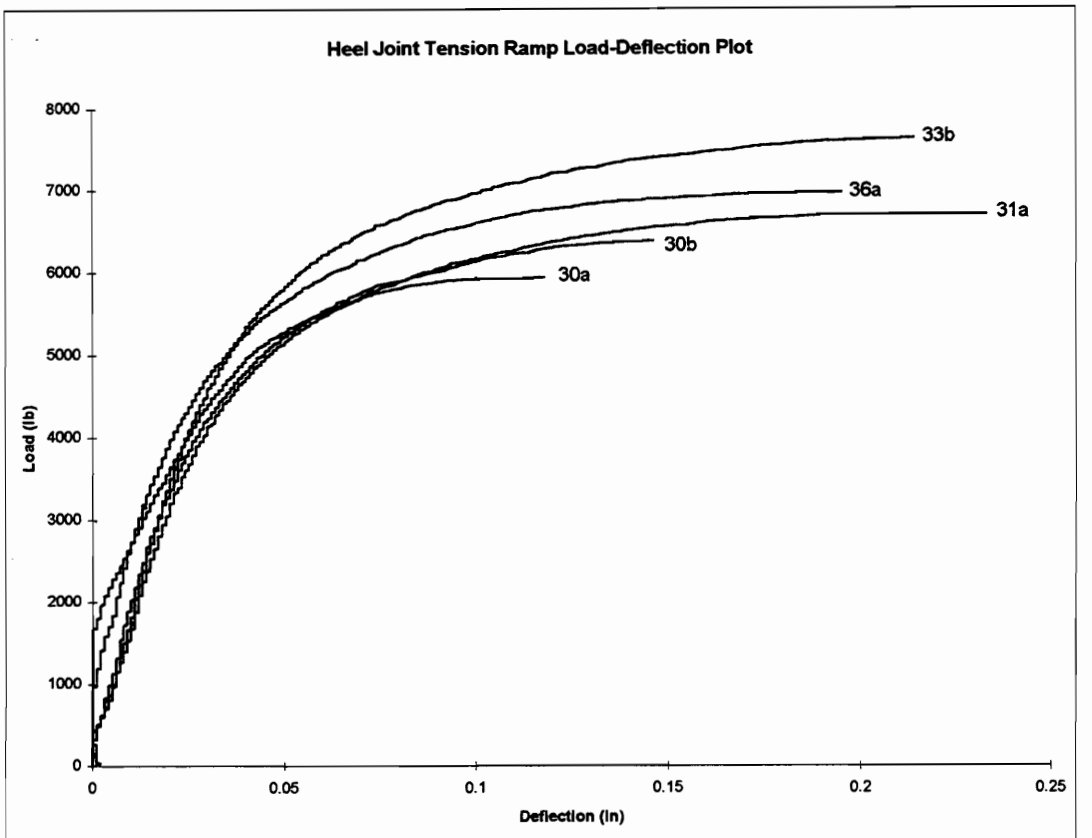
Heel Joint Tension Ramp Load-Deflection Plot
Load (lb)
Deflection (In)
33b
36a
31a
30b
30a
0
1000
2000
3000
4000
5000
6000
7000
8000
0
0.05
0.1
0.15
0.2
0.25

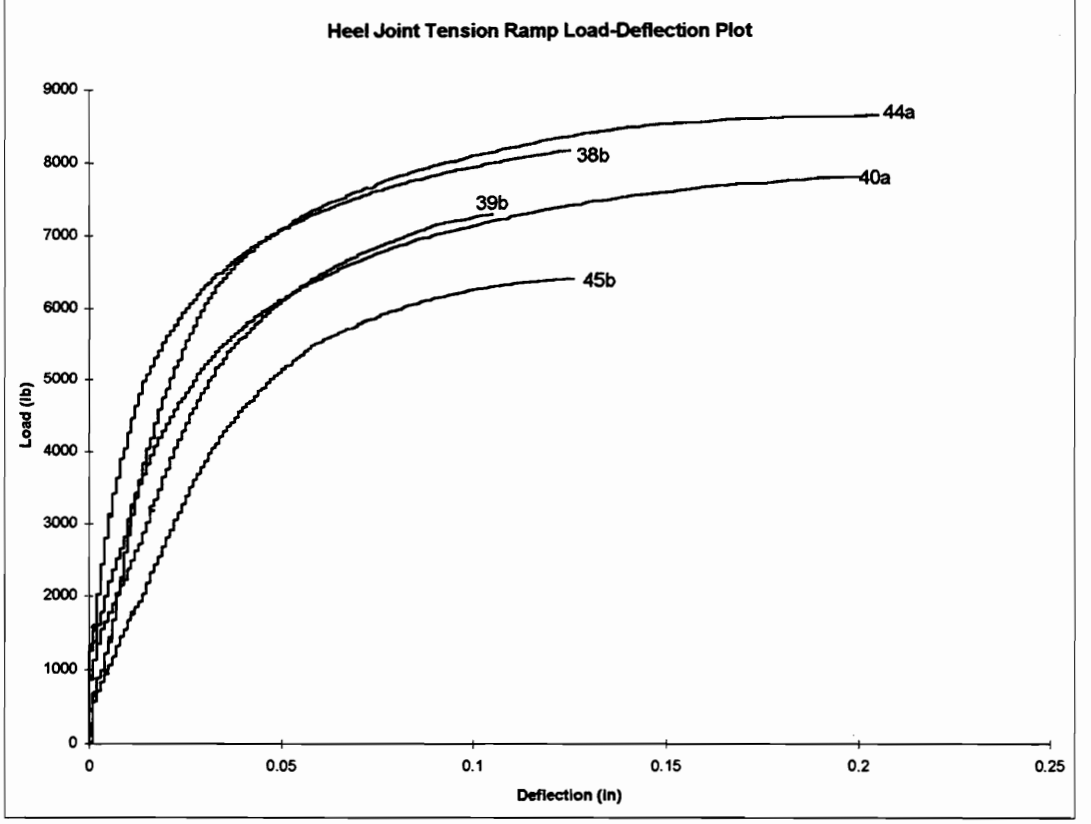
Heel Joint Tension Ramp Load-Deflection Plot
Load (lb)
Deflection (In)
44a
38b
40a
39b
45b
0
1000
2000
3000
4000
5000
6000
7000
8000
9000
0
0.05
0.1
0.15
0.2
0.25

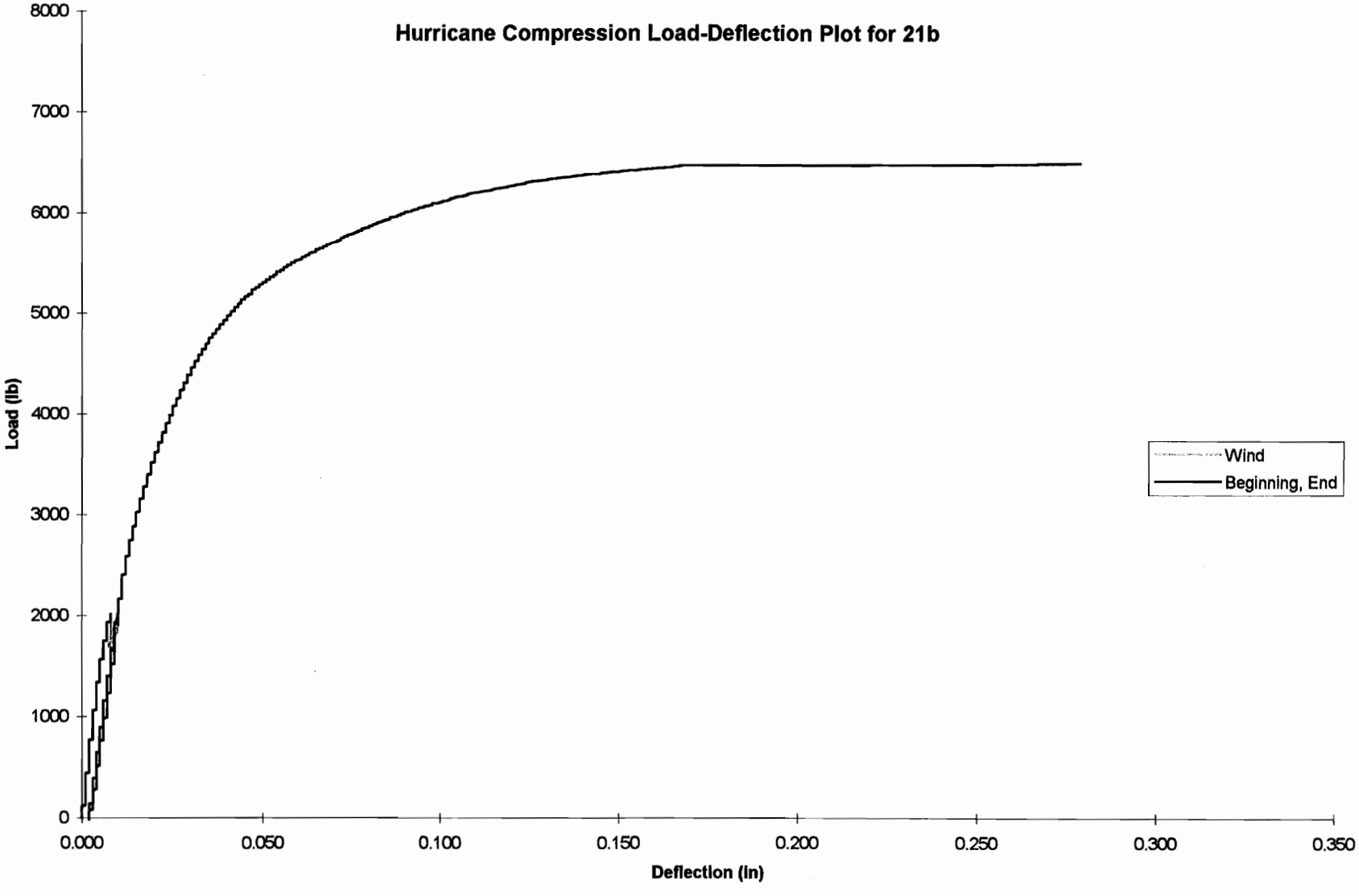
Hurricane Compression Load-Deflection Plot for 21b
Load (lb)
8000
7000
6000
5000
4000
3000
2000
1000
0
0.000
0.050
0.100
0.150
0.200
0.250
0.300
0.350
Deflection (in)
Wind
Beginning, End

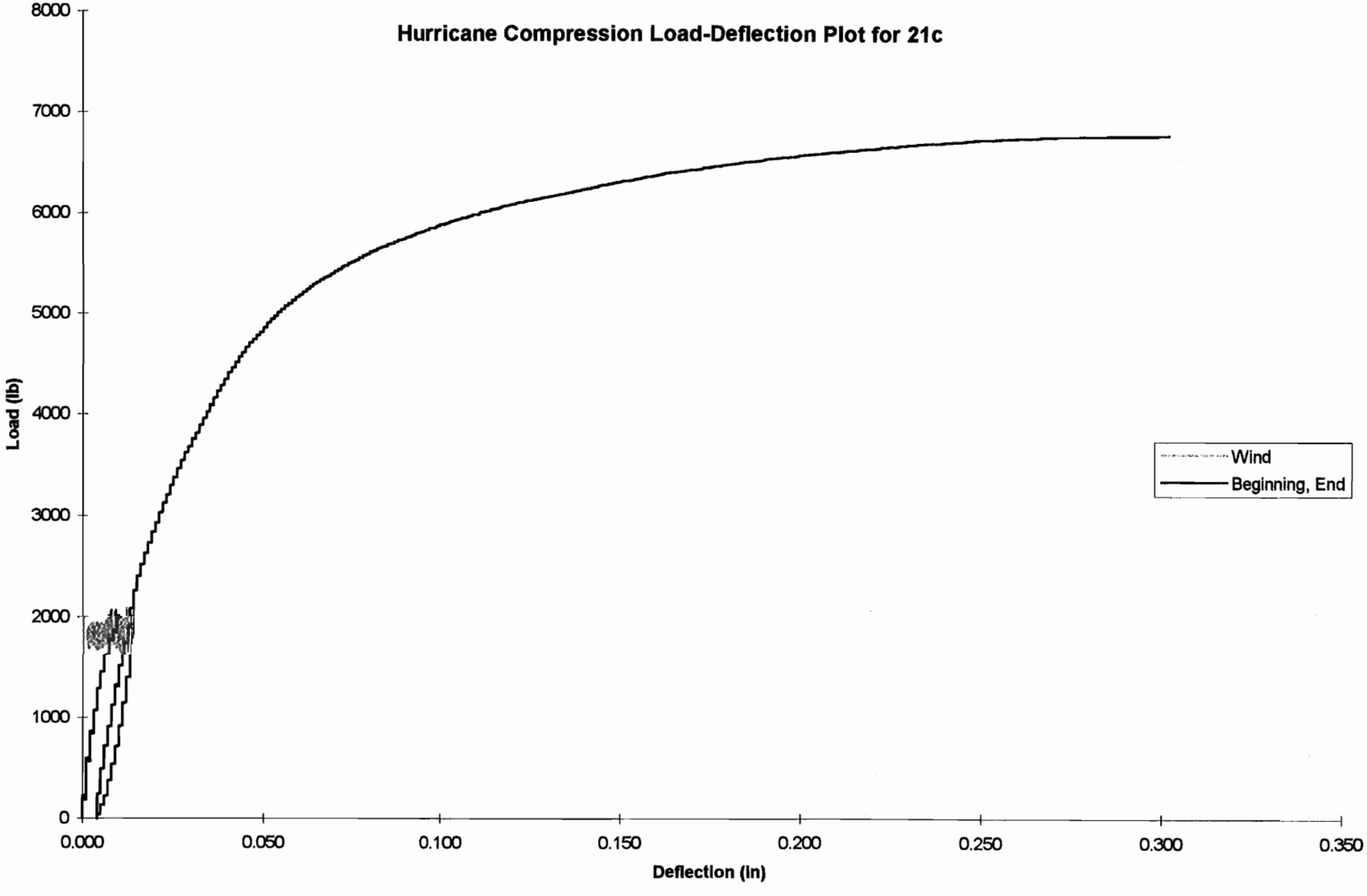
Hurricane Compression Load-Deflection Plot for 21c
Load (lb)
8000
7000
6000
5000
4000
3000
2000
1000
0
0.000
0.050
0.100
0.150
0.200
0.250
0.300
0.350
Deflection (In)
Wind
Beginning, End

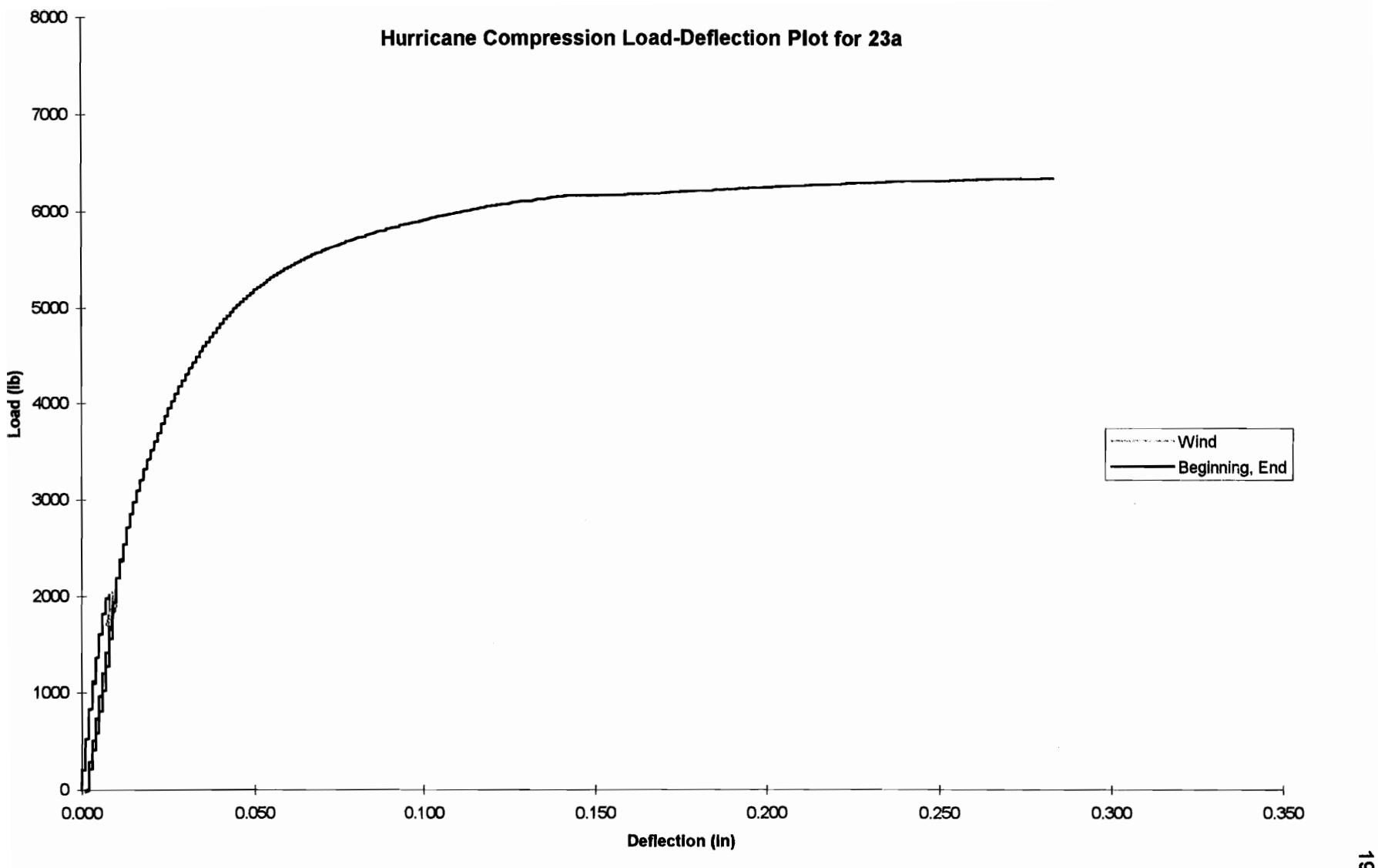
Hurricane Compression Load-Deflection Plot for 23a
Load (lb)
8000
7000
6000
5000
4000
3000
2000
1000
0
0.000
0.050
0.100
0.150
0.200
0.250
0.300
0.350
Deflection (in)
Wind
Beginning, End

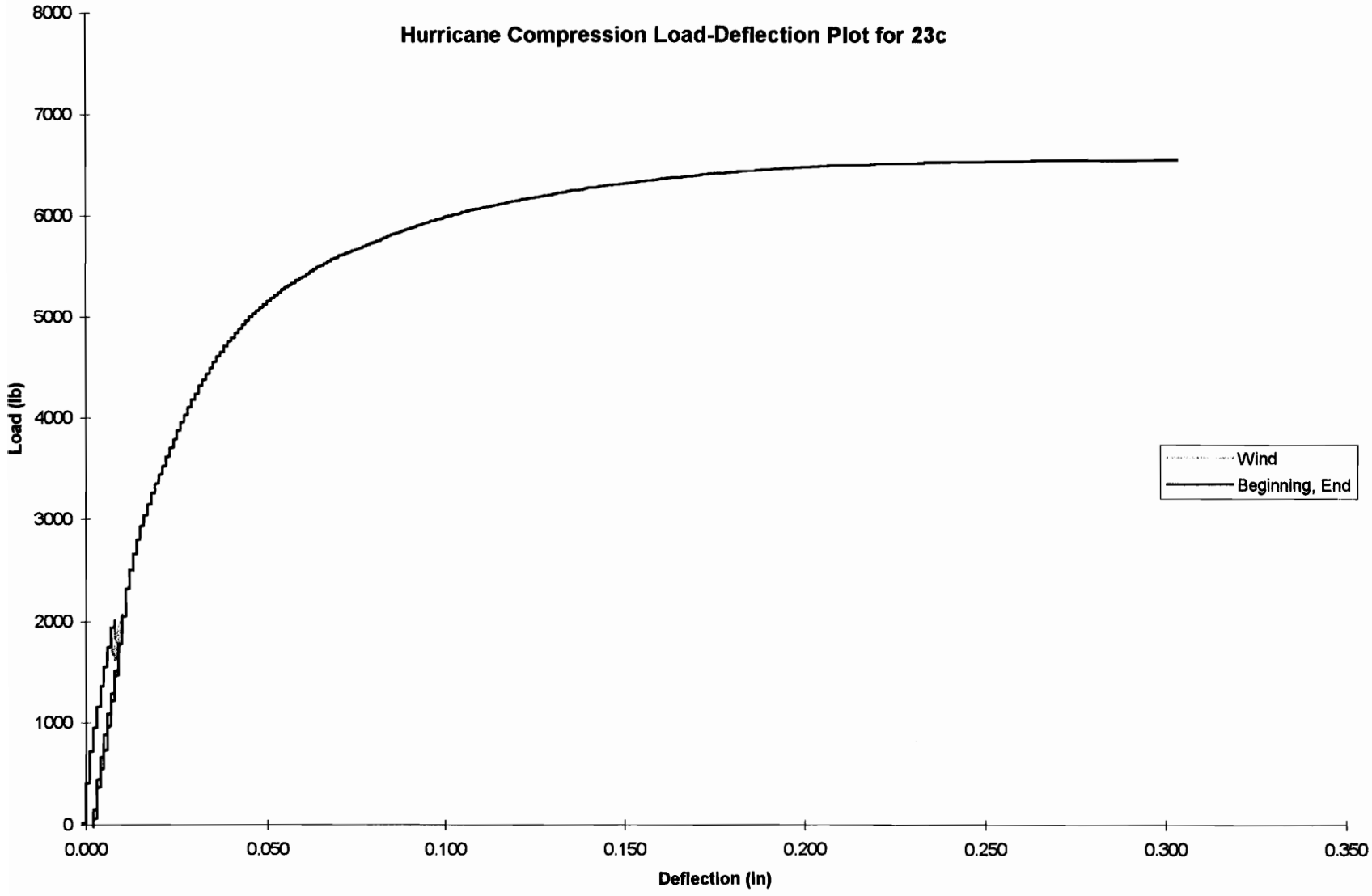
Hurricane Compression Load-Deflection Plot for 23c
Load (lb)
8000
7000
6000
5000
4000
3000
2000
1000
0
0.000
0.050
0.100
0.150
0.200
0.250
0.300
0.350
Deflection (In)
Wind
Beginning, End

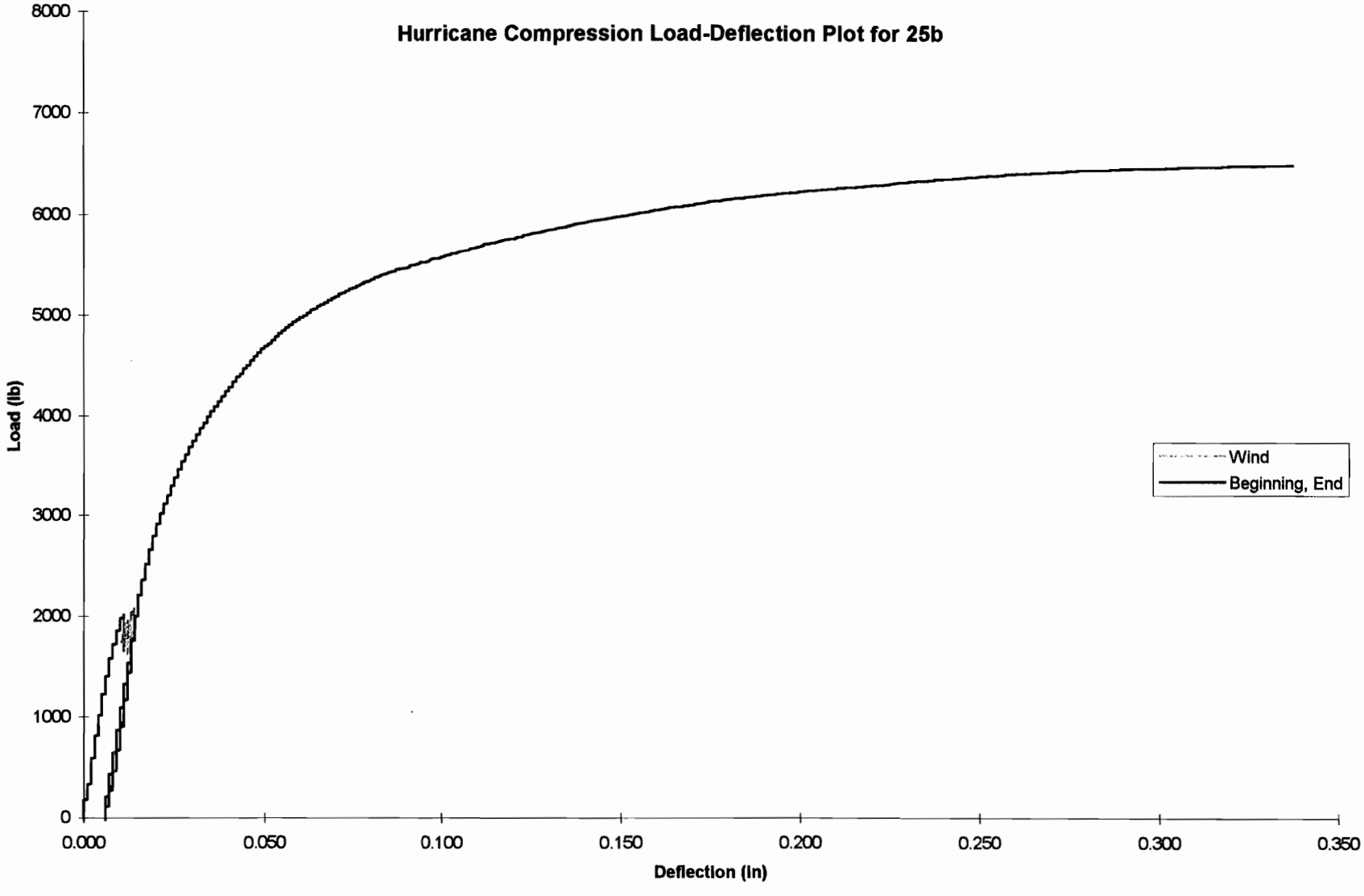
Hurricane Compression Load-Deflection Plot for 25b
Load (lb)
8000
7000
6000
5000
4000
3000
2000
1000
0
0.000
0.050
0.100
0.150
0.200
0.250
0.300
0.350
Deflection (in)
Wind
Beginning, End

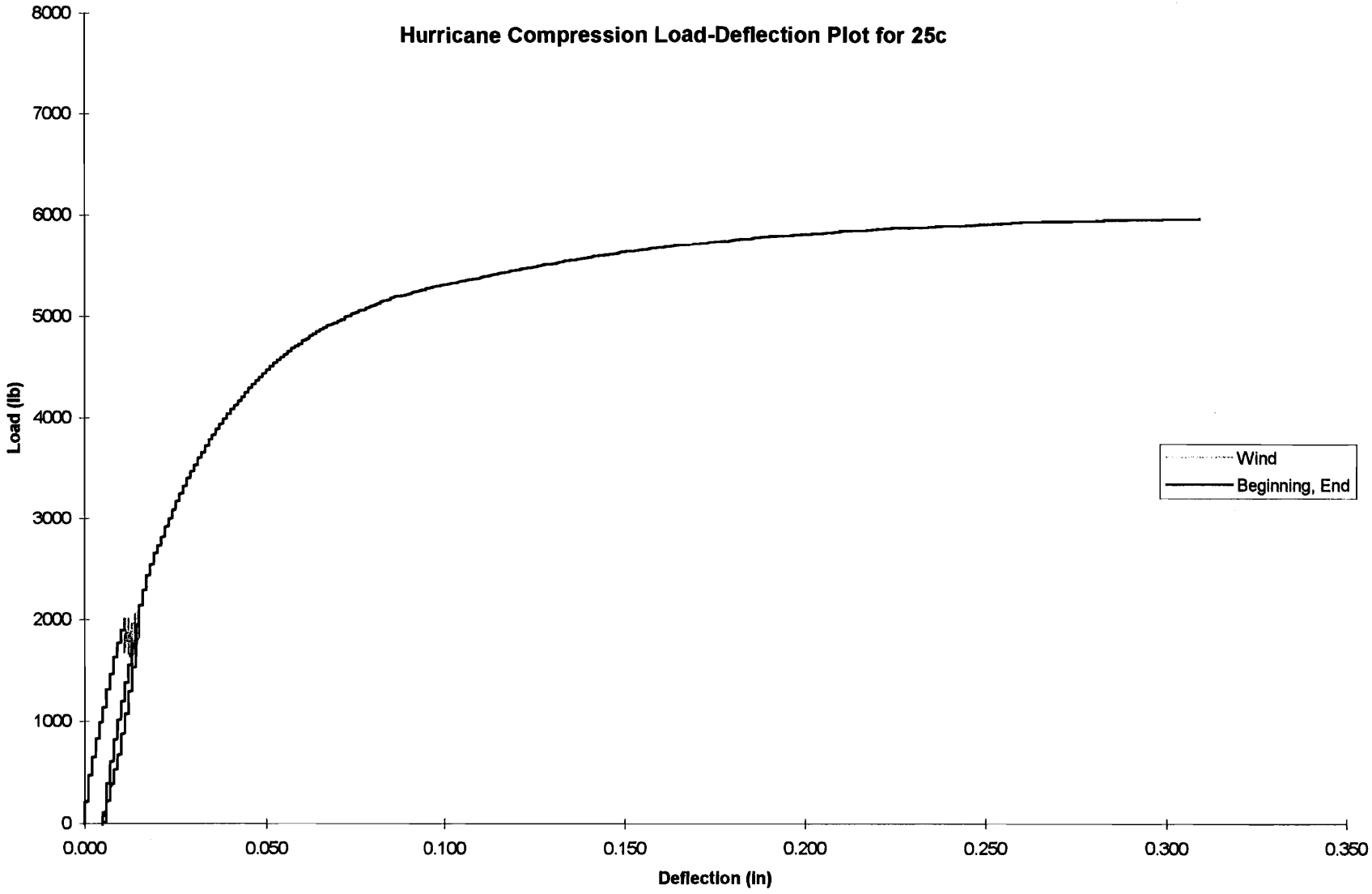
Hurricane Compression Load-Deflection Plot for 25c
Load (lb)
8000
7000
6000
5000
4000
3000
2000
1000
0
0.000
0.050
0.100
0.150
0.200
0.250
0.300
0.350
Deflection (in)
Wind
Beginning, End

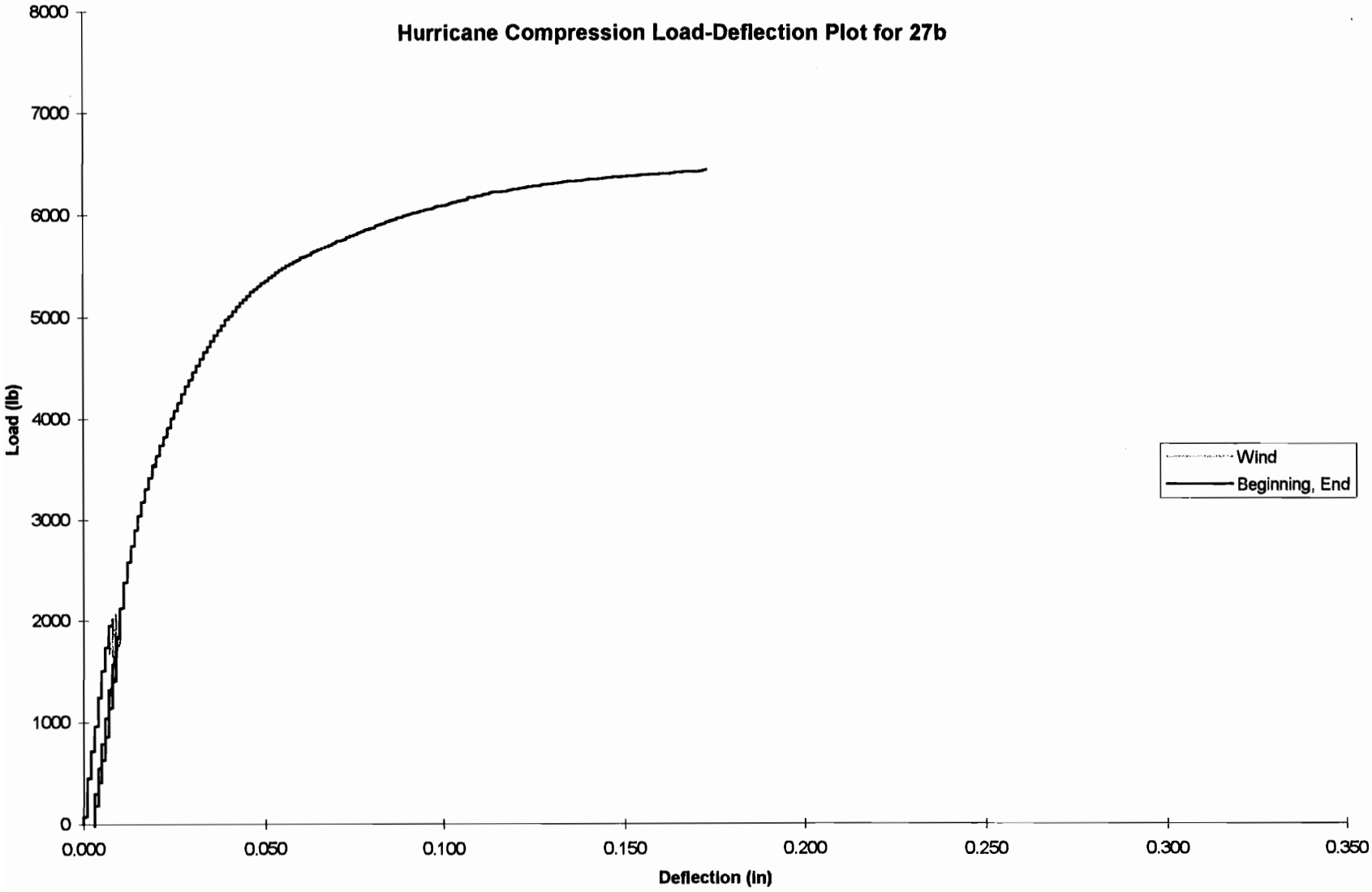
Hurricane Compression Load-Deflection Plot for 27b
Load (lb)
8000
7000
6000
5000
4000
3000
2000
1000
0
0.000
0.050
0.100
0.150
0.200
0.250
0.300
0.350
Deflection (in)
Wind
Beginning, End

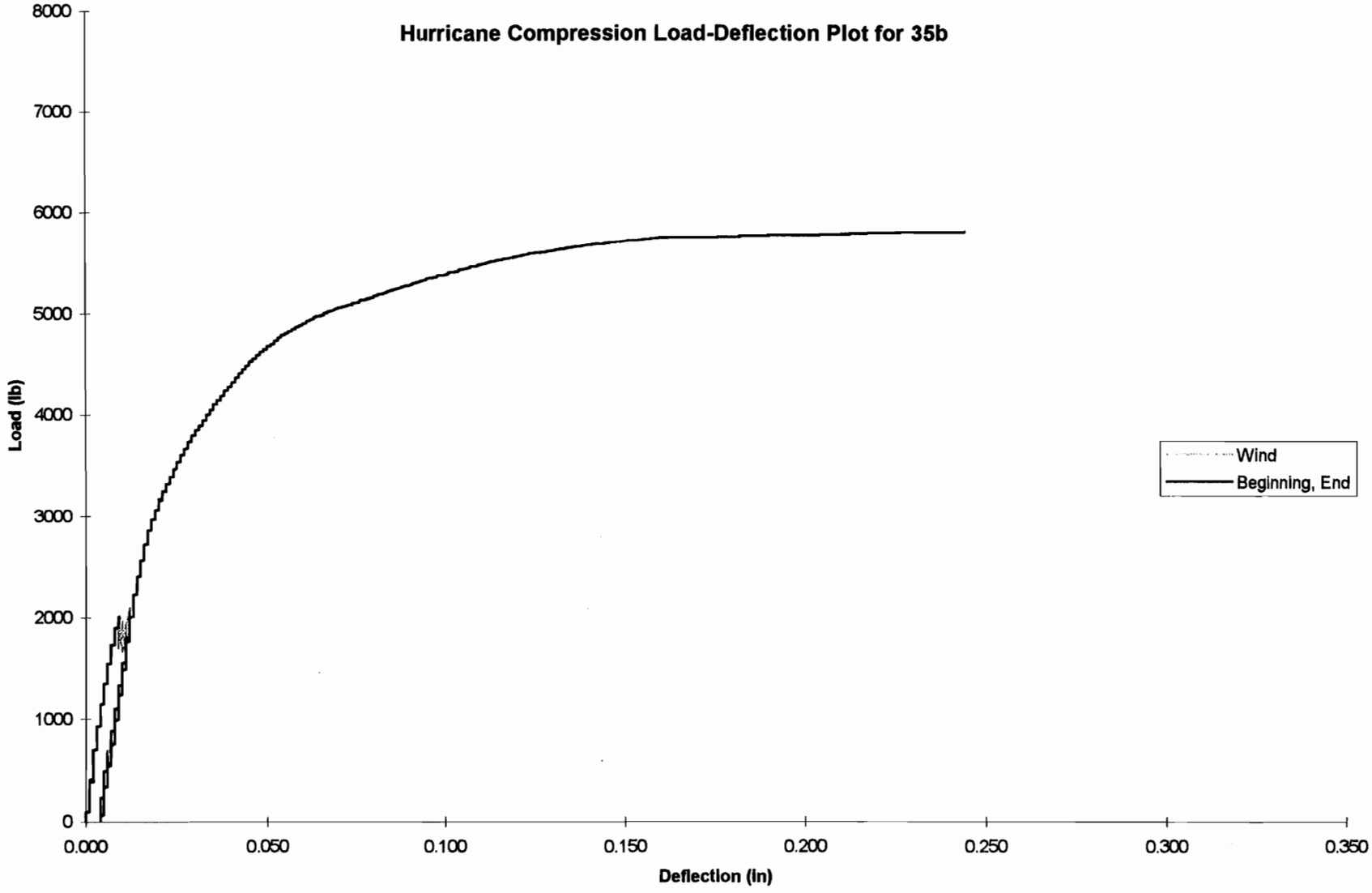
Hurricane Compression Load-Deflection Plot for 35b
Load (lb)
8000
7000
6000
5000
4000
3000
2000
1000
0
0.000
0.050
0.100
0.150
0.200
0.250
0.300
0.350
Deflection (in)
Wind
Beginning, End

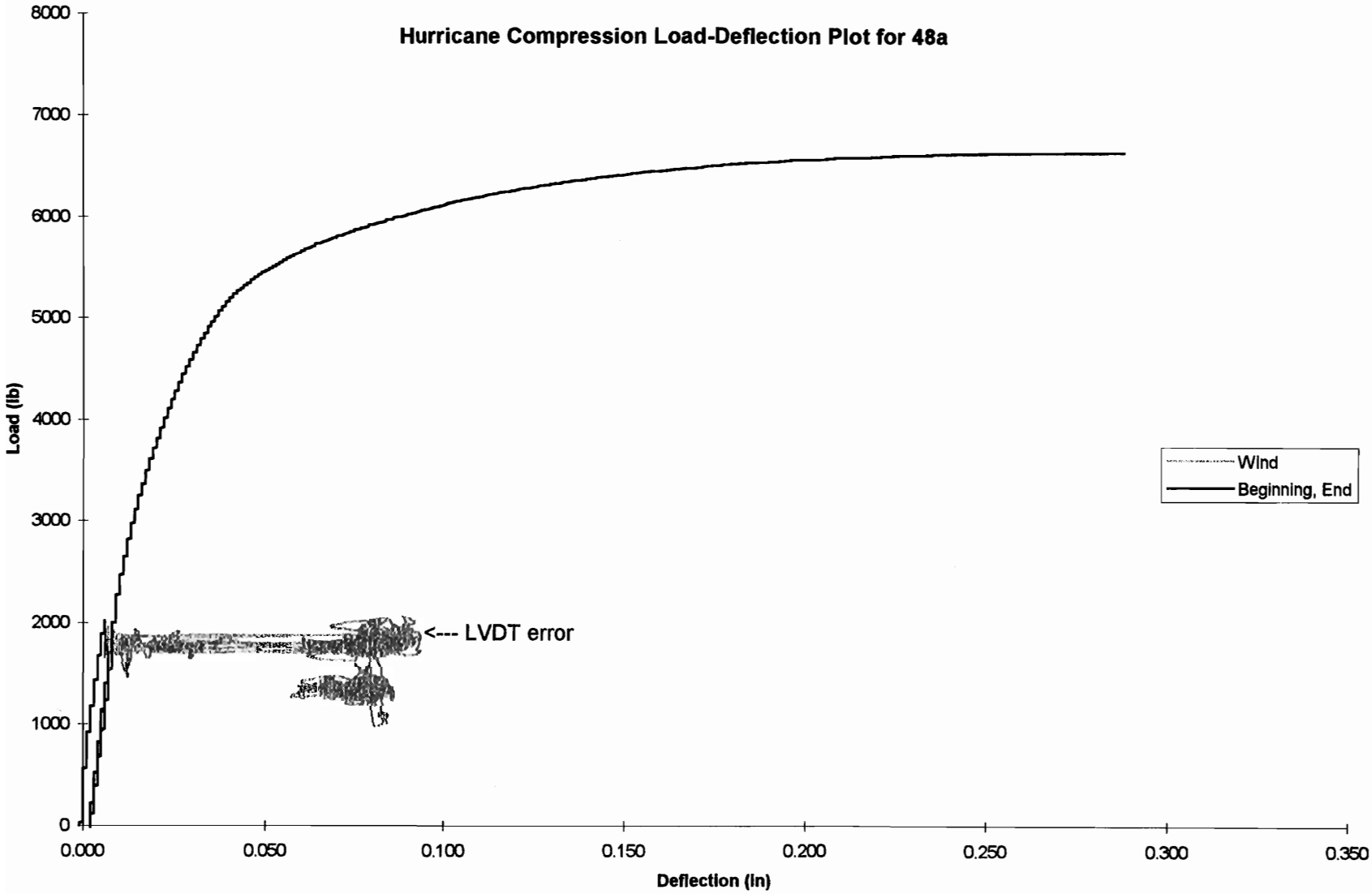
Hurricane Compression Load-Deflection Plot for 48a
Load (lb)
8000
7000
6000
5000
4000
3000
2000
1000
0
0.000
0.050
0.100
0.150
0.200
0.250
0.300
0.350
Deflection (in)
<--- LVDT error
Wind
Beginning, End

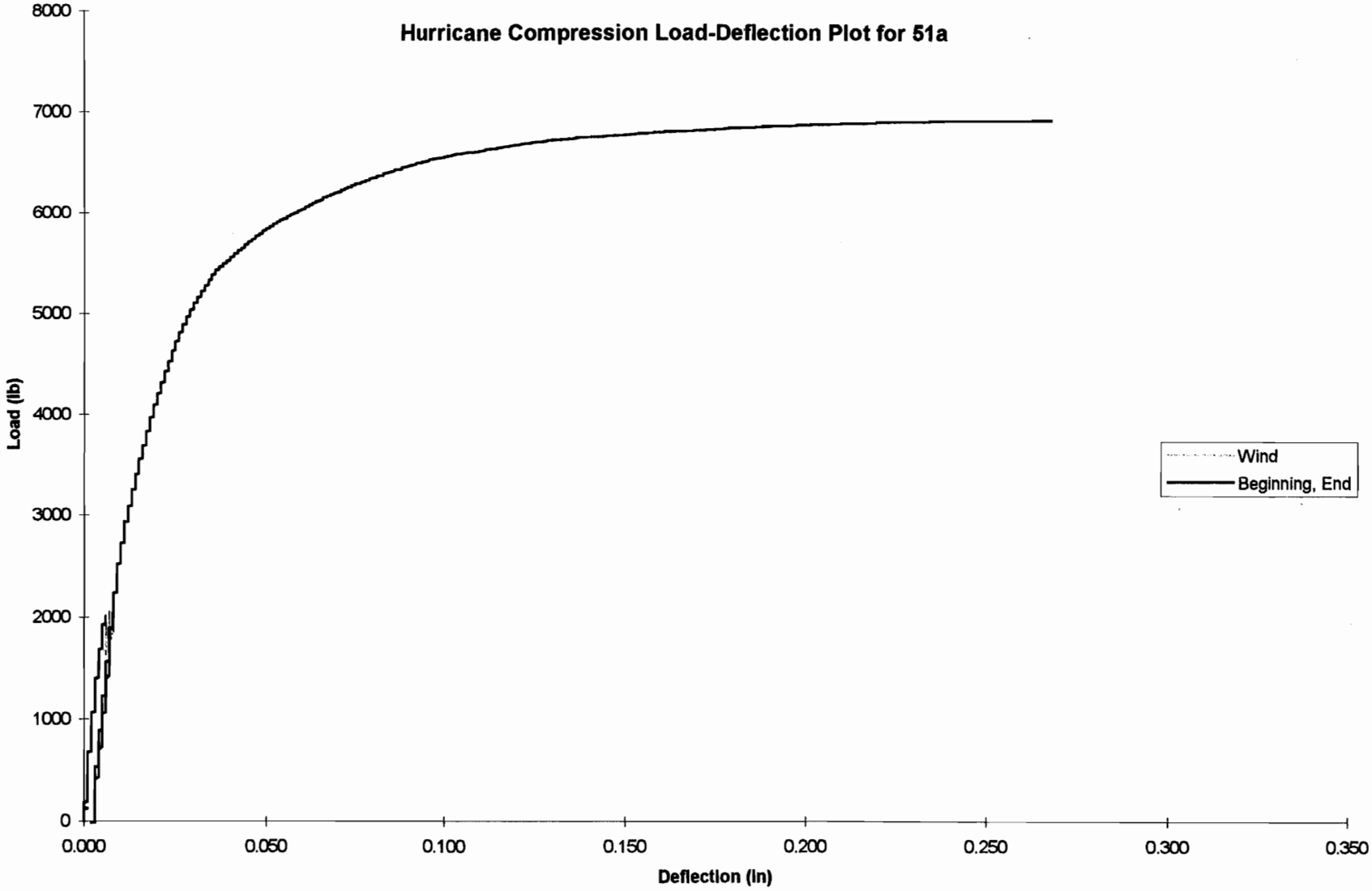
Hurricane Compression Load-Deflection Plot for 51a
Load (lb)
8000
7000
6000
5000
4000
3000
2000
1000
0
0.000
0.050
0.100
0.150
0.200
0.250
0.300
0.350
Deflection (in)
Wind
Beginning, End

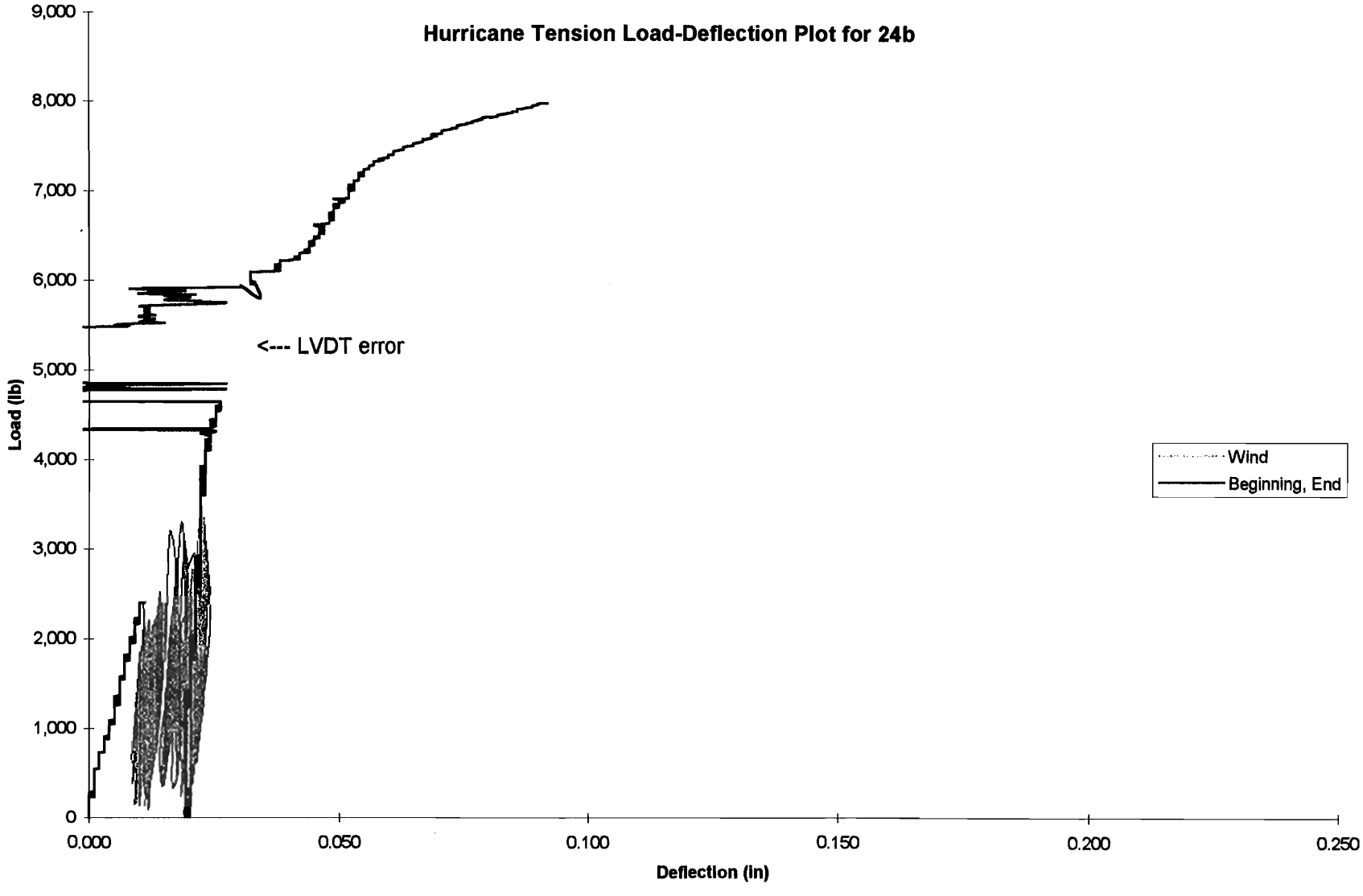
Hurricane Tension Load-Deflection Plot for 24b
9,000
8,000
7,000
6,000
5,000
4,000
3,000
2,000
1,000
0
Load (lb)
<--- LVDT error
Wind
Beginning, End
0.000
0.050
0.100
0.150
0.200
0.250
Deflection (in)

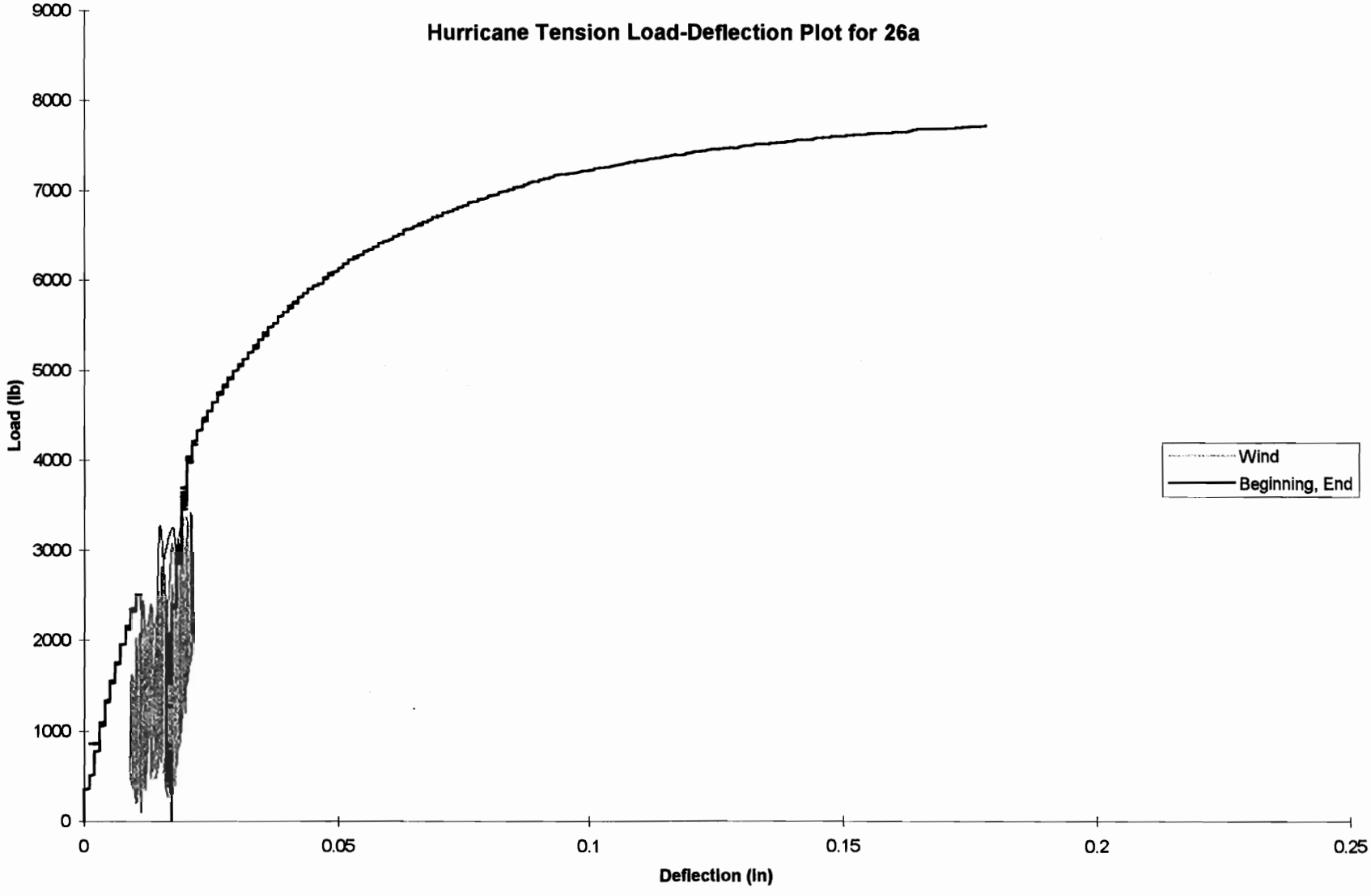
Hurricane Tension Load-Deflection Plot for 26a
Load (lb)
9000
8000
7000
6000
5000
4000
3000
2000
1000
0
0
0.05
0.1
0.15
0.2
0.25
Deflection (in)
Wind
Beginning, End

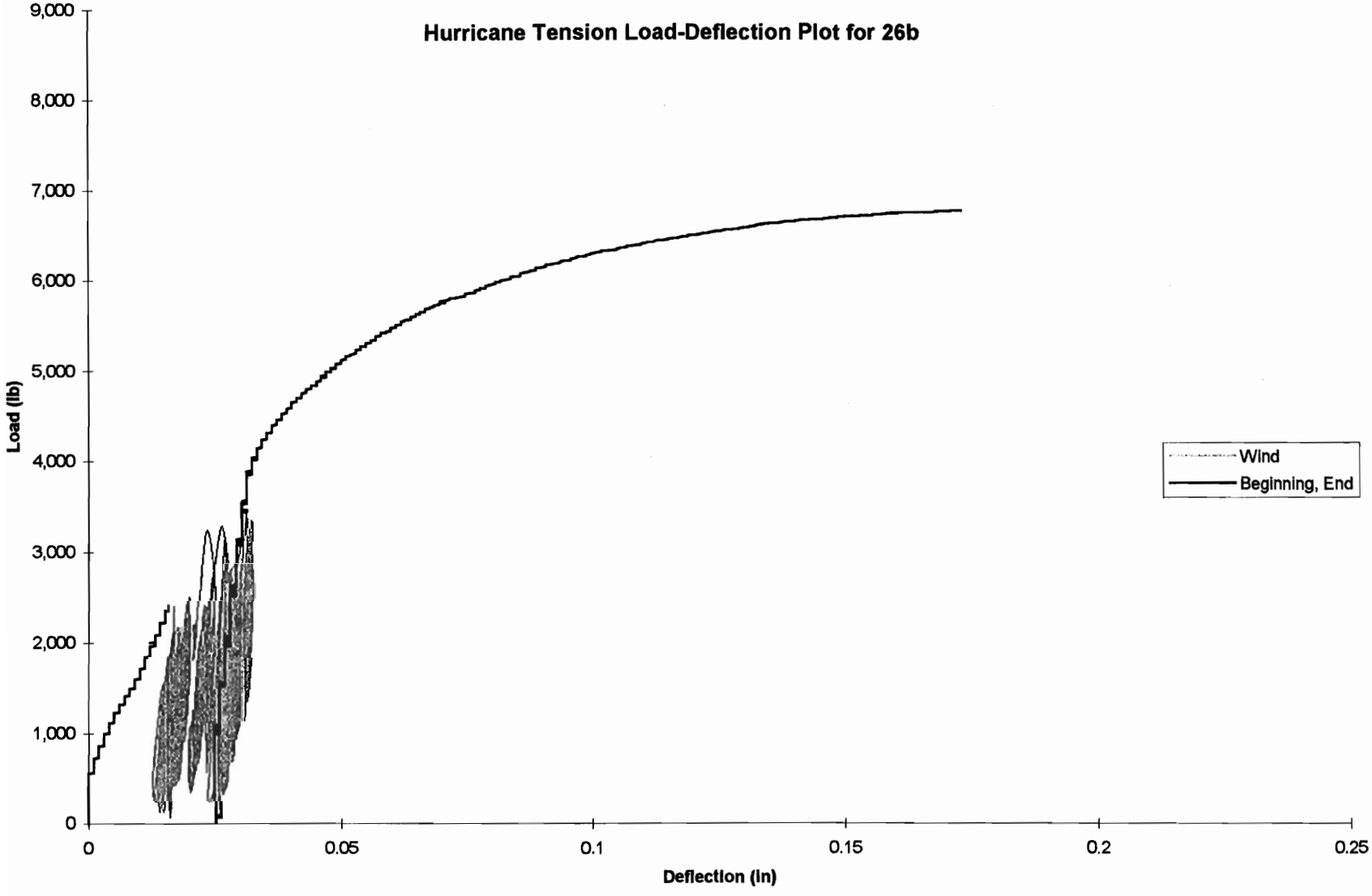
Hurricane Tension Load-Deflection Plot for 26b
9,000
8,000
7,000
6,000
5,000
4,000
3,000
2,000
1,000
0
Load (lb)
0
0.05
0.1
0.15
0.2
0.25
Deflection (in)
Wind
Beginning, End

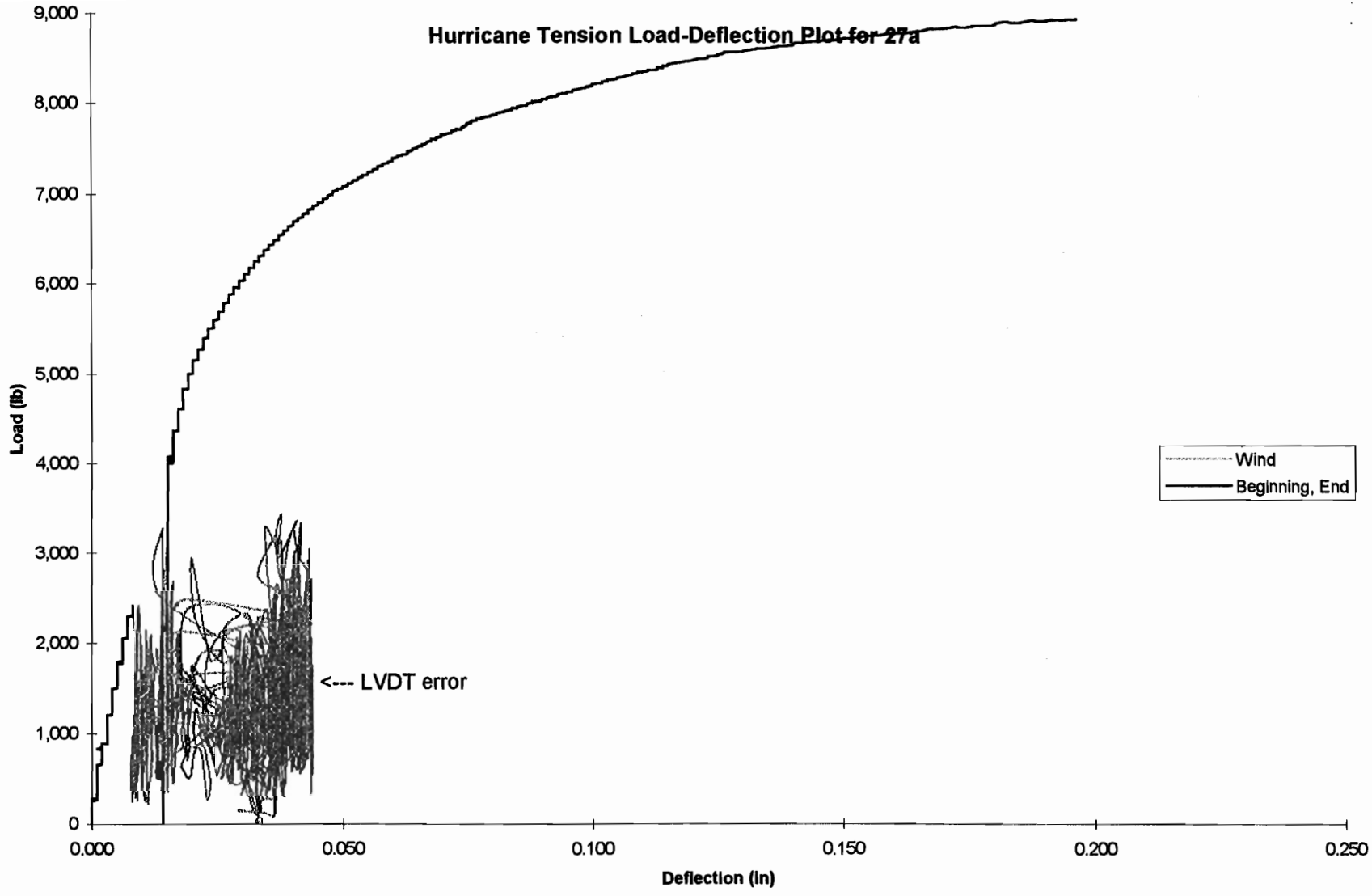
Hurricane Tension Load-Deflection Plot for 27a
Load (lb)
9,000
8,000
7,000
6,000
5,000
4,000
3,000
2,000
1,000
0
0.000
0.050
0.100
0.150
0.200
0.250
Deflection (in)
<--- LVDT error
Wind
Beginning, End

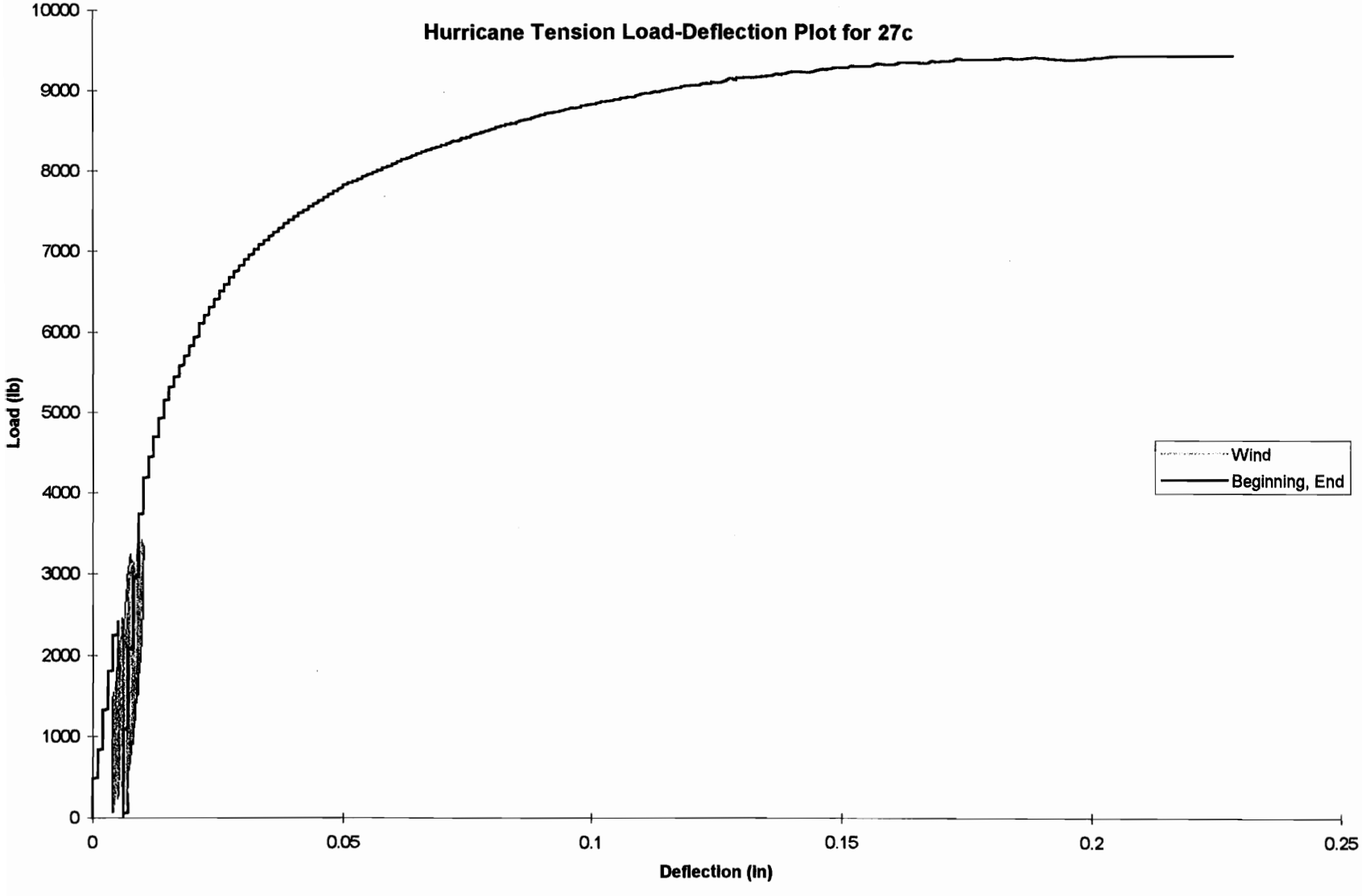
Hurricane Tension Load-Deflection Plot for 27c
Load (lb)
10000
9000
8000
7000
6000
5000
4000
3000
2000
1000
0
0
0.05
0.1
0.15
0.2
0.25
Deflection (in)
Wind
Beginning, End

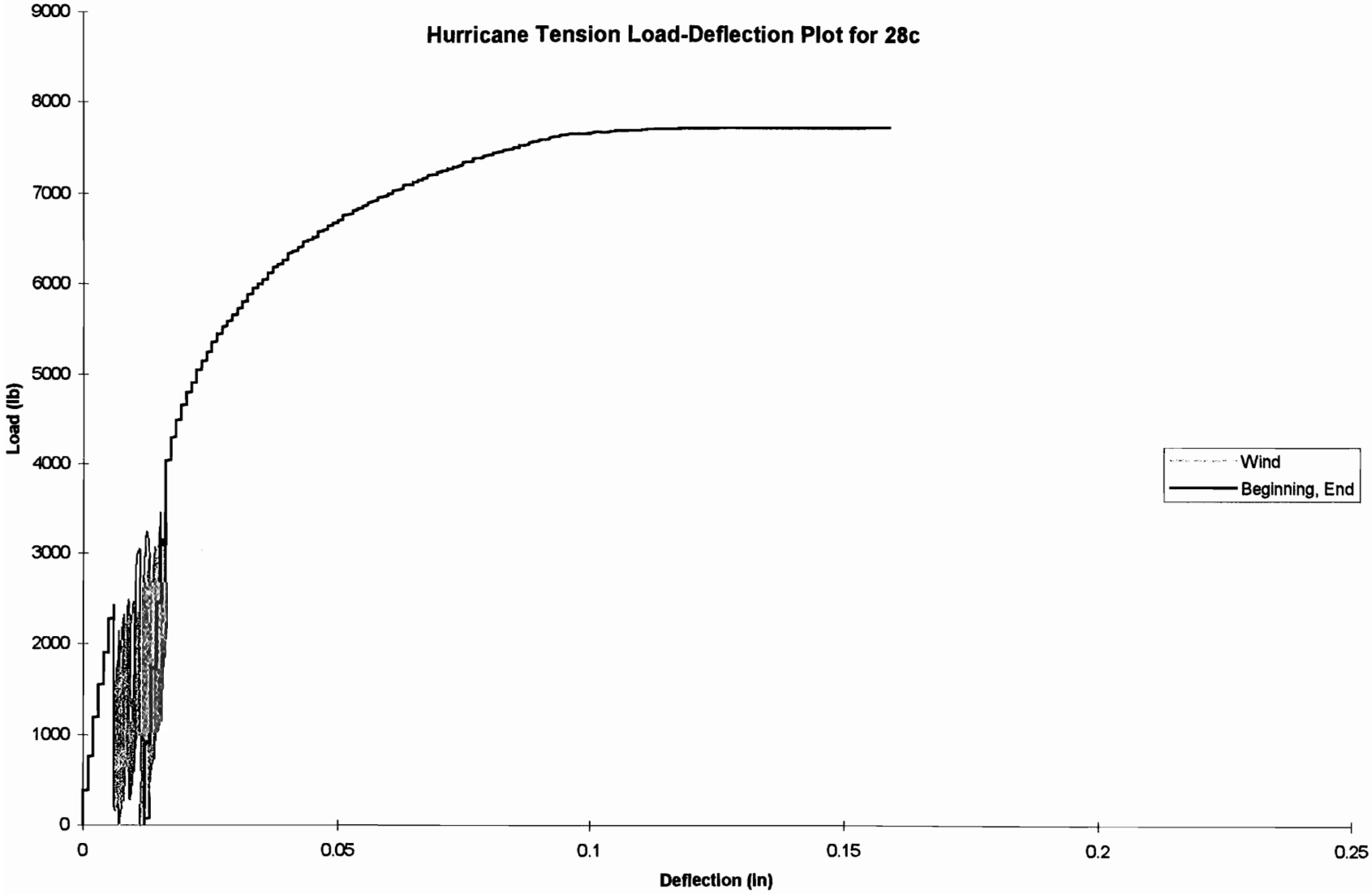
Hurricane Tension Load-Deflection Plot for 28c
Load (lb)
9000
8000
7000
6000
5000
4000
3000
2000
1000
0
0
0.05
0.1
0.15
0.2
0.25
Deflection (in)
Wind
Beginning, End

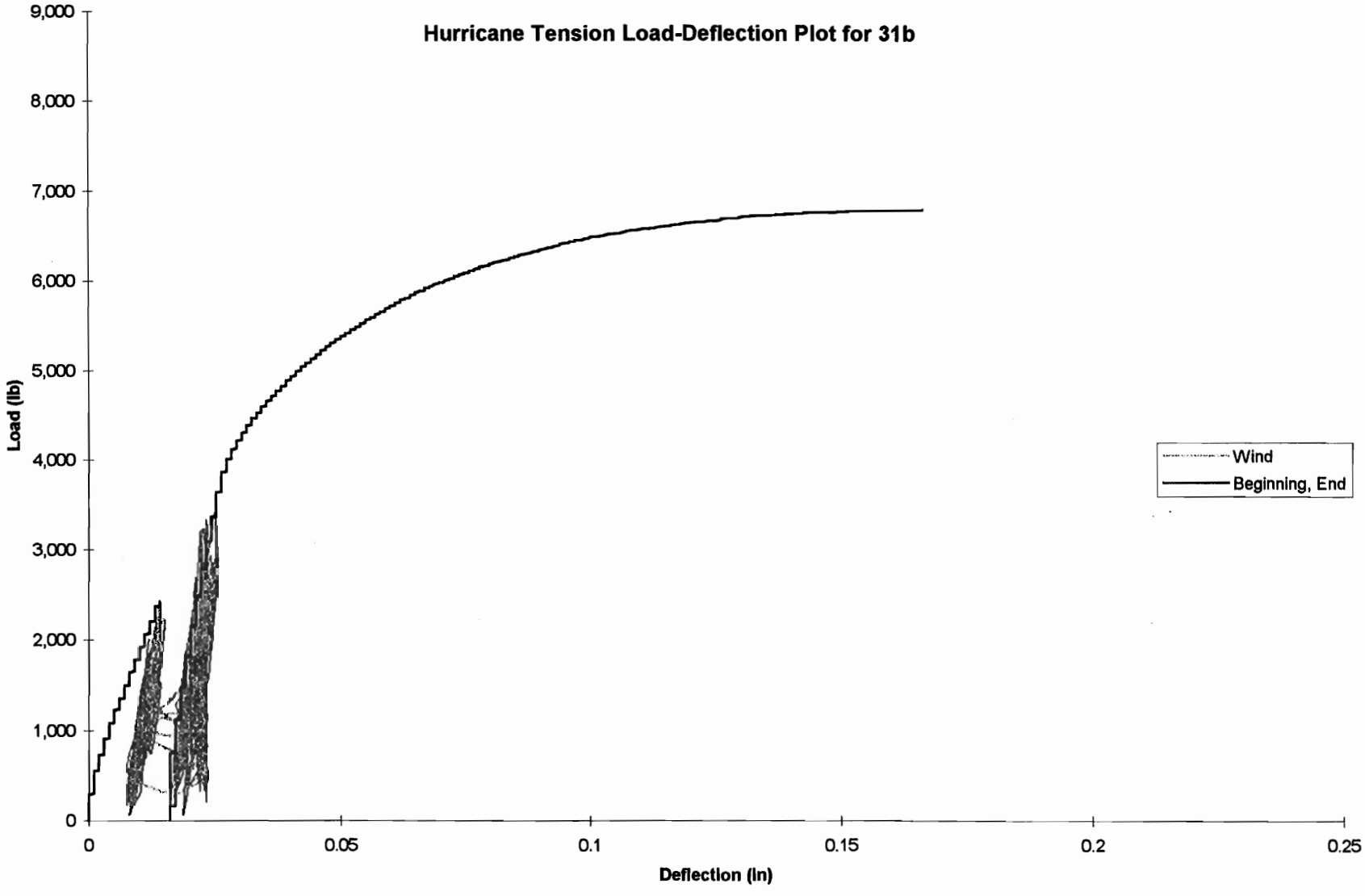
Hurricane Tension Load-Deflection Plot for 31b
9,000
8,000
7,000
6,000
5,000
4,000
3,000
2,000
1,000
0
Load (lb)
0
0.05
0.1
0.15
0.2
0.25
Deflection (in)
Wind
Beginning, End

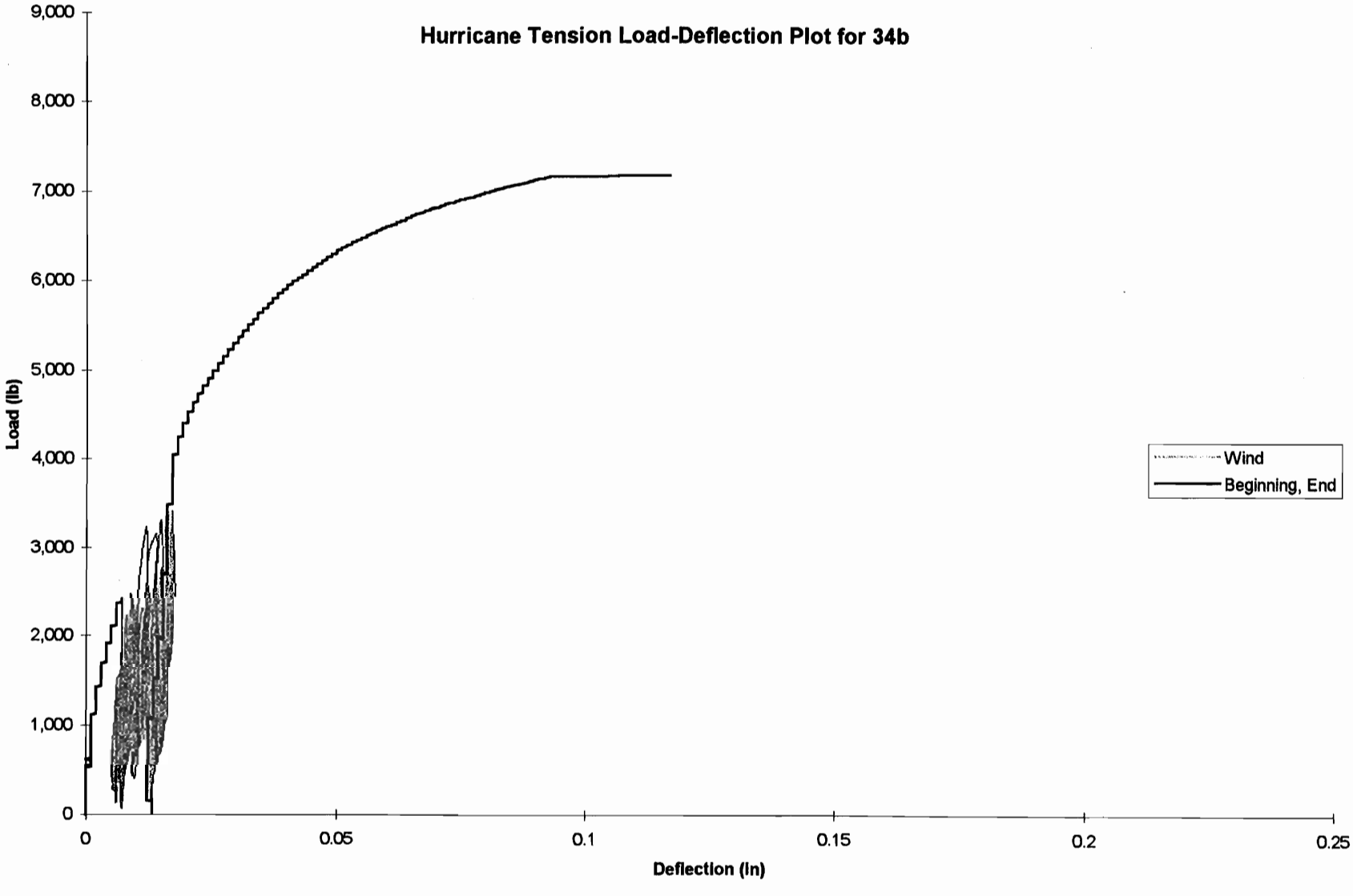
Hurricane Tension Load-Deflection Plot for 34b
Load (lb)
9,000
8,000
7,000
6,000
5,000
4,000
3,000
2,000
1,000
0
0
0.05
0.1
0.15
0.2
0.25
Deflection (In)
Wind
Beginning, End

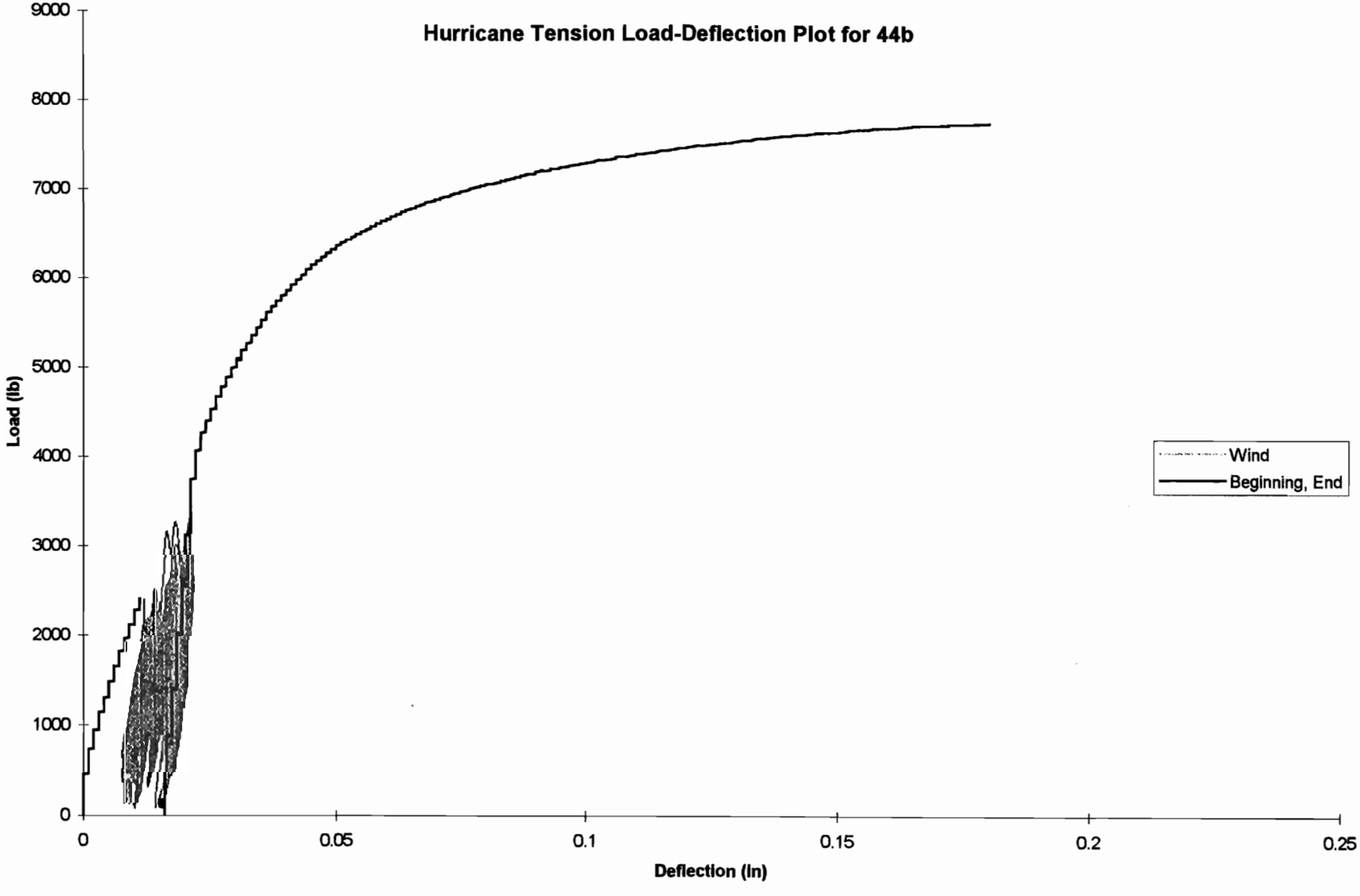
Hurricane Tension Load-Deflection Plot for 44b
Load (lb)
9000
8000
7000
6000
5000
4000
3000
2000
1000
0
0
0.05
0.1
0.15
0.2
0.25
Deflection (in)
Wind
Beginning, End

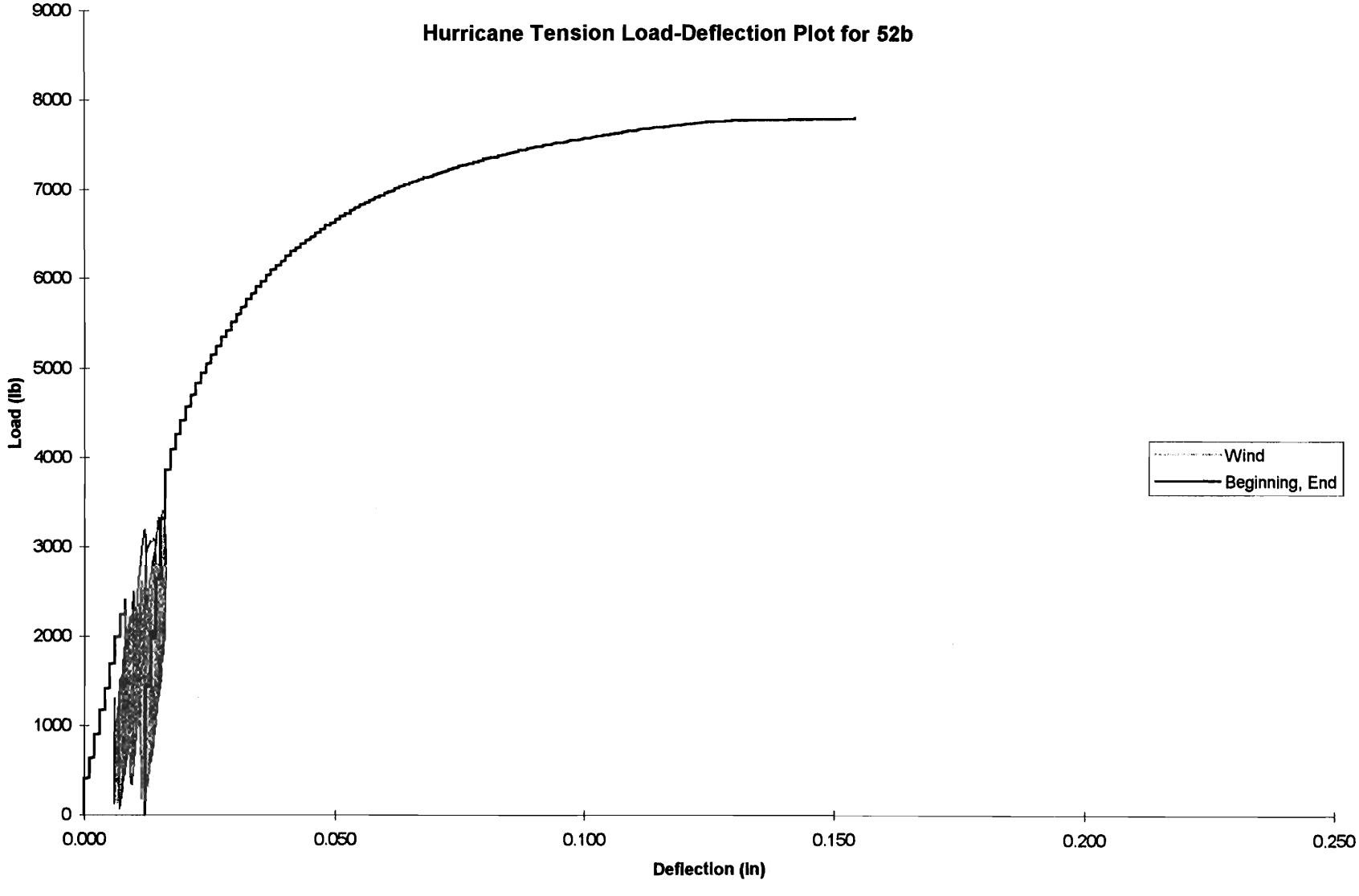
Hurricane Tension Load-Deflection Plot for 52b
Load (lb)
9000
8000
7000
6000
5000
4000
3000
2000
1000
0
0.000
0.050
0.100
0.150
0.200
0.250
Deflection (in)
Wind
Beginning, End

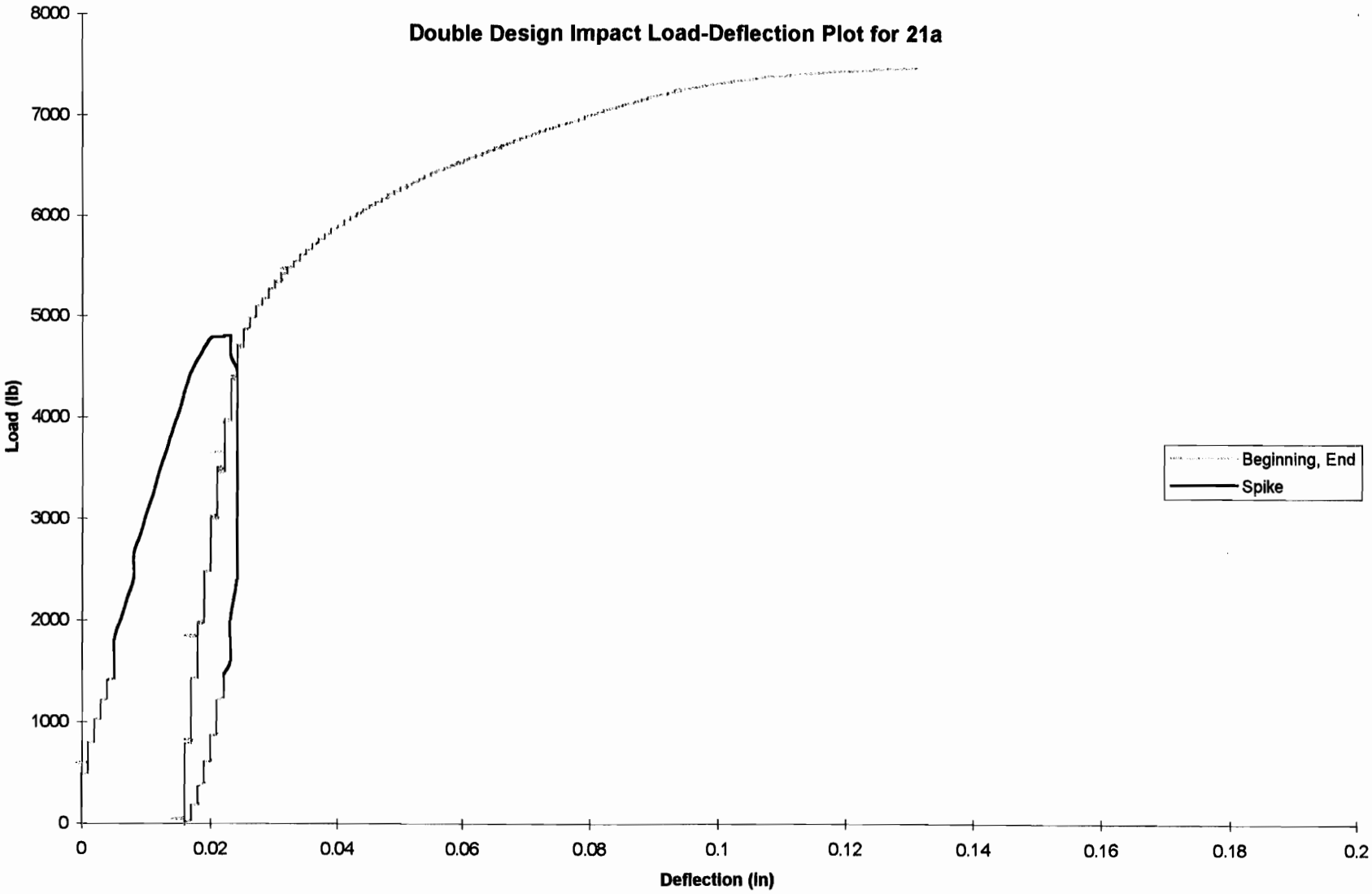
Double Design Impact Load-Deflection Plot for 21a
Load (lb)
8000
7000
6000
5000
4000
3000
2000
1000
0
0
0.02
0.04
0.06
0.08
0.1
0.12
0.14
0.16
0.18
0.2
Deflection (in)
Beginning, End
Spike

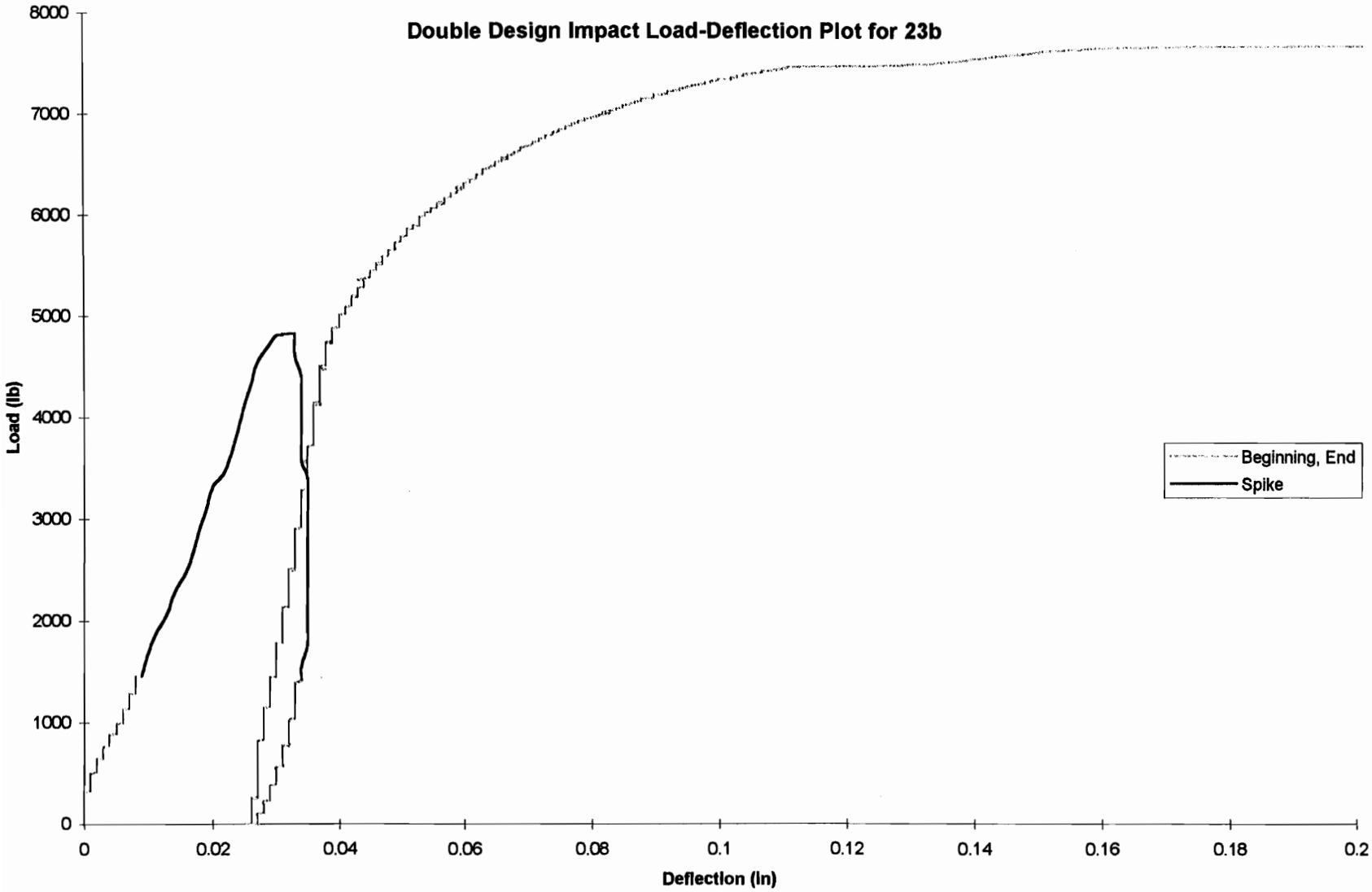
Double Design Impact Load-Deflection Plot for 23b
Load (lb)
8000
7000
6000
5000
4000
3000
2000
1000
0
0
0.02
0.04
0.06
0.08
0.1
0.12
0.14
0.16
0.18
0.2
Deflection (in)
Beginning, End
Spike

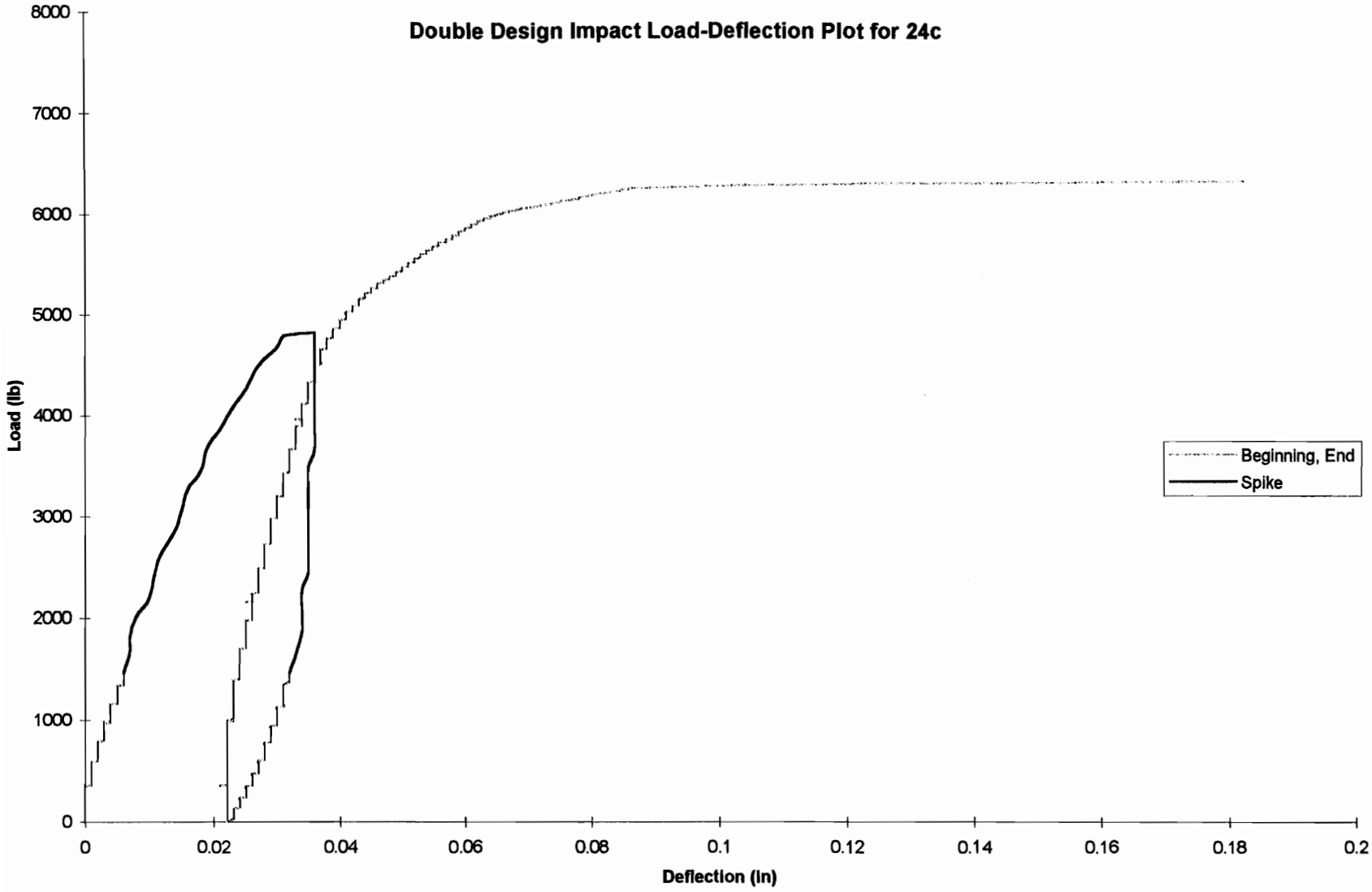
Double Design Impact Load-Deflection Plot for 24c
Load (lb)
8000
7000
6000
5000
4000
3000
2000
1000
0
0
0.02
0.04
0.06
0.08
0.1
0.12
0.14
0.16
0.18
0.2
Deflection (in)
Beginning, End
Spike

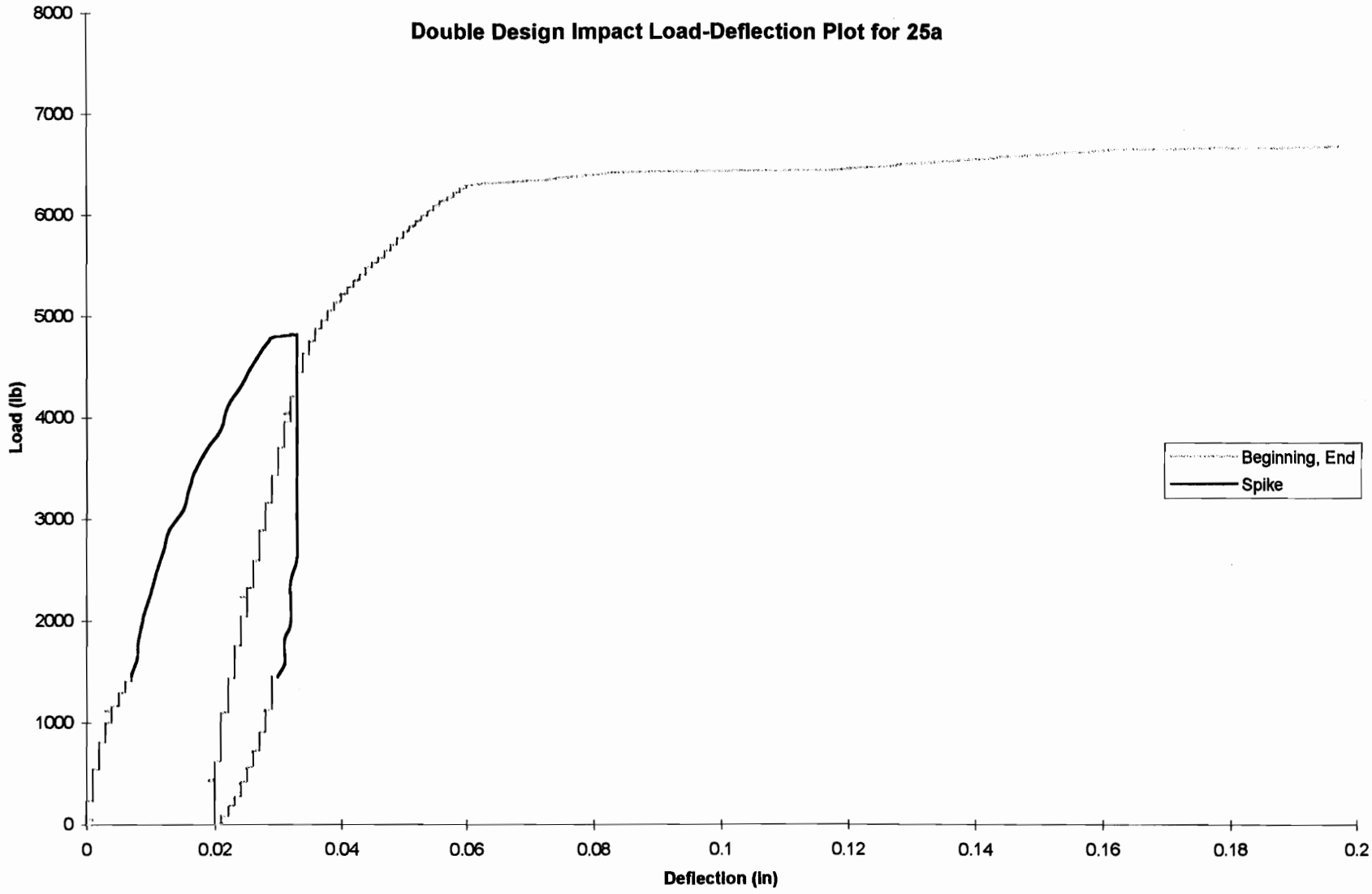
Double Design Impact Load-Deflection Plot for 25a
Load (lb)
8000
7000
6000
5000
4000
3000
2000
1000
0
0
0.02
0.04
0.06
0.08
0.1
0.12
0.14
0.16
0.18
0.2
Deflection (in)
Beginning, End
Spike

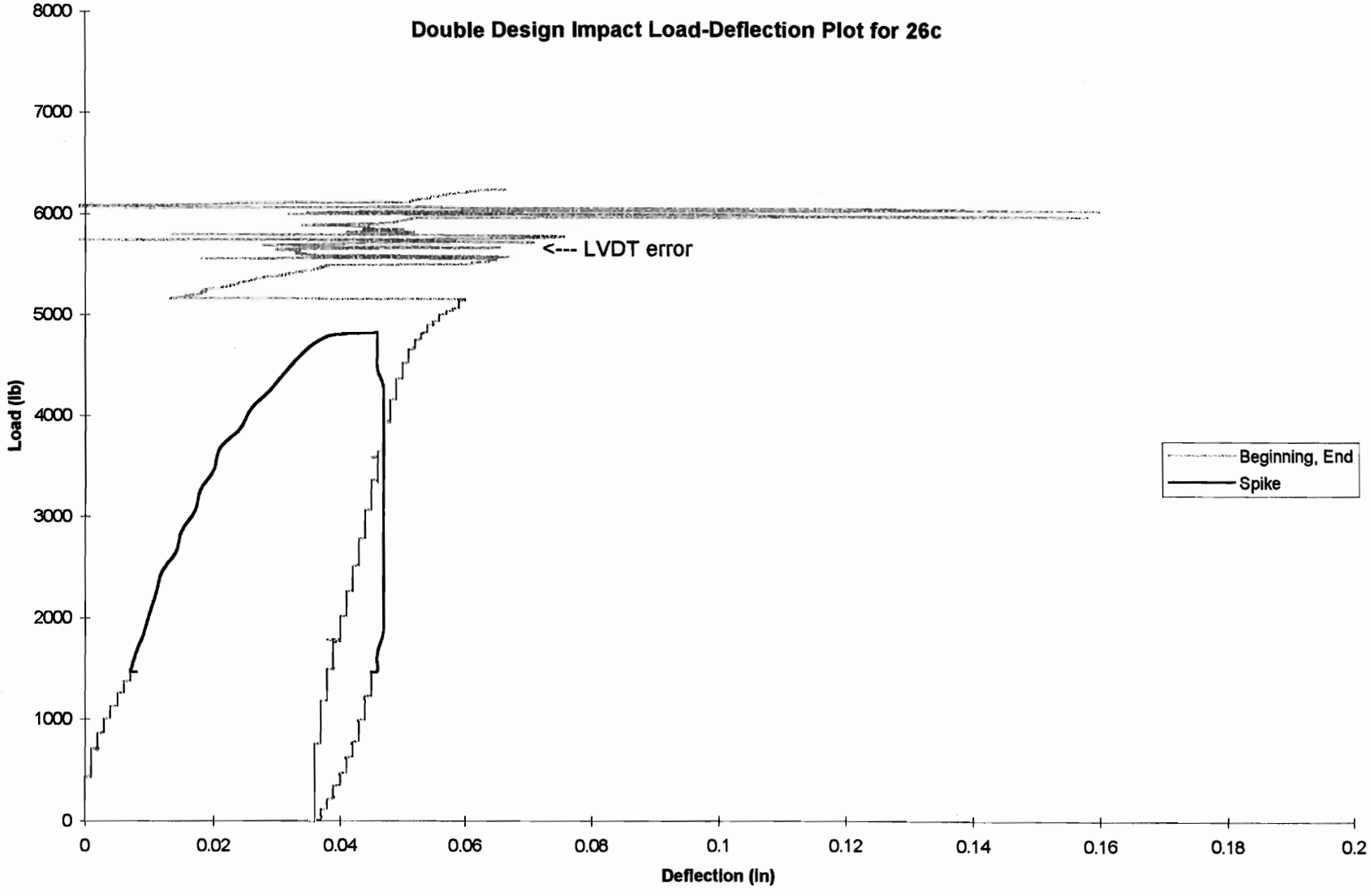
Double Design Impact Load-Deflection Plot for 26c
<--- LVDT error
Load (lb)
Deflection (in)
Beginning, End
Spike
8000
7000
6000
5000
4000
3000
2000
1000
0
0
0.02
0.04
0.06
0.08
0.1
0.12
0.14
0.16
0.18
0.2

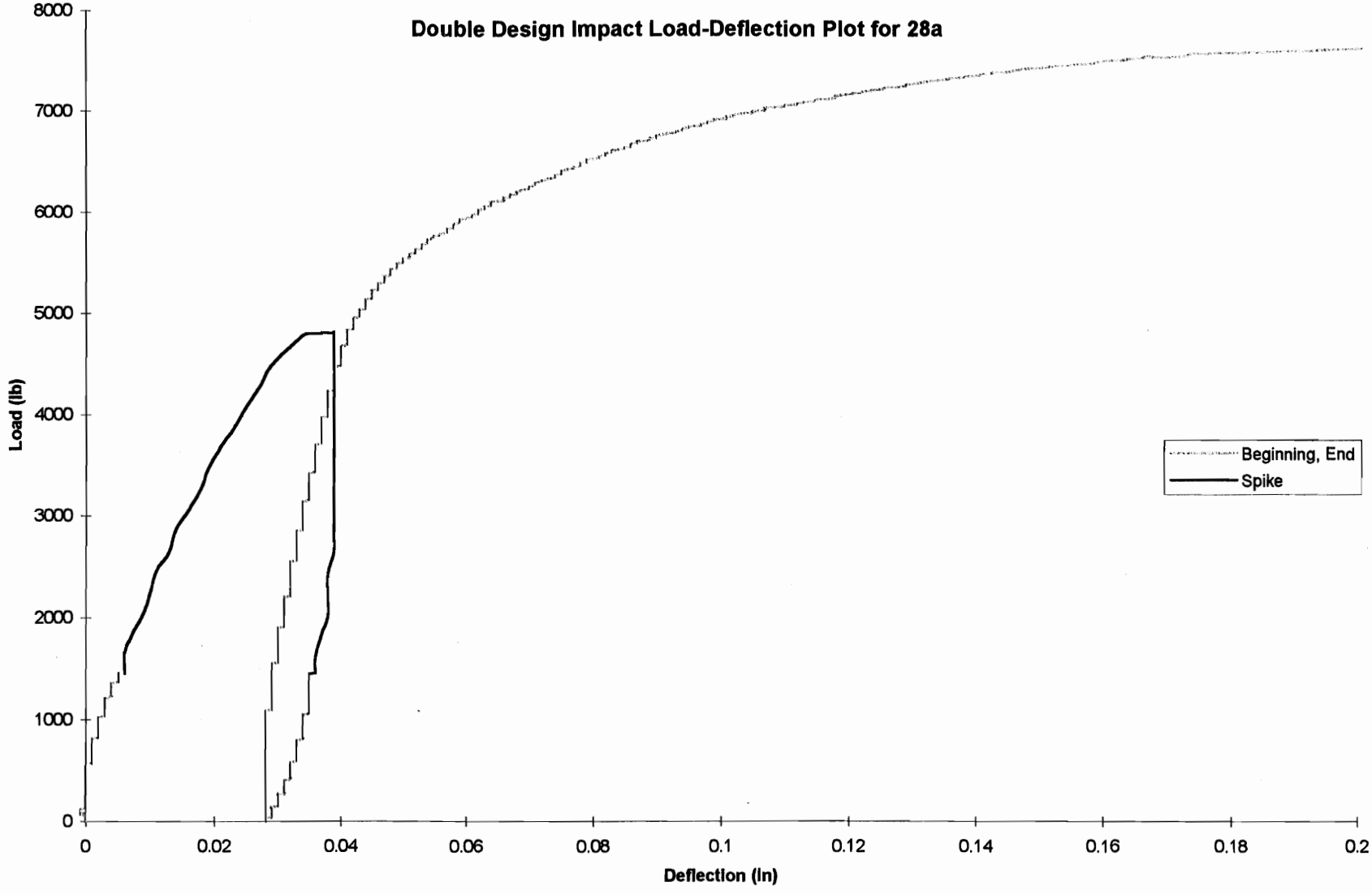
Double Design Impact Load-Deflection Plot for 28a
Load (lb)
8000
7000
6000
5000
4000
3000
2000
1000
0
0
0.02
0.04
0.06
0.08
0.1
0.12
0.14
0.16
0.18
0.2
Deflection (In)
Beginning, End
Spike

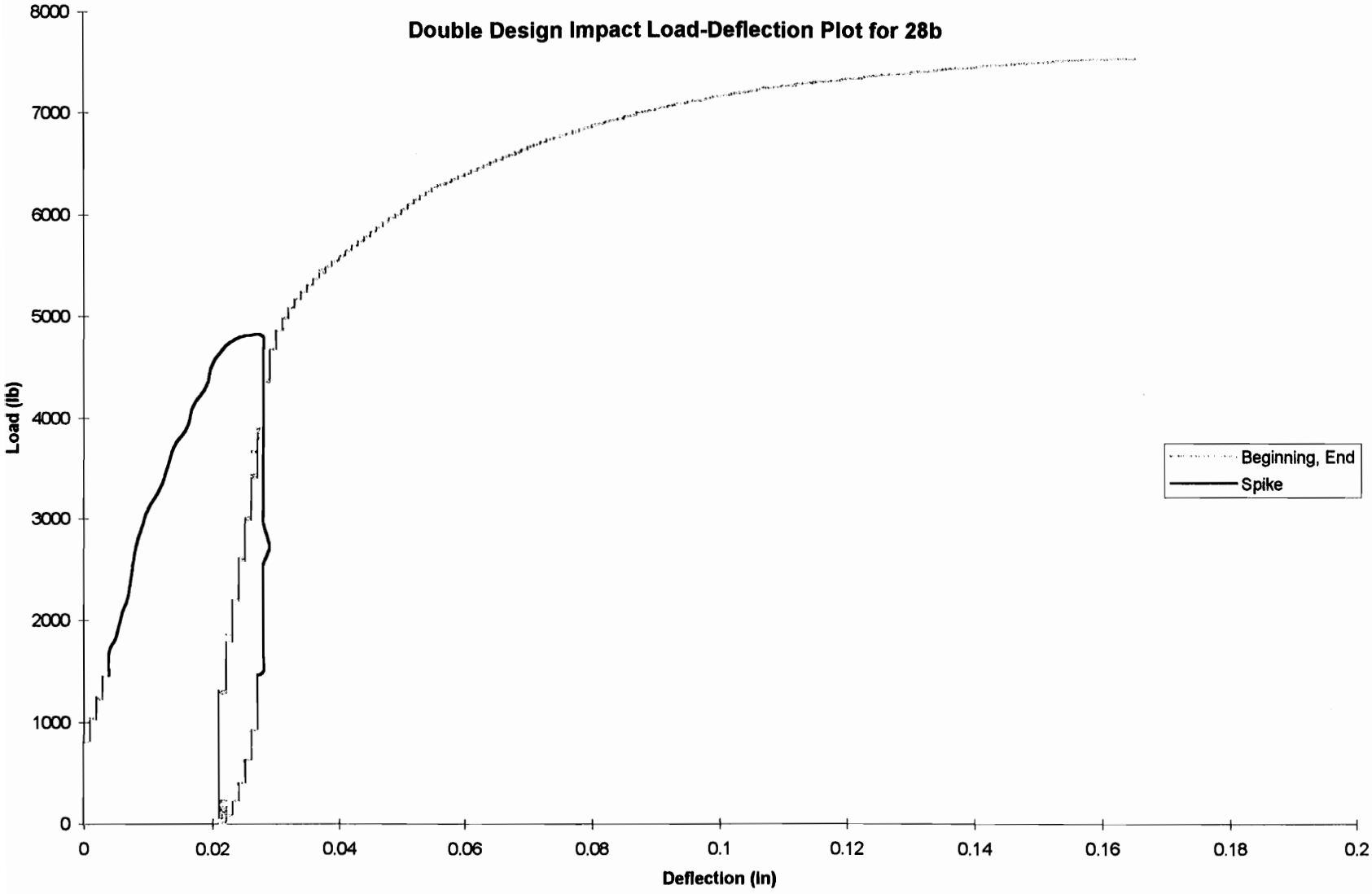
Double Design Impact Load-Deflection Plot for 28b
Load (lb)
8000
7000
6000
5000
4000
3000
2000
1000
0
0
0.02
0.04
0.06
0.08
0.1
0.12
0.14
0.16
0.18
0.2
Deflection (in)
Beginning, End
Spike

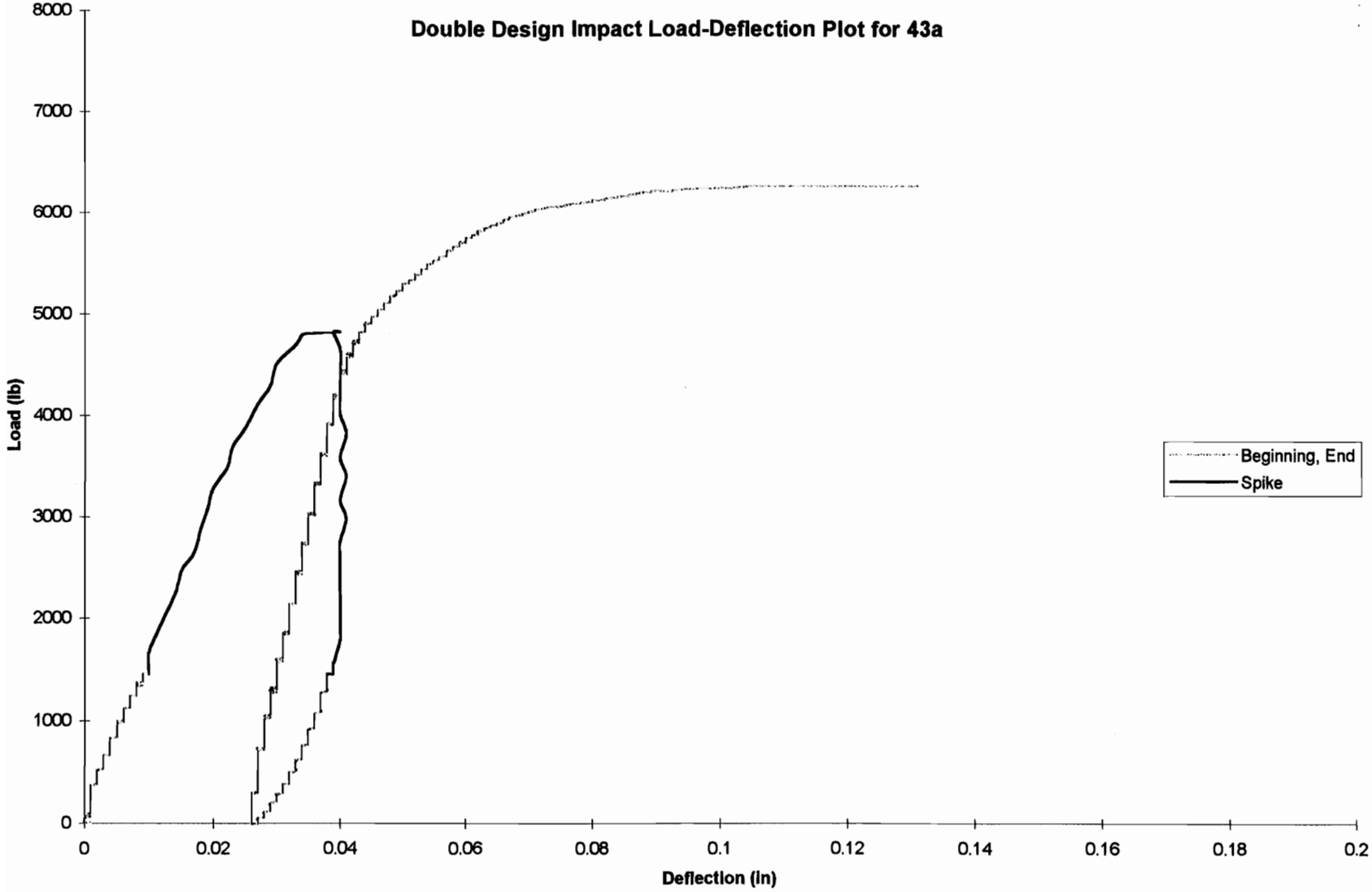
Double Design Impact Load-Deflection Plot for 43a
Load (lb)
8000
7000
6000
5000
4000
3000
2000
1000
0
0
0.02
0.04
0.06
0.08
0.1
0.12
0.14
0.16
0.18
0.2
Deflection (in)
Beginning, End
Spike

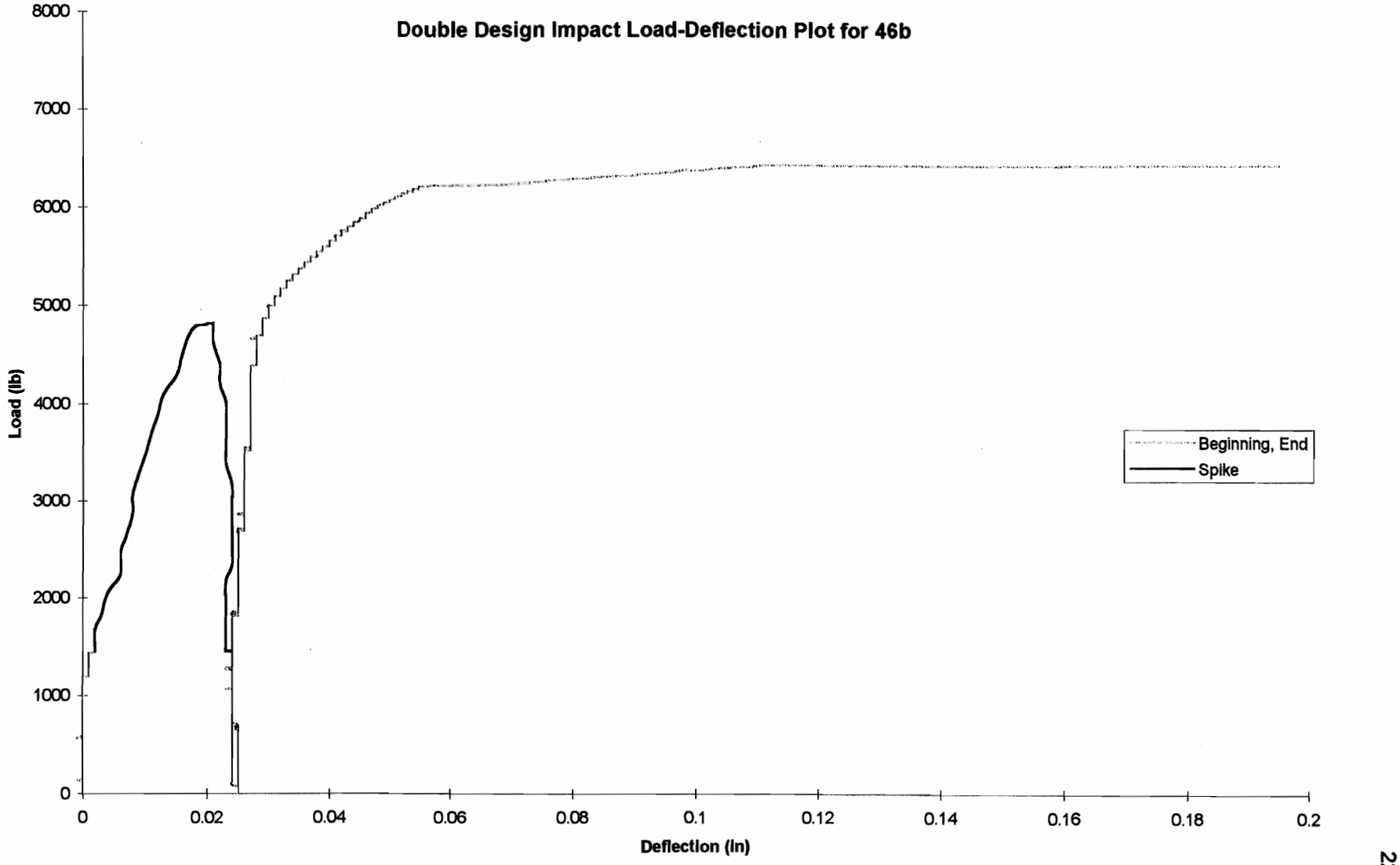
Double Design Impact Load-Deflection Plot for 46b
Load (lb)
8000
7000
6000
5000
4000
3000
2000
1000
0
0
0.02
0.04
0.06
0.08
0.1
0.12
0.14
0.16
0.18
0.2
Deflection (in)
Beginning, End
Spike

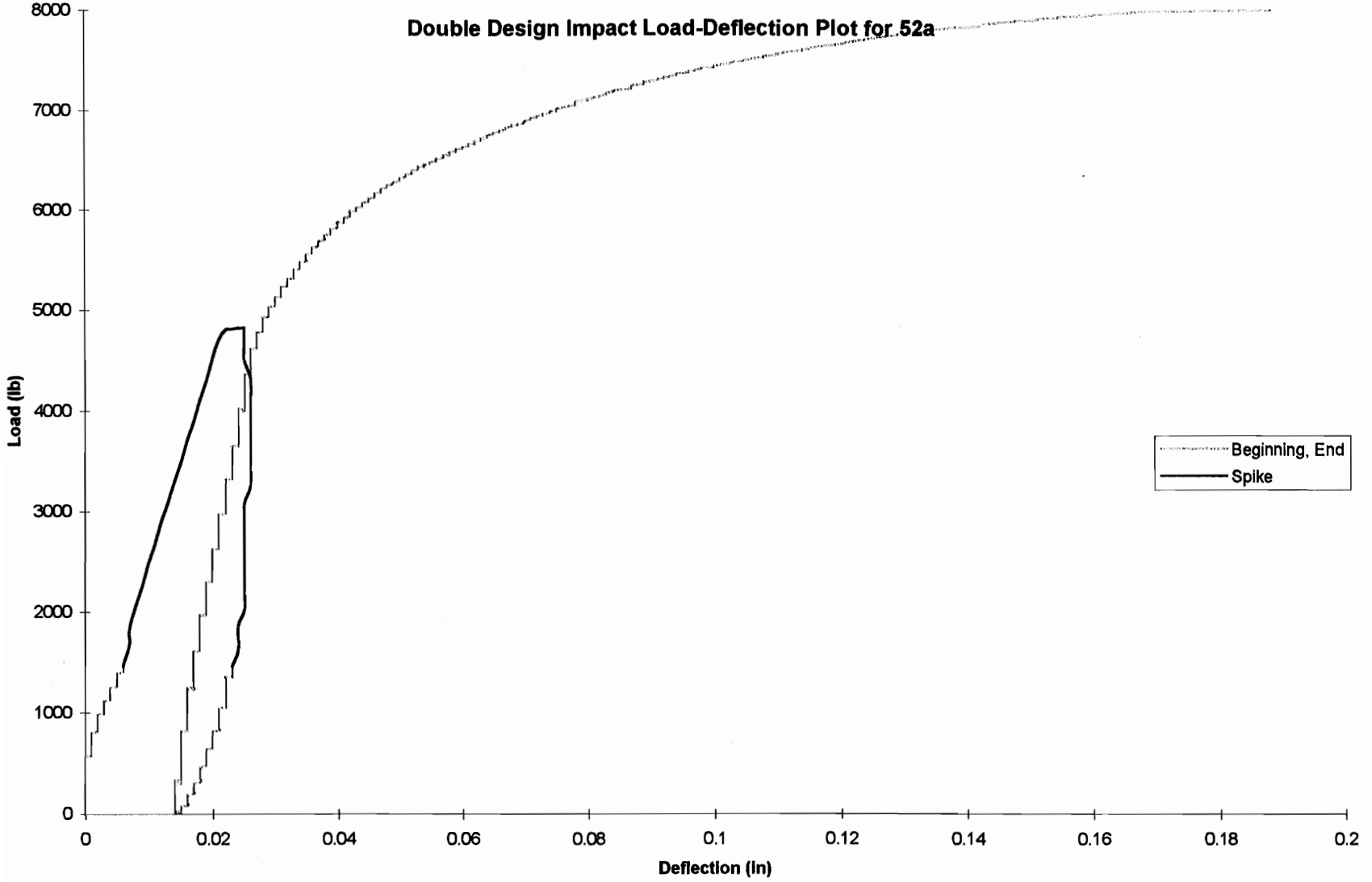
Double Design Impact Load-Deflection Plot for 52a
Load (lb)
8000
7000
6000
5000
4000
3000
2000
1000
0
0
0.02
0.04
0.06
0.08
0.1
0.12
0.14
0.16
0.18
0.2
Deflection (in)
Beginning, End
Spike

Appendix D
Tension splice joint test results

Static Ramp	Ultimate Strength (lb)	Design Load Stiffness (lb/in)	Dead Load Stiffness (lb/in)	Ultimate Deflection (in)	Moisture Content (%)	Time to Failure (min)
1a	6,781	410,992	573,333	0.065	11.5	7.5
2c	6,803	302,376	430,000	0.064	12.7	7.6
5c	7,224	601,966	688,000	0.072	13.0	8.0
8a	7,941	441,182	860,000	0.127	11.8	8.8
15b	7,526	501,766	860,000	0.097	12.0	8.4
17c	6,577	292,297	430,000	0.091	11.1	7.3
18c	5,865	488,734	860,000	0.047	11.9	6.5
19c	4,717	449,210	573,333	0.066	11.8	5.2
20c	7,978	443,225	573,333	0.100	11.5	8.9
Average	6,824	437,000	650,000	0.081	11.9	7.6
COV	15.2%	22.0%	27.1%	30.3%	4.9%	15.2%
# of samples	9	9	9	9	9	9

Static Ramp	Rings per inch	% Late Wood	Specific Gravity	Modulus of Elasticity (10^6 psi)	Failure Mode	Grain Orientation
1a	5	25	0.55	1.80	WS	Both
2c	7	25	0.55	1.73	WS	Flat
5c	8	50	0.36	1.82	TW	Quarter
8a	5	20	0.50	1.95	TW and PF	Flat
15b	4	25	0.50	1.72	WS and PF	Both
17c	5	14	0.57	1.8	TW	Flat
18c	10	25	0.54	1.87	WS	Flat
19c	7	25	0.57	1.67	WS and TW	Flat
20c	5	20	0.53	1.76	WS and PF	Both
Average	6	25	0.52	1.79		
COV	30.9%	39.2%	12.3%	4.7%		
# of samples	9	9	9	9		

NA: Not Available
Flat: Flat-Sawn Lumber (Growth Rings Parallel to Wide Face of Lumber)
Quarter: Quarter-Sawn Lumber (Growth Rings Perpendicular to Wide Face of Lumber)
Both: Combination of Flat and Quarter-Sawn Lumber
TW: Tooth Withdrawal Failure
WS: Wood Shear Failure
PF: Metal Plate Failure

Accelerated Ramp	Ultimate Strength (lb)	Design Load Stiffness (lb/in)	Dead Load Stiffness (lb/in)	Ultimate Deflection (in)	Moisture Content (%)	Time to Failure (s)
1c	6,100	677,760	865,000	0.051	11.8	40.7
3b	8,017	381,761	576,667	0.100	12.4	53.4
5a	8,310	461,677	576,667	0.111	12.8	55.4
6b	8,585	572,336	865,000	0.108	12.1	57.2
7b	5,423	451,942	576,667	0.047	11.4	36.2
9a	7,371	491,391	865,000	0.085	12.3	49.1
12c	8,236	422,359	865,000	0.118	12.2	54.9
14b	6,927	461,786	576,667	0.080	11.6	46.2
16b	7,934	528,919	865,000	0.091	12.2	52.9
19b	4,951	471,481	865,000	0.049	12.1	33.0
Average	7,185	492,000	750,000	0.084	12.1	47.9
COV	17.9%	17.0%	19.9%	31.8%	3.3%	17.9%
# of samples	10	10	10	10	10	10

Accelerated Ramp	Rings per inch	% Late Wood	Specific Gravity	Modulus of Elasticity (10^6 psi)	Failure Mode	Grain Orientation
1c	6	25	0.52	1.80	WS	Flat
3b	6	30	0.49	1.99	TW	Flat
5a	12	50	0.39	1.82	TW and PF	Quarter
6b	4	25	0.49	1.79	PF	Flat
7b	4	15	0.61	1.76	WS	Flat
9a	9	25	0.52	1.98	WS and TW	Flat
12c	4	20	0.54	2.05	TW and PF	Flat
14b	6	30	0.53	1.73	TW	Flat
16b	6	15	0.52	1.88	TW	Flat
19b	8	20	0.60	1.67	WS and TW	Flat
Average	7	26	0.52	1.85		
COV	39.2%	39.7%	11.6%	6.7%		
# of samples	10	10	10	10		

NA: Not Available
Flat: Flat-Sawn Lumber (Growth Rings Parallel to Wide Face of Lumber)
Quarter: Quarter-Sawn Lumber (Growth Rings Perpendicular to Wide Face of Lumber)
Both: Combination of Flat and Quarter-Sawn Lumber
TW: Tooth Withdrawal Failure
WS: Wood Shear Failure
PF: Metal Plate Failure

Double Design Impact	Ultimate Strength (lb)	Design Load Stiffness (lb/in) ending	Dead Load Stiffness (lb/in) beginning	Dead Load Stiffness (lb/in) ending	Ultimate Deflection (in)	Dynamic Deflection (in)	Moisture Content (%)
2b	7,516	294,754	576,667	346,000	0.1015	0.005	9.9 *
3c	7,607	461,016	576,667	432,500	0.098	0.008	10.3 *
6a	7,527	386,014	865,000	432,500	0.082	0.005	9.7 *
9b	6,394	355,207	576,667	432,500	0.0595	0.010	9.6 *
10b	7,408	493,841	865,000	576,667	0.077	0.006	9.6 *
13a	6,883	305,922	865,000	346,000	0.099	0.010	9.6 *
13b	6,061	310,817	865,000	346,000	0.0515	0.010	9.1 *
15c	7,527	418,182	865,000	432,500	0.082	0.005	10.1 *
16a	7,434	381,213	576,667	432,500	0.09	0.008	10.2 *
20a	7,992	484,378	576,667	576,667	0.0735	0.005	10.0 *
Average	7,235	389,000	721,000	435,000	0.081	0.007	9.8 *
COV	8.29%	19.01%	21.08%	19.36%	20.55%	35.32%	3.6%
# of samples	10	10	10	10	10	10	10

Double Design Impact	Time to Failure (min)	Rings per inch	% Late Wood	Specific Gravity	Modulus of Elasticity (10^6 psi)	Failure Mode	Grain Orientation
2b	8.4	6	15	0.56	1.73	WS	Flat
3c	8.5	5	25	0.46	1.99	TW	Flat
6a	8.4	3	20	0.49	1.79	TW	Both
9b	7.1	8	30	0.53	1.98	WS	Flat
10b	8.2	5	15	0.51	1.78	WS	Both
13a	7.6	4	25	0.55	1.75	WS and TW	Flat
13b	6.7	5	20	0.55	1.75	WS and TW	Both
15c	8.4	4	20	0.49	1.72	TW and PF	Both
16a	8.3	5	20	0.52	1.88	TW and PF	Flat
20a	8.9	4	20	0.52	1.76	WS	Both
Average	8.0	5	21	0.52	1.81		
COV	8.29%	28.0%	21.9%	6.2%	5.6%		
# of samples	10	10	10	10	10		

NA: Not Available
Flat: Flat-Sawn Lumber (Growth Rings Parallel to Wide Face of Lumber)
Quarter: Quarter-Sawn Lumber (Growth Rings Perpendicular to Wide Face of Lumber)
Both: Combination of Flat and Quarter-Sawn Lumber
* Unreliable Moisture Content - sample was left out of standard room
TW: Tooth Withdrawal Failure
WS: Wood Shear Failure
PF: Metal Plate Failure

Ultimate Impact	Ultimate Strength (lb)	Design Load Stiffness (lb/in) ending	Dead Load Stiffness (lb/in) beginning	Dead Load Stiffness (lb/in) ending	Ultimate Deflection (in)	Dynamic Deflection (in)	Moisture Content (%)
5b	7,641	363,839	576,667	576,667	0.061	0.021	11.5 *
6c	7,673	341,019	1,730,000	432,500	0.083	0.040	10.6 *
7c	6,336 ***	NA	432,500 **	NA	NA	NA	9.5 *
8c	7,723	321,779	576,667	432,500	0.096	0.034	10.0 *
9c	6,429 ***	NA	432,500 **	NA	NA	NA	9.9 *
11b	7,625	363,109	865,000	432,500	0.07	0.033	10.3 *
11c	8,017	334,035	576,667	432,500	0.088	0.029	10.8 *
13c	6,708	343,996	865,000	432,500	0.035	0.029	9.4 *
17a	7,257	322,524	865,000	346,000	0.053	0.038	9.6 *
19a	5,190 ***	NA	432,500 **	NA	NA	NA	9.4 *
Average	7,520	341,000	865,000	441,000	0.069	0.032	10.1 *
COV	5.60%	5.04%	47.14%	15.40%	31.20%	20.30%	6.9%
# of samples	7	7	7	7	7	7	10

Ultimate Impact	Time to Failure (min)	Rings per inch	% Late Wood	Specific Gravity	Modulus of Elasticity (10^6 psi)	Failure Mode	Grain Orientation
5b	8.5	10	50	0.37	1.82	TW and PF	Quarter
6c	8.5	4	20	0.49	1.79	TW and PF	Flat
7c	NA	4	20	0.59	1.76	WS	Flat
8c	8.6	6	15	0.54	1.95	PF	Flat
9c	NA	10	30	0.53	1.98	WS	Flat
11b	8.5	3	15	0.50	1.77	TW and PF	Flat
11c	8.9	3	15	0.51	1.77	TW and PF	Both
13c	7.5	5	20	0.54	1.75	WS and TW	Both
17a	8.1	6	20	0.53	1.80	WS and TW	Flat
19a	NA	6	20	0.62	1.67	WS and TW	Flat
Average	8.4	6	23	0.52	1.81		
COV	5.60%	44.6%	47.1%	12.5%	5.1%		
# of samples	7	10	10	10	10		

NA: Not Available
Flat: Flat-Sawn Lumber (Growth Rings Parallel to Wide Face of Lumber)
Quarter: Quarter-Sawn Lumber (Growth Rings Perpendicular to Wide Face of Lumber)
Both: Combination of Flat and Quarter-Sawn Lumber
* Unreliable Moisture Content - sample was left out of standard room
** Value not included in average, COV, or number of samples calculation
*** Strength value determined as the maximum load achieved during the impact load but not included in average, COV, or number of samples calculation
TW: Tooth Withdrawal Failure
WS: Wood Shear Failure
PF: Metal Plate Failure

Appendix E
Load-deflection plots for tension splice joints

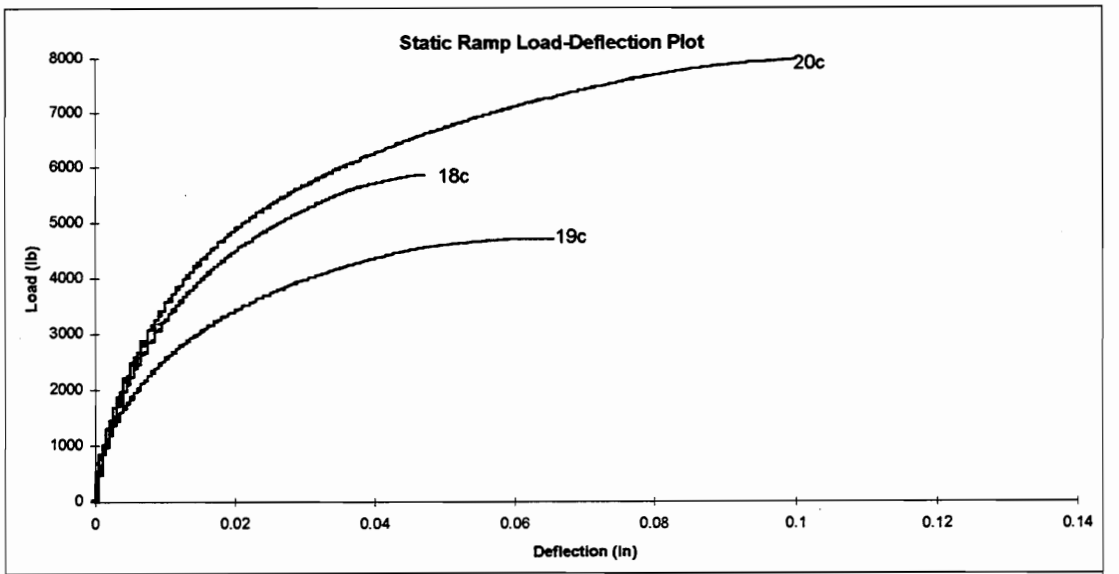
Static Ramp Load-Deflection Plot
Load (lb)
Deflection (in)
20c
18c
19c
0
1000
2000
3000
4000
5000
6000
7000
8000
0.02
0.04
0.06
0.08
0.1
0.12
0.14

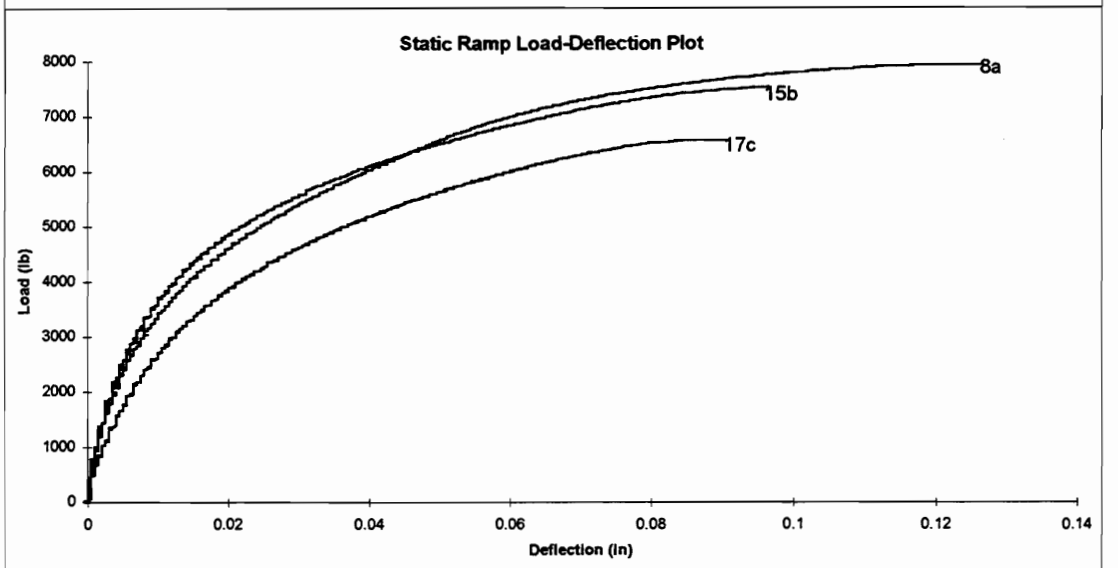
Static Ramp Load-Deflection Plot
Load (lb)
Deflection (in)
8a
15b
17c
0
1000
2000
3000
4000
5000
6000
7000
8000
0.02
0.04
0.06
0.08
0.1
0.12
0.14

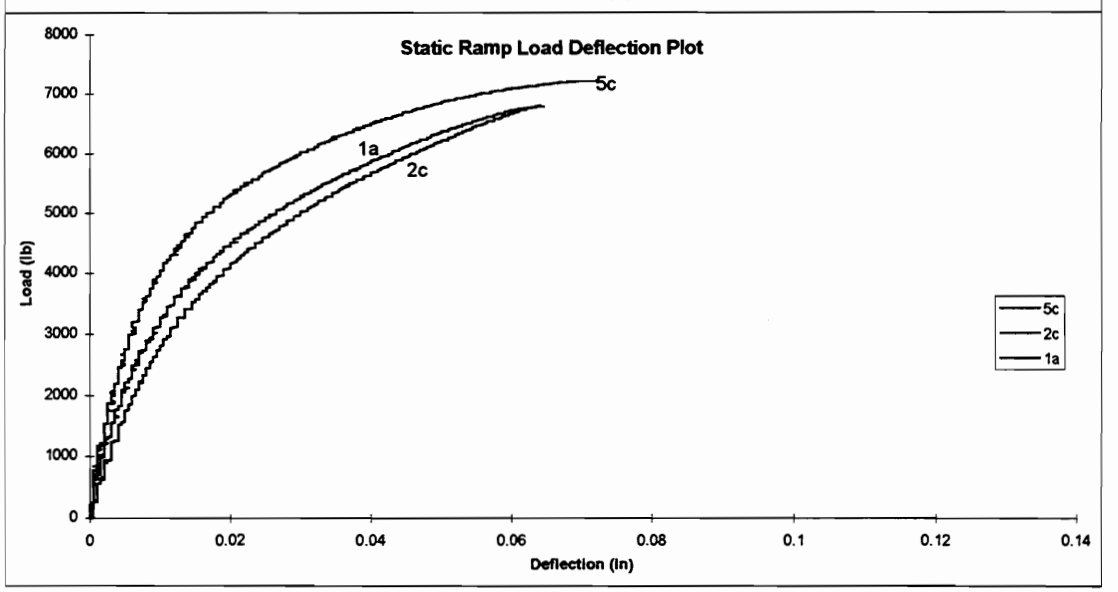
Static Ramp Load Deflection Plot
Load (lb)
Deflection (in)
5c
1a
2c
5c
2c
1a
0
1000
2000
3000
4000
5000
6000
7000
8000
0.02
0.04
0.06
0.08
0.1
0.12
0.14

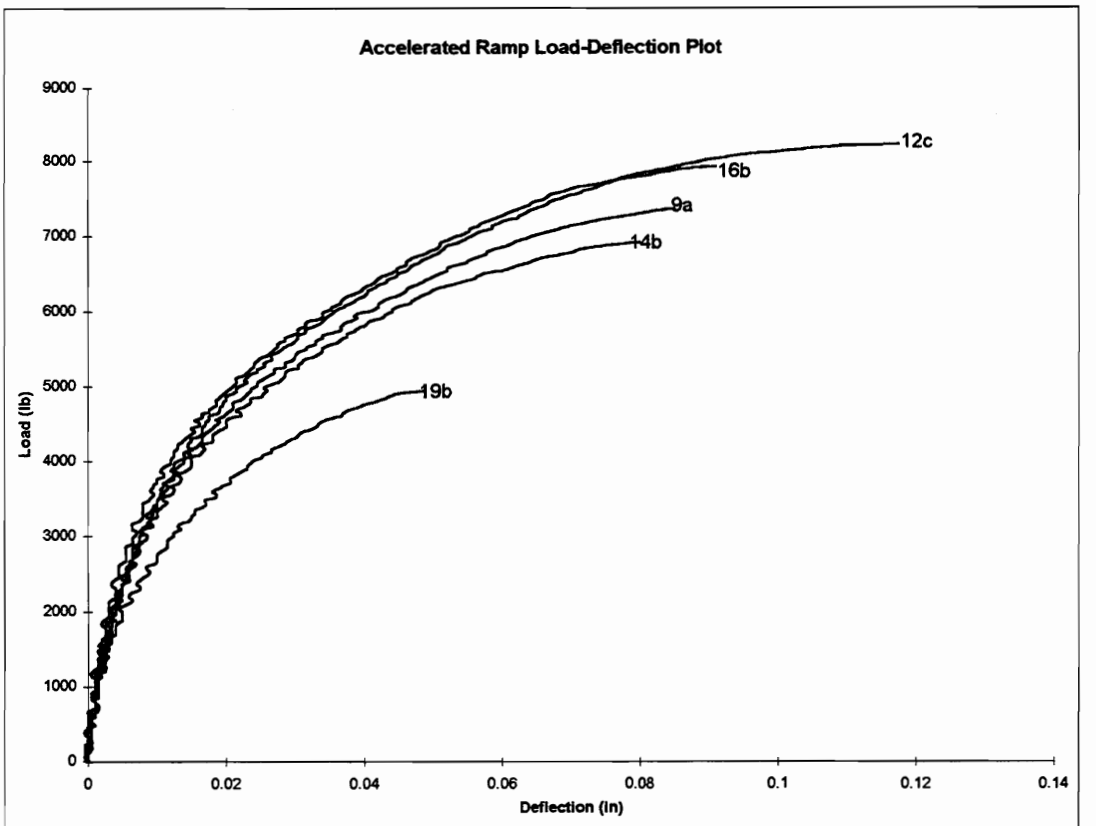
Accelerated Ramp Load-Deflection Plot
Load (lb)
Deflection (in)
12c
16b
9a
14b
19b

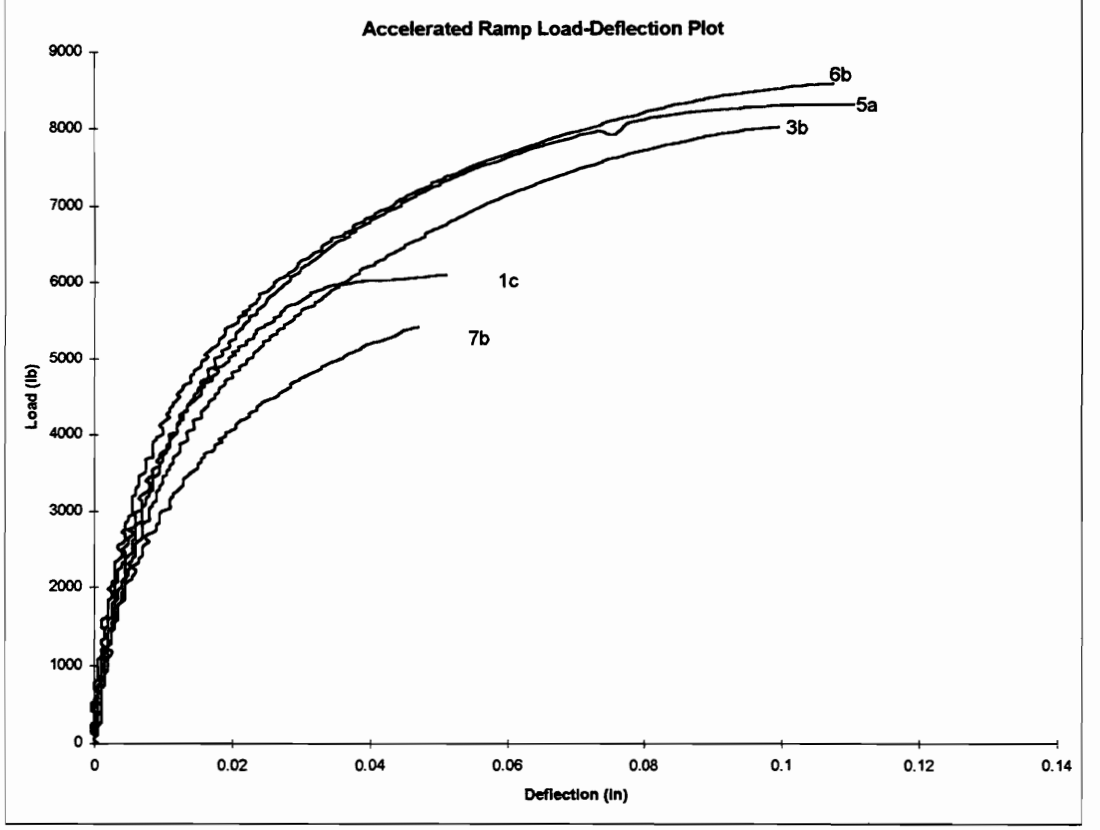
Accelerated Ramp Load-Deflection Plot
Load (lb)
Deflection (in)
6b
5a
3b
1c
7b

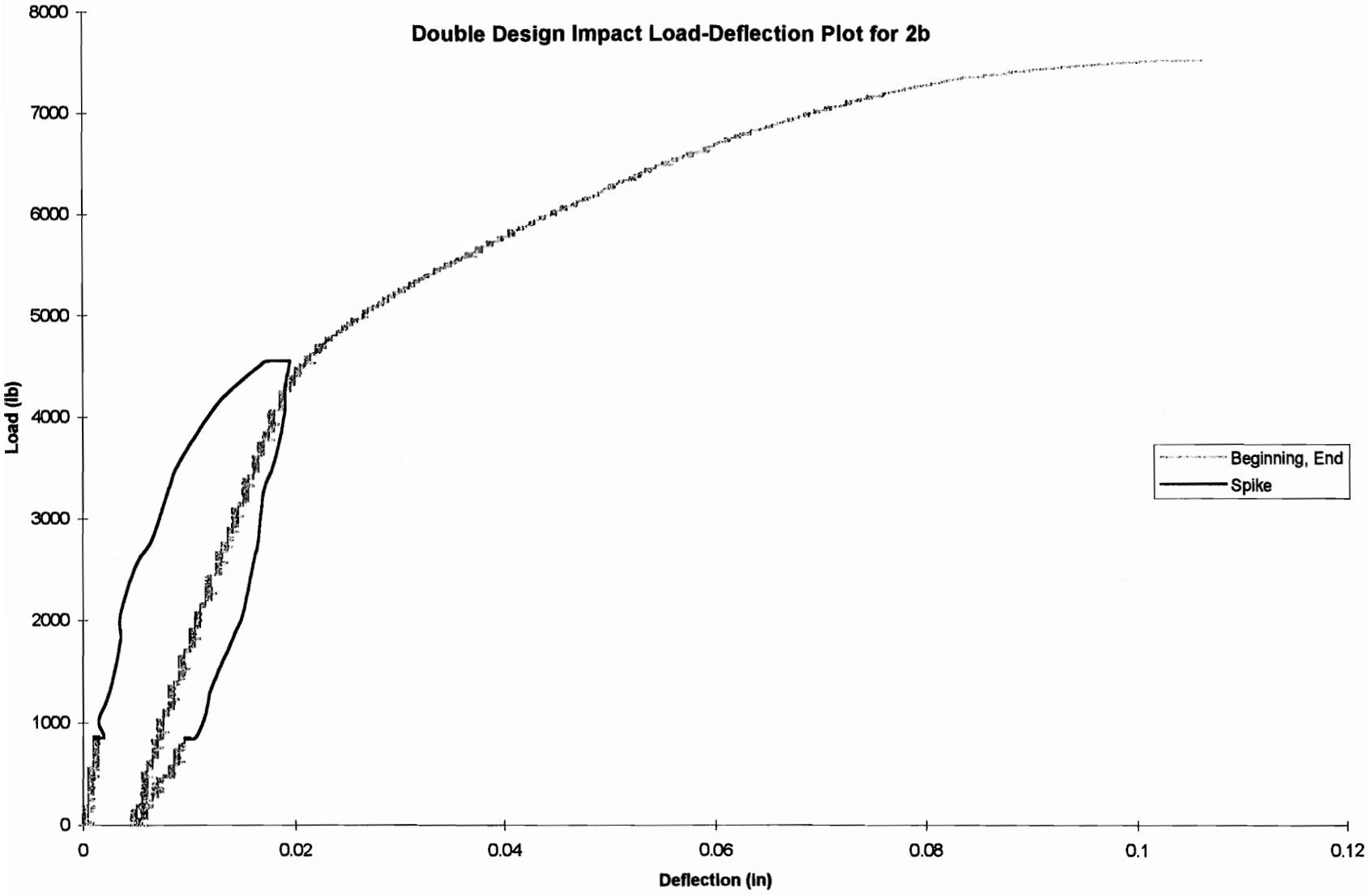
Double Design Impact Load-Deflection Plot for 2b
Load (lb)
8000
7000
6000
5000
4000
3000
2000
1000
0
0
0.02
0.04
0.06
0.08
0.1
0.12
Deflection (in)
Beginning, End
Spike

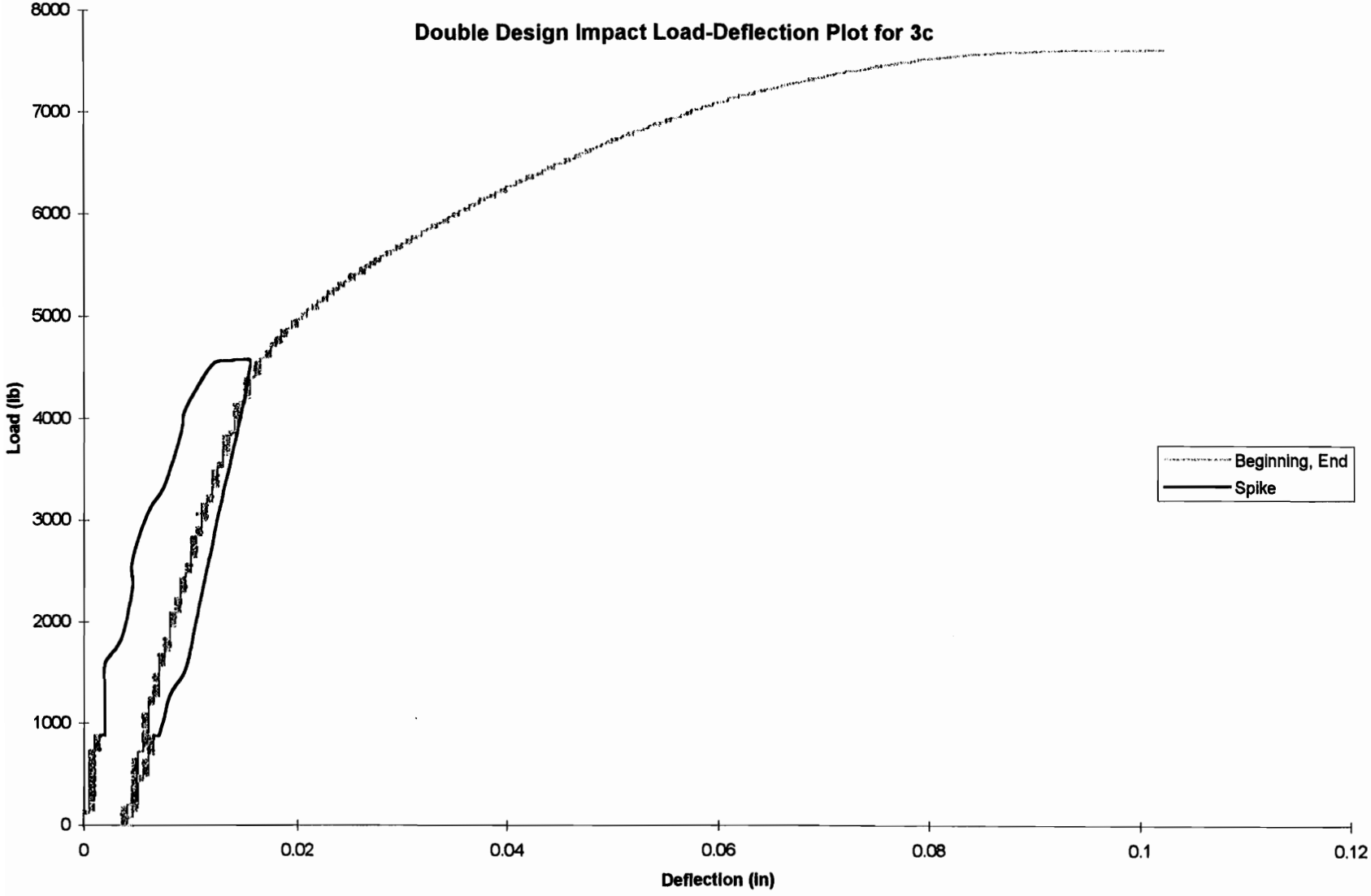
Double Design Impact Load-Deflection Plot for 3c
Load (lb)
8000
7000
6000
5000
4000
3000
2000
1000
0
0
0.02
0.04
0.06
0.08
0.1
0.12
Deflection (in)
Beginning, End
Spike

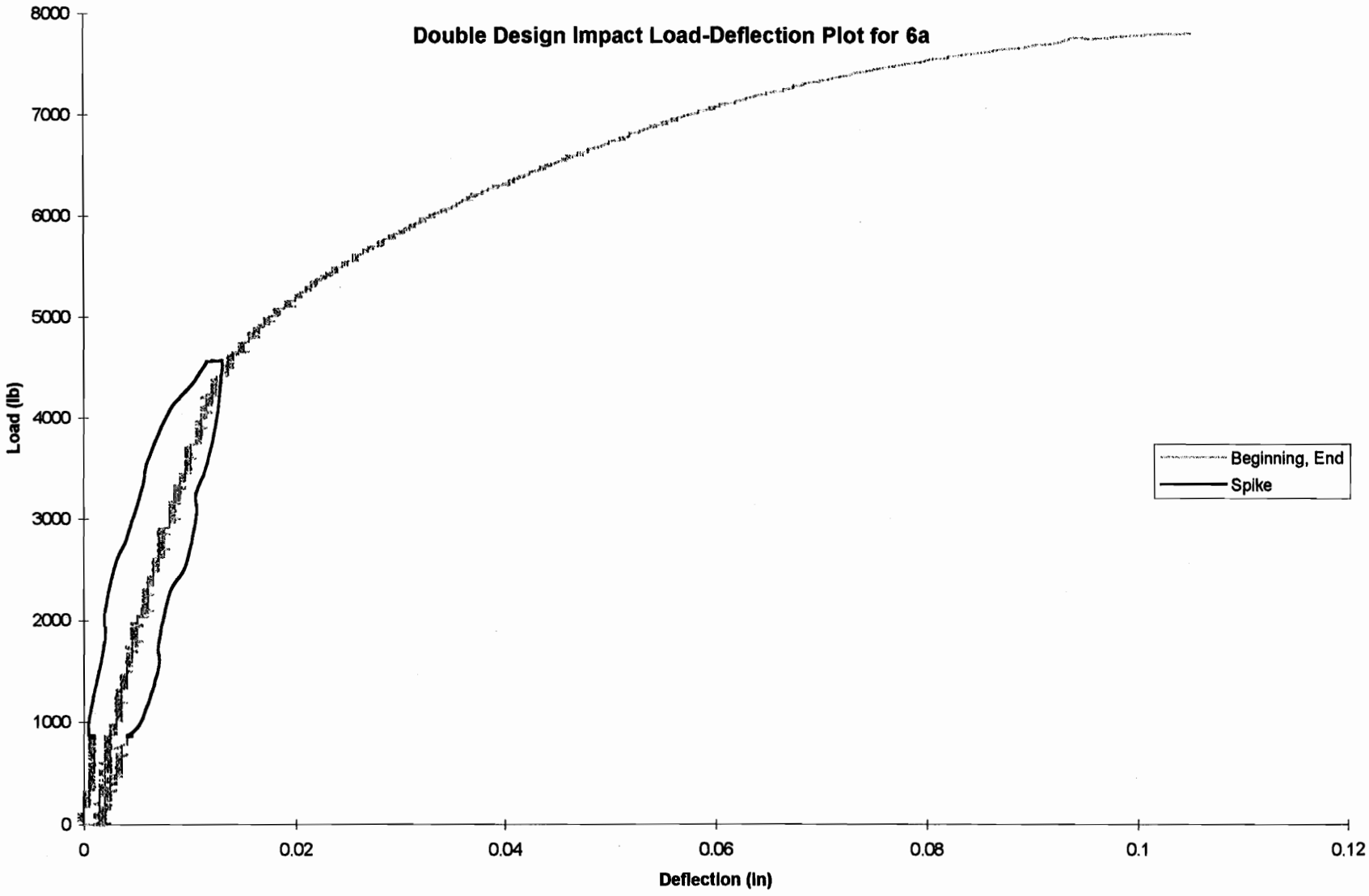
Double Design Impact Load-Deflection Plot for 6a
Load (lb)
8000
7000
6000
5000
4000
3000
2000
1000
0
0
0.02
0.04
0.06
0.08
0.1
0.12
Deflection (in)
Beginning, End
Spike

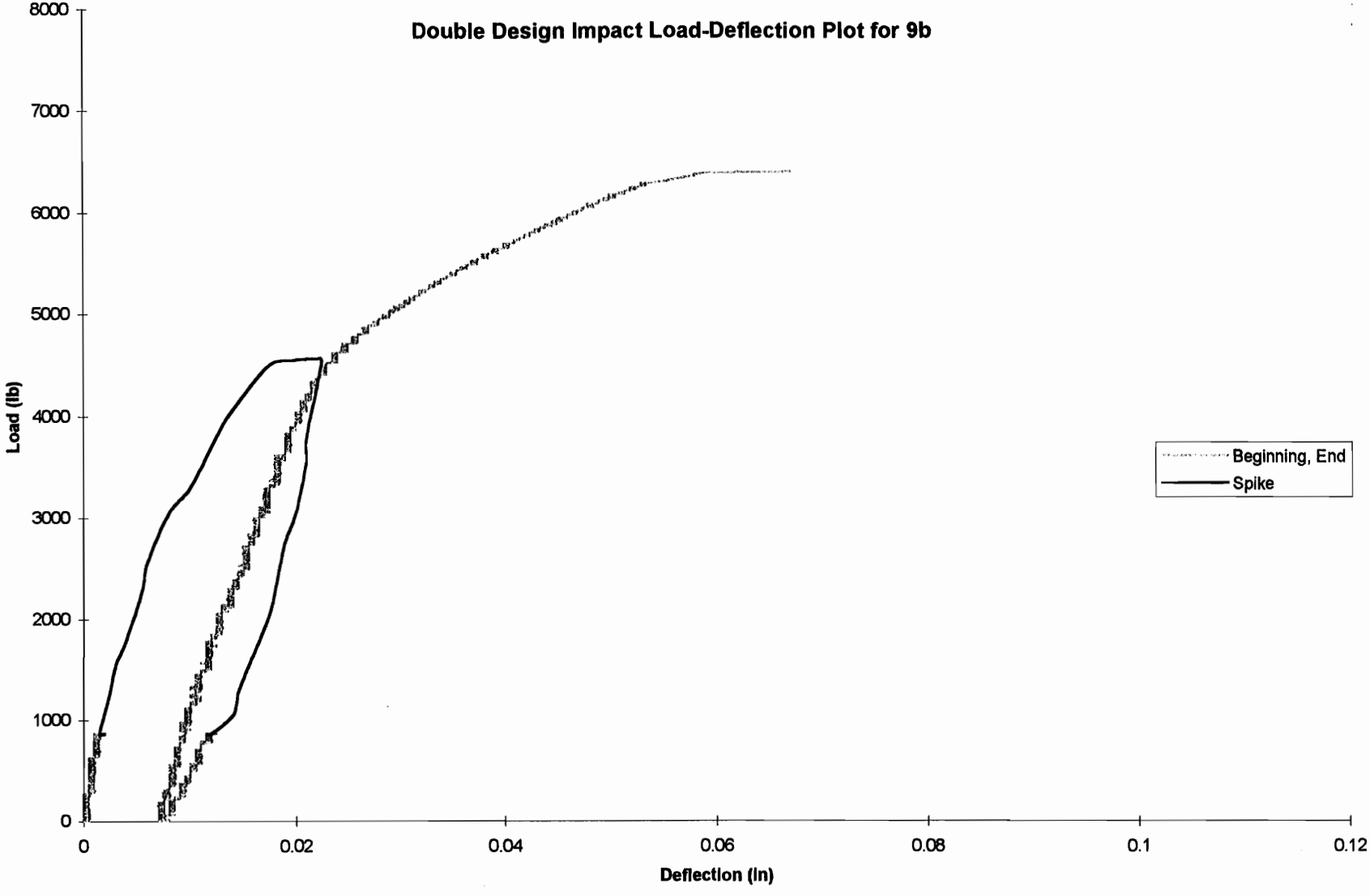
Double Design Impact Load-Deflection Plot for 9b
Load (lb)
8000
7000
6000
5000
4000
3000
2000
1000
0
0
0.02
0.04
0.06
0.08
0.1
0.12
Deflection (in)
Beginning, End
Spike

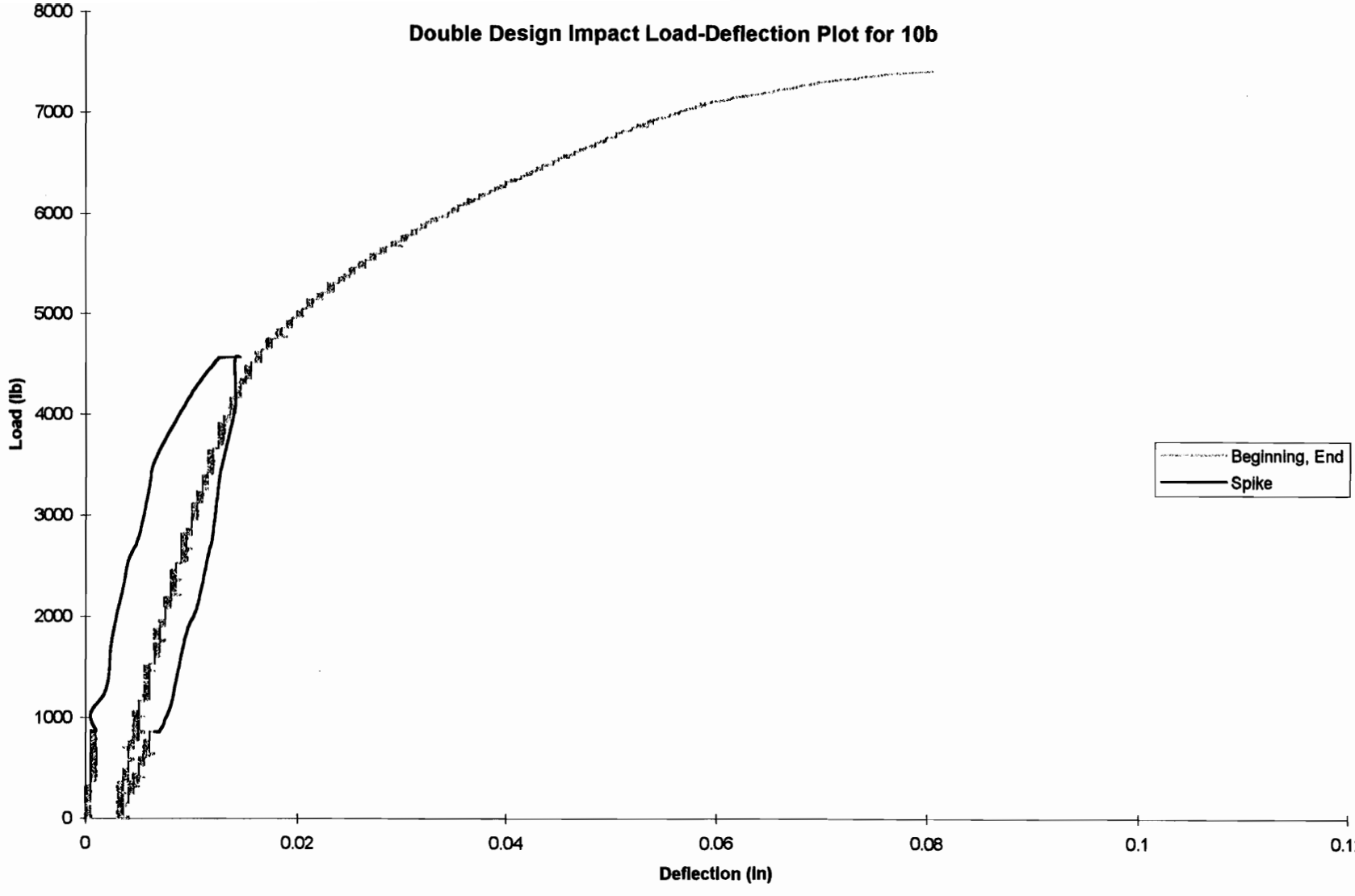
Double Design Impact Load-Deflection Plot for 10b
Load (lb)
8000
7000
6000
5000
4000
3000
2000
1000
0
0
0.02
0.04
0.06
0.08
0.1
0.12
Deflection (in)
Beginning, End
Spike

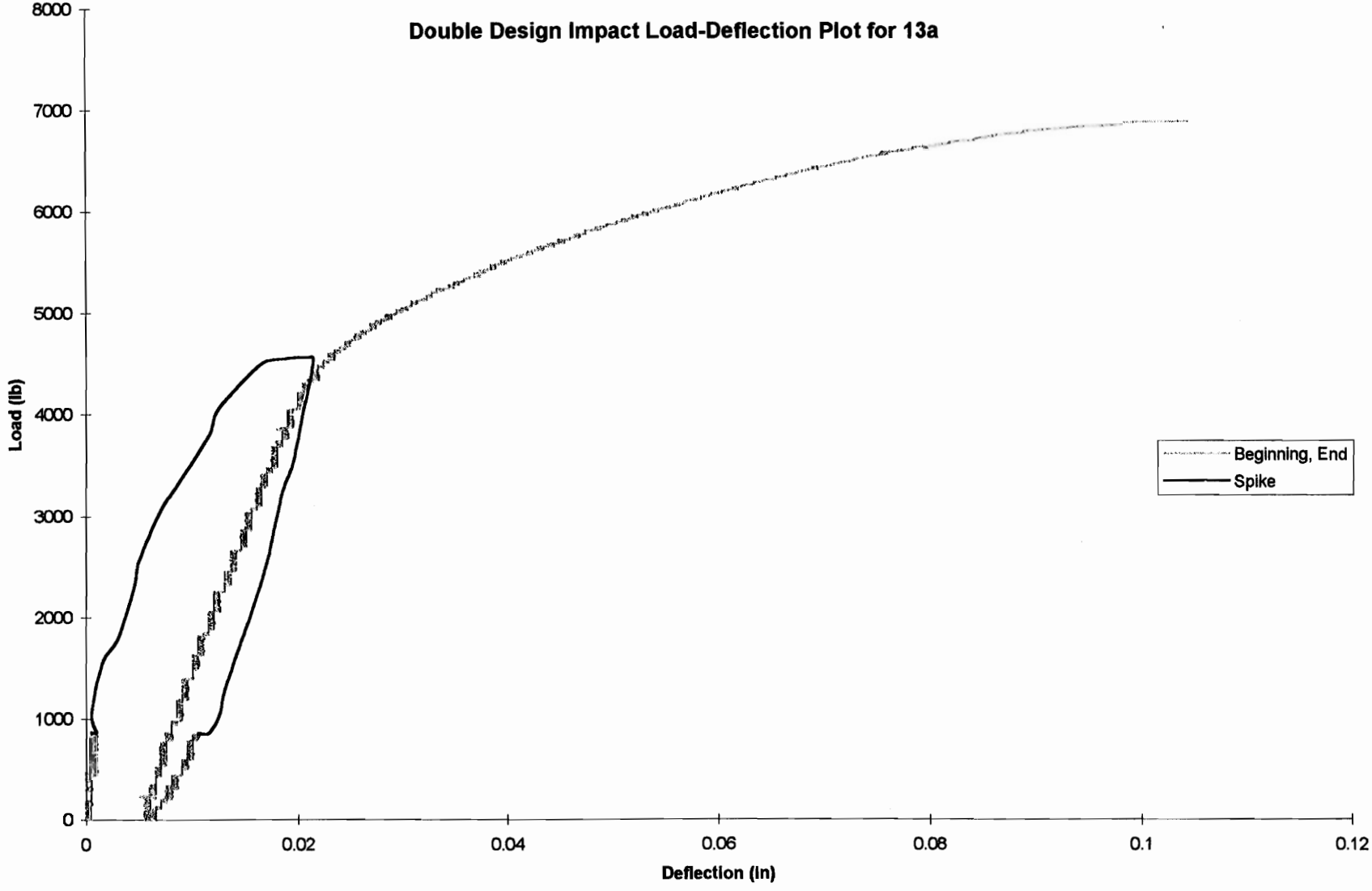
Double Design Impact Load-Deflection Plot for 13a
Load (lb)
8000
7000
6000
5000
4000
3000
2000
1000
0
0
0.02
0.04
0.06
0.08
0.1
0.12
Deflection (in)
Beginning, End
Spike

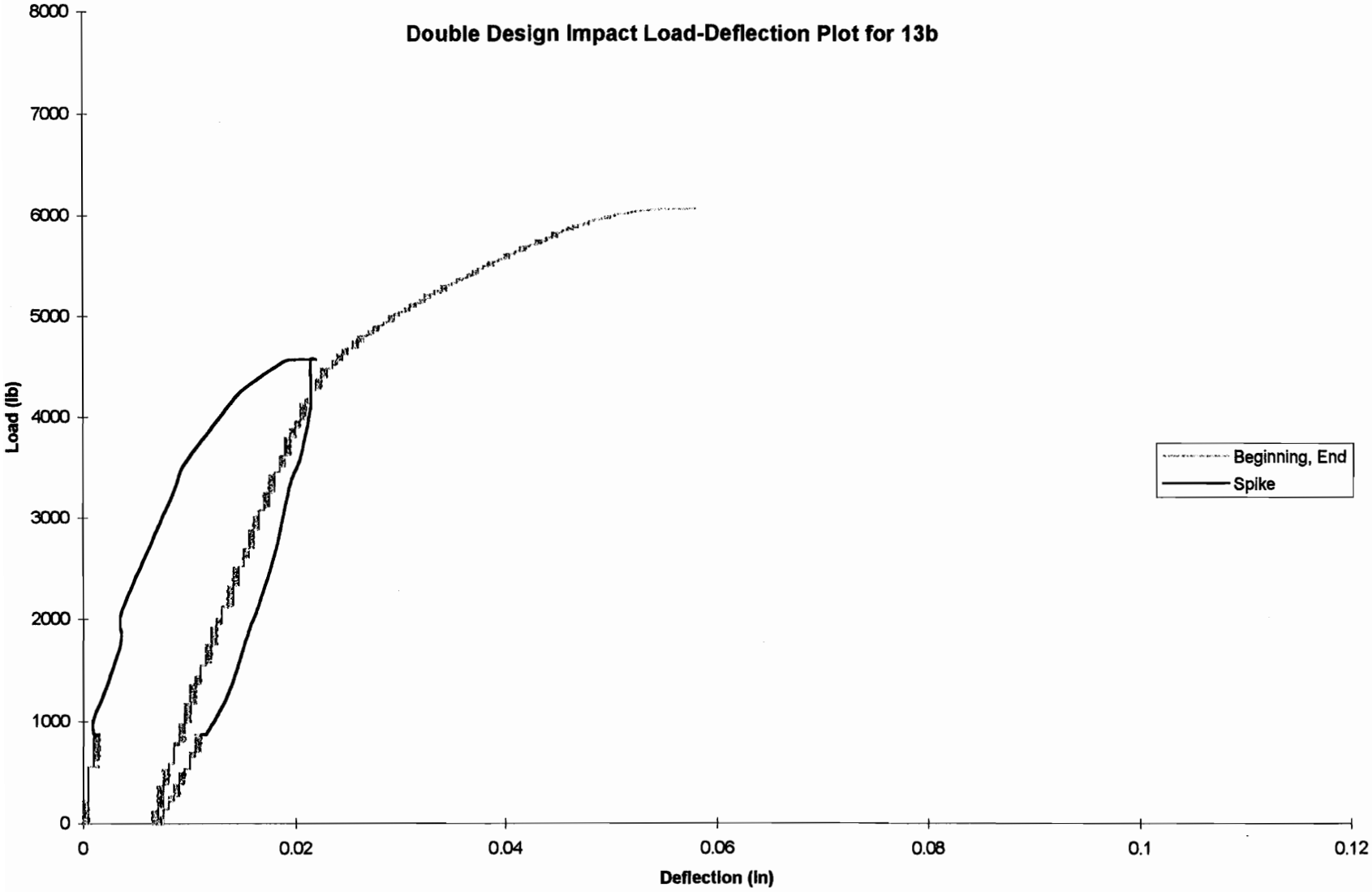
Double Design Impact Load-Deflection Plot for 13b
Load (lb)
8000
7000
6000
5000
4000
3000
2000
1000
0
0
0.02
0.04
0.06
0.08
0.1
0.12
Deflection (In)
Beginning, End
Spike

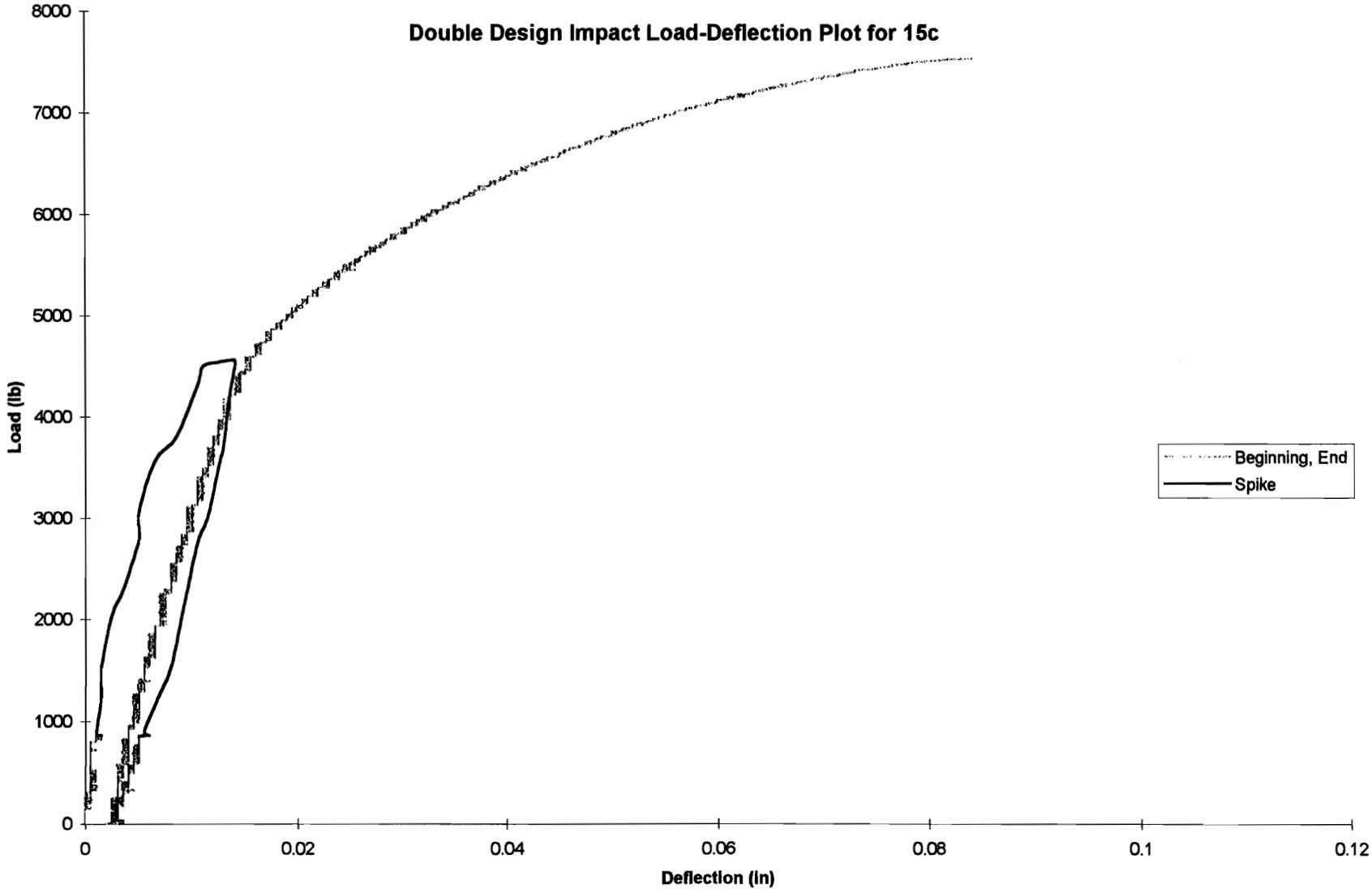
Double Design Impact Load-Deflection Plot for 15c
Load (lb)
8000
7000
6000
5000
4000
3000
2000
1000
0
0
0.02
0.04
0.06
0.08
0.1
0.12
Deflection (in)
Beginning, End
Spike

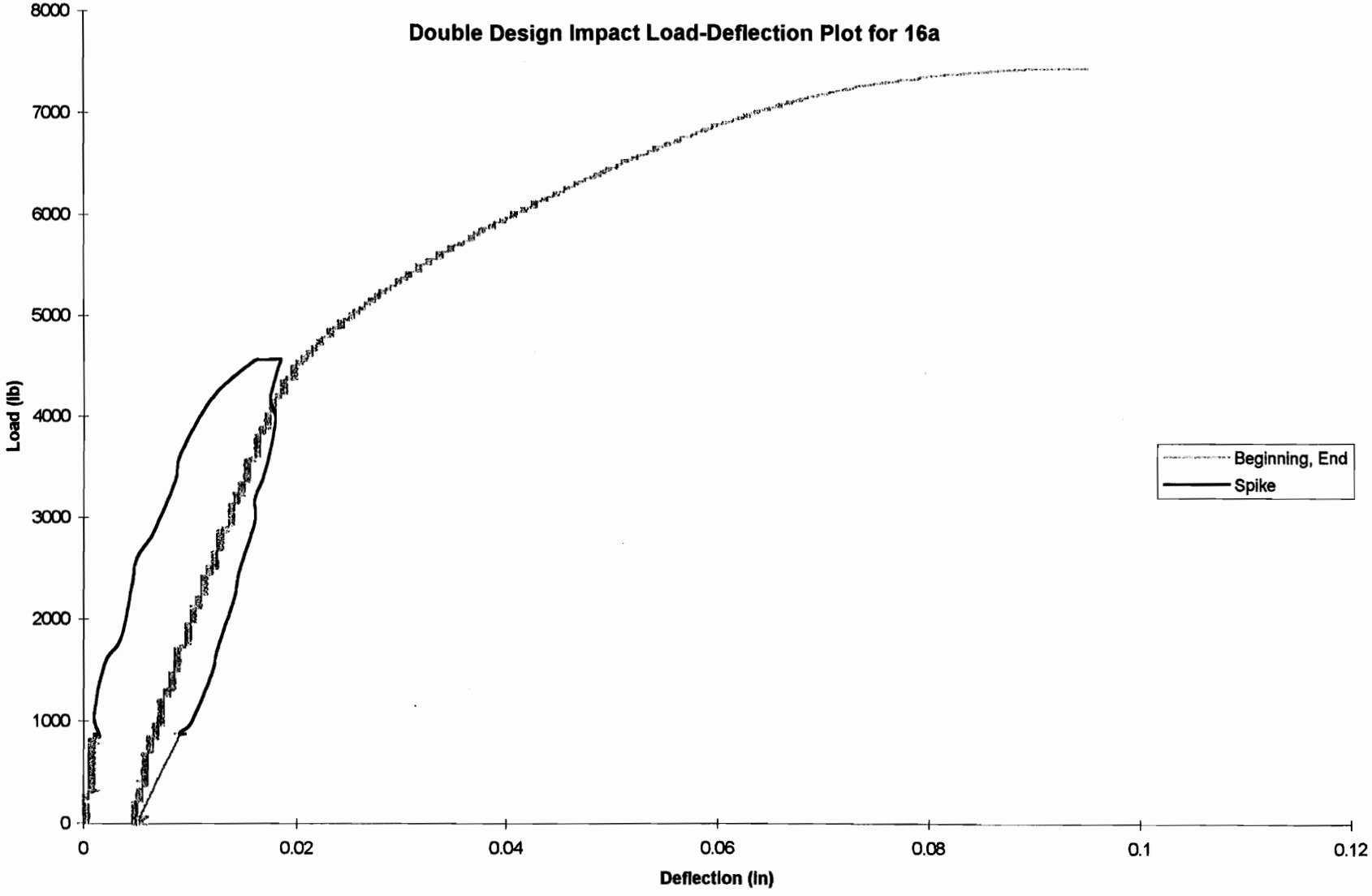
Double Design Impact Load-Deflection Plot for 16a
Load (lb)
8000
7000
6000
5000
4000
3000
2000
1000
0
0
0.02
0.04
0.06
0.08
0.1
0.12
Deflection (in)
Beginning, End
Spike

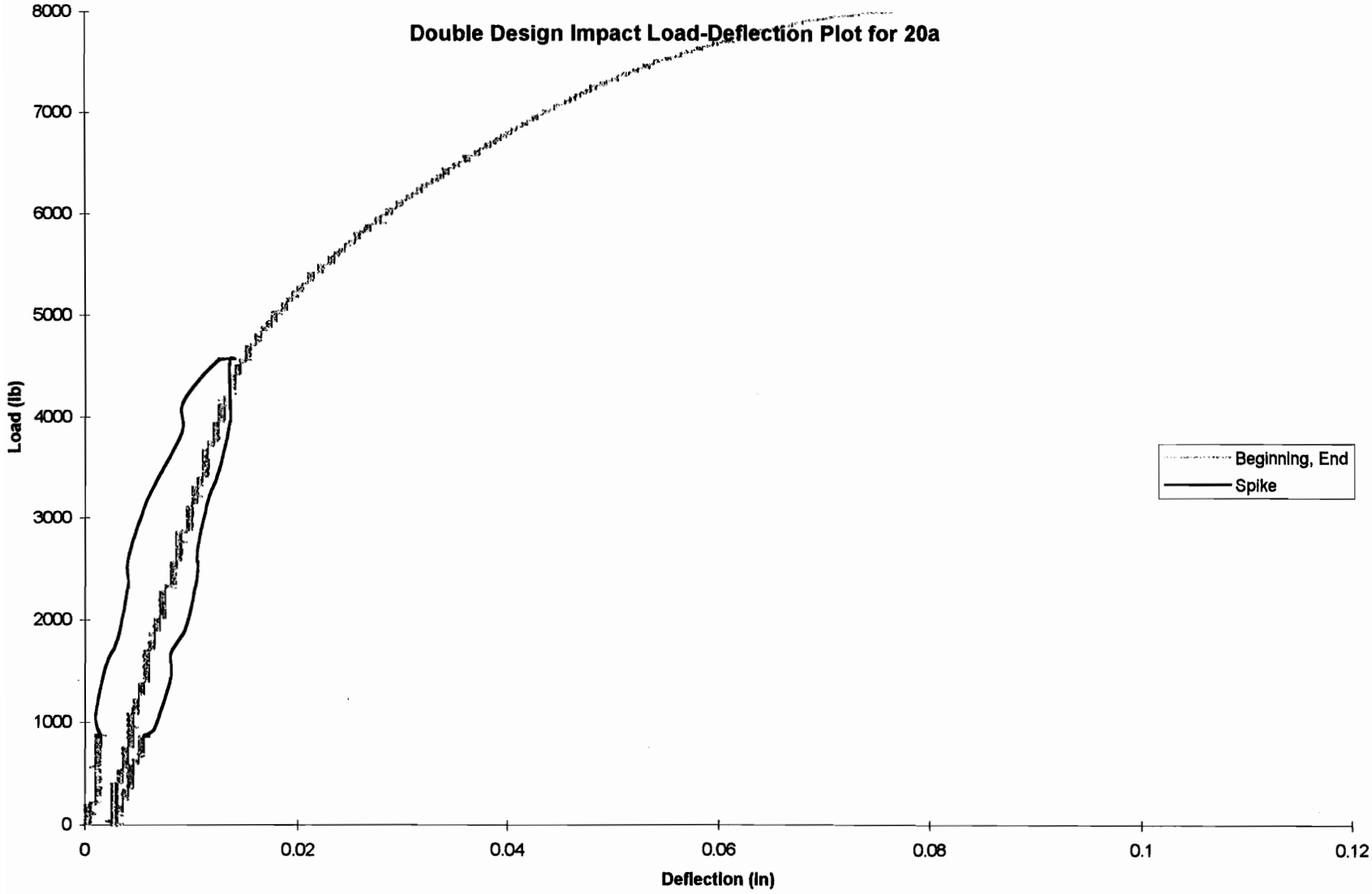
Double Design Impact Load-Deflection Plot for 20a
Load (lb)
8000
7000
6000
5000
4000
3000
2000
1000
0
0
0.02
0.04
0.06
0.08
0.1
0.12
Deflection (in)
Beginning, End
Spike

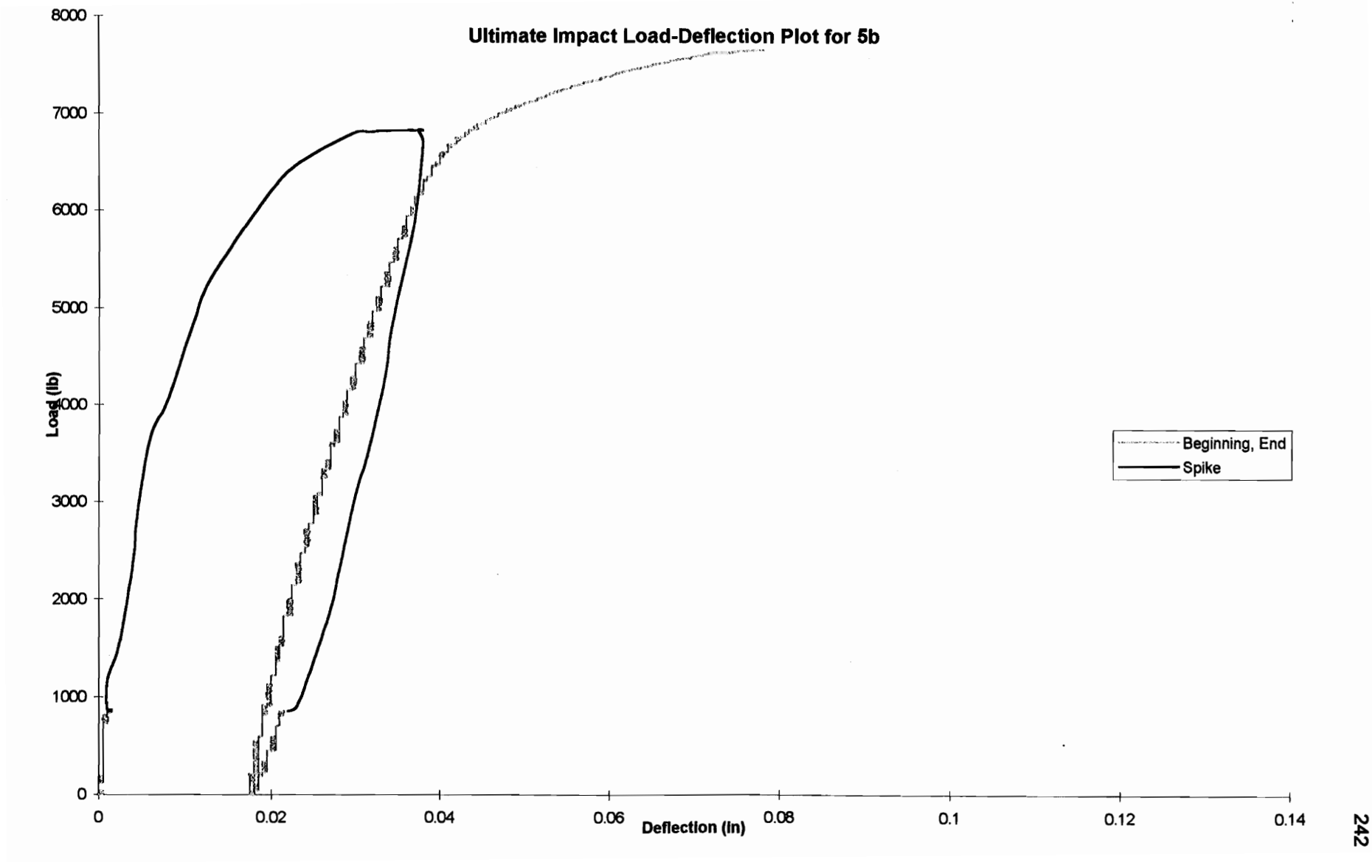
Ultimate Impact Load-Deflection Plot for 5b
Load (lb)
8000
7000
6000
5000
4000
3000
2000
1000
0
0
0.02
0.04
0.06
0.08
0.1
0.12
0.14
Deflection (in)
Beginning, End
Spike

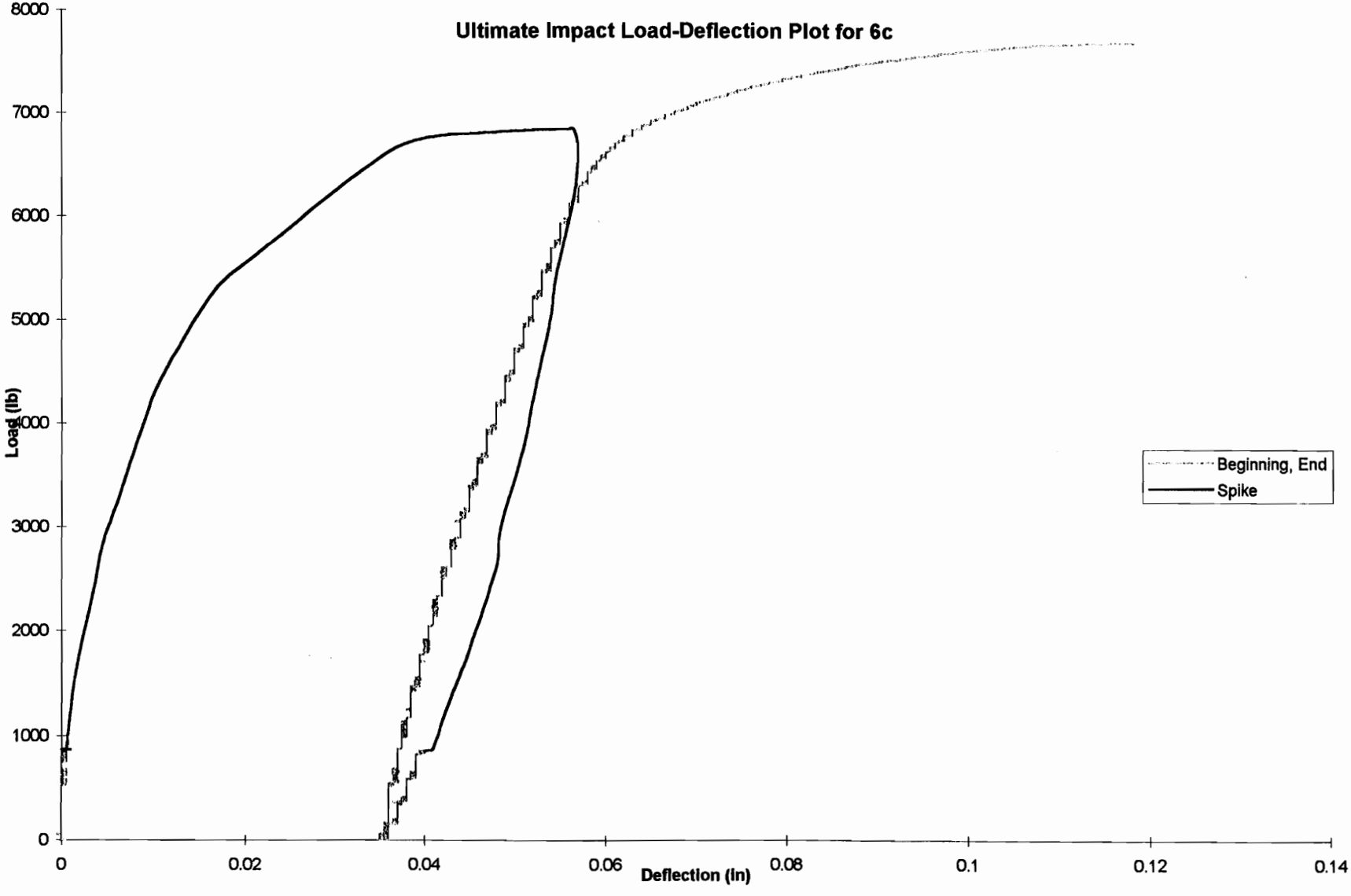
Ultimate Impact Load-Deflection Plot for 6c
Load (lb)
8000
7000
6000
5000
4000
3000
2000
1000
0
0
0.02
0.04
0.06
0.08
0.1
0.12
0.14
Deflection (in)
Beginning, End
Spike

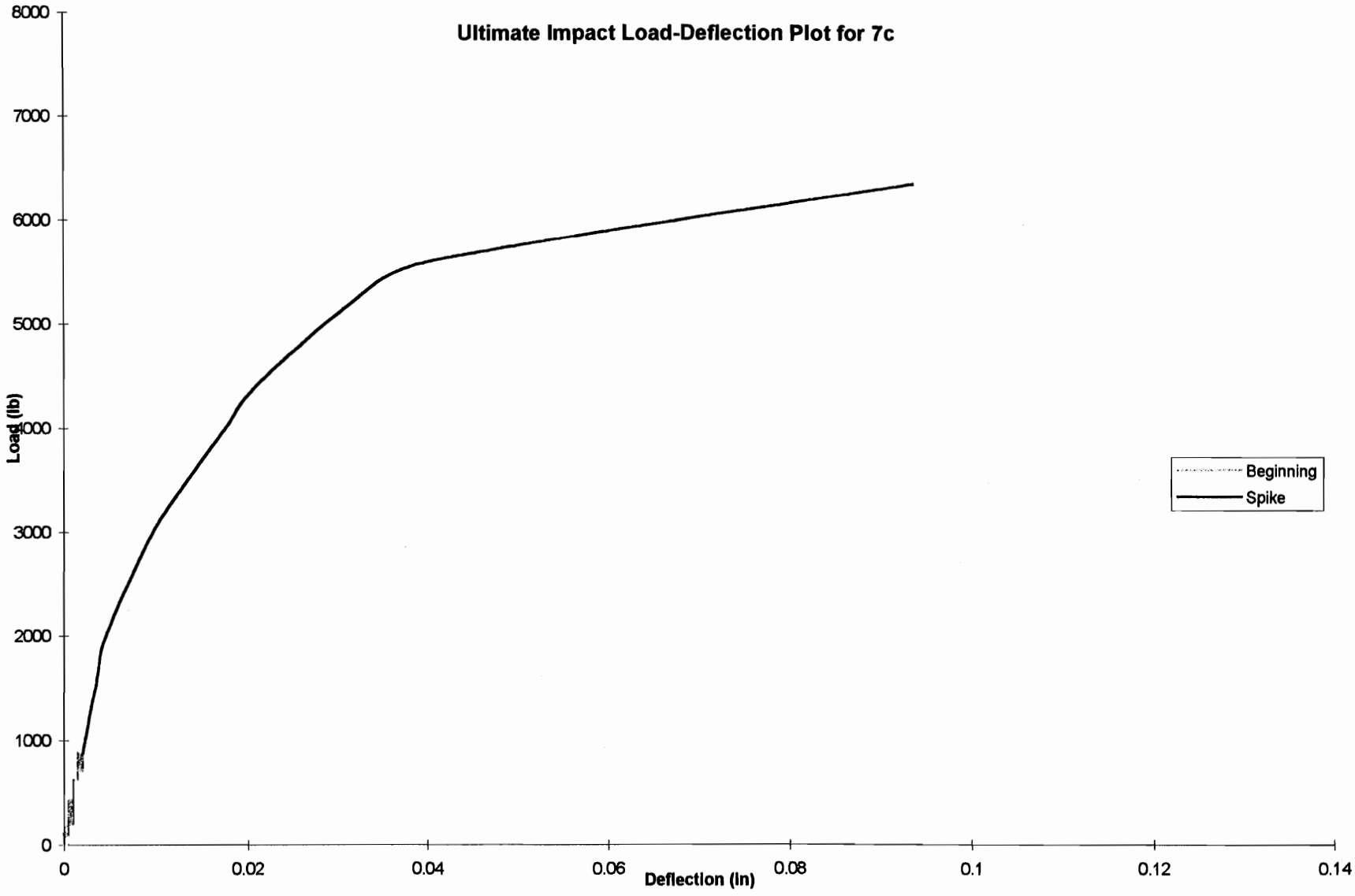
Ultimate Impact Load-Deflection Plot for 7c
Load (lb)
8000
7000
6000
5000
4000
3000
2000
1000
0
0
0.02
0.04
0.06
0.08
0.1
0.12
0.14
Deflection (in)
Beginning
Spike

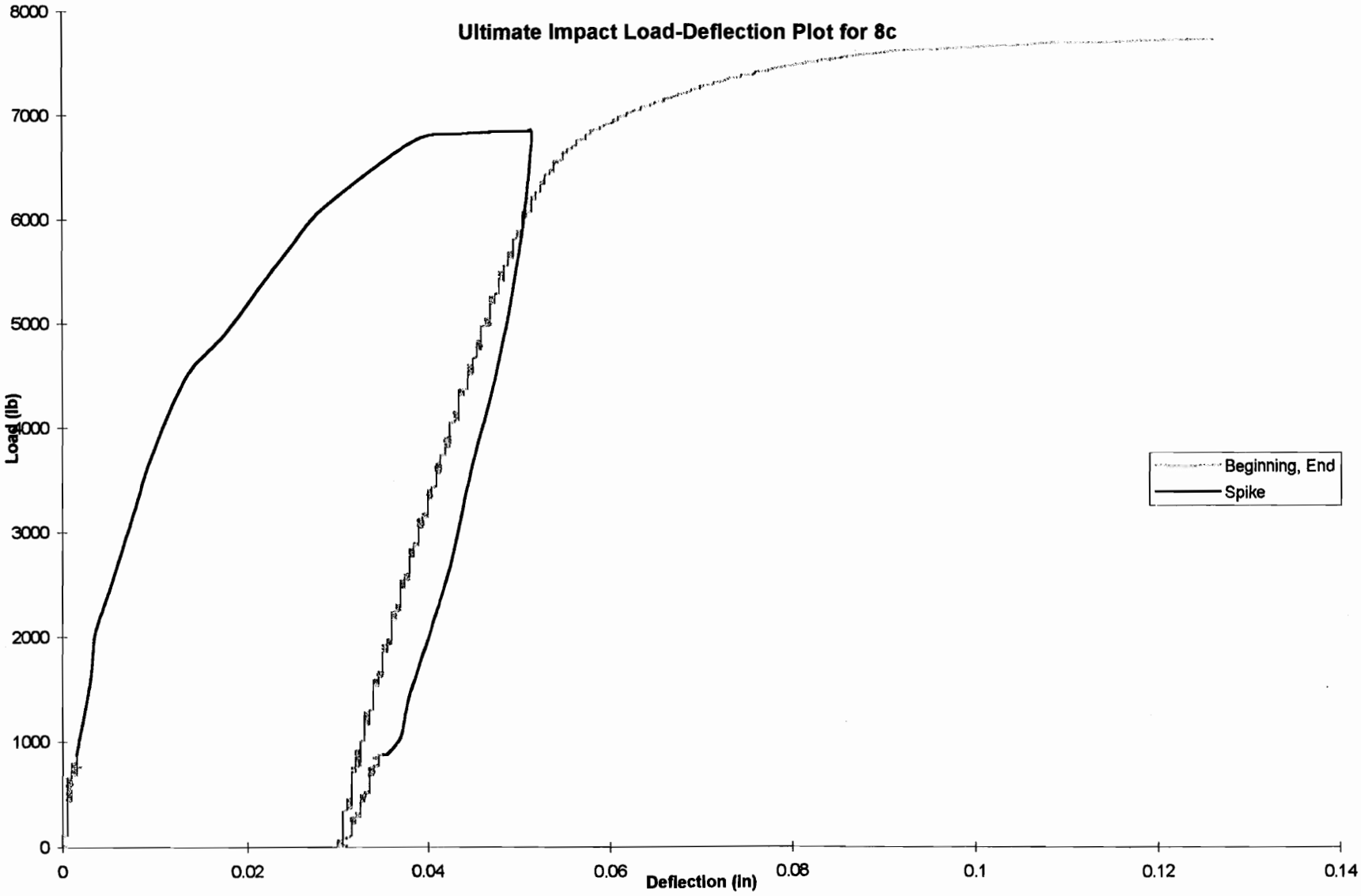
Ultimate Impact Load-Deflection Plot for 8c
Load (lb)
8000
7000
6000
5000
4000
3000
2000
1000
0
0
0.02
0.04
0.06
0.08
0.1
0.12
0.14
Deflection (in)
Beginning, End
Spike

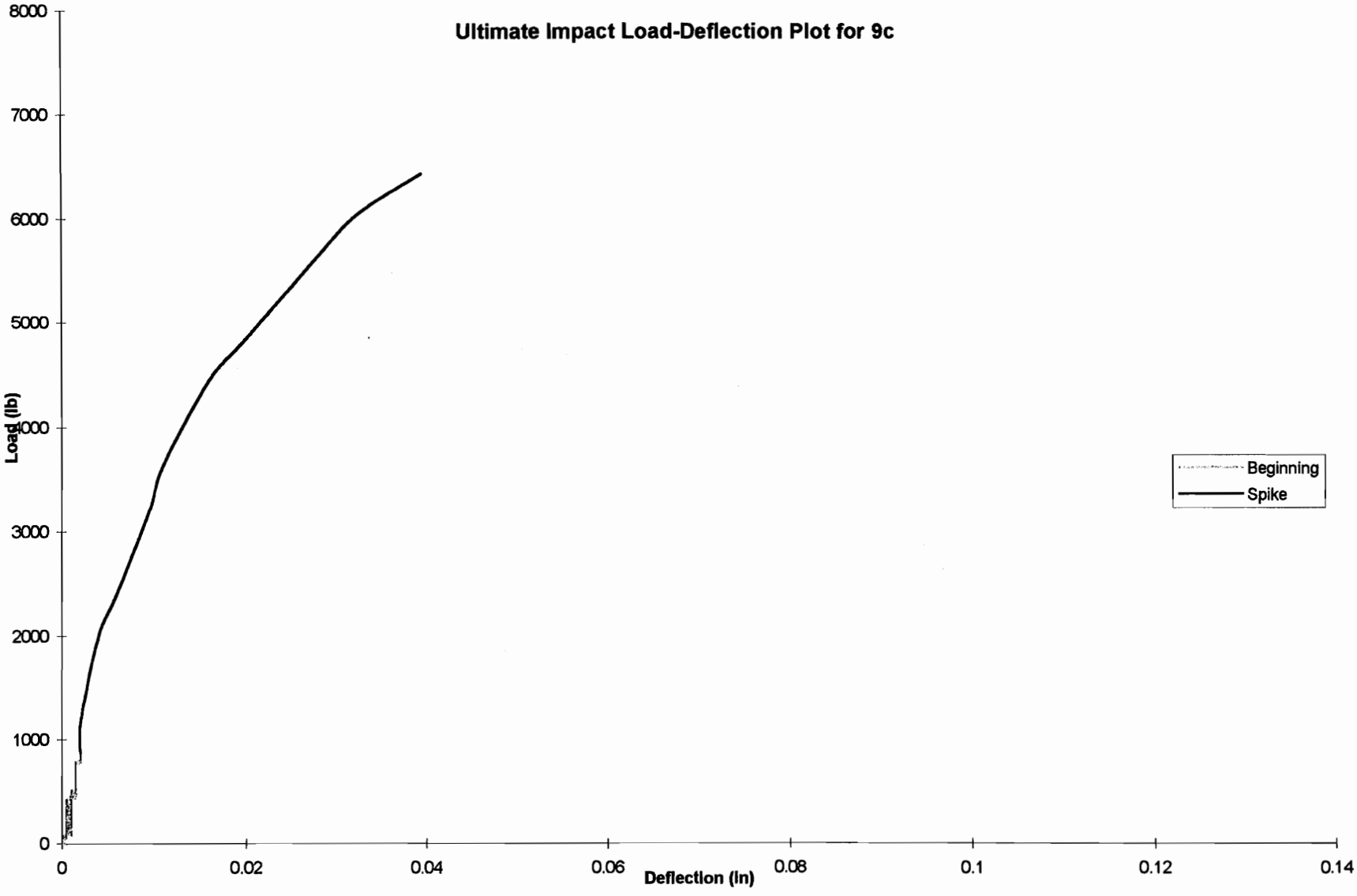
Ultimate Impact Load-Deflection Plot for 9c
Load (lb)
8000
7000
6000
5000
4000
3000
2000
1000
0
0
0.02
0.04
0.06
0.08
0.1
0.12
0.14
Deflection (in)
Beginning
Spike

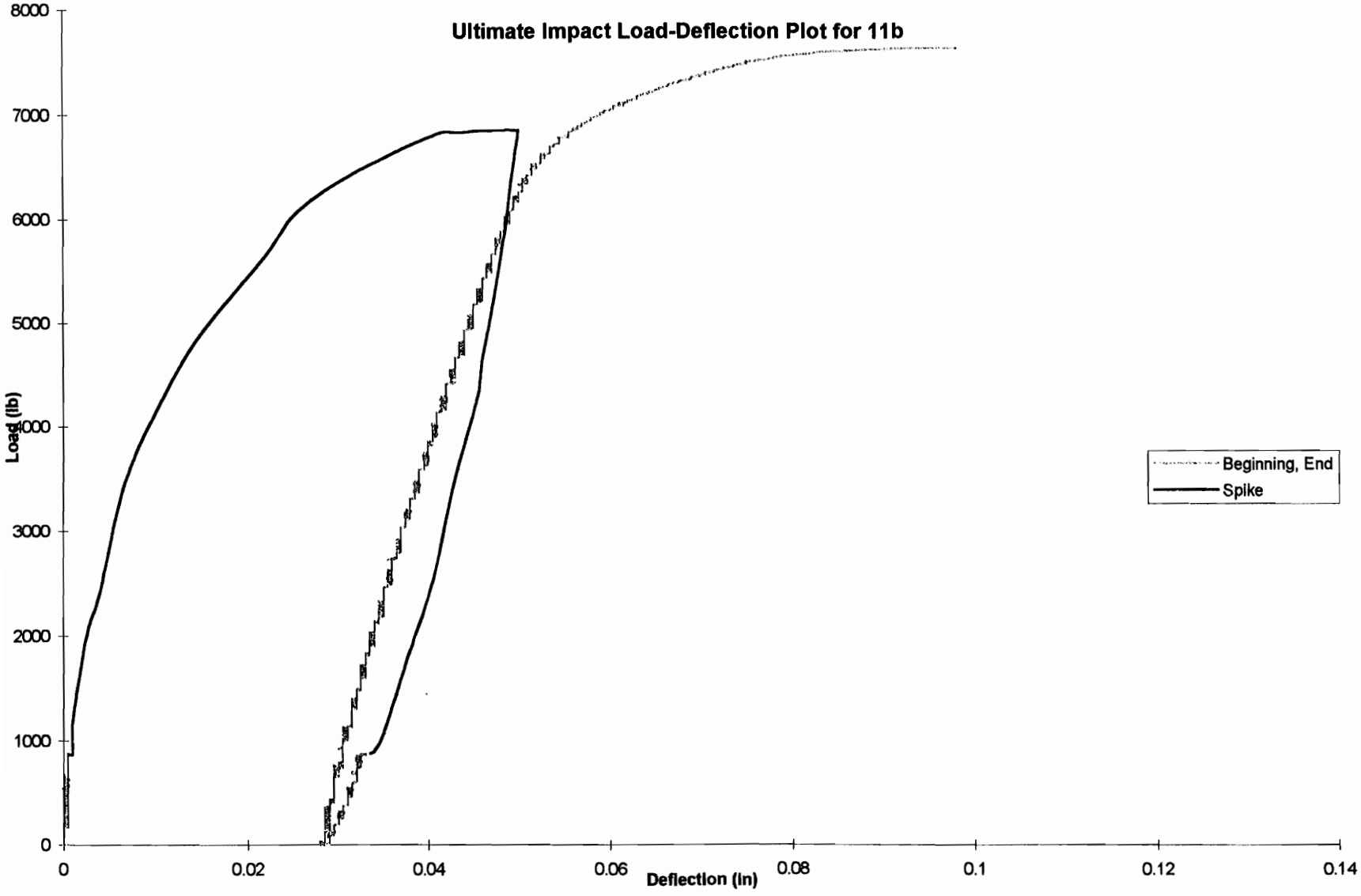
Ultimate Impact Load-Deflection Plot for 11b
Load (lb)
8000
7000
6000
5000
4000
3000
2000
1000
0
0
0.02
0.04
0.06
0.08
0.1
0.12
0.14
Deflection (in)
Beginning, End
Spike

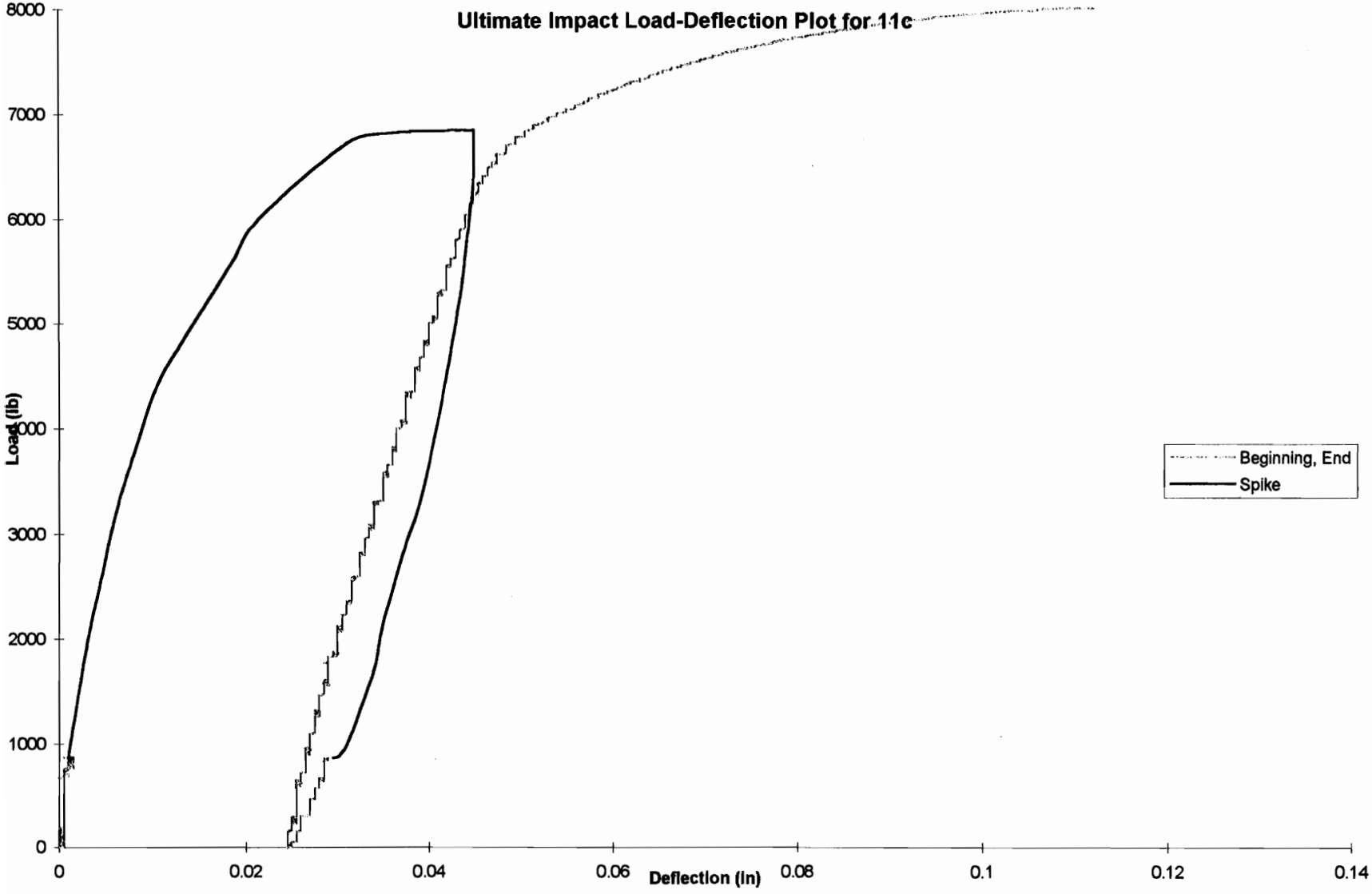
Ultimate Impact Load-Deflection Plot for 11c
Load (lb)
8000
7000
6000
5000
4000
3000
2000
1000
0
0
0.02
0.04
0.06
0.08
0.1
0.12
0.14
Deflection (in)
Beginning, End
Spike

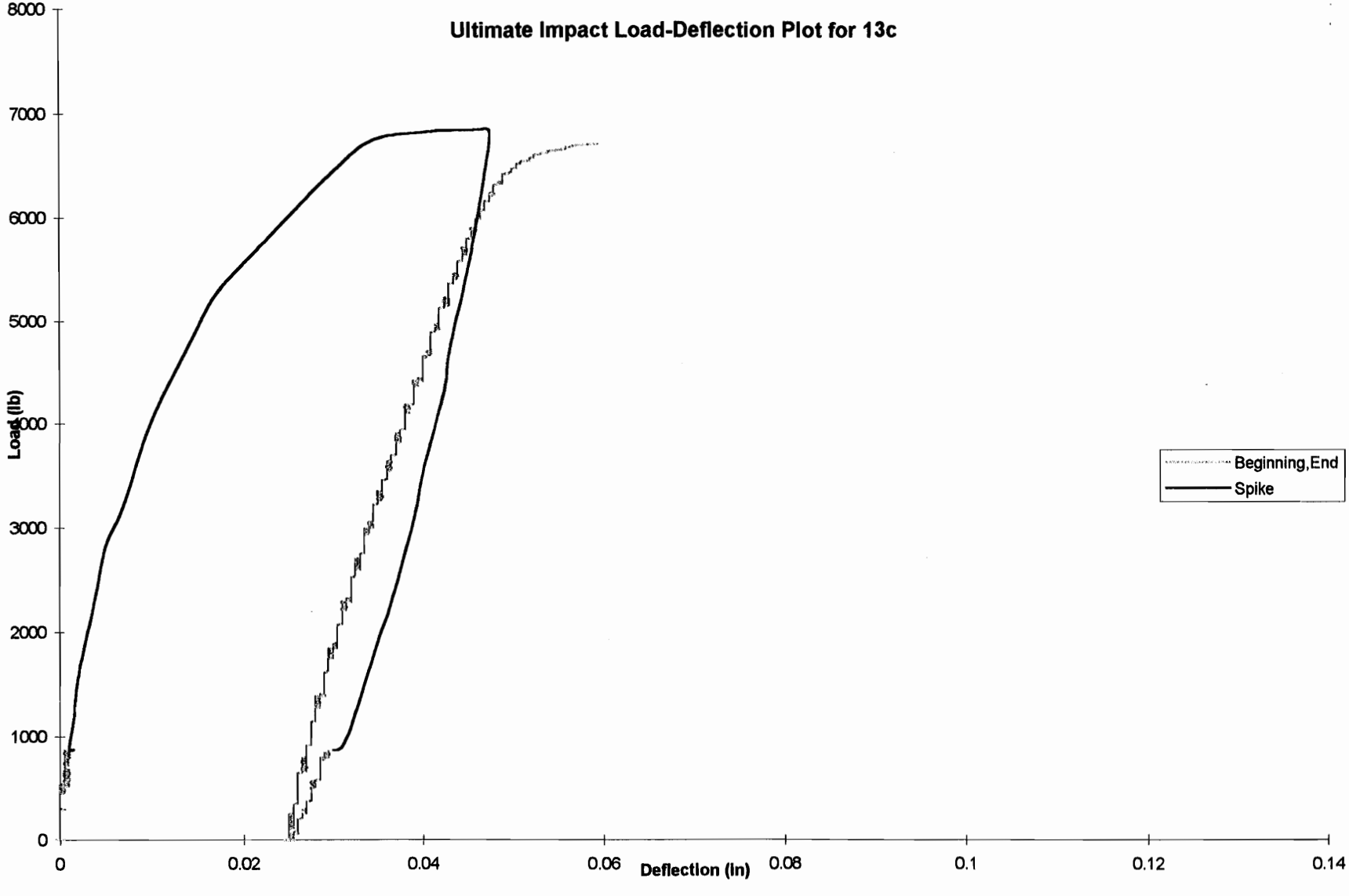
Ultimate Impact Load-Deflection Plot for 13c
Load (lb)
8000
7000
6000
5000
4000
3000
2000
1000
0
0
0.02
0.04
0.06
0.08
0.1
0.12
0.14
Deflection (in)
Beginning,End
Spike

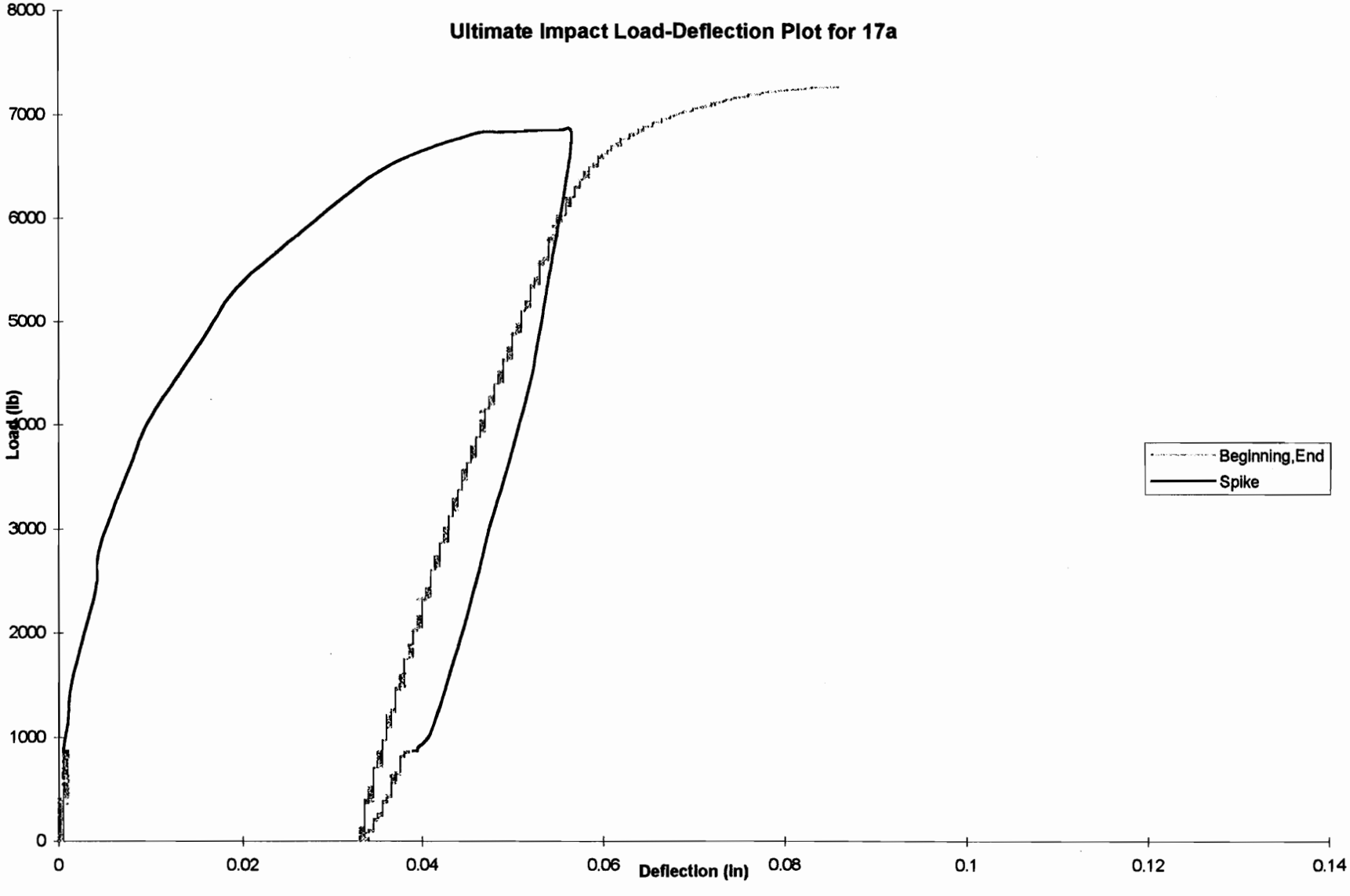
Ultimate Impact Load-Deflection Plot for 17a
Load (lb)
8000
7000
6000
5000
4000
3000
2000
1000
0
0
0.02
0.04
0.06
0.08
0.1
0.12
0.14
Deflection (in)
Beginning,End
Spike

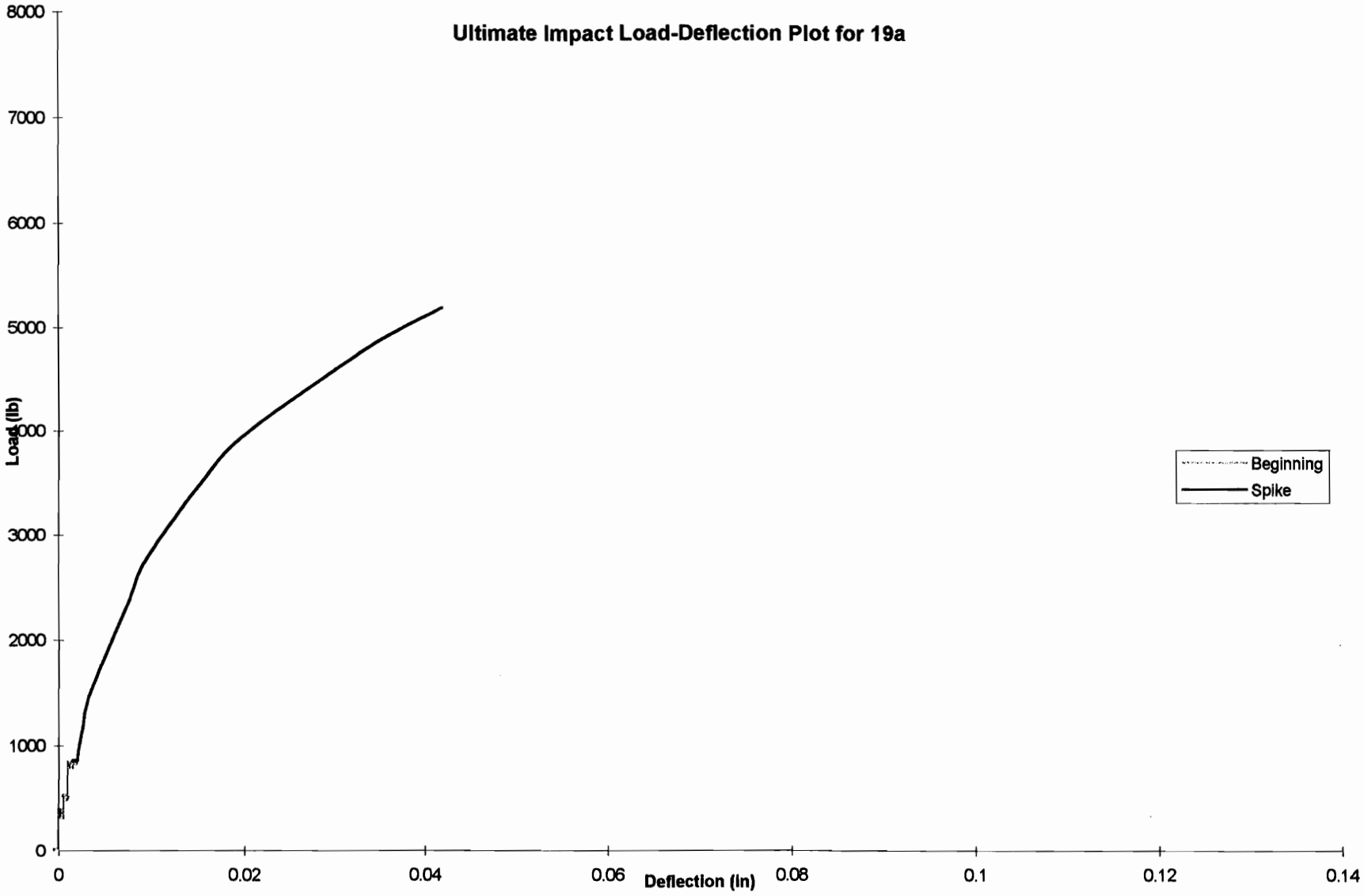
Ultimate Impact Load-Deflection Plot for 19a
8000
7000
6000
5000
4000
3000
2000
1000
0
Load (lb)
0
0.02
0.04
0.06
0.08
0.1
0.12
0.14
Deflection (in)
Beginning
Spike